TRIAXIAL FREQUENCY SWEEP CHARACTERIZATION FOR DENSE GRADED HOT MIX ASPHALT CONCRETE MIX DESIGN

A Thesis Submitted to the College of
Graduate Studies and Research
in Partial Fulfillment of the Requirements
for the Degree of Master of Science
in the Department of Civil and Geological Engineering
University of Saskatchewan
Saskatoon

By
Erin Dawn Baumgartner

PERMISSION TO USE

In presenting this thesis in partial fulfillment of the requirements for a Postgraduate degree from the University of Saskatchewan, I agree that the Libraries of this University may make it freely available for inspection. I further agree that permission for copying of this thesis in any manner, in whole or in part, for scholarly purposes may be granted by the professor or professors who supervised my thesis work or, in their absence, by the Head of the Department or the Dean of the College in which my thesis work was done. It is understood that any copying, publication, or use of this thesis or parts thereof for financial gain shall not be allowed without my written permission. It is also understood that due recognition shall be given to me and to the University of Saskatchewan in any scholarly use which may be made of any material in my thesis.

Requests for permission to copy or to make other use of material in this thesis in whole or part should be addressed to:

Head of the Department of Civil Engineering

University of Saskatchewan

Saskatoon, Saskatchewan S7N 5A9

ABSTRACT

Asphalt concrete mix design methods, such as the Marshall method, have historically been based on physical and phenomenological material testing empirically correlated to observed field performance. Changing pavement field state conditions such as increased trucking, poorer quality aggregate resources, and the aged state of road infrastructure in Saskatchewan have resulted in recent pavement performance to be outside traditional empirical performance prediction inference.

It has been recognized worldwide that a mechanistic based asphalt concrete mix design methodology that directly quantifies structural behaviour of pavement under diverse field state conditions could significantly assist pavement design engineers. However, SHRP Level II and III mechanistic asphalt concrete characterization has been shown not to be pragmatic for characterizing asphalt concrete mixes.

The objective of this research was to investigate the use of mechanistic material properties obtained from triaxial frequency sweep characterization in the rapid triaxial tester (RaTT) in conjunction with SHRP gyratory compaction properties for designing asphalt concrete for different asphalt cement contents, traffic loads, traffic speeds, and temperatures.

RaTT testing was more responsive to variation in asphalt cement content outside of acceptable ranges of volumetric properties relative to Marshall stability and flow. This demonstrated the importance of specifying acceptable volumetric properties of asphalt concrete mixes. Correlation of material properties with volumetric measurements validated triaxial frequency sweep characterization in the RaTT.

Dynamic modulus, Poisson's ratio, and phase angle results were in accordance with expected material behaviour, indicating that the RaTT provides reasonable asphalt concrete material properties. Also, the RaTT identified asphalt concrete to be a nonlinear viscoelastic material, as observed in the field.

The RaTT was able to characterize SHRP gyratory compacted samples for the typical range of traction states, load frequencies, and temperatures that simulated a range

of Saskatchewan field state conditions. Triaxial frequency sweep testing in the RaTT could significantly augment conventional volumetric mix analysis as well as the SHRP Superpave^{TM} Level I asphalt concrete mix design system. RaTT testing was found to be cost effective, time efficient, and provided mechanistic material constitutive relations that can be employed for inelastic mechanistic mix design, road structural modelling, and asset management.

ACKNOWLEDGEMENTS

The research work reported here was supported in part by the Saskatchewan Department of Highways and Transportation. The author is grateful for this support. Thanks also to Alex Kozlow and Amélie Couraud for their assistance in the laboratory.

The author also acknowledges the efforts made on her behalf by Debbie Forgie, Joanne Skeates, Cynthia Hanke, and Melissa Zink.

The author is grateful to the advisory committee for their guidance of the research work: Dr. Gordon Putz, Dr. Bruce Sparling, and Dr. Gordon Sparks. The author is also appreciative of the efforts of the external advisor, Greg Chartier. The author extends special acknowledgements and thanks to the research supervisor, Dr. Curtis Berthelot.

TABLE OF CONTENTS

LIST OF TABLES

LIST OF FIGURES

LIST OF ABBREVIATIONS

AASHTO – American Association of Highway and Transportation Officials
ASTM – American Society for Testing and Materials
CGSB – Canadian General Standards Board
CHST – Constant height shear test
COS – City of Saskatoon
DHT – Saskatchewan Department of Highways and Transportation
ESAL – Equivalent Single Axle Load
FC – Fatigue cracking
FSCH – Frequency sweep at constant height
IDT – Indirect tension test
LCPC – Laboratoire Central des Ponts et Chausseés
LVDT – Linear variable differential transducer
N – Number of gyratory revolutions
N_{des} – Design number of gyrations
N_{ini} – Initial number of gyrations
N_{max} – Maximum number of gyrations
PD – Permanent deformation
PG – Performance Grade
RaTT – Rapid triaxial test
RSCH – Repeated shear at constant height
SHRP – Strategic Highway Research Program
SST – Superpave™ shear tester
T_{EFF} – Effective temperature
T_{PD} – Permanent deformation temperature
T_{FC} – Fatigue cracking temperature
VFA – Voids Filled with Asphalt
VMA – Voids in the Mineral Aggregate
VTM – Voids in the Total Mix

1.0 INTRODUCTION

Asphalt concrete is the primary road surfacing system in Canada (Haas and Karan 1993). Asphalt concrete is a viscoelastic particulate composite material (Dietrich *et al.* 1998). Traditionally, the primary objectives of a hot mix asphalt concrete mix design have been to: 1) determine the optimal grain size distribution of locally available aggregate sources; 2) determine the optimal asphalt cement content for a given mix aggregate gradation; and 3) ensure adequate distress resistance for expected field state conditions.

Asphalt concrete mix design has historically been based on physical and phenomenological material testing empirically correlated to observed field performance. Saskatchewan road agencies currently employ Marshall asphalt concrete mix design and specifications (COS 2000, DHT 2003), which has traditionally been the most widely employed conventional empirical based mix design method in North America (Linden *et al*. 1989). However, empirical mix design methods, such as the Marshall method, have several limitations including (Mamlouk and Sarofim 1988, Monismith 1992):

- Results are dependent upon the test apparatus configuration and therefore do not characterize the fundamental thermomechanical behaviour of asphalt concrete;
- Empirical mix design test results may rank the relative behaviour of hot mix asphalt concrete, however, the material indices obtained can not be used for road modelling or structural design; and
- Field state conditions and material types under which the conventional empirical mix design methods were historically calibrated have changed significantly over recent decades.

In particular, a serious limitation to conventional asphalt concrete design inference is that Saskatchewan has experienced significant increases in commercial truck loadings over recent years. As a result, Saskatchewan asphalt concrete pavements are experiencing increased load related distress and structural deterioration, particularly on concentrated commercial haul corridors. Further, urban asphalt concrete mixes are subjected to even higher damage due to channelized commercial trucking, minimal local weight enforcement, and stop-and-go traffic conditions. In addition, poorer quality aggregate resources have resulted in many pavements that do not comply with modern structural performance expectations.

Although high quality aggregates specified by advanced asphalt concrete mixes, such as stone matrix asphalt, may improve the performance of asphalt concrete mixes, high quality aggregates are difficult to manufacture from depleted glacial deposits typical in Saskatchewan. In fact, it is estimated that Saskatchewan contains approximately 150 million metric tonnes of quality aggregate and Saskatchewan consumes 6-10 million metric tonnes of aggregate per year (DHT Internal Report 2003). As a result, it is projected that Saskatchewan will be facing a severe aggregate shortage within the next two decades. Because higher performing aggregate specifications typically result in significantly increased manufacturing costs and wastage of scarce and non-renewable high quality aggregate resources, more accurate performance based mix design improvements must be developed.

Researchers have made considerable advancements in developing performance based asphalt binder characterization specifications, such as the Strategic Highway Research Program Performance Grading (SHRP-PG) system. The SHRP-PG system has led to higher performing modified asphalt cement binders. However, these recent advancements in asphalt cement technologies are only effective when employed within acceptable asphalt concrete volumetric mix properties, structural design parameters, aggregate properties, and asphalt cement content.

It has further been recognized that pavement structural design methods typically employed by road agencies do not account for differences in asphalt concrete mixes. Therefore, asphalt concrete mix design methodology that can directly quantify the

structural capacity and predict life cycle performance of asphalt concrete mixes under diverse field state conditions is required (Baladi 1989). As a result, researchers have been developing mechanistic based asphalt mix theory and laboratory characterization equipment and protocols that quantify the fundamental mechanistic behaviour of asphalt concrete mixes (SHRP 1994 and AASHTO 2004). Specifically this research has focused on mechanistic asphalt concrete mix analysis procedures that quantify the fundamental properties of asphalt concrete mixes over the full range of stress and strain states and temperatures experienced in the field (Finn *et al.* 1976, Potter 1989, SHRP 1994, Berthelot 1999, and Crockford *et al.* 2002).

A mechanistic mix design system that could assist the evaluation of new asphalt concrete mixes and structures as they are developed would be a powerful tool in pavement performance prediction, especially under continually changing traffic loading conditions. A mechanistic based mix design method would significantly compliment mechanistic based asphalt cement binder and structural design and road modelling technologies such as numerical finite element analysis. In addition, pavement life cycle costing and pavement asset management require accurate mechanistic characterization of road material behaviour to predict road performance (Berthelot *et al.* 1997).

Over recent years, considerable research has been undertaken to develop and deploy improved rut resistant asphalt concrete mixes such as stone matrix asphalt (Kreide *et al*. 2003), open graded friction course (Watson *et al*. 2003), and SHRP Superpave^{TM} coarse mixes (Superpave Mix Design 1996) specifically designed for high commercial traffic conditions in high temperature applications. A mechanistic mix design system would assist in the implementation of advanced asphalt concrete mixes (Rowe *et al.* 1995) and would be a powerful tool in pavement rehabilitation optimization analysis (Patrick and Bailey 2003).

Several road agencies have already adopted some form of mechanistic based asphalt concrete mix design procedures, including the majority of European countries, South Africa, Illinois, Kentucky, and Washington (Theyse *et al.* 1996, Corté and Goux 1996, and Harichandran *et al.* 2001). In many cases, these mechanistic based design methods have led to the adoption of higher quality performance-based asphalt concrete

systems. However, a fundamental limitation of these current mechanistic mix design methods is the lack of accurate material constitutive characterization capabilities.

1.1 Review of Asphalt Concrete Mix Design Methods

1.1.1 Marshall Mix Design

The Marshall mix design method was developed during the 1930's (U.S. Army Corps of Engineers 1944) as a portable asphalt concrete mix design method that involved minimal effort and time as a basis for determining the optimum asphalt content of the given aggregate gradation. The Marshall mix design method is empirically based and is the most widely employed mix design method employed by North American road agencies (Linden *et al*. 1989).

The Marshall mix design method uses an impact hammer to compact samples in a 102 mm diameter mould to a height of approximately 63.5 mm (Roberts *et al*. 1996). Compaction effort in the field is represented by the number of Marshall hammer blows per side of the sample. Standard compaction is 50 blows per side of the sample. However, the paving industry may specify a compaction effort of 25, 50 or 75 blows depending on traffic conditions (Maupin 1995). Research has shown poor correlation between the mechanical properties of Marshall impact hammer compacted samples and field specimens (Consuegra *et al.* 1989, and Carlberg 2003). In addition, Marshall stability and flow measurements do not characterize the fundamental behaviour of asphalt mixes, and, as a result, can not be used to model the structural behaviour of asphalt concrete mixes.

1.1.2 SHRP Superpave™ Mix Design

The Superpave™ (*Su*perior *Per*forming Asphalt *Pave*ments) mix design system is a product of the Strategic Highway Research Program (SHRP) developed from 1987 through 1992 (Roberts *et al*. 1996). The Superpave™ mix design system was developed to minimize permanent deformation, fatigue cracking, and low temperature cracking in asphalt concrete (SHRP-A-408 1994). Unlike the Marshall mix design method,

Superpave™ is a mechanistic mix design system that directly accounts for constituent material properties and design environmental conditions in addition to traffic level.

Superpave™ employs the SHRP gyratory compactor to compact asphalt concrete specimens. The gyratory compactor (Harman *et al.* 2001):

- Is adaptable to both laboratory mix design and field quality control;
- Better simulates air void content as obtained in the field both after placement and after traffic loading relative to Marshall impact hammer compaction; and
- Approximates aggregate degradation in the field.

The Superpave™ performance prediction system provides the means to determine fundamental properties of asphalt concrete such as stiffness modulus, fatigue resistance, and permanent deformation resistance which can be used for road structural modelling. Although the theory behind Superpave™ mix design and performance prediction characterization is sound, the mix characterization methods specified by Superpave™ are not pragmatic in that they are very time consuming and therefore not cost effective (Berthelot 1999). In addition, the Superpave™ mix evaluation protocols are not proven to be related to performance in the field. Therefore an accurate, time efficient and cost efficient performance verification test would be a beneficial addition to the Superpave™ mix design and analysis system.

1.1.3 Triaxial Frequency Sweep Testing

Triaxial frequency sweep testing is a mechanistic based asphalt concrete characterization method that is a time and cost effective method for determining mechanistic asphalt concrete material properties. Triaxial frequency sweep testing in the rapid triaxial tester (RaTT) is a recent advancement towards accurately reproducing field traffic loading conditions in the laboratory. The RaTT employed in this research has the ability to perform frequency sweep characterization using pneumatic confining traction in a rubber membrane while a sinusoidal traction is applied vertically to the sample. Sinusoidal loading reasonably simulates repeat axle loads experienced by the pavement (Crockford *et al.* 2002, Anthony and Berthelot 2004). Confining traction allows close duplication of pavement service stress states in addition to preventing premature sample

failure (Brown *et al.* 2001). The RaTT employs 150 mm diameter by 150 mm tall samples SHRP gyratory compacted samples.

Both vertical and confining tractions can be user defined as per the specific field state conditions, allowing for characterization of a range of traffic loads. In addition, the vertical sinusoidal traction frequency can be varied, allowing for characterization of a range of traffic speeds for specific situations. For example, a 10.0 Hz test frequency approximately simulates traffic at highway speeds, depending on truck axle spacing and configuration. Test temperature can also be varied to accommodate a range of temperatures experienced in the field.

In summary, the RaTT is a continuum based test apparatus with the ability to characterize the fundamental mechanistic behaviour of asphalt concrete mixes which may be used to better classify asphalt mixes as well as model pavement structures.

1.2 Project Objectives

The objective of this research was to employ triaxial frequency sweep characterization in the rapid triaxial tester (RaTT) for characterizing asphalt concrete mixes at typical mix design parameters for typical Saskatchewan asphalt cement contents, traffic loads, traffic speeds, and temperatures.

A second objective of this research was to compare the results of the Marshall mix design method to Superpave^{TM} Level I gyratory compaction results and linear viscoelastic material properties obtained from RaTT test results of typical Saskatchewan dense graded asphalt concrete mixes.

1.3 Research Hypothesis

The hypothesis of this research is that the material properties obtained from triaxial frequency sweep characterization of asphalt concrete in the RaTT will concur with changes in physical material properties as characterized using conventional mix design methods.

1.4 Scope

City of Saskatoon (COS) Type A1 (COS 2000) and Saskatchewan Department of Highways and Transportation (DHT) Type 71 (DHT 2003) asphalt concrete mixes were considered in this research. Both mixes are dense graded hot mix asphalt concrete mixes typically used for high traffic corridors. Other high performing asphalt concrete mixes, such as open graded friction course and stone matrix asphalt, being investigated by other road agencies are not considered economically feasible in Saskatchewan given aggregate depletion and therefore were not considered.

The three aggregate blend gradations that were considered in this research were based on COS Type A1 gradation specifications and included the middle of the aggregate gradation envelope, the fine side (top) of the gradation envelope, and the coarse side (bottom) of the gradation envelope. Straight run 150-200A penetration grade asphalt cement was employed for all mixes employed in this research.

In this research, triaxial frequency sweep testing in the RaTT was employed to characterize asphalt concrete material properties based on typical Saskatchewan field state conditions including:

- Temperatures;
- Multi-axial stress states; and
- Traffic load rates.

Two repeat Marshall impact hammer compacted samples and one SHRP gyratory compacted sample were compacted for each of the three blend gradations at six different asphalt cement contents typical to Saskatchewan asphalt concrete mix designs. Only one SHRP gyratory compacted sample was characterized in this research because previous research has shown the RaTT to have high repeatability when testing asphalt concrete (Berthelot 1999).

Each sample was subjected to volumetric characterization. The SHRP gyratory samples were then subjected to triaxial frequency sweep testing in the RaTT which consisted of applying five traction magnitudes at five loading frequencies as summarized in Table 1.1 and Table 1.2, respectively.

Table 1.1 Triaxial Frequency Sweep Load Frequencies

Frequency Test Order	Axial Loading Frequency (Hz)
1	10.0
2	5.0
3	1.0
4	0.5
5	0.125

Table 1.2 Applied Triaxial Frequency Sweep Peak Traction States

Traction State Order	Maximum Axial Traction (kPa)	Minimum Axial Traction (kPa)	Confining Traction (kPa)	Resulting Deviatoric Stress (kPa)
1	200	50	50	150
2	300	75	75	225
3	400	100	100	300
4	600	150	150	450
5	800	200	200	600

1.5 Methodology

The project elements and tasks employed to accomplish the objectives of this research are outlined below:

- Project Element 1: Background and Literature Review
  - Task 1 – Review of literature pertaining to the effect of gradation, air void content, and asphalt content on typical dense graded mixes.
  - Task 2 – Review of literature pertaining to conventional asphalt mix design methods, including the Marshall method, and SHRP Level I volumetric characterization criterion of asphalt concrete mixes.
  - Task 3 – Review of literature pertaining to alternate mix design procedures and specifications.
  - Task 4 – Review of literature pertaining to mechanistic evaluation techniques developed for asphalt concrete mixes.

- Project Element 2: Field Sampling
  - Task 1 – Sample aggregate materials from a local aggregate source used for asphalt concrete paving.
  - Task 2 – Sample 150-200 penetration grade asphalt cement from a standard supplier commonly used in Saskatchewan.
- Project Element 3: Laboratory Characterization
  - Task 1 – Characterization of asphalt cement binder.
    - Perform penetration test on asphalt concrete as per AASHTO T49 (AASHTO 1995).
    - Perform absolute viscosity test on asphalt concrete as per AASHTO T202 (AASHTO 1995).
    - Classify asphalt cement penetration-viscosity as per CAN/CGSB-16-3M90.
  - Task 2 – Marshall mix design and characterization.
    - Determine volumetric properties of the asphalt concrete samples of aggregate gradations and asphalt cement contents as per AASHTO T269 (AASHTO 1995).
    - Perform Marshall stability and flow test as per AASHTO T245 (AASHTO 1995).
    - Determine the optimum asphalt cement content for the mix blend gradations based on volumetric properties.
  - Task 3 – SHRP Level I gyratory mix design and characterization.
    - Examine SHRP gyratory compaction profile as per AASHTO TP4 (AASHTO 1995).
    - Determine the volumetric properties of the asphalt concrete for aggregate gradations and asphalt cement content as per AASHTO T269 (AASHTO 1995).
    - Determine the optimum asphalt cement content for the mix blend gradations based on volumetric properties.

- Task 4 – Triaxial frequency sweep mechanistic mix characterization.
    - Perform triaxial frequency sweep testing of the asphalt concrete samples for five load frequencies (0.125 Hz, 0.5 Hz, 1.0 Hz, 5.0 Hz, and 10.0 Hz) and five peak vertical compressive and confining traction states (200 kPa-50 kPa, 300 kPa-75 kPa, 400 kPa-100 kPa, 600 kPa-150 kPa, and 800 kPa-200 kPa) at 25^{o}C and 60^{o}C.

➢ Project Element 4: Analysis of Laboratory Mix Characterization Results

- Task 1 – Quantify and compare Marshall volumetrics and SHRP gyratory volumetrics relative to DHT, COS, and SHRP specified bandwidths.
- Task 2 – Quantify Marshall stability and flow as a function of asphalt content for mix aggregate blend gradations.
- Task 3 – Identify the optimum asphalt cement content for the mix blend gradations and characterization method.

➢ Project Element 5: Analysis of Triaxial Frequency Sweep Characterization Results

- Task 1 – Quantify the triaxial frequency sweep mechanistic material properties (dynamic modulus, Poisson's ratio, and phase angle) as a function of asphalt content for aggregate gradations.
- Task 2 – Determine the mechanistic material property ranges corresponding to acceptable volumetric specifications.
- Task 3 – Compare of Marshall volumetrics, stability and flow to triaxial frequency sweep material properties.
- Task 4 – Quantify the variability of the triaxial frequency sweep testing and mix design parameters (temperature, deviatoric stress state, loading rate, blend gradation, and asphalt content).
- Task 5 – Determine the linear and elastic limits of asphalt concrete mixes of gradation, asphalt cement content, and field state conditions.

➢ Project Element 6: Summary, Conclusions, and Future Recommendations

1.6 Summary

Conventional phenomenological-empirical asphalt concrete mix design methods, such as the Hveem and Marshall mix design systems, are widely used in the pavement industry. However, these traditional design methods have several limitations for designing asphalt concrete mixes for modern field state conditions. Therefore an asphalt concrete mix design and analysis method is required to more accurately characterize the field performance related properties of asphalt concrete mixes.

Triaxial frequency sweep testing in the rapid triaxial tester (RaTT) is a recent advancement towards accurately reproducing field traffic loading conditions in the laboratory. The RaTT employed in this research applies a confining traction to the sample while a sinusoidal traction is applied vertically. Confining traction, vertical traction, vertical traction frequency, and test temperature may be varied to simulate field state conditions for specific locations.

However, prior to adopting new mechanistic based asphalt concrete mix design and analysis methods, new proposed methods must first be compared to conventional mix design parameters and the field performance inference related to those methods. Once validated based on past field performance inference, the mechanistic asphalt concrete mix characterization system and protocols can be applied to asphalt mixes, road structural design, and asset management applications.

The asphalt concrete mixes employed in this research were based on City of Saskatoon Type A1 and the Saskatchewan Department of Highways and Transportation Type 71 dense graded mixes typically used for high traffic corridors in Saskatchewan. The RaTT was employed to characterize asphalt concrete material properties based on typical Saskatchewan traffic loads, traffic speeds, and temperatures.

2.0 LITERATURE SEARCH AND BACKGROUND

This chapter introduces and reviews literature regarding hot mix asphalt concrete distresses and physical properties, traditional empirical mix design methods, and recently developed mechanistic mix design methods. Asphalt concrete pavements are designed to provide a smooth, dust free surface to facilitate public and commercial ground transportation. More than 90 percent of all paved roads in the United Sates and Canada are surfaced with asphalt concrete (Consedine 2004).

2.1 Asphalt Concrete Distresses

Asphalt concrete is intended to resist distresses throughout its design life. Damage within hot mix asphalt concrete pavement falls primarily into three categories:

1) Mix disintegration including:
   - Stripping; and
   - Ravelling.
2) Fracture including:
   - Fatigue cracking; and
   - Thermal cracking.
3) Viscoplastic flow including:
   - Rutting; and
   - Shoving.

This thesis will focus on characterizing permanent deformation behaviour of asphalt concrete pavements.

2.1.1 Mix Disintegration

Stripping is the loss of adhesive bond between the aggregate and asphalt cement binder (McCann and Sebaaly 2003). Stripping is usually the result of moisture between the aggregate surface and asphalt cement. Problems associated with stripping include accelerated asphalt cement aging, loss of asphalt concrete stability, and other distresses such as ravelling, rutting, and cracking. (Ruth 1985, Mohamed 1993, Kandhal 1994)

Ravelling is the disintegration of asphalt concrete beginning from the surface and progressing downward because of dislodged aggregate particles. Aggregate particle dislodgement is a result of the loss of bond between the asphalt binder and aggregate particles. Causes of ravelling include insufficient asphalt content, segregation of the asphalt concrete mix during placement, high air void content, and excessively oxidized asphalt binder (Sontowski 1995, Bischoff *et al*. 1998). Problems associated with ravelling include loose aggregate causing loss of skid resistance and aggregate picked up and thrown by tires. Severe ravelling may create a large depression in the road surface allowing water ponding and therefore increasing the risk of hydroplaning.

2.1.2 Fatigue Cracking

Fatigue cracking typically initiates longitudinally along the edge of the wheel path or in short cracks in the wheel path perpendicular to the direction of traffic, depending on the structural composition of the pavement (Epps and Monismith 1971, Terrel 1971, Leahy *et al*. 1996), as illustrated in Figure 2.1. Severe fatigue cracking propagates to form a network of interconnected cracks that resembles the skin of an alligator and is therefore sometimes referred to as alligator cracking. Fatigue cracking develops because of repeated applied tractions which result in stresses that are higher than the tensile and shear strength of the asphalt concrete. Fatigue cracking is the principal load-associated cracking that occurs in asphalt concrete.

Problems associated with fatigue cracking include roughness, loss of load transfer through the asphalt concrete layer to the substructure, and water infiltration through the pavement causing weakening of the substructure.

Figure 2.1 Fatigue Cracking of Asphalt Concrete

2.1.3 Thermal Cracking

Thermal cracks typically propagate transversely in asphalt concrete (Roque and Ruth 1990, Shen and Kirkner 2001), as illustrated in Figure 2.2. Thermal cracking is mostly associated with environmental effects (Jeng *et al*. 1993). As the ambient air temperature decreases, the temperature of the asphalt cement decreases causing shrinkage, inducing tensile stresses into the asphalt cement (SHRP-A-357). Once the tensile stress exceeds the tensile strength of the asphalt cement and/or the asphalt cement-aggregate interface, thermal cracking occurs (Sebaaly *et al*. 2002). The change in strain in the asphalt cement as a result of temperature change from 40^{o}C to -40^{o}C is approximately 0.010 mm/mm. However, the change in strain in the aggregate is only 0.001 mm/mm. The order of magnitude strain difference between the aggregate and the asphalt results in thermal cracking.

Problems associated with thermal cracking include ride roughness, depression at the crack, as illustrated in Figure 2.3, loss of load transfer to the substructure, and water infiltration through the pavement causing weakening of the substructure (Epps 2000).

Figure 2.2 Thermal Cracking in Asphalt Concrete

Figure 2.3 Thermal Crack Depression in Asphalt Concrete

2.1.4 Permanent Deformation

Permanent deformation, or rutting, in asphalt pavement is exhibited by longitudinal bowl-shaped depressions in the wheel paths of a road surface, as illustrated in Figure 2.4 through Figure 2.8. Permanent deformation can be a result of weak substructure material below the pavement surfacing as illustrated in Figure 2.4 and Figure 2.5, a weak pavement layer as illustrated in Figure 2.6 through Figure 2.8, or both. Permanent deformation has traditionally been a common cause of failure in asphalt concrete pavements (Monismith and Finn 1977, and Majidzadeh *et al.* 1979), and is the most common cause of premature asphalt concrete mix failure in Saskatchewan (Beshara 2000). Failure due to rutting is defined as rut depth of 12.5 mm (Highway Research Board 1961). As a result, at least ten percent of the DHT asphalt concrete maintenance budget is spent on rut treatments (Davies 2004).

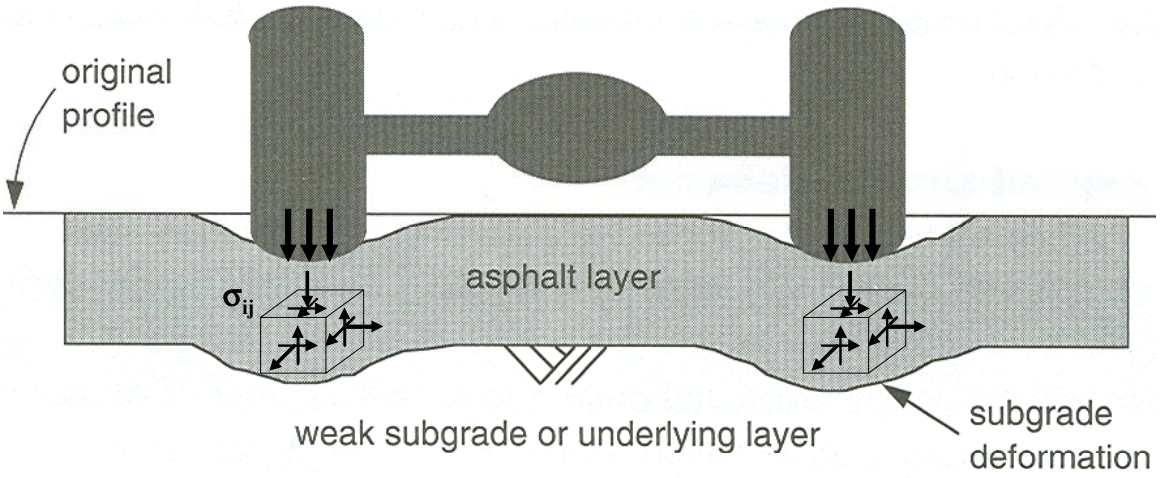

Figure 2.4 Rutting in Weak Substructure Layer (After Superpave Mix Design 1996)

Figure 2.5 Substructure Rutting with Fatigue Cracking

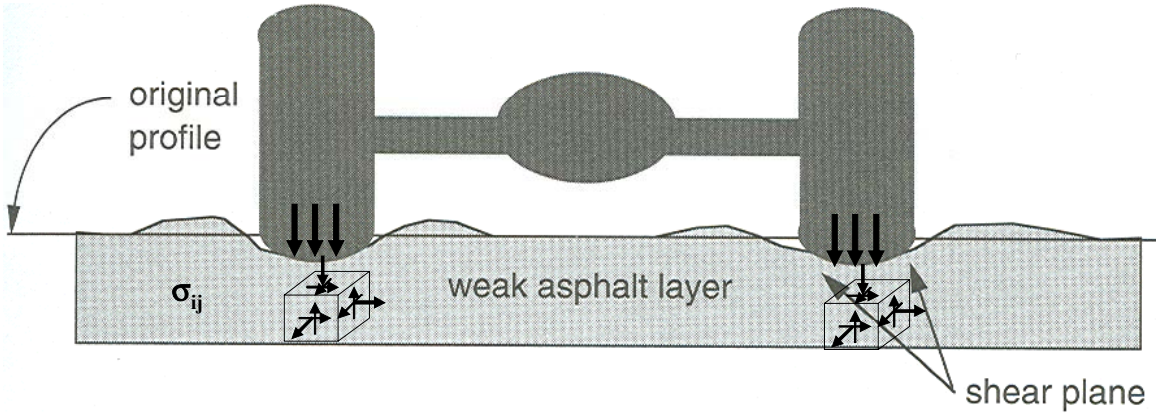

Figure 2.6 Rutting in Weak Asphalt Concrete Layer (After Superpave Mix Design 1996)

Figure 2.7 Asphalt Concrete Layer Viscoplastic Rutting

Figure 2.8 Cross Section of Asphalt Concrete Layer Isolated Wheel Path Rutting Due to Viscoplasticity (Courtesy of DHT)

Rutting in asphalt concrete pavement is caused by cumulative non-recoverable plastic strain in road materials spatially within the wheel paths due to the collective effects of repeated high axle loads, high traffic volumes, high service temperature, and high tire pressures. Tractions are applied by vehicle wheels at the pavement surface, resulting in stress and strain state in the pavement layer. Rutting is a function of the cumulative permanent plastic strain occurring in all materials comprising the road structure (Barksdale 1977, Croney 1977). In structurally sound pavement structures, most rutting in asphalt concrete pavement occurs in the top 75 mm to 100 mm of the pavement structure (Sebaaly *et al.* 1997).

Consolidation of the asphalt concrete layer occurs in most dense graded asphalt concrete pavements under commercial truck traffic loading soon after construction and tapers off with time (SHRP-A-357 1993, Hanson *et al.* 1994, Roberts *et al.* 1996). Commercial trucks are the major cause of plastic strains because they induce large tractions and therefore plastic strains in the asphalt concrete mix (Sousa and Solaimanian 1994). Excessive mix consolidation typically occurs when the asphalt concrete has too high asphalt cement content, too soft asphalt cement, excessive rounded aggregate, and/or too low initial air void content in the mix due to improper compaction or poor mix formula during construction (Button *et al.* 1990, Foster 1993). Rutting is exacerbated in areas with slow moving traffic or in areas with severe braking and acceleration tractions, such as at urban intersections (Blight 1974), particularly at high ambient air temperatures. The increased permanent deformation resulting from slow moving traffic is due to high horizontal shear tractions is caused by two mechanisms: 1) braking and accelerating which result in stress states greater than the shear strength of the asphalt mix thereby causing rutting and shoving, and 2) viscoplastic flow due to extended load periods. In addition, the strain gradient across the tire footprint and at tire edges induces high viscoplastic strain relative to elastic strain in the asphalt concrete.

Given the thermal viscoelastic behaviour of asphalt cement, high temperatures significantly influence the mechanical behaviour of asphalt concrete mixes. High ambient air temperatures cause asphalt cement to expand. However, aggregate has a thermal coefficient of expansion that is an order of magnitude lower than asphalt

cement. As a result, asphalt cement will expand more than aggregate at high temperatures. Therefore, air voids are required to allow for the expansion of asphalt cement at high temperatures. If the mix has insufficient air voids, the asphalt cement will expand filling the air void space and may cause the aggregate particles to push apart, decreasing the air void content, reducing interparticle friction, and therefore strength, of the mix. This can result in weak asphalt concrete in hot weather producing viscoplastic flow rutting in wheel paths under commercial traffic loading (Davis 1994).

Rutting may also be a result of a weak substructure below the asphalt concrete pavement. Tractions in the wheel paths may be transferred through the pavement layer to the substructure material, which consolidates causing rutting (Blight 1974, Matheson and Simmons 1990).

Problems associated with rutting include loss of structural integrity, roughness, and manoeuvrability difficulty when changing lanes. In addition, rutting results in loss of transverse drainage causing water ponding in ruts, therefore increasing risk of hydroplaning, lowering skid resistance, and channelling drainage water into transverse cracks.

2.2 Hot Mix Asphalt Concrete Conventional Physical Material Properties

Asphalt concrete is a particulate composite material composed of aggregate particles, asphalt cement binder, and the air voids between them (Papagiannakis *et al*. 2002) as illustrated in Figure 2.9. The interlocking aggregate skeleton transfers the traffic loads to the substructure, while the asphalt cement is the matrix that holds the aggregate skeleton together. Approximate proportions of each material are 5.0 to 6.0 percent asphalt cement by weight of dry aggregate and 3.0 to 5.0 percent air voids, depending on road agency design requirements.

Figure 2.9 Coarse Dense Graded Hot Mix Asphalt Concrete Mix Particulate Composite Cross Section

Physical volumetric properties are commonly used when designing asphalt concrete. When performing mix designs, a proper balance of physical properties, such as air void content, along with asphalt cement content and stockpile aggregate properties, such as grain size distribution and fracture, must be obtained to satisfy the requirements specified by the road agency.

2.2.1 Aggregate Gradation

Aggregate gradation is the distribution of aggregate particle sizes expressed as a percent of the total dry weight of the aggregate. Aggregate gradation affects many important properties of an asphalt concrete mix including stiffness, stability, durability, permeability, workability, fatigue resistance, frictional resistance, and moisture damage resistance (Roberts *et al*. 1996). To ensure these properties are adequate in the asphalt concrete mix, road agencies specify limits for the aggregate gradation.

Gradation envelope specifications for COS Type A1 (COS 2000) are summarized in Table 2.1 and illustrated in Figure 2.10. Gradation envelope specifications for DHT Type 71 (DHT 2003) are summarized in Table 2.2 and illustrated in Figure 2.11. In DHT Type 71, the aggregate top and bottom sizes are smaller than for COS Type A1. Mixes with larger aggregate top size are thought to have better rutting resistance than mixes with smaller top size (Roberts *et al*. 1996).

Table 2.1 COS Type A1 Aggregate Gradation Envelope Specifications

Sieve Size (mm)	Percent Passing by Weight	
	Minimum	Maximum
20.0	100	100
16.0	93	100
12.5	88	95
9.00	78	86
5.00	65	76
2.00	48	59
0.900	32	54
0.400	22	42
0.160	3	10
0.071	2	5

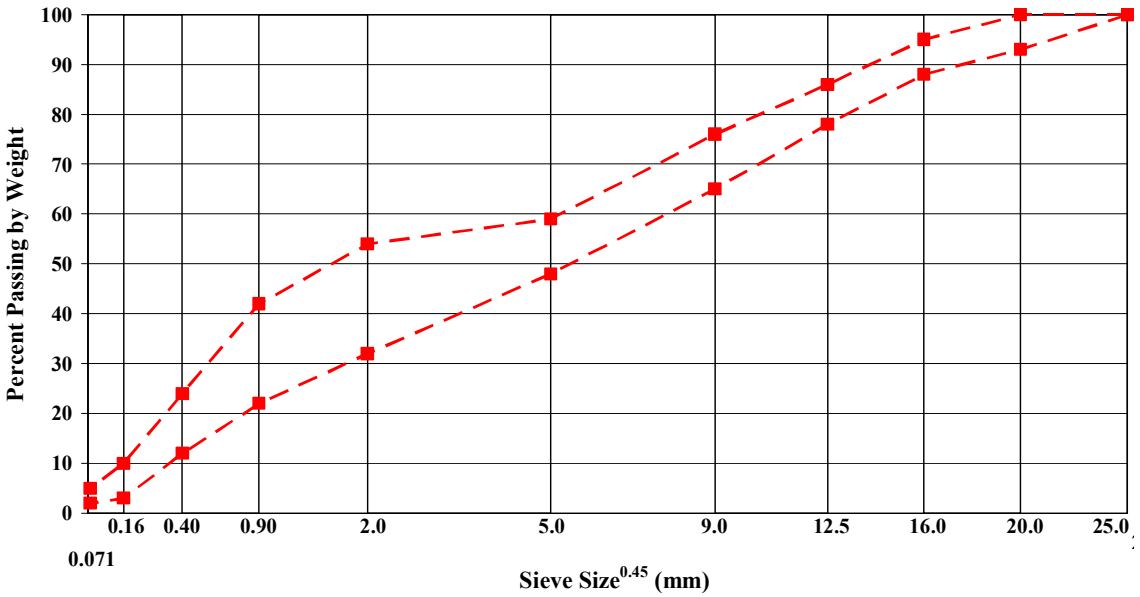

Figure 2.10 COS Type A1 Aggregate Gradation Envelope

Table 2.2 DHT Type 71 Aggregate Gradation Envelope Specifications

Sieve Size (mm)	Percent Passing by Weight	
	Minimum	Maximum
18.0	100	100
16.0	78	98
12.5	68	92
9.00	54	80
5.00	38	65
2.00	18	46
0.900	10	33
0.400	5	25
0.160	3	13
0.071	2	9

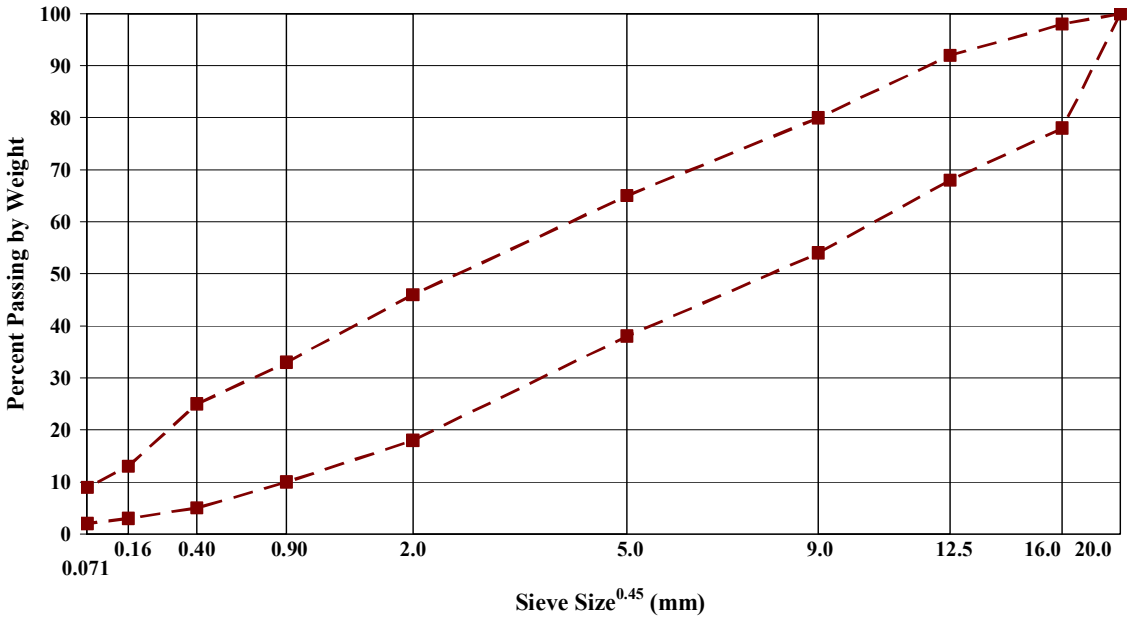

Figure 2.11 DHT Type 71 Aggregate Gradation Envelope

2.2.2 Sand Equivalence

Sand equivalence is the relative proportions of plastic fines and dust in fine aggregate. Aggregate with less plastic fines and dust will have a higher sand equivalence than aggregate with more fines and dust. Sand equivalence specifications are employed to limit the amount of plastic fines in aggregate.

COS Type A1 and DHT Type 71 specify a minimum sand equivalence of 45 (COS 2000, DHT 2003), whereas Superpave™ specifies a minimum sand equivalence of 40 for traffic levels less than 3 million equivalent single axle loads (ESALs) (Superpave Mix Design 1996).

2.2.3 Organic Content

Organic content is the amount of pieces of an aggregate source that float in water expressed as a percent of the total dry weight of the aggregate. Organic content specifications are employed to limit the amount of lightweight and porous aggregate particles. COS Type A1 specifies a maximum organic content of 1.0 percent (COS 2000), whereas DHT Type 71 specifies a maximum organic content of 2.0 percent (DHT 2003).

2.2.4 Aggregate Angularity

Aggregate angularity is the percent of aggregate particles which have mechanically fractured faces. It is well known that the shear strength of asphalt concrete under confined field state conditions can be improved by increasing the internal friction between the aggregate particles in the mix (Kim *et al*. 1992, Parker and Brown 1992, Rao and Tutumluer 2000, Kim *et al*. 2002, Rao *et al*. 2002). This can be accomplished by adjustments in aggregate gradation or increasing the angularity of the aggregate particles through increased crushing which results in the aggregate particles "locking" together. However, increasing aggregate particle angularity of glacial aggregate deposits typically requires increased aggregate crushing during manufacturing. Given the increasing shortage of high quality aggregates in Saskatchewan, aggregate quality is a growing barrier to manufacturing high crush fraction aggregate blends.

COS Type A1 specifies that a minimum of 70 percent of the aggregate retained on the 5.0 mm sieve must have two or more fractured faces (COS 2000). DHT Type 71 specifies that a minimum of 75 percent of the aggregate must have one or more fractured faces (DHT 2003). Superpave™ specifies a minimum of 75 percent of coarse aggregate

(retained on the 4.75 mm sieve) have one or more fractured faces in addition to a minimum of 40 percent of fine aggregate (Superpave Mix Design 1996).

2.2.5 Manufactured Fines

Manufactured fines are the percent by weight of fines which have been mechanically crushed. COS Type A1 specifies a manufactured fines minimum of 70 percent of the material passing the 5.0 mm sieve (COS 2000). DHT and Superpave^{TM} do not have a manufactured fines requirement.

2.2.6 Asphalt Cement

Asphalt concrete pavements on Saskatchewan high traffic arterial highways are typically constructed using 150-200A penetration grade asphalt cement. Stiffer asphalt cements, such as 85-100, will become very brittle at cold temperatures decreasing crack resistance. Softer asphalt cements, such as 300-400, become very soft at high temperatures decreasing rutting resistance. Penetration at 25^{o}C and absolute viscosity at 60^{o}C of 150-200A asphalt cement must fall within the limits specified by the Canadian General Standards Board (CGSB) CAN/CGSB-16-3M90 as illustrated in Figure 2.12.

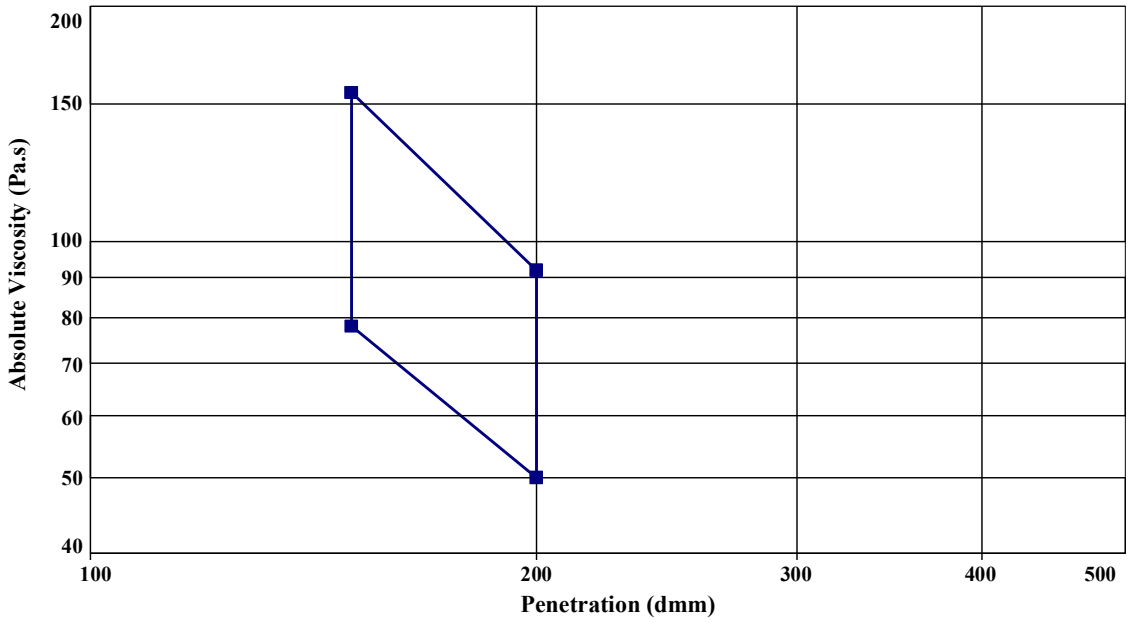

Figure 2.12 150-200A Asphalt Cement CGSB Absolute Viscosity and Penetration Limits

2.2.7 Voids in the Total Mix

Voids in the total mix (VTM) constitute all air voids between the coated aggregate particles in compacted asphalt concrete (Roberts *et al.* 1996), as illustrated in Figure 2.13. VTM contribute to the thermal stability of compacted asphalt concrete by allowing for thermal expansion of asphalt cement between the aggregate particles as well as volumetric strain under repeated heavy traffic loading (Huber 1989). However, high VTM can decrease the durability of a pavement by increasing the possibility for water and air to permeate the mix, increasing the oxidization and stripping potential, resulting in reduced cracking resistance, popouts, and ravelling (Monismith and Epps 1969, Linden *et al*. 1989, Abdullah *et al*. 1998). Insufficient VTM may cause aggregate particles to lose contact with each other due to asphalt cement expansion at elevated temperatures, resulting in a loss of strength and increased potential for rutting under traffic load tractions.

The design VTM is targeted to simulate VTM in the field after five to ten years of traffic loading. The COS Type A1 mix specifies an acceptable VTM range between 3.5 and 5.0 percent. The DHT Type 71 mix design specifies an acceptable VTM range between 2.5 and 5.0 percent. The SHRP Superpave^{TM} mix design system specifies a VTM of 4.0 percent at the design number of gyrations for all mix designs. Research has shown that pavements with less than 2.0 percent VTM (Beshara 2000) and 3.0 percent VTM (Sebaaly *et al.* 1997, and Mallick 1999) have experienced premature rutting, which is consistent with the minimum VTM requirements for both COS and SHRP. It should be noted that the DHT minimum VTM specification is much lower than for the other agencies. Table 2.3 summarizes the VTM mix design specifications.

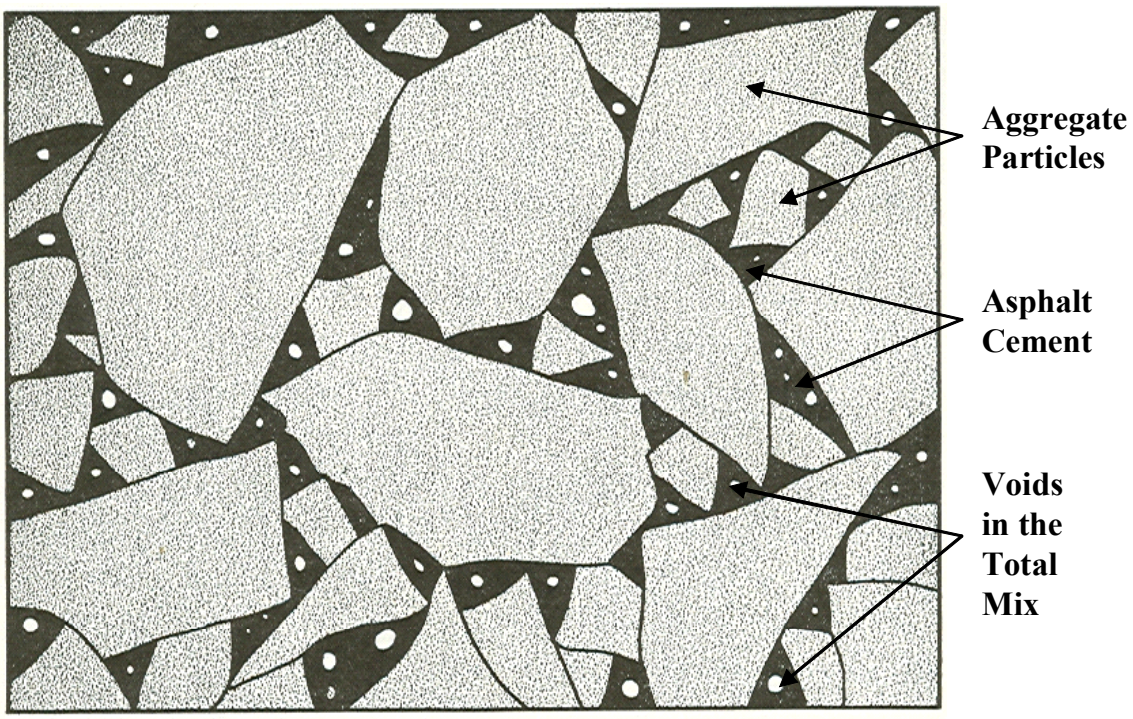

Figure 2.13 Voids in the Total Mix and Voids Filled with Asphalt (After Wallace and Martin 1967)

Table 2.3 VTM Specifications for Dense Graded Mix Designs

	Voids in Total Mix (%)	
	Minimum	**Maximum**
COS Type A1	3.5	5.0
DHT Type 71	2.5	5.0
SHRP Superpave™ (Target)	4.0	

For a given aggregate gradation, VTM are controlled by asphalt cement content, compaction effort during construction, and compaction under traffic loading (Hanson *et al*. 1994, D'Angelo 2001). Increasing the proportion of large aggregate in a mix increases VTM. However, a large maximum particle size may result in poor workability and segregation in the mix during placement in the field. It should be noted that an increase in asphalt content and/or natural sand content may push the larger particles away from each other, therefore increasing VTM but also decreasing interparticle friction. Sand will increase VTM but may also weaken the mix and reduce thermal durability due to reduced asphalt cement film thickness.

2.2.8 Voids in the Mineral Aggregate

Voids in the mineral aggregate (VMA) is the total void space between aggregate particles in compacted asphalt concrete, including air voids and asphalt not absorbed by the aggregate, as illustrated in Figure 2.14. VMA must provide sufficient void space for adequate asphalt cement content and VTM (Huber 1989, D'Angelo 2001). VMA is a function of aggregate gradation, particle shape, and surface texture. VMA can be increased by increasing the proportion of large aggregate, adding sand, or by increasing aggregate angularity (Aschenbrener and MacKean 1994). It should be noted that an increase in natural sand content may push the larger particles away from each other, therefore increasing VMA but also decreasing interparticle friction. Too high VMA may result in high permeability and therefore climatic durability problems. Too low VMA may result in stability problems, such as rutting, due to air void collapse in hot weather (Harvey and Tsai 1996).

Table 2.4 summarizes VMA mix design specifications. COS Type A1 does not have a VMA requirement. The VMA of a DHT Type 71 mix must be between 14.0 and 16.0 percent. The minimum VMA of a SHRP Superpave^{TM} 12.5 mm nominal size mix is 14.0 percent.

Table 2.4 VMA Specifications for Dense Graded Mix Designs

	Voids in Mineral Aggregate (%)	
	Minimum	**Maximum**
COS Type A1	---	---
DHT Type 71	14.0	16.0
SHRP 12.5 mm Nominal Size	14.0	---

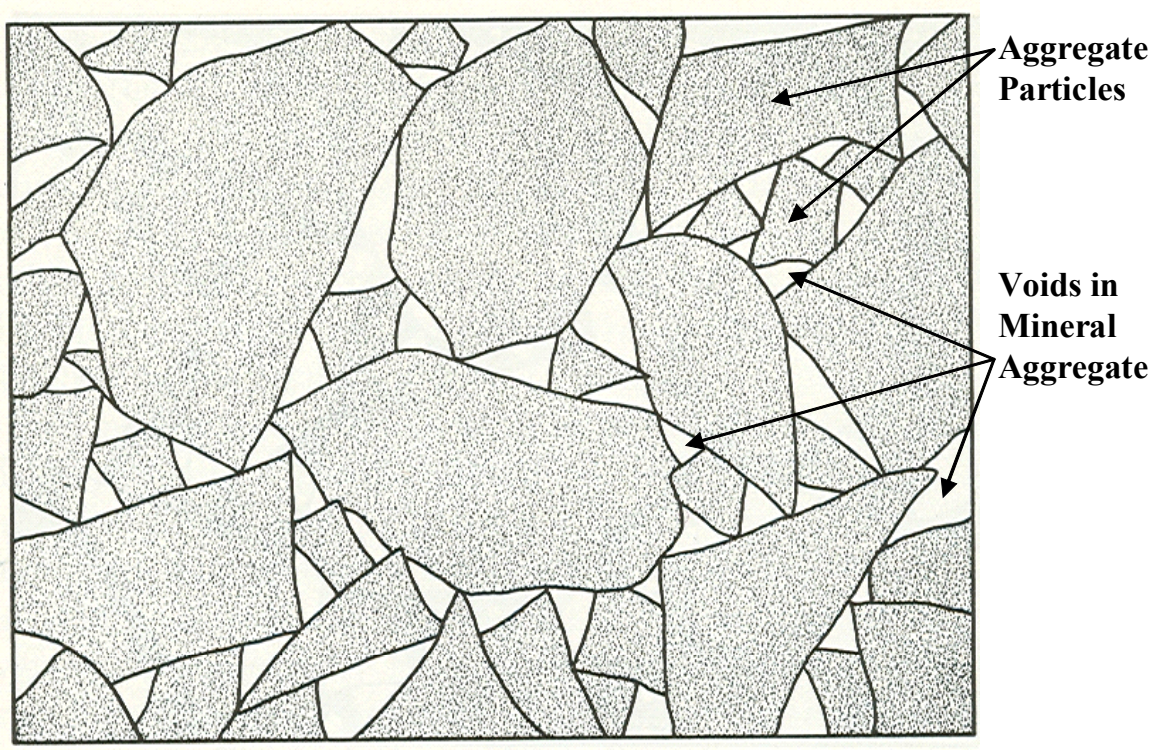

Figure 2.14 Voids in the Mineral Aggregate(After Wallace and Martin 1967)

2.2.9 Voids Filled with Asphalt

Voids filled with asphalt cement (VFA) is the percent of the VMA that is filled with asphalt cement (Roberts *et al*. 1996), as illustrated in Figure 2.15. VFA specifications for COS, DHT, and SHRP Superpave™ volumetric specifications are summarized in Table 2.5. The VFA of a COS Type A1 must be between 65 and 75 percent. The VFA of a DHT Type 71 mix must be between 65 and 80 percent. The VFA of a SHRP Superpave™ mix with a design life of less than 3 million ESALs and 12.5 mm nominal size mix must be between 65 and 78 percent.

Table 2.5 VFA Specifications for Dense Graded Mix Designs

	Voids Filled with Asphalt (%)	
	Minimum	**Maximum**
COS Type A1	65	75
DHT Type 71	65	80
SHRP 12.5 mm Nominal Size	65	78

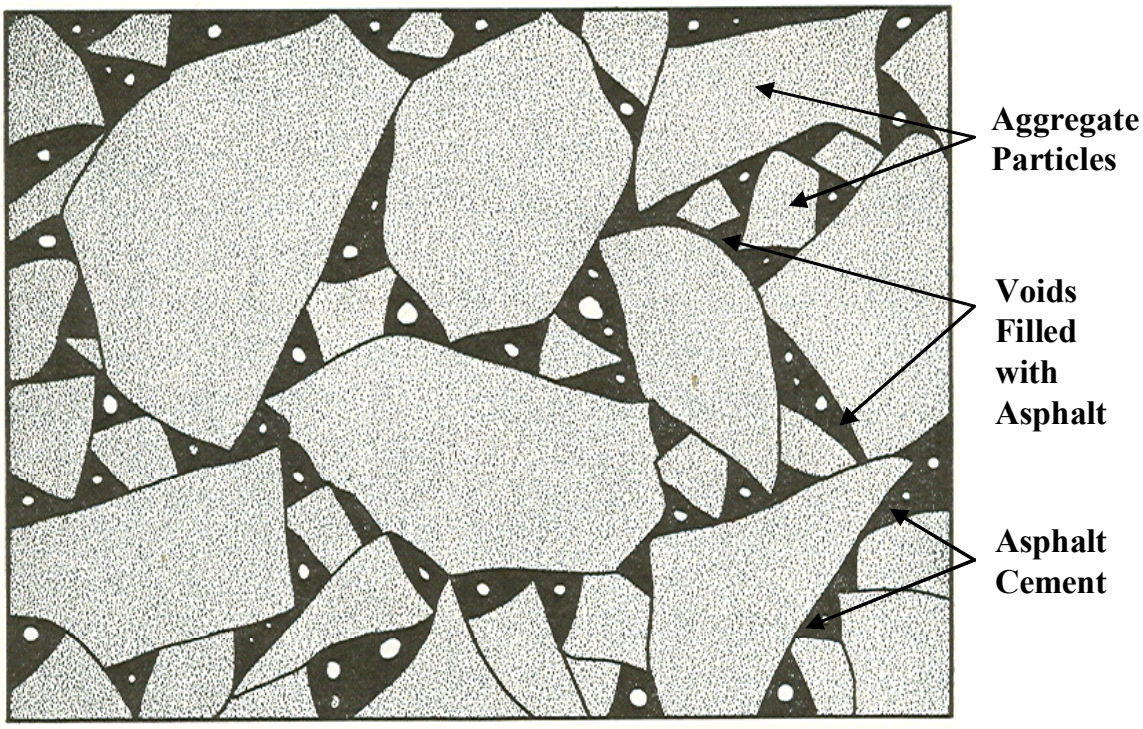

Figure 2.15 Voids Filled with Asphalt (After Wallace and Martin 1967)

2.2.10 Asphalt Cement Film Thickness

Asphalt cement film thickness is the average thickness of the asphalt cement layer covering each aggregate particle in the asphalt concrete mix. Film thickness has been linked to mix durability, or aging resistance (Kandhal and Chakraborty 1996, Roberts *et al.* 1996). Asphalt concrete with insufficient film thickness is more susceptible to oxidation which causes the mix to become brittle, reducing cracking resistance. In addition, thinner asphalt cement films can be more easily penetrated by water causing moisture induced damage such as rutting, shoving, ravelling, and bleeding. Film thickness is dependent upon the nature of the aggregate surface, the pressure between aggregate surfaces, and the direction of shear in the mix (Huang *et al.* 1998). COS and DHT specify a minimum asphalt cement film thickness of 7.5 μm.

2.2.11 Theoretical Maximum Specific Gravity

The theoretical maximum specific gravity, or theoretical maximum density, is the density of an asphalt concrete mix if all air voids were removed, or the highest possible density of the mix. Theoretical maximum specific gravity is employed to

calculate the voids values in an asphalt concrete mix and to provide target density values for pavement compaction during construction (Roberts *et al*. 1996).

2.2.12 Anti-stripping Agents

Anti-stripping agents are products added to hot mix asphalt concrete to reduce the stripping potential of the mix. Hydrated lime is a common anti-stripping agent in hot mix asphalt concrete (Roberts *et al*. 1996). Saskatchewan road agencies typically add approximately 1.0 percent hydrated lime to asphalt concrete mixes. Although hydrated lime is an effective anti-stripping agent, lime's anti-strip mechanism is not well understood. Lime typically increases the Marshall stability of the asphalt concrete mix (Akili 1993). Hydrated lime also adds fines to the asphalt concrete mix and can result in a tighter mix. Lime anti-stripping agent is typically employed by COS and DHT. Lime typically substantially increases the Marshall stability of the mix and somewhat homogenizes mix behaviour as a function of aggregate gradation. Therefore lime was not employed in this research in order to minimize homogeneity of the mixes.

2.2.13 Oxidation

Oxidation, or aging, is the interaction between oxygen and asphalt cement in the asphalt concrete mix (Abdullah *et al*. 1998). Oxidation increases the stiffness of the asphalt cement decreasing cracking resistance of the mix (Roberts *et al*. 1996). The oxidation rate depends on temperature and properties of asphalt cement such as fines/sand content, porosity, VTM, and film thickness (Linden *et al*. 1989).

2.3 Hot Mix Asphalt Concrete Types

2.3.1 Dense Graded

Dense graded asphalt concrete mixes consist of a well graded aggregate blend that generally follows the maximum density line. Because of the high density of the mix it is relatively impermeable if designed and constructed properly. Dense graded mixes can be used for most pavement layers and traffic conditions. Desirable VTM values range from 3.0 to 5.0 percent. Figure 2.16 illustrates typical dense graded mix gradation limits.

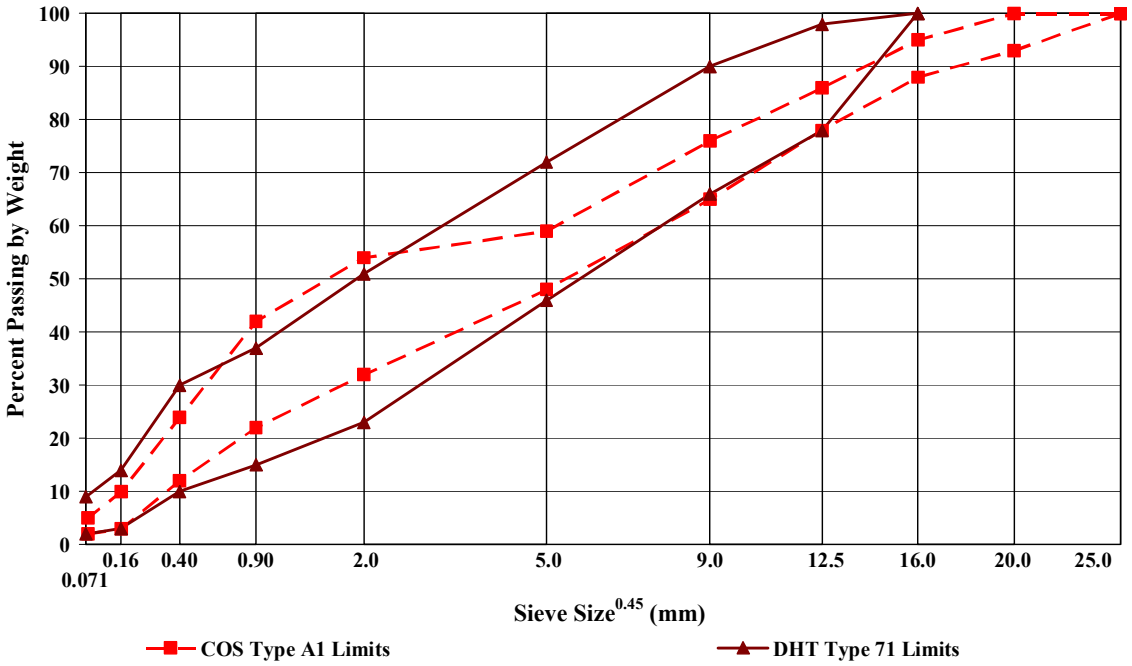

Figure 2.16 Dense Graded Aggregate Gradation

2.3.2 Stone Matrix Asphalt

Stone matrix asphalt is a gap-graded asphalt concrete mix which typically consists of 70 to 80 percent high quality crushed coarse aggregate with crushed fine aggregate, mineral filler, asphalt cement, and a stabilizing agent. The mineral filler and stabilizing agent prevent draindown of the asphalt cement and usually consist of fibres and/or polymers. In stone matrix asphalt, the crushed coarse aggregate supports the load which results in a mix with high shear stiffness and is therefore highly rut resistant mix (Mogawer and Stuart 1994, Partl *et al*. 1994, Partl *et al*. 1996). The high proportion of crushed coarse aggregate results in stone-on-stone contact, as illustrated in Figure 2.18, forming an interlocking aggregate skeleton, unlike conventional asphalt concrete. The aggregate skeleton allows loads to be transferred from the pavement surface to the underlying layers of the road structure. It can be seen that the fine aggregate "floats" in the asphalt cement of the conventional mix which causes more of the fine aggregate to support the load. Stone matrix asphalt mixes have been used as a surface course on high volume roads and highways in Europe for over 30 years and in the United States for over 10 years (Kreide *et al*. 2003). Figure 2.17 illustrates a typical stone matrix asphalt gradation relative to typical dense graded mix gradation limits.

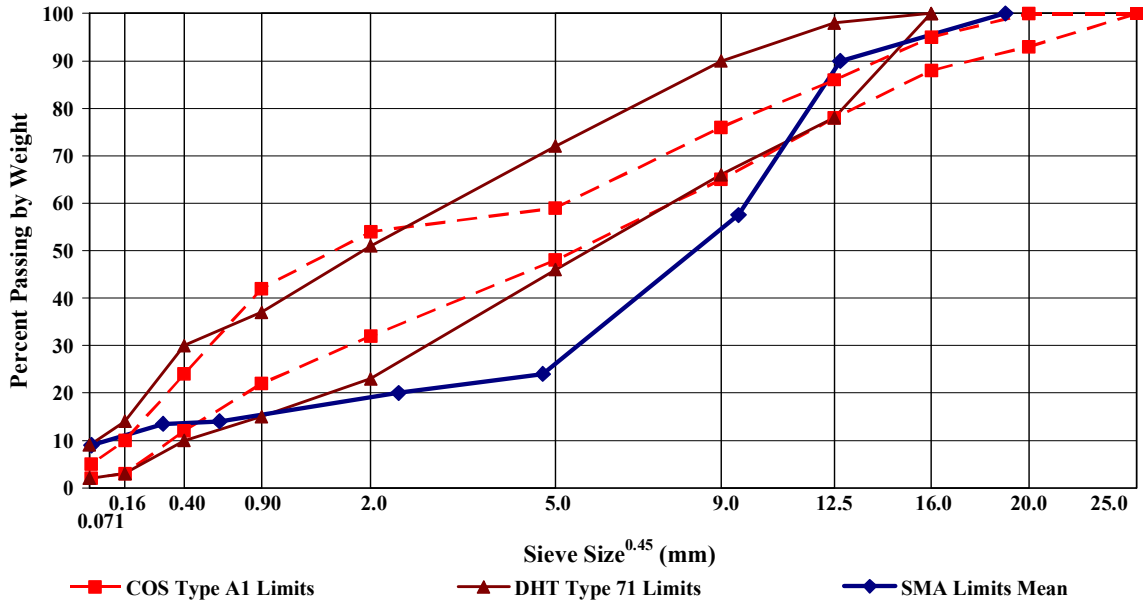

Figure 2.17 Dense Graded and SMA Aggregate Gradation

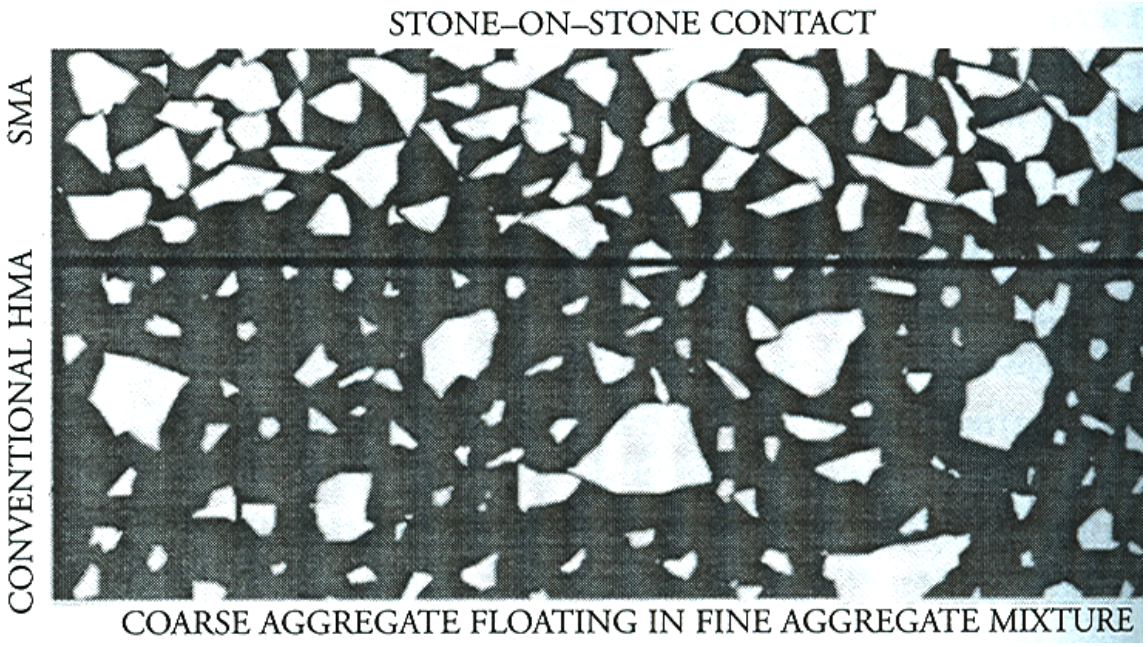

Figure 2.18 Cross Section Comparison of SMA and Conventional Asphalt Concrete (After Roberts *et al.* 1996)

2.3.3 Open Graded Friction Course

Open graded friction course mixes are designed with a high air void content to enable water drainage over the surface, through the pavement, and out to the road shoulder (Roberts *et al*. 1996, Watson *et al*. 2003). Rapid removal of water from the pavement surface reduces the risk of hydroplaning and improves skid resistance. However, use of these mixes is restricted to climates with limited freeze-thaw activity because water trapped in the pavement may freeze and expand causing cracking. High air void content is achieved by using a larger proportion of coarse aggregate in the mix. Rubberized asphalt cement binder is often used since it has a greater ability than neat asphalt cement to hold aggregate particles in place. Open graded friction course mixes are primarily used on high traffic roads since their susceptibility to oil and gasoline drippings make them unsuitable for parking lots or roads with slow-moving traffic. Figure 2.19 illustrates a typical open graded friction course gradation relative to typical dense graded mix gradation limits and Figure 2.20 illustrates a typical open graded friction course pavement.

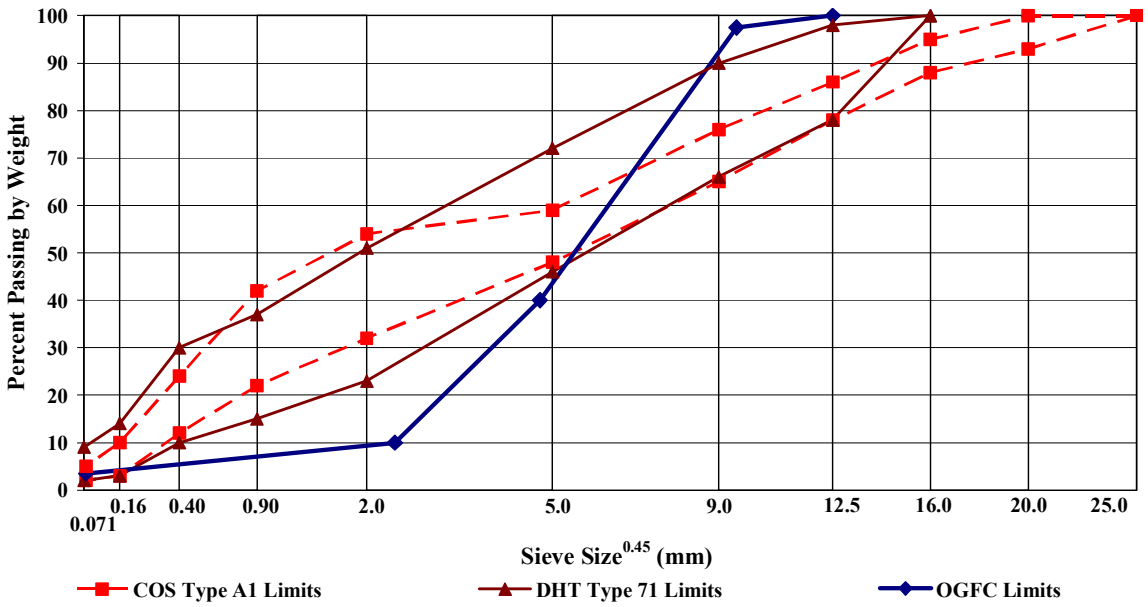

Figure 2.19 Typical Open Graded Friction Course Gradation and Dense Graded Mean of Grain Size Limits

Figure 2.20 Florida Department of Transportation Open Graded Friction Course

2.4 Elastic and Inelastic Material Behaviour

Material behaviour may be either elastic or inelastic. Material properties that characterize elastic material behaviour include elastic modulus, Poisson's ratio, shear modulus, and resilient modulus. Material properties that characterize inelastic material behaviour include creep compliance, relaxation modulus, complex modulus, phase angle, and dynamic modulus. The Bauschinger effect may also be a characteristic of inelastic material behaviour.

2.4.1 Elastic Material Behaviour

Elastic materials experience instantaneous load and relaxation as illustrated in Figure 2.21. Also load and relaxation follow the same path as illustrated in Figure 2.22. Therefore elastic materials do not experience permanent deformation (Allen and Haisler 1985). When an elastic material is subjected to small loads and deformations, the deflection of the material is directly proportional to the applied load. The proportional limit is the point at which the stress-strain relationship of the elastic material deviates from linearity, as illustrated in Figure 2.22. At loads beyond this point, the deflection of

the material is not directly proportional to the applied load. Linear elasticity can be completely characterized using elastic modulus and Poisson's ratio (Mamlouk and Sarofim 1988).

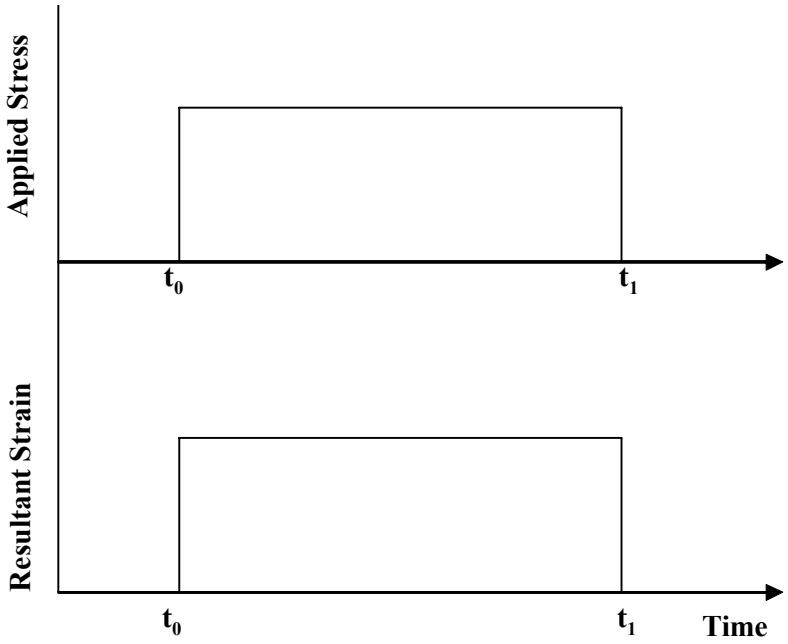

Figure 2.21 Elastic Material Behaviour

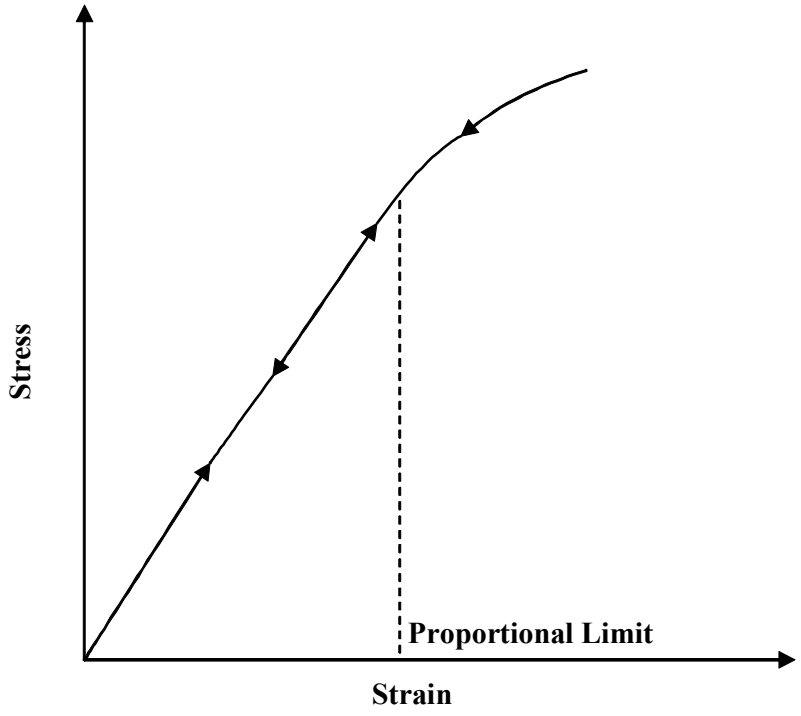

Figure 2.22 Elastic Material Behaviour

2.4.1.1 Elastic Modulus

The elastic modulus (or Young's modulus) is the linear elastic relationship between axial stress and strain:

$$E = \frac{\sigma}{\varepsilon} \quad \textbf{(2.1)}$$

Where:

E = Elastic modulus;

σ = Stress (Pa); and

ε = Strain (mm/mm).

2.4.1.2 Poisson's Ratio

Poisson's ratio (ν) is the relationship between the lateral and longitudinal deformation of a material (Allen and Haisler 1985). As a result, Poisson's ratio is an important factor in three-dimensional modelling and behaviour of asphalt concrete (Buttlar and Roque 1994). Poisson's ratio is expressed as:

$$\nu = -\frac{\varepsilon_{22}(t)}{\varepsilon_{11}(t)} = -\frac{\varepsilon_{33}(t)}{\varepsilon_{11}(t)} \quad \textbf{(2.2)}$$

Where:

$$\varepsilon_{11} = \frac{1}{E}[\sigma_{11} - \nu(\sigma_{22} + \sigma_{33})]$$

$$\varepsilon_{22} = \frac{1}{E}[\sigma_{22} - \nu(\sigma_{11} + \sigma_{33})]$$

$$\varepsilon_{33} = \frac{1}{E}[\sigma_{33} - \nu(\sigma_{11} + \sigma_{22})]$$

Where:

ε_{ii} = Strain in the X_1, X_2, X_3 orthogonal coordinate directions (mm/mm); and

σ_{ii} = Stress in the X_1, X_2, X_3 orthogonal coordinate directions (Pa).

Poisson's ratio is an important factor that influences the stiffness of unbound particulate materials (Park and Lytton 2004). Since the majority of rutting in asphalt concrete occurs at high temperatures, it is important to ensure adequate stiffness in the aggregate skeleton. This may be done by comparing Poisson's ratios for different

mixes. As the road industry moves towards high crush fraction mixes, it will become increasingly important to measure Poisson's ratio to ensure adequate asphalt concrete mixes while avoiding wastage of quality aggregate (Bouchard 1992).

Poisson's ratio of asphalt concrete has been shown to vary with material temperature and triaxial stress state (Kennedy 1977, Tayebali *et al*. 1995). The stiffness of asphalt concrete in a confined stress state is typically dependent upon Poisson's ratio and temperature (Whitmoyer and Kim 1994, Chua and Tenison 2003). Poisson's ratio is also a function of aggregate gradation, aggregate crush fraction, and aggregate top size. As temperature increases, the aggregate skeleton becomes the primary load bearing component of asphalt concrete due to the decreased viscosity of the asphalt cement binder. As a result of the decreased cohesiveness of asphalt cement, at high temperatures asphalt concrete behaves similarly to an unbound material (SHRP-A-357 1993). It is therefore hypothesized that Poisson's ratio of conventional asphalt concrete mixes will be larger at higher temperatures.

2.4.1.3 Shear Modulus

Shear modulus (G) is the ratio of shear stress to shear strain and is a measure of resistance to shear distortion (Allen and Haisler 1985). Shear modulus is a function of temperature and load application rate (Sousa and Monismith 1988, Whitmoyer and Kim 1994). The shear modulus is also known as the modulus of rigidity, and may be expressed as:

$$G = \frac{\tau}{\gamma} = \frac{E}{2(1+\nu)} \quad \textbf{(2.3)}$$

Where:

τ = Shear stress (Pa); and

γ = Shear strain (mm/mm).

2.4.1.4 Resilient Modulus

The resilient modulus (M_R) is defined as the ratio of the repeated deviatoric stress to the recoverable axial strain and represents the elastic stiffness of the material after many load repetitions (Mamlouk and Sarofim 1988). The resilient modulus is used

to quantify the stress dependent stiffness of asphalt concrete under dynamic loads. Resilient modulus is a function of temperature and stress state (Ayres and Witczak 1995, Park and Lytton 2004).

The resilient modulus of asphalt concrete is typically determined using the indirect tension test as described in ASTM D4123 (ASTM 1996). The resilient modulus under multi-axial loading is illustrated in Figure 2.23 and may be expressed as:

$$M_R = \frac{\sigma_d}{\varepsilon_R} = k_1 (I_1)^{k_2} (J_2)^{k_3} \quad \textbf{(2.4)}$$

Where:

σ_d = Deviatoric stress (Pa);

ε_R = Resilient axial strain (mm/mm);

I_1 = First stress invariant (Pa);

J_2 = Second deviatoric stress invariant (Pa); and

$k_{1,2,3}$ = Statistical regression parameters.

Deviatoric stress state is defined as the total stress state minus the mean hydrostatic stress state, and is synonymous with shear stress (Berthelot 2003). Hydrostatic stress state is one with equal tractions in three orthogonal directions. A hydrostatic stress state results in change of volume without change of shape in an isotropic material, whereas deviatoric stress results in change of shape (Malvern 1969). A stress invariant is a constant scalar derived from the stress or strain tensor and is constant regardless of coordinate direction (Allen and Haisler 1985). The resilient modulus statistical regression parameters are defined as the power law coefficients that produce the lowest least squared linear regressions relationship between resilient modulus and the applied stress state invariants.

As illustrated in Figure 2.23, the resilient modulus of asphalt concrete is dependent on the amount of time that has passed before the resilient modulus is determined (Mamlouk and Sarofim 1988, Hopman 1994).

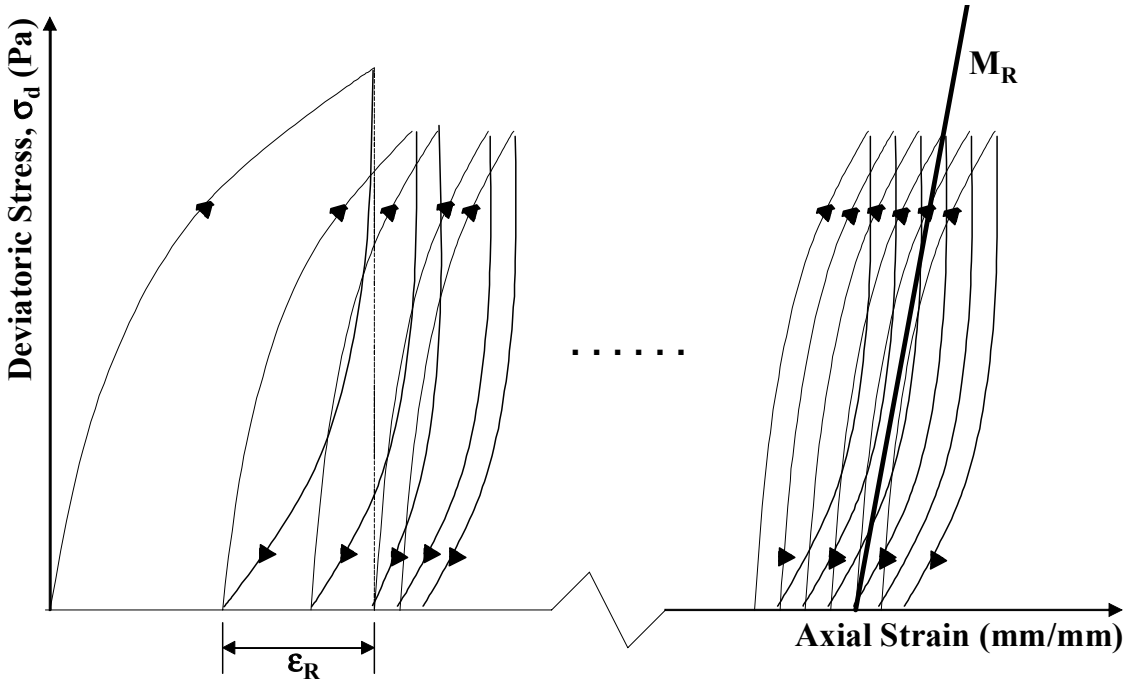

Figure 2.23 Resilient Modulus

2.4.2 Inelastic Material Behaviour

Plastic material behaviour is when a material experiences irrecoverable deformation as a result of an applied traction. Plastic materials initially resist deformation until the material's yield stress is reached. In a plastic material, deformation ceases when the applied load is removed. Plastic behaviour is dependent upon load magnitude and is not dependent upon load application rate (Uzan 1996).

Viscosity is a material's resistance to deformation under an applied shear stress. Viscous behaviour is dependent upon load application rate and is not dependent upon load magnitude. Viscosity in solid materials may be accompanied by elastic behaviour (viscoelasticity) and/or plastic behaviour (viscoplasticity).

A viscoelastic material exhibits both elastic, or solid-like, and viscous, or fluid-like, mechanical behaviour (Malvern 1969). Although viscoelasticity is similar to plastic behaviour, purely plastic behaviour does not account for time dependent creep behaviour exhibited by asphalt concrete below the yield point. The incorporation of viscous behaviour in asphalt concrete performance models produces the ability to take

into account rate dependent creep. Viscoelastic materials' stress-strain behaviour is dependent upon:

- The duration of applied surface traction;
- The rate of applied surface traction; and
- Temperature.

Viscoelastic materials have a "memory" of their load history. Therefore, the stress in a viscoelastic material depends upon the entire strain history of the material (Malvern 1969, Allen and Haisler 1985). Viscoelastic material constitutive relations must account for the full history of stresses and the resulting strains experienced by the material (Kim *et al*. 1995, Berthelot 2003). Viscoelastic materials can also exhibit both linear and nonlinear behaviour, as well as a range of viscosities depending on the factors stated above. Characterization of viscoelastic material behaviour requires Poisson's ratio, a modulus, and a time-dependent term to fully describe material behaviour (Mamlouk and Sarofim 1988). Viscoelastic material properties are required to predict rutting, thermal cracking, and fatigue cracking in asphalt concrete (SHRP-A-357 1993).

It has been widely accepted that performance of asphalt concrete can be approximately characterized using linear viscoelastic theory (Blight 1977, Huhtala *et al.* 1990, Berthelot 1999). Linear viscoelastic materials exhibit stress-strain behaviour such that at any given time the magnitude of stress is directly proportional to the magnitude of the resulting strain (Blight 1977). It has been recognized that asphalt concrete is a nonlinear visco-elasto-plastic material (Uzan 1996).

The mechanical behaviour of a linear viscoelastic material is illustrated in Figure 2.24 and can be represented as:

$$D(t) = \frac{\varepsilon(t)}{\sigma_0}$$
$$E(t) = \frac{\sigma(t)}{\varepsilon_0} \qquad \textbf{(2.5)}$$

Where:

D(t) = Creep compliance (Pa^{-1});

E(t) = Relaxation modulus (Pa);

σ = Stress (Pa);

ε = Strain (mm/mm); and

t = Specified time interval (seconds).

Creep compliance is the time-dependent strain modulus of a material subjected to constant stress. Stress relaxation is the time-dependent modulus of a material subjected to a constant strain. Creep compliance and relaxation modulus are required for viscoelastic damage prediction (Gibson *et al*. 2003).

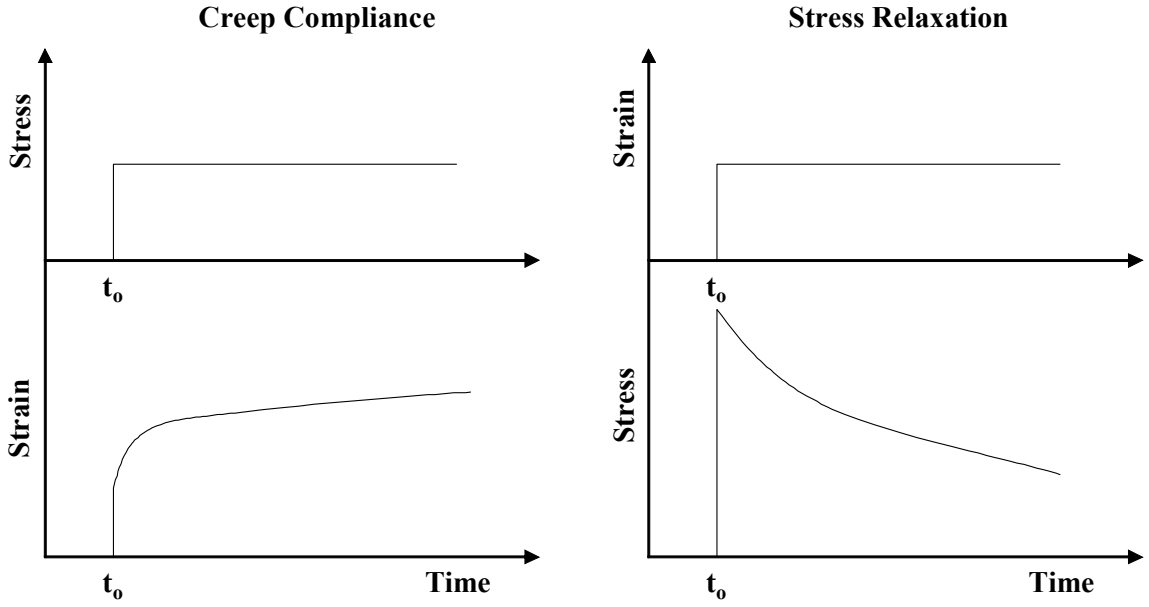

Figure 2.24 Viscoelastic Material Behaviour

Linear viscoelastic material behaviour may be expressed in terms of time-dependent hereditary integrals of stress and strain to account for the full load history of the material as (Berthelot 2003):

$$\sigma(t) = \int_0^t E(t-\tau)\frac{\partial \varepsilon}{\partial \tau} d\tau$$
$$\varepsilon(t) = \int_0^t D(t-\tau)\frac{\partial \sigma}{\partial \tau} d\tau \qquad \textbf{(2.6)}$$

Where:

σ = Stress (Pa)

ε = Strain (mm/mm)

E = Modulus of elasticity (Pa)

D = Compliance (Pa^{-1})

t = Time 1 (seconds)

τ = Time 2 (seconds)

If the viscoelastic creep and relaxation behaviour over long loading times is relatively smooth in log-log space, a linear Prony Series can be used to model the creep compliance and relaxation modulus as (Berthelot 2003):

$$E(t) = E_{\infty} + \sum_{i=1}^{N} E_i e^{-\frac{E_i}{\eta_i}t} \quad \textbf{(2.7)}$$

Where:

E(t) = Relaxation modulus (Pa);

η = Viscosity (Pa.seconds);

E_{∞} = Elastic modulus at time infinity (Pa); and

N = Step function.

2.4.2.1 Complex Modulus

The complex modulus (E^*) defines the relationship between stress and strain under an applied dynamic load for a linear viscoelastic material. The complex modulus of asphalt concrete is determined by subjecting a cylindrical specimen to sinusoidal loading while measuring the resulting horizontal and vertical deformations (Mamlouk and Sarofim 1988, Kim and Lee 1995). The complex modulus is a useful measure of asphalt concrete behaviour because it quantifies linear elastic and viscous material properties under dynamic loading representative of field state conditions.

The complex modulus is composed of a real component and an imaginary component (Roberts *et al.* 1996), as illustrated in Figure 2.25. The real component is the elastic, or recoverable, portion of the deformation, while the imaginary component is the

viscous, or irrecoverable, portion of the deformation (Mamlouk and Sarofim 1988). The complex modulus may be expressed as:

$$E^* = E' + i\,E'' \tag{2.8}$$

Where:

E' = Elastic component (Pa);

E'' = Inelastic component (Pa); and

i = Imaginary component, i.e. $\sqrt{-1}$, (Pa).

Making use of Euler's equations, the applied traction waveform and strain response of vertical sinusoidal loading may be expressed as (Pellinen and Witczak 2002):

$$\begin{aligned} T_{11}(t) &= T_{11p} e^{i\omega t} \\ \varepsilon_{11}(t) &= \varepsilon_{11p} e^{i(\omega t - \delta)} \end{aligned} \tag{2.9}$$

Where:

$T_{11}(t)$ = Time dependent boundary traction in the X_1 coordinate direction (Pa);

T_{11p} = Peak applied boundary traction in the X_1 coordinate direction (Pa);

$\varepsilon_{11}(t)$ = Time dependent axial strain response in the X_1 coordinate direction;

ε_{11p} = Peak axial strain response in the X_1 coordinate direction;

ω = Angular load frequency (radians per second);

t = Elapsed time (seconds); and

δ = Phase angle (radians).

By substitution and expansion of terms, the complex modulus of a time dependent material may be expressed as:

$$E^* = \frac{T_{11}(t)}{\varepsilon_{11}(t)} = \frac{T_{11p} e^{i\omega t}}{\varepsilon_{11p} e^{i(\omega t - \delta)}} = \frac{T_{11p} \sin(\omega t)}{\varepsilon_{11p} \sin(\omega t - \delta)} \tag{2.10}$$

Therefore, a high complex modulus means that a given stress results in a relatively low permanent strain, or deformation, in the pavement (Shenoy and Romero 2002). It may therefore desirable to choose an asphalt concrete mix with a relatively high complex modulus.

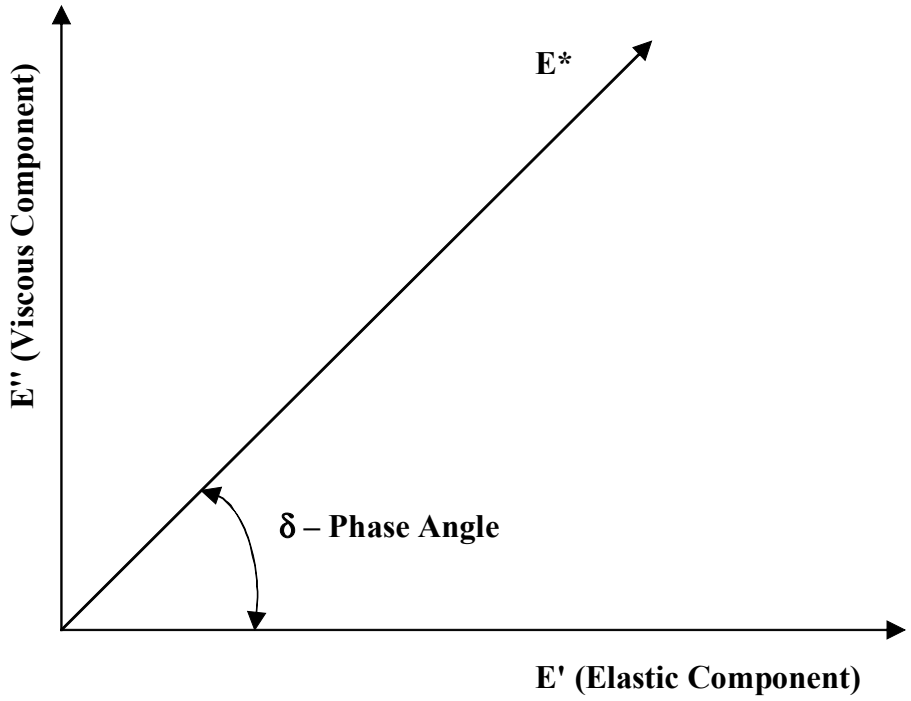

Figure 2.25 Phase Angle and Complex Modulus in Polar Coordinates

2.4.2.2 Dynamic Modulus

Dynamic modulus is the absolute value of the complex modulus ($|E^*|$) and has long been considered a convenient characteristic in estimating pavement behaviour (Majidzadeh *et al.* 1979). Dynamic modulus is the ratio of the peak axial stress over the peak axial strain in a linear viscoelastic material under sinusoidal loading. The procedure for conducting the dynamic modulus test is described in ASTM D3497 (ASTM 1996). Dynamic modulus is expressed as the absolute value of the complex modulus (Kim and Lee 1995, Saadeh *et al*. 2003):

$$E_D = \left|E^*\right| = \sqrt{\left(\frac{T_{11p}}{\varepsilon_{11p}}\cos\delta\right)^2 + \left(\frac{T_{11p}}{\varepsilon_{11p}}\sin\delta\right)^2} = \frac{T_{11p}}{\varepsilon_{11p}} \qquad \textbf{(2.11)}$$

Dynamic modulus of asphalt concrete is known to be dependent upon VTM, temperature, and stress state (Cragg and Pell 1971, Shook 1984, Chehab *et al*. 2000). Because of the decreasing viscosity of asphalt cement with increasing temperature, asphalt concrete would behave less stiff and experience higher strains at higher temperatures. It is therefore hypothesized that dynamic modulus will be smaller at higher temperatures. It is also hypothesized that dynamic modulus will decrease with increasing asphalt cement content due to decreasing aggregate interparticle friction and the increasing amount of viscous material in the sample.

2.4.2.3 Phase Angle

Phase angle (δ) is the fraction of the period that one periodic wave function lags another periodic wave function. The phase angle for asphalt concrete is determined by measuring the lag in strain response relative to the stress from the application of a sinusoidal load (Witczak *et al*. 2002), or the time difference between material loading and the resulting deformation and may be calculated:

$$\delta = \omega T \quad \textbf{(2.12)}$$

Where:

T = Time lag between stress and strain (seconds)

Phase angle is a measure of the relative contributions of viscous flow and elasticity to the overall stiffness of a material. The strain response of a purely elastic material will be in-phase with stress, resulting in a phase angle of 0 degrees (Pellinen and Witczak 2002) as illustrated in Figure 2.26. For a purely viscous material, strain response will be 90 degrees out of phase with applied stress, as illustrated in Figure 2.27. Viscoelastic materials will therefore exhibit a phase angle between 0 degrees and 90 degrees as illustrated in polar coordinates in Figure 2.25.

For a viscoelastic material, phase angle is dependent upon temperature, load application rate, and stress state (Malvern 1969, Cragg and Pell 1971). As temperature increases the viscosity of asphalt cement decreases, thereby resulting in the aggregate skeleton increasingly becoming the primary distribution component. Since aggregate

behaves similarly to an elastic material, it is hypothesized that phase angle will decrease at higher temperatures.

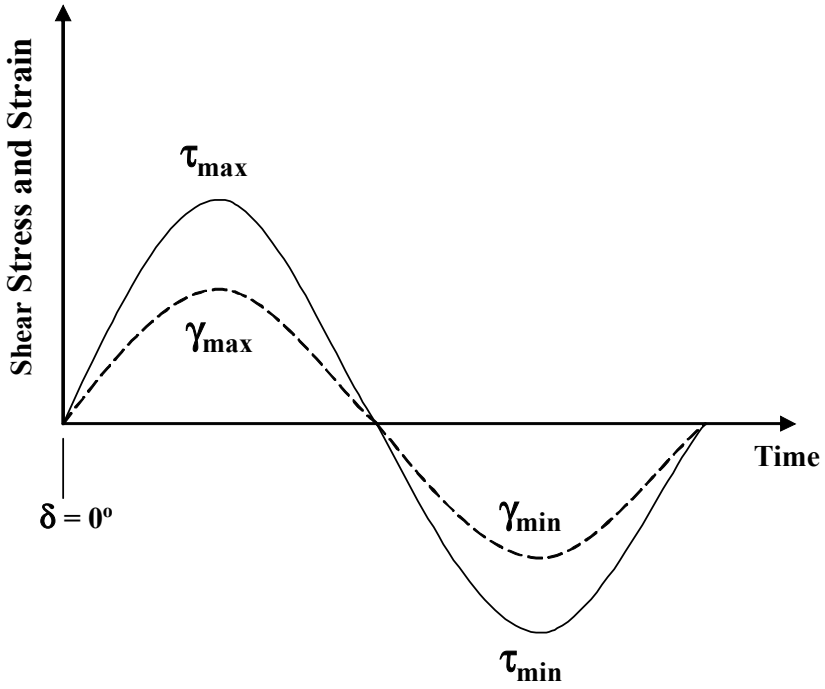

Figure 2.26 In-Phase Shear Strain Response

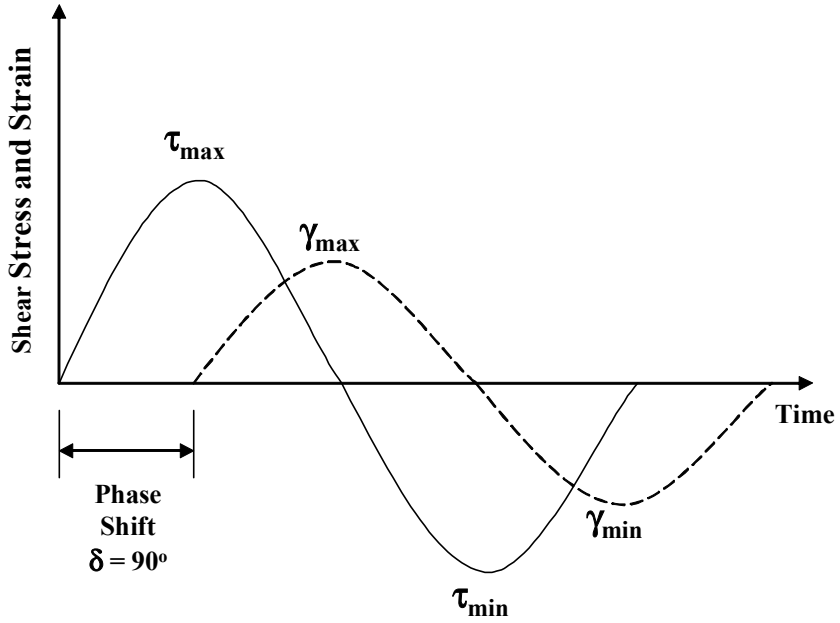

Figure 2.27 Out of Phase Shear Strain Response

2.4.3 Bauschinger Effect

The Bauschinger effect is an attempt to quantify the directional anisotropy induced by plastic strain. Directional anisotropy is when an increase in plastic deformation in one direction causes a decrease in yield stress in the opposite direction during subsequent reversed loading (Malvern 1969, Chen 1994). The Bauschinger effect can occur in asphalt concrete under repeated loading in the lab and may be related to repeated traffic loads on asphalt concrete pavements, particularly those that experience significant plastic deformation.

The Bauschinger effect in asphalt concrete is characterized by hardening, or increasing of the yield point, when the sample is reloaded in compression, but softening, or lowering of the yield point, when the stress is reversed and the sample is reloaded in tension, as illustrated in Figure 2.28. This effect, however, is reversed at high temperatures when the asphalt binder softens, increasing of the yield point in tension and lowering of the yield point in compression.

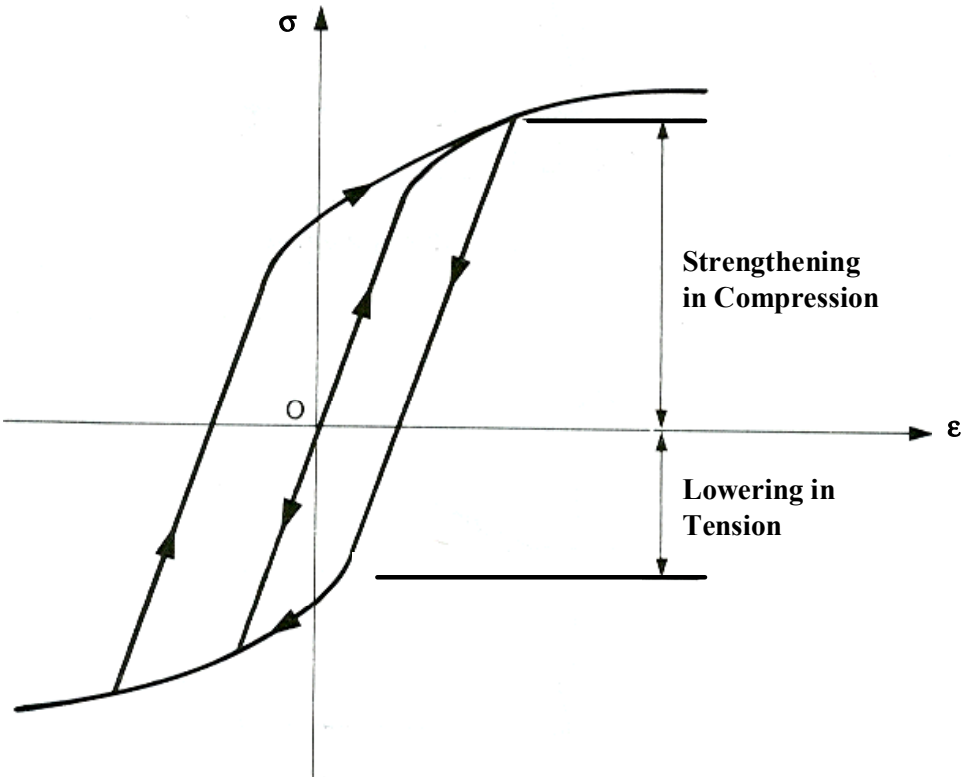

Figure 2.28 Bauschinger Effect (After Chen 1994)

2.5 Three-Dimensional Material Constitutive Characterization and Road Modelling

Most modern engineered systems employ two or three-dimensional models for material behaviour performance prediction. Material properties resulting from mechanistic material characterization can be input into a two or three-dimensional primary response model that considers road geometry, climate, and traffic loads. Accurately modelling of three-dimensional material behaviour is essential in asphalt concrete structural design and analysis. The following is a summary of three-dimensional material behaviour.

Anisotropic materials exhibit unique mechanical behaviour in all coordinate directions (Malvern 1969, Chen 1994). Hooke's Law for anisotropic materials can be generalized in terms of nine unique stresses (σ_{ij}), nine unique strains (ε_{kl}), and 81 material property constants (C_{ijkl}) (Allen and Haisler 1985) as:

$$\{\sigma_{ij}\} = [C_{ijkl}]\{\varepsilon_{kl}\} \qquad \textbf{(2.13)}$$

If the conservation of linear and angular momentum of the body is satisfied, the stress and strain tensors must be symmetric, simplifying the above constitutive relation. Therefore, anisotropic material behaviour may be reduced to six unique strains, six unique stresses, and 36 material property constants.

Orthotropic materials exhibit unique mechanical behaviour in three orthogonal directions (Malvern 1969, Chen 1994), so the constitutive relation may be reduced to nine material property constants (Allen and Haisler 1985). Conversely, isotropic materials exhibit uniform mechanical behaviour in all directions (Malvern 1969), so the constitutive relation matrix may be reduced to three material property constants (Allen and Haisler 1985). Transversely isotropic materials exhibit uniform mechanical behaviour in two orthogonal directions (Malvern 1969) so the material constitutive relation matrix may be reduced to five material property constants (Allen and Haisler 1985).

Asphalt concrete is an anisotropic material, but may be accurately represented by transversely isotropic behaviour. It is therefore beneficial to employ a testing procedure that applies a traction resulting in a uniform stress field within the sample where measurements can be made on the sample in order to accurately quantify mechanical properties.

2.6 Conventional Hot Mix Asphalt Concrete Mix Design Frameworks

The traditional objective of asphalt concrete mix design is to find the blend of asphalt cement and aggregate to provide the maximum distress resistance under a variety of specified field state conditions, such as traffic and environmental loading throughout the pavement design life. This is achieved by determining the required type and proportion of aggregate and its corresponding optimum asphalt cement content to produce physical properties in the range specified by the road agency.

Several mix design methods have been developed to determine the optimum asphalt cement content of asphalt concrete mixes. The types of available mix design methods include purely-empirical, phenomenological-empirical, and mechanistic.

2.6.1 Empirical Mix Design

Empiricism is "relying upon observation, experimentation, or induction…and replacing it with some sort of theory" (Webster 1993). Purely-empirical mix designs rely solely on observation of past pavement performance and classical statistical regression to formulate performance based design relationships. The road industry has performed several full scale road experiments to obtain performance data in order to formulate empirical performance models. These road tests include the Western Association of State Highway Officials (WASHO) road test conducted in the early 1950's (Highway Research Board 1955), and the Association of American State Highway Officials (AASHO) road test conducted in Illinois from 1958 to 1960 (Highway Research Board 1961). Several road tests have been conducted by road agencies in western Canada, including DHT, to model road behaviour in Canadian conditions. Typical limitations of road tests include (Huang 1993):

- High construction and data collection costs;
- Limited geographical area, construction materials, traffic types and conditions, and environmental conditions;
- The results are only applicable to the environmental, material, and traffic loading conditions of the specific road test; and
- The inability to account for coupled long term life cycle effects between road structure, environmental, and traffic loading conditions.

2.6.2 Phenomenological-Empirical Mix Design

Phenomenological-empirical hot mix asphalt concrete characterization involves simulative tests coupled with observation of past field performance to quantify the behaviour of road materials for pavement performance prediction. Limitations of phenomenological-empirical tests include (Mamlouk *et al*. 1983, Mamlouk and Sarofim 1988, Monismith 1992, Berthelot *et al.* 1999):

- The results are dependent upon the test apparatus configuration and therefore do not characterize the material's fundamental thermomechanical behaviour which is directly related to damage prediction; and
- The traffic and material conditions under which the mix design methods were developed have changed.

2.6.3 Mechanistic Mix Design

Since the early 1960's, pavement design procedures have been shifting from empirical based to mechanistic based (Zafir *et al*. 1994). The primary advantage of a mechanistic design procedure is that mechanistic methods quantify the fundamental properties of the asphalt concrete layer over the full range of stress and strain states and temperatures experienced in the field. Mechanistic road modelling is based upon recent advancements in material science, thermomechanics, and computational capacities. Mechanistic models can greatly decrease the amount of empirical data required for field performance validation. Advantages of mechanistic-empirical road modelling include (Lee *et al*. 2003):

- Thermomechanical principles are universal for all engineering materials;
- Thermomechanical principles do not change over time, allowing for continual modifications to performance models and changing pavement conditions; and
- Thermomechanical constitutive relations are directly related to pavement performance.

The development of a mechanistic asphalt concrete mix design procedure may be outlined as follows (Ali and Tayabji 1998):

- Form a hypothesis regarding the mechanism of the development of pavement distresses;
- Perform comprehensive material characterization incorporating changes in the material properties as a function of stress state, traffic loading rate, and environmental conditions;
- Determine the fundamental behaviour of the material, namely stress, strain, and deformation;
- Estimate the damage due to traffic and environmental loading; and
- Estimate the accumulation of damage over a period of time.

Conventional hot mix asphalt concrete mix design methods are phenomenological-empirically based and include the Hveem and Marshall mix design methods.

2.6.4 Hveem Mix Design Method

The development of the Hveem mix design method began in the late 1920's when Francis Hveem started to work with "oil mixes". However, the final form of the procedure for use with asphalt concrete was not complete until 1959 (Hveem 1983, Roberts *et al.* 1996). Several western States implemented and continue to employ the Hveem asphalt mix design procedure (Linden *et al*. 1989, Chua and Tenison 2003).

Hveem recognized the importance of multi-axial mechanical behaviour of asphalt mixes, particularly the ability of the material to resist induced shear stress from

applied wheel tractions. The result was the development of the Hveem stabilometer to evaluate the multi-axial mechanical behaviour of an asphalt concrete mix at different asphalt contents. However, the stabilometer test was established through correlation of laboratory testing to field performance and stabilometer results are not directly related to pavement performance, the results can not be used as pavement performance modelling inputs (Hadley *et al*. 1970).

Asphalt concrete samples for use in the Hveem mix analysis system are compacted using a kneading compactor. The samples have a diameter of 102 mm to simulate a tire footprint area and a height of 63.5 mm to approximate an asphalt concrete layer thickness. The Hveem kneading compactor, illustrated in Figure 2.29, is a device which applies pressure to the specimen through a hydraulically operated tamper foot that has a surface area of one quarter of the cross sectional area of the specimen. The foot applies a specified pressure to the specimen, after which the foot is raised, the base rotates one sixth of a revolution, and the specified pressure is applied again. This process continues until the entire perimeter of the sample has been compacted. The kneading action produces the rolling loading effect of traffic and therefore allows the aggregate particles to become oriented similarly to asphalt concrete compacted in the field. The vertical stress versus time profile of one kneading compactor blow is illustrated in Figure 2.30.

The Hveem stabilometer, illustrated in Figure 2.31, applies a vertical load to the asphalt concrete specimen and measures the resulting horizontal displacement. Hveem believed that the amount of load transmitted laterally through the specimen would reflect the degree of plasticity (Chua and Tenison 2003). The circumference of the specimen is retained by a neoprene diaphragm surrounded by an oil reservoir to simulate field confinement conditions. The optimum asphalt cement content is chosen by increasing the asphalt cement content until such a point that stability is compromised. Optimum asphalt content is taken as the highest asphalt content that does not compromise stability to maximize environmental durability.

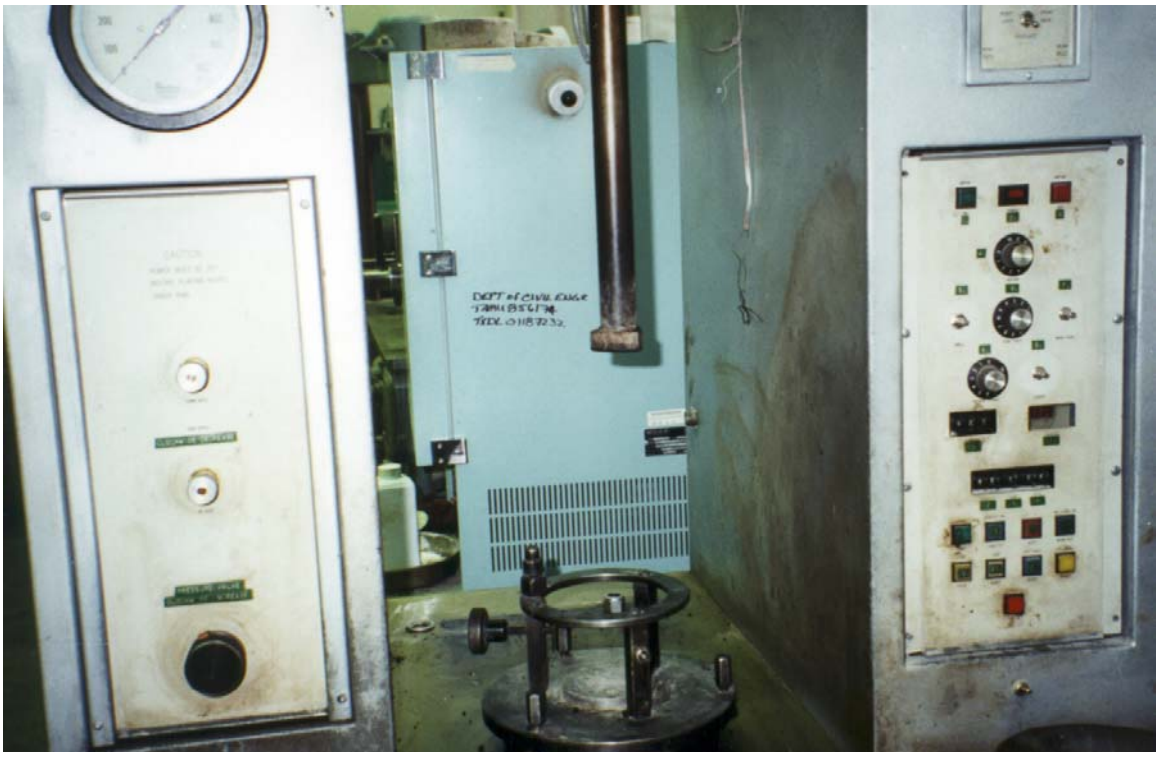

Figure 2.29 Mechanical Kneading Compactor Tamping Foot

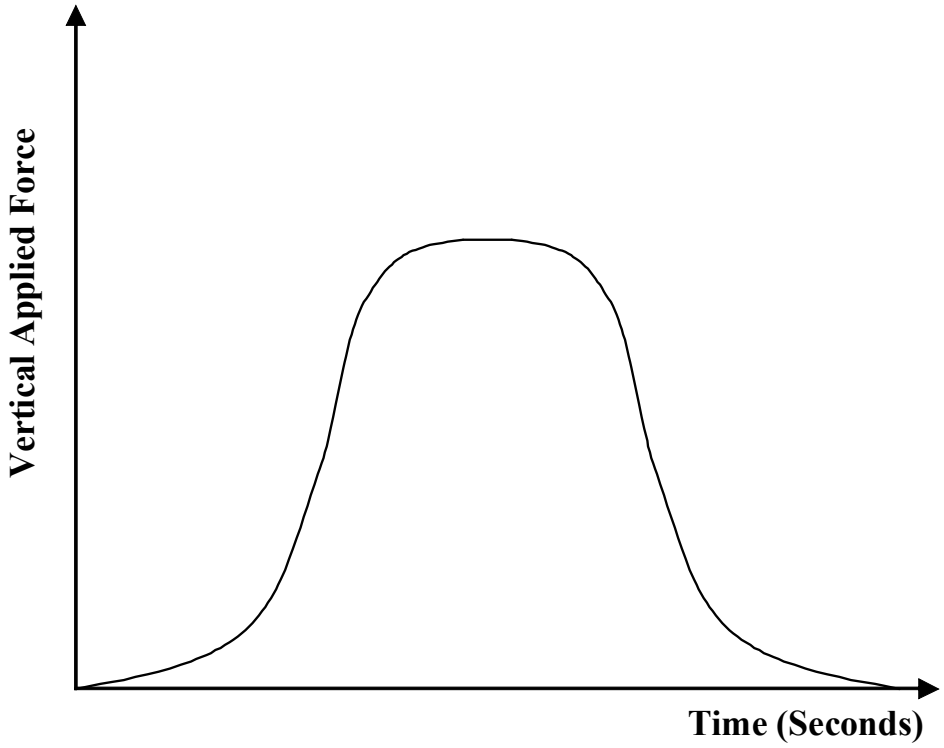

Figure 2.30 Kneading Compactor Loading Profile

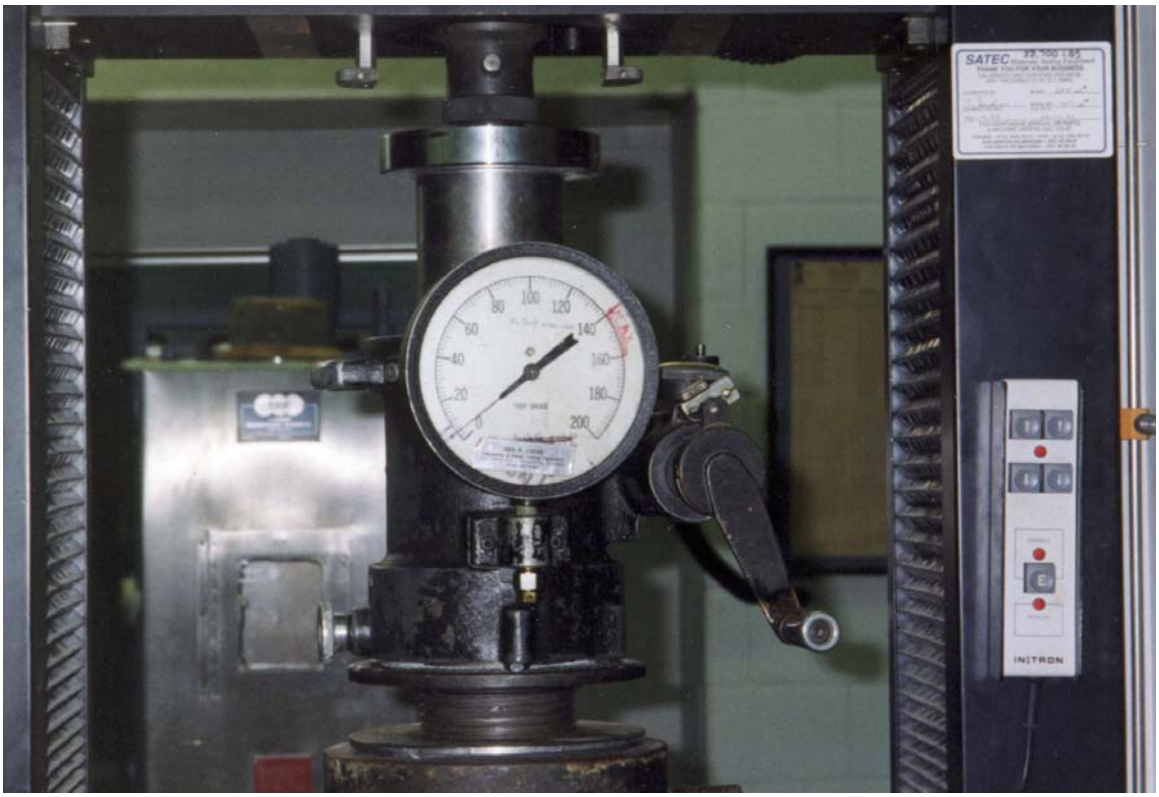

Figure 2.31 Hveem Stabilometer

Although the Hveem mix design method attempts to quantify the effect of multi-axial loading, the Hveem method has several limitations including (Berthelot *et al.* 1999):

- The Hveem method is based on empirical performance relationships and therefore does not produce properties directly related to field performance;
- The high capacity load frame results in relatively high capital and operating costs and precludes testing in the field; and
- The Hveem stabilometer does not provide feedback controlled multi-axial measurements and, as a result, cannot be used to characterize the performance characteristics of asphalt concrete at stress states representative of field state conditions.

2.6.5 Marshall Mix Design Method

The Marshall mix design method was developed by Bruce Marshall during the 1930's (U.S. Army Corps of Engineers 1944). Marshall's goal was to develop a portable asphalt concrete mix design method that involved minimal effort and time as a basis for determining the optimum asphalt content. The Marshall mix design method has traditionally been the most widely employed conventional empirical mix design method in use by North American road agencies (Linden *et al*. 1989).

Marshall sample compaction employs an impact hammer, illustrated in Figure 2.32, to compact samples in a 102 mm diameter mould to a height of approximately 63.5 mm (Roberts *et al*. 1996). The vertical stress versus time profile for one Marshall impact hammer blow with respect to the Hveem kneading compactor profile is illustrated in Figure 2.33.

Compaction effort in the field is represented by the number of Marshall hammer blows per side of the sample. Standard compaction is considered as 50 blows per side of the sample. However, compaction effort of 25, 50 or 75 blows per side have been specified for projects with low, medium, and high traffic conditions, respectively (Maupin 1995). As a result, the optimum asphalt content is theoretically influenced by traffic level. More compaction effort is required in the field to reach the 75 blow Marshall mix design density relative to the same mix compacted using 50 blows. Therefore, the higher density of the 75 blow Marshall mix design should theoretically consolidate less under traffic loading.

Marshall stability is determined by placing the sample on its side in the Marshall stabilometer, as illustrated in Figure 2.34, and determining the maximum load supported by the specimen at a fixed deformation rate of 50.8 mm per minute. The maximum load is defined as the stability value, and the flow is defined as the sample displacement at the time of maximum applied load, as illustrated in Figure 2.35. Marshall stability and flow measurements are employed to compare samples at several asphalt cement contents. The purpose of the stability requirement is to ensure adequate strength of the mix. The flow requirement ensures adequate strain energy capacity to provide cracking resistance

while limiting viscoplastic flow to provide rutting resistance. Retained stability is the percentage of a sample's original Marshall stability of a sample's Marshall stability following a 24 hour conditioning in water at 60°C. Retained stability is intended to represent resistance to moisture damage.

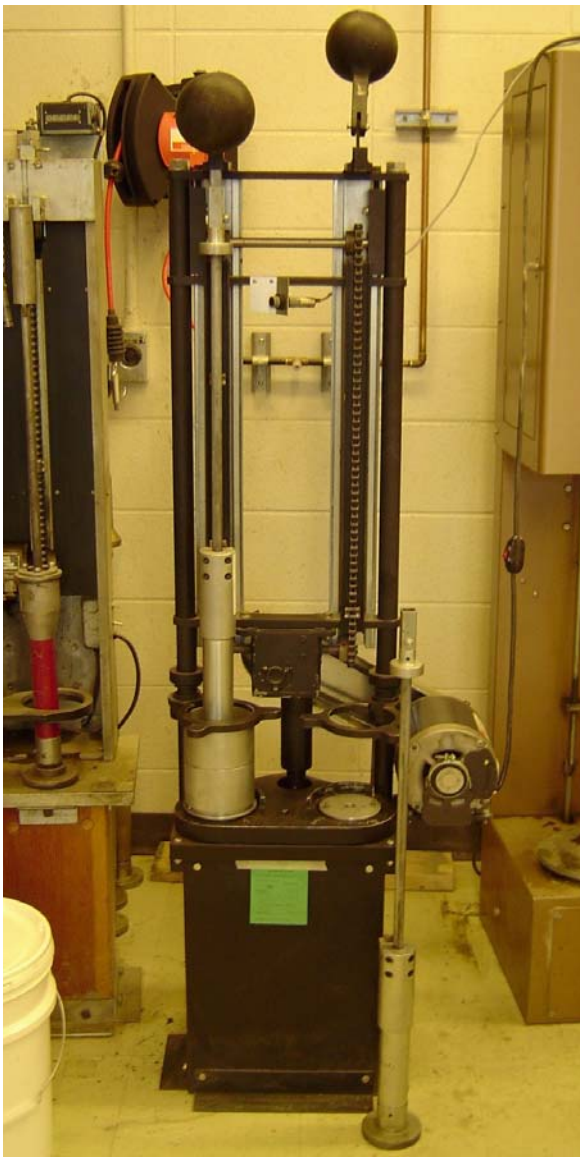

Figure 2.32 Mechanical Marshall Impact Hammer

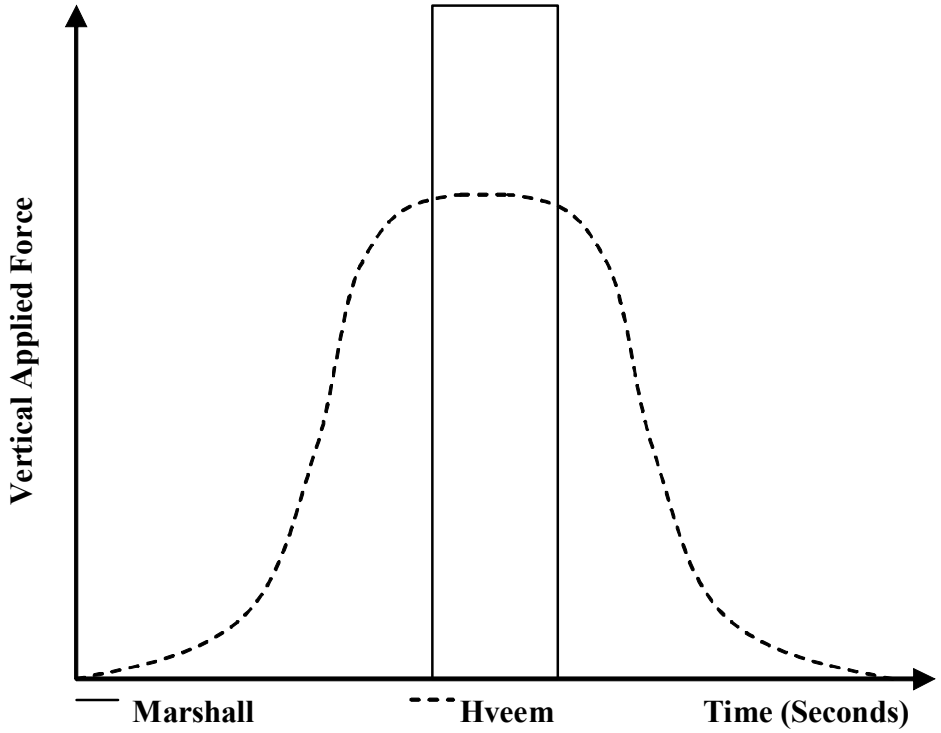

Figure 2.33 Marshall Impact Hammer and Hveem Kneading Compaction Loading Profiles

Figure 2.34 Marshall Stabilometer

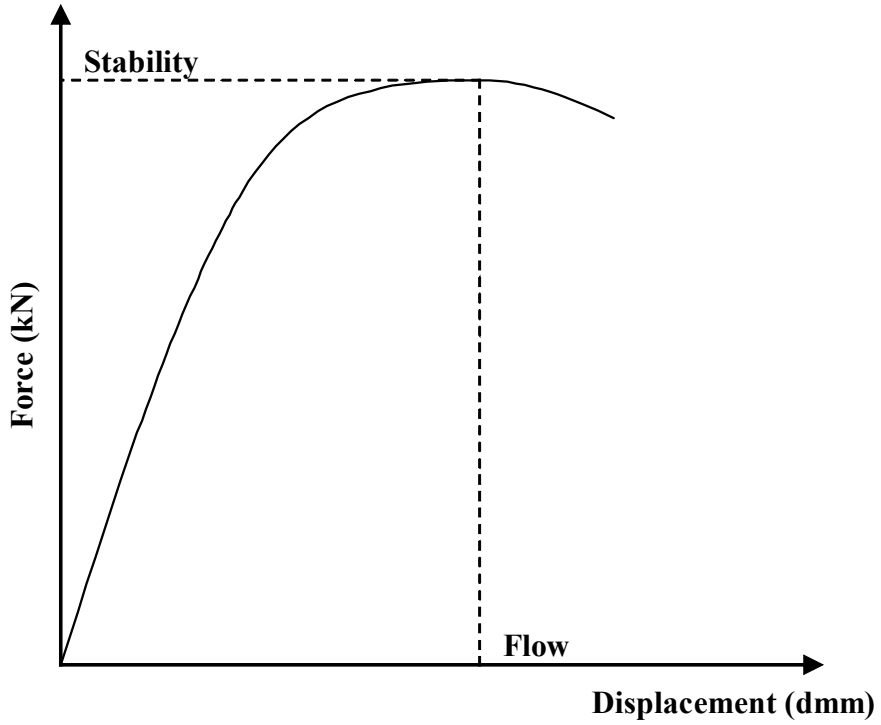

Figure 2.35 Marshall Stability and Flow

Limitations of the Marshall mix design method include (van de Loo 1976, Mamlouk *et al*. 1983, Consuegra *et al.* 1989, Berthelot *et al.* 1999, Carlberg 2003):

- The Marshall method is based on empirical field performance relationships and therefore does not produce properties directly related to performance;
- The Marshall stabilometer does not provide feedback controlled multi-axial measurements and, as a result, cannot be used to characterize the performance characteristics of asphalt concrete at stress states representative of field state conditions;
- The Marshall stabilometer cannot be used to characterize mechanistic properties of asphalt concrete at stress states representative of field state conditions because the curved mould applies boundary tractions to the sample, producing highly nonlinear stress-strain fields within the sample;
- Even though the Marshall procedure was created to decrease rutting in pavements, many pavements show significant rutting; and

- Research has shown poor correlation between the mechanical properties of laboratory compacted samples and field specimens, likely due to the uniform impact load applied by the Marshall hammer.

Marshall mix design specifications for 75 blow COS Type A1 and DHT Type 71 are summarized in Table 2.6. The COS Type A1 minimum Marshall stability is 11.0 kN at 60°C, the minimum retained Marshall stability is 75 percent, and the flow must be between 2.0 mm and 4.0 mm. The DHT Type 71 minimum Marshall stability is 7.0 kN at 60°C, the minimum retained Marshall stability is 70 percent, and the flow must be between 1.5 mm and 3.5 mm.

Table 2.6 75-Blow Marshall Mix Design Specifications

	COS Type A1			DHT Type 71		
	Stability (kN)	**Retained Stability (%)**	**Flow (mm)**	**Stability (kN)**	**Retained Stability (%)**	**Flow (mm)**
Minimum	11.0	75	2.0	7.0	70	1.5
Maximum	---	---	4.0	---	---	3.5

2.6.6 Unconfined Compressive Strength

Unconfined compressive strength (UCS) testing involves applying a vertical load at a fixed deformation rate to a cylindrical asphalt concrete sample, as specified in ASTM D1074 (ASTM 1996) and AASHTO T167 (AASHTO 1995). Unconfined compressive strength is the peak applied load divided by the original cross sectional area of the sample perpendicular to the direction of the load, as illustrated in Figure 2.36. Unconfined compressive strength is expressed as:

$$UCS = \sigma_f = \frac{P_{11f}}{A_0} \quad \textbf{(2.14)}$$

Where:

σ_f = Peak stress at failure (Pa);

P_{11f} = Peak applied load at failure (N); and

A_0 = Original cross sectional area (m^2).

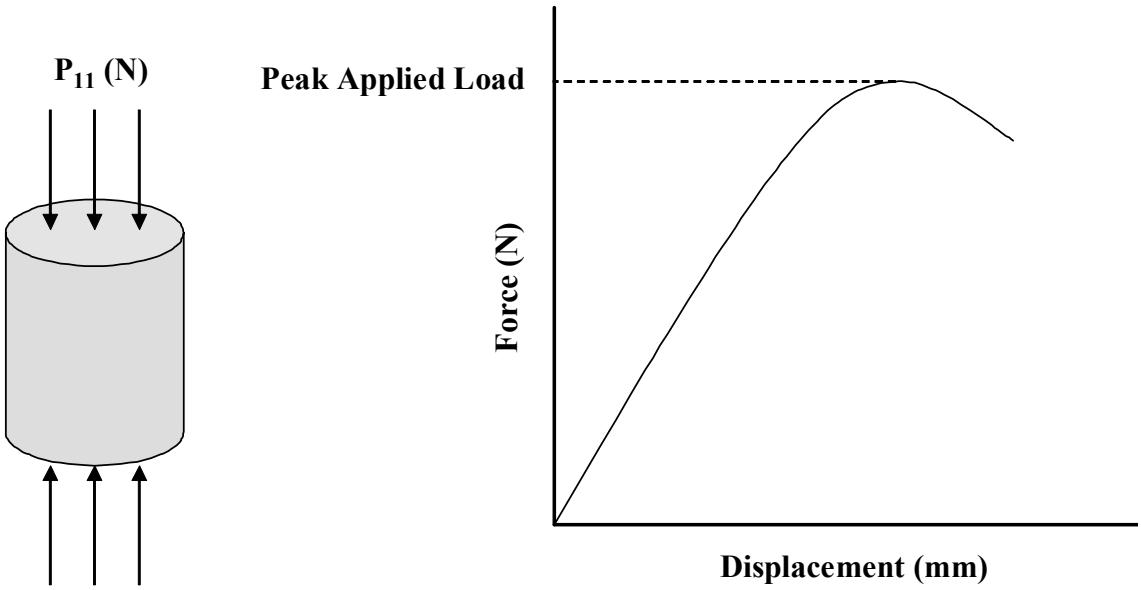

Figure 2.36 Unconfined Compressive Strength Testing

Limitations of unconfined compressive strength characterization include:

- The stress state generated during testing is highly deviatoric in nature and unrepresentative of field state loading conditions;
- The results are largely dependent upon load application rate (Mamlouk and Sarofim 1988); and
- The UCS does not provide feedback controlled multi-axial deflection measurements and, as a result, cannot be used to characterize the fundamental performance characteristics of asphalt concrete.

2.7 SHRP Superpave^{TM} Mix Design Method

Since the conventional empirical Marshall mix design method does not provide direct relation to performance properties of asphalt concrete mixes (Baladi 1989) it was essential to develop a performance based asphalt concrete mix design method. SHRP undertook a major research effort from 1987 through 1992 to investigate the thermomechanical properties of asphalt concrete related to field performance and develop first generation performance prediction models for various road structure types and traffic and environmental conditions (Roberts *et al*. 1996).

The Superpave™ (*Su*perior *Per*forming Asphalt *Pave*ments) mix design method is a product of SHRP and was developed to minimize permanent deformation, fatigue cracking, and low temperature cracking in asphalt concrete (SHRP-A-408 1994). Superpave™ mixes are dense graded mixes with lower proportions of natural fines and sand combined with increased aggregate crushing requirements than standard dense graded mixes. Unlike the Marshall method, Superpave™ directly accounts for aggregate properties and environmental conditions in addition to traffic level. In addition, the Superpave™ system incorporates performance prediction tests to determine the fundamental properties of asphalt concrete such as stiffness modulus, fatigue resistance, and permanent deformation resistance.

2.7.1 Superpave™ Aggregate Gradation

Superpave™ aggregate gradations must fall within gradation control points while avoiding the restricted zone. The restricted zone is intended to prevent the aggregate gradation of the mix from following the maximum density line, therefore increasing VTM to enhance high temperature rut resistance (Hand *et al*. 2001, Kandhal and Mallick 2001, Kandhal *et al*. 2002). Gradations that follow the maximum density line can have inadequate VMA and are typically very responsive to asphalt content for field state temperatures. The gradation limits depend on the nominal maximum aggregate size. The nominal maximum size is one sieve size larger than the largest sieve to retain more than ten percent of the aggregate. To illustrate, the Superpave™ 12.5 mm nominal size control points and restricted zone specifications are summarized in Table 2.7 and illustrated in Figure 2.37.

Table 2.7 Superpave™ 12.5 mm Nominal Size Gradation Specifications

Sieve Size (mm)	Percent Passing by Weight			
	Control Points		Restricted Zone Boundary	
			Minimum	Maximum
19.0		100		
12.5	90	100		
2.36	28	58	39.1	39.1
1.18			25.6	31.6
0.60			19.1	23.1
0.30			15.5	15.5
0.075	2	10		

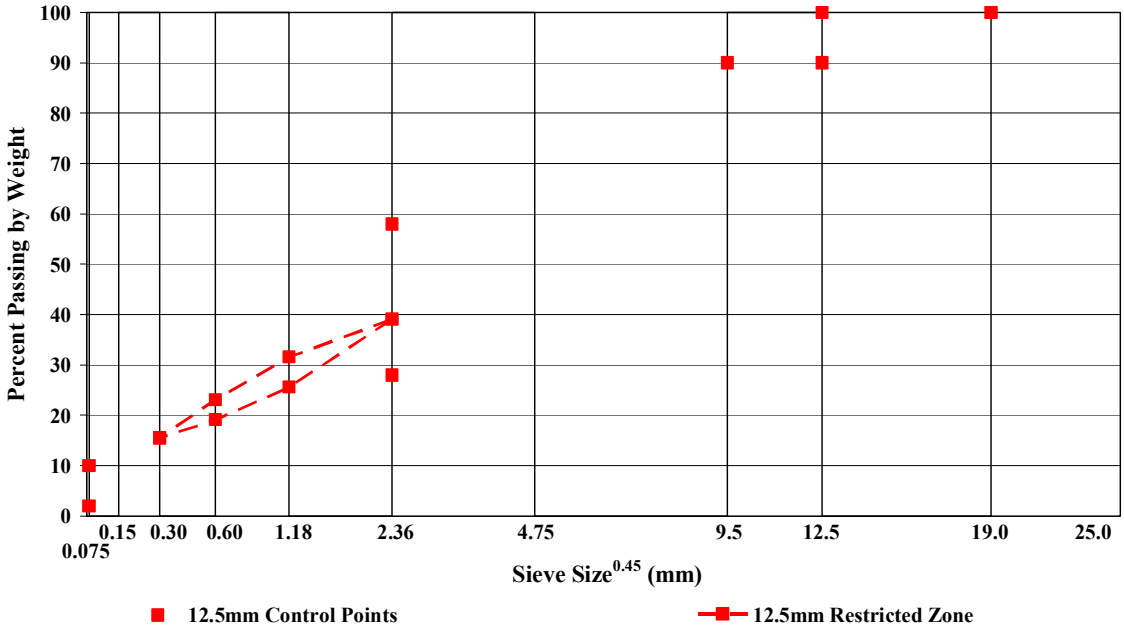

Figure 2.37 SHRP 12.5 mm Nominal Size Aggregate Gradation Control Points and Restricted Zone

2.7.2 Superpave™ Asphalt Concrete Gyratory Compaction

One of the primary benefits of the Superpave™ system is that specimen compaction involves the use of a gyratory compactor, as illustrated in Figure 2.38. The mix is subjected to both vertical and shear stresses during compaction as a result of the gyratory motion (Anderson and Bahia 1997, Mallick 1999). The vertical load and gyratory angle may be adjusted by the operator. As a result, the SHRP gyratory

compactor is able to simulate a wide variety of traffic compaction including cars, trucks, and aircraft by using different combinations of vertical pressure and gyratory angle. Of the current asphalt concrete laboratory compaction methods, it is widely accepted that gyratory compaction best simulates asphalt concrete compaction in the field (Butcher 1998).

Figure 2.38 Gyratory Compactor with Mould and Asphalt Concrete Sample

Research has indicated a higher degree of correlation of final pavement VTM after traffic loading with the gyratory compactor than with the 75 blow Marshall test (Hanson *et al*. 1994, Maupin 1995). The one-directional impact nature of Marshall compaction results in minimal reorientation and densification of the aggregate skeleton relative to SHRP gyratory samples. The difference in compaction results may be because gyratory compaction generates higher compaction shear effort, thereby

providing a better measure of mix compactability relative to the Marshall compaction method.

Research has indicated that the brand of gyratory compactor has no consistent significant effect on the complex shear modulus (G^*) or the maximum shear strain (γ_{max}) of individual samples as measured by SHRP Superpave^{TM} (Anderson *et al.* 1999). The variability in VTM and bulk specific gravity of compacted gyratory samples has been found to be greatly reduced by using the same machine for all samples and by using a sample diameter of 150 mm (Buchanan *et al*. 2001, D'Angelo *et al*. 2001). The same research also determined that the precision of the gyratory compactor has reduced sample variability relative to the mechanical Marshall hammer.

Sample height, bulk specific gravity, VTM, and shear strength are continuously measured during compaction allowing for the analysis of sample throughout the compaction process. Shear strength may be used to quantify the relative compactability of asphalt concrete mixes. As a mix is compacted its shear strength increases because of the increasing interparticle friction, or stone-on-stone contact. If the shear strength of the mix is adequate for the design (greater than the shear stress applied by the gyratory compactor) the shear strength recorded during compaction will plateau and remain constant throughout the remaining gyrations, indicating a stable mix. If the shear strength of the mix is inadequate, the shear strength recorded during compaction will decrease after a certain number of gyrations, indicating an unstable mix. In addition, identification of unstable mixes is possible since unstable mixes densify more rapidly than stable mixes. Field data has shown similar trends between rutting and the loss of shear strength during gyratory compaction. (Mallick 1999)

2.7.2.1 Development of the Gyratory Compactor

The first gyratory compactor was developed in 1939 when the Texas Highway Department initiated research of the design and control of asphalt mixtures. At the time, it was desired to develop laboratory compaction methods that (Harman *et al.* 2001):

- Were adaptable to both mix design and field control;

- Produced the same air void content as obtained in the field both after placement and after a period of traffic loading; and
- Approximated aggregate degradation in the field.

The protocol for the Texas gyratory compactor, illustrated in Figure 2.39, involves applying a constant pressure and rotating the mould at a 6.0 degree angle at 30 revolutions per minute (Huber *et al.* 1996). A 102 mm Texas gyratory compacted sample is illustrated in Figure 2.40. A Texas gyratory compactor with a 152 mm mould was also developed for designing mixes with large size aggregate as well as large stone bases. The modern SHRP gyratory compactor was developed based on the Texas gyratory machine.

In the late 1950's, the United States Corps of Engineers developed the gyratory kneading compactor, as illustrated in Figure 2.41, in response to experience showing Marshall impact hammer compaction did not accurately simulate wheel path densities under heavy aircraft loading (Harman *et al.* 2001).

The gyratory compaction concept was brought to France in the late 1950's. The result was the development of the French Laboratoire Central des Ponts et Chaussées (LCPC) gyratory protocol in the 1960's and early 1970's to replace the Marshall mix design method. The LCPC protocol involves rotating a 160 mm diameter mould at a 1.0 degree angle at six revolutions per minute (SHRP-A-408 1994). Unlike the Marshall method of standardizing laboratory compaction, the LCPC method standardized field compaction effort during pavement construction. (Huber 1996)

Figure 2.39 Texas Gyratory Compactor

Figure 2.40 Texas Gyratory Compaction Sample

Figure 2.41 United States Corps of Engineers Gyratory Kneading Compactor

2.7.2.2 Superpave^{TM} Gyratory Compaction Protocol

The SHRP testing protocol specifies the application of a vertical compressive pressure of 600 kPa to a specimen in a mould while the mould is tilted at 1.25 degrees and is rotated at 30 revolutions per minute. The number of revolutions (N) depends upon traffic level and field air temperatures. The initial number of gyrations, N_{ini}, is an indication of mixture compactability. The design number of gyrations, N_{des}, is the number of gyrations required to produce a sample density equivalent to the expected field density after the design amount of traffic loading. The maximum number of gyrations, N_{max}, is used to produce a density that should, theoretically, never be exceeded in the field.

Superpave^{TM} specifies a design VTM of 4.0 percent at N_{des} for mixes of all aggregate gradation nominal sizes to ensure adequate VTM after pavement consolidation due to heavy traffic loading to mitigate rutting during the service life of the pavement. All mixes require a minimum VTM of 11.0 percent at N_{ini} and a minimum of 2.0 percent at N_{max} in order to ensure adequate mix stability, as summarized

in Table 2.8. For a 12.5 mm nominal size aggregate gradation, the minimum VMA is 14.0 percent, and the VFA must be between 65 and 78 percent.

Table 2.9 summarizes the N_{ini}, N_{des}, and N_{max} specifications as a function of traffic level and environmental conditions. It can be seen that the focus of the Superpave™ system is high volumes of heavy traffic loads and high temperature conditions. Typical traffic levels in Saskatchewan are less than 3.0 million ESALs and the average design high air temperature is 39°C.

Table 2.8 Superpave™ Volumetric Specifications

			VTM (%)	VMA (%)	VFA (%)
12.5 mm Nominal Size	N_{ini}	Minimum	11.0	---	---
	N_{des}	Minimum	4.0	14.0	65
		Maximum	---	---	78
	N_{max}	Minimum	2.0	---	---

Table 2.9 Superpave™ Design Gyratory Compaction Effort

Design ESALs ($x10^6$)	Average Design High Air Temperature											
	< 39°C			39 - 40°C			41 - 42°C			43 - 44°C		
	N_{ini}	N_{des}	N_{max}	N_{ini}	N_{des}	N_{max}	N_{ini}	N_{des}	N_{max}	N_{ini}	N_{des}	N_{max}
< 0.3	7	68	104	7	74	114	7	78	121	7	82	127
0.3 - 1	7	76	117	7	83	129	7	88	138	8	93	146
1 - 3	7	86	134	8	95	150	8	100	158	8	105	167
3 - 10	8	96	152	8	106	169	8	113	181	9	119	192
10 - 30	8	109	174	9	121	195	9	128	208	9	135	220
30-100	9	126	204	9	139	228	9	146	240	10	153	253
> 100	9	143	235	10	158	262	10	165	275	10	172	288

(After Superpave Mix Design 1996)

2.7.3 Superpave^{TM} Performance Prediction Testing

There are three levels of Superpave^{TM} asphalt concrete mix design. Level I mix design involves asphalt cement and aggregate material selection, blend gradation determination, and volumetric analysis. The VTM compaction profiles at N_{ini}, N_{des}, and N_{max} are used to indicate mixture quality. Although the gyratory compactor is able to determine the compactability and physical properties of the mixes, the critical weakness of the Level I mix design is that it does not include a mechanical test to ensure adequate mix performance. The addition of a reliable, fast, and economical performance test to measure the fundamental properties asphalt concrete is required (Witczak *et al*. 2002).

In addition to the volumetric characterization of Level I, Level II includes an intermediate performance prediction system employing accelerated performance tests using the indirect tension test (IDT) and Superpave^{TM} shear tester (SST). Level II performance prediction is performed at an effective temperature (T_{eff}), which repersents year-round service temperatures. Testing at T_{eff} simplifies testing but does not produce complete performance prediction for a broad spectrum of field state conditions. Two different effective temperatures are used since permanent deformation and fatigue cracking occur at different temperatures. The temperature at which predicted permanent deformation would be the same as that predicted by a multiple temperature analysis is represented by T_{eff}(PD). The temperature at which predicted fatigue cracking would be the same as that predicted by a multiple temperature analysis is represented by T_{eff}(FC). Both effective temperatures are determined by Superpave^{TM} computer software using historical weather information at the project location and asphalt concrete layer thickness. Level II test temperatures are summarized in Table 2.10. (Superpave Mix Design 1996)

Level III is a complete performance prediction system which involves varying test temperatures and stress states. Level III performance prediction is performed at a range of temperatures dependent on the test type, as illustrated in Table 2.10. The wider range of temperatures represents a more accurate prediction of environmental effects. (Superpave Mix Design 1996)

Table 2.10 SHRP Superpave™ Performance Testing

Analysis Level	Performance Distress Model		
	Permanent Deformation	**Fatigue Cracking**	**Low Temperature Cracking**
II	Single shear test at constant height at T_{eff}(PD). Frequency sweep test at constant height at T_{eff}(PD).	Simple shear test at constant height at T_{eff}(FC). Frequency sweep test at constant height at T_{eff}(FC). Indirect tensile strength at T_{eff}(FC).	Indirect tensile creep compliance at 0^o, -10^o, -20^oC. Binder creep stiffness and creep rate.
III	Frequency sweep test at constant height at 4^o, 20^o, 40^oC. Uniaxial strain test at 4^o, 20^o, 40^oC. Volumetric test at 4^o, 20^o, 40^oC. Simple shear test at constant height at 4^o, 20^o, 40^oC.	Indirect tensile strength at -10^o, 4^o, 20^oC.	Indirect tensile creep compliance at 0^o, -10^o, -20^oC. Binder creep stiffness and creep rate.

(After Superpave Mix Design 1996)

Most mix designs use either Level I or Level II procedures. However, Level III should be used for high volume roads and mixes using modified asphalt cement binders to ensure proper consideration of environmental effects (Leahy *et al.* 1996). Performance prediction is accomplished using models for material properties, environmental effects, pavement response, and pavement distress. (Superpave Mix Design 1996)

The Superpave™ shear tester is employed to perform the performance prediction tests, and is illustrated in Figure 2.42. The SST is a closed-loop feedback servo-hydraulic system that can apply axial loads, shear loads, and confinement pressures simultaneously to asphalt concrete specimens at controlled temperatures ranging from 1^oC to 80^oC. The response of asphalt concrete to these loads is measured by linear variable differential transducers (LVDTs) attached to the sample, as illustrated in Figure 2.43. The response is then used as inputs to the performance prediction models. Six

Superpave™ testing protocols can be performed using the SST including (Superpave Mix Design 1996):

- Volumetric hydrostatic;
- Uniaxial strain;
- Repeated shear at constant height;
- Repeated shear at constant stress ratio;
- Constant height shear test; and
- Frequency sweep at constant height.

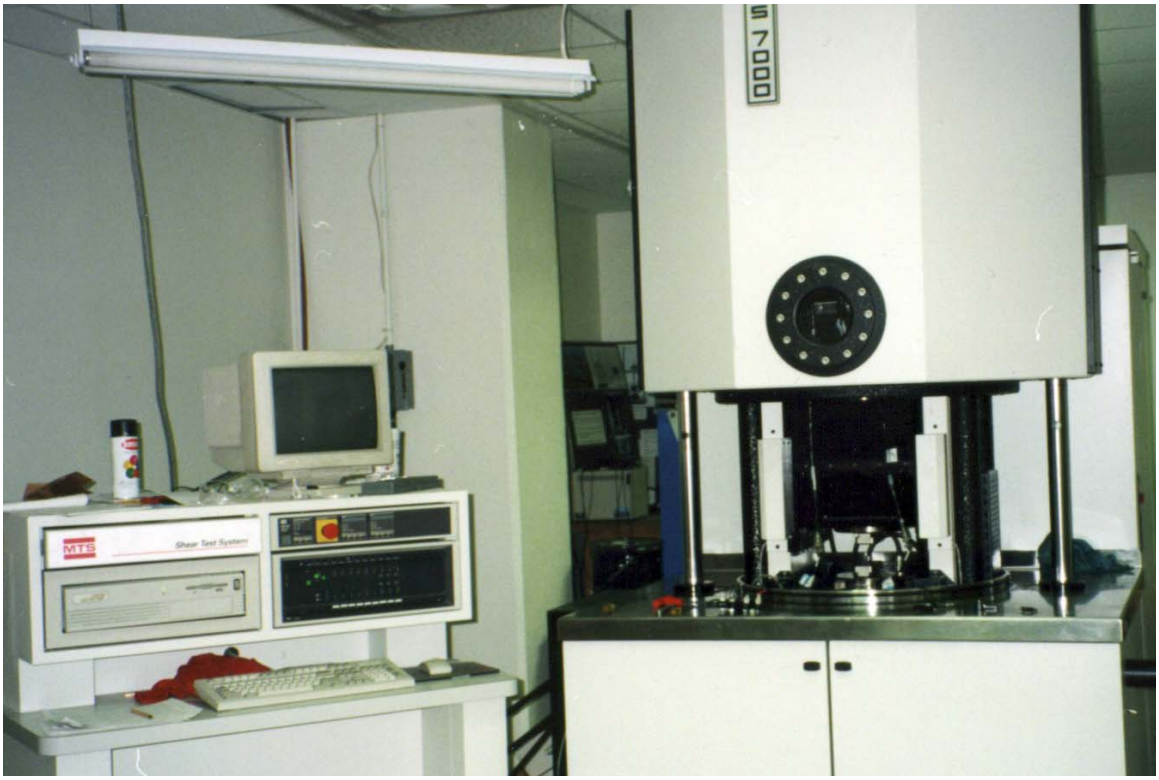

Figure 2.42 Superpave™ Shear Tester

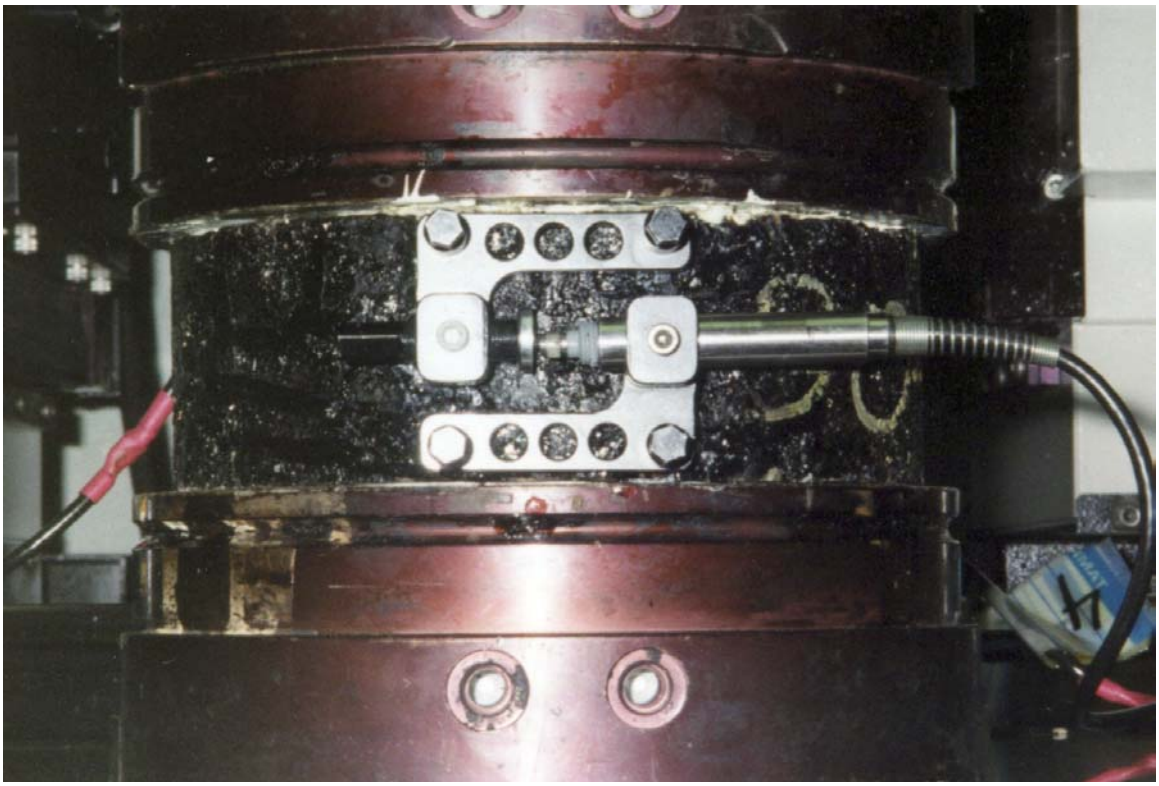

Figure 2.43 Superpave™ Shear Tester Liner Variable Displacement Transducer Configuration

Disadvantages of the SST include (Berthelot *et al.* 1997, Berthelot 1999, Weissman *et al.* 1999Chehab *et al*. 2000, Brown *et al.* 2001, Christensen *et al*. 2002):

- It has high capital and operating costs;
- It is complicated to operate;
- Testing time is considerably longer than conventional testing making it impractical for use by most road agencies, contractors, and consultants;
- Samples must be sawed and glued to end platens which is excessively time consuming for quality control testing;
- Cutting and gluing of specimens may affect sample response; and
- The SST tests are not sufficiently developed for immediate adoption.

It can therefore be concluded that an accurate, repeatable, reproducible, time efficient, and cost efficient performance verification test would be a beneficial addition to the Superpave™ mix design and analysis system.

2.7.3.1 Volumetric Hydrostatic Test

The volumetric hydrostatic test is performed for Level III permanent deformation and fatigue cracking prediction. The test evaluates the bulk elastic properties of asphalt concrete at three hydrostatic stress state and temperature combinations, as summarized in Table 2.11. The sample is subjected to a stress which is increased at a rate of 70 kPa per second until the desired stress level is reached. The resulting circumferential strain is measured using LVDTs as illustrated in Figure 2.44. The procedure for conducting this test is described in AASHTO TP7 (AASHTO 1995).

Table 2.11 Volumetric Test Parameters

Temperature (^{o}C)	Confining Stress (kPa)
4	830
20	690
40	550

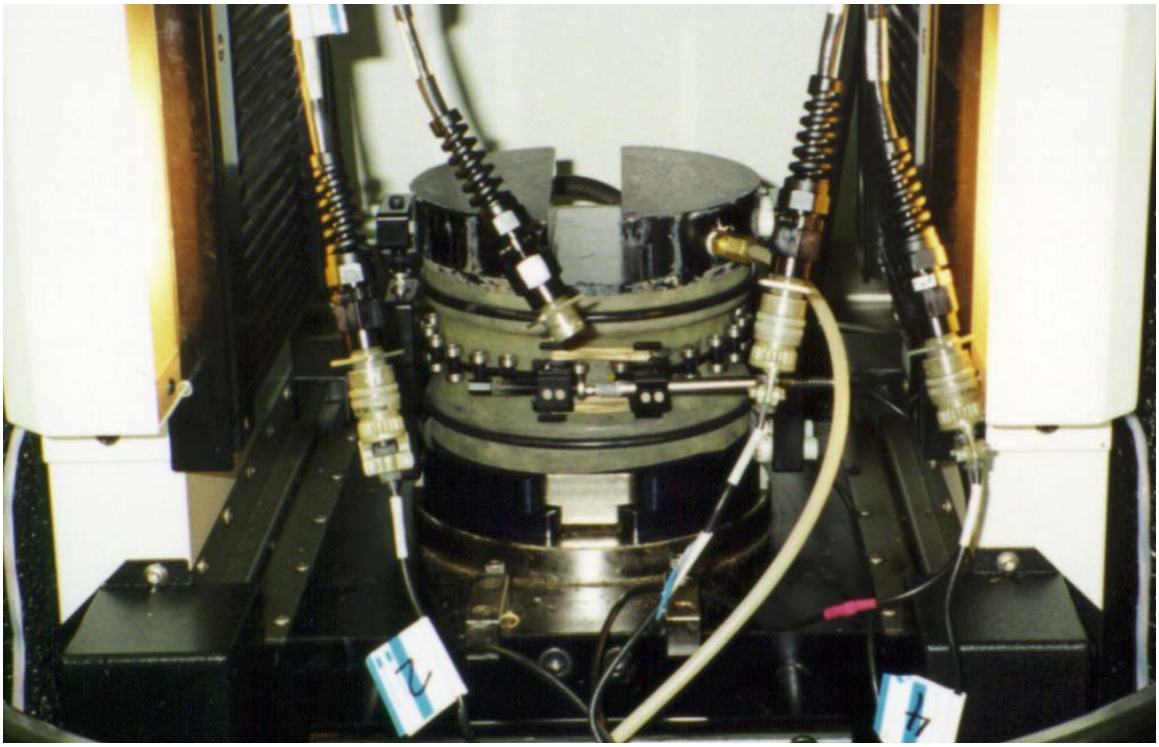

Figure 2.44 Superpave Shear Tester Volumetric Hydrostatic Sample

2.7.3.2 Uniaxial Strain Test

The uniaxial strain test is performed for permanent deformation and fatigue cracking prediction. The sample is subjected to an axial stress which tends to cause the sample to dilate and increase in circumference. However, air pressure is applied to keep the sample circumference constant. Three axial stress levels are applied to the sample depending on the test temperature, as summarized in Table 2.12.

The uniaxial strain test is performed in Level III performance prediction for determination of the uniaxial constrained compression modulus. The procedure for conducting this test is described in AASHTO TP7 (AASHTO 1995).

Table 2.12 Uniaxial Strain Test Parameters

Temperature (^{o}C)	Confining Stress (kPa)
4	655
20	550
40	345

2.7.3.3 Repeated Shear at Constant Height Test

The repeated shear at constant height test (RSCH) is performed to estimate rut depth. A shear load is applied to the sample to achieve a shear stress level of 68 kPa. The applied shear load tends to cause the sample to dilate and increase in height. However, the vertical actuator applies enough axial pressure to keep the sample height constant. The sample is subjected to 5000 load cycles consisting of a 0.1 second applied shear load followed by a 0.6 second rest period. Deformations and axial and shear loads are measured throughout the duration of the test. The RSCH test is not required for Superpave^{TM} performance prediction. The procedure for conducting this test is described in AASHTO TP7 (AASHTO 1995).

RSCH test results have shown high variability and six or more samples may be required for accurate characterization (Romero and Anderson 2001).

2.7.3.4 Repeated Shear Test at Constant Stress Ratio Test

The repeated shear test at constant stress ratio is performed to determine the cumulative shear strain in asphalt concrete and to identify asphalt concrete mixtures prone to tertiary rutting. Tertiary flow is the permanent deformation that occurs when VTM of the asphalt concrete decreases below approximately 3.0 percent. The sample, as illustrated in Figure 2.45, is subjected to between 5000 and 120,000 synchronized shear and axial load cycles, depending on traffic and climate conditions. Each load cycle consists of a 0.1 second applied shear load followed by a 0.6 second rest period. The axial stress to shear stress ratio is maintained at a constant level in the range from 1.2 to 1.5, and the stress magnitudes are selected based on stress conditions that will be experienced by the asphalt concrete in the field. This test was designed to be a non-destructive test; however, it has been discovered that many Superpave^{TM} samples fail in the repeated shear test. Failure may be due to excessive shear concentrations, excessive stress state at elevated temperatures, and sample geometry. A typical failed sample is illustrated in Figure 2.46. Test parameters are summarized in Table 2.13.

Table 2.13 Repeated Shear Test at Constant Stress Ratio Parameters

Base Condition	Asphalt Content					
	High		Medium		Low	
	Shear	Axial	Shear	Axial	Shear	Axial
Weak	84	119	63	98	49	56
Strong	98	175	84	105	56	91

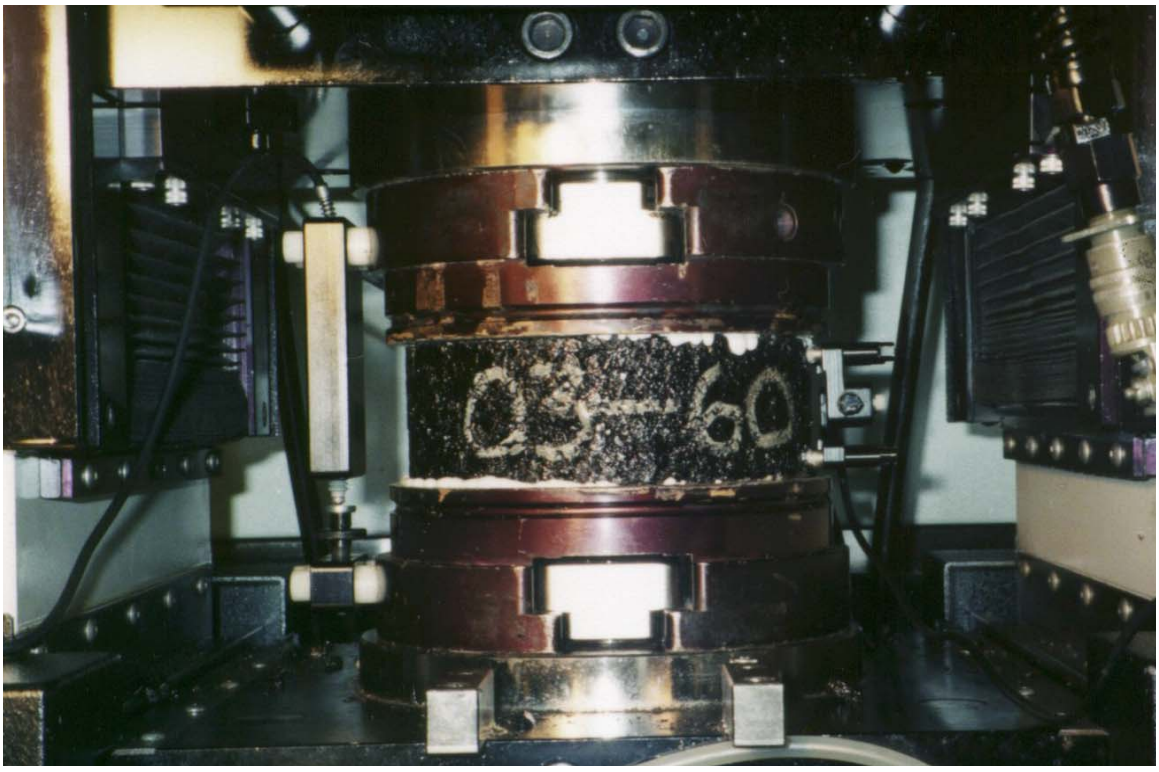

Figure 2.45 Superpave Shear Tester Sample

Figure 2.46 Superpave Repeated Shear Tester Failed Sample

The repeated shear test at constant stress ratio is performed in both Level II and Level III mix designs. The repeated shear test at constant stress ratio is performed at a critical temperature determined by Superpave^{TM} computer software. The critical temperature depends on T_{eff} (PD) and the design number of gyrations (Superpave Mix Design 1996). The procedure for conducting this test is described in AASHTO TP7 (AASHTO 1995).

2.7.3.5 Constant Height Shear Test

The constant height shear test (CHST) is performed for permanent deformation and fatigue cracking prediction by determining the maximum shear strain of asphalt concrete. The test evaluates the elastic, viscoelastic, and plastic behaviour of asphalt concrete. A controlled shear stress is applied to the sample at a rate of 70 kPa/s which tends to cause the sample to dilate and increase in height. However, the vertical actuator applies enough axial pressure to keep the sample height constant. The shear stress level and test temperature depend on the level of performance prediction.

The CHST test is performed in both Level II and Level III performance prediction. The procedure for conducting this test is described in AASHTO TP7 (AASHTO 1995).

Table 2.14 Constant Height Shear Test Parameters

Analysis Level	Temperature (^{o}C)	Maximum Shear Stress (kPa)
II	T_{eff}(PD) T_{eff}(FC)	By Interpolation
III	4	345
	20	105
	40	35

2.7.3.6 Frequency Sweep at Constant Height Test

The frequency sweep at constant height test (FSCH) is performed for permanent deformation and fatigue cracking prediction by determining the complex shear modulus of asphalt concrete. A shear load is applied to the sample to obtain a shear strain of 0.05 percent. The applied shear load tends to cause the sample to dilate and increase in

height. However, the vertical actuator applies enough axial pressure to keep the sample height constant. The sample is subjected to 100 load cycles at ten different frequencies. The test temperature depends on the level of performance prediction, as summarized in Table 2.15. Deformations and axial and shear loads are measured throughout the duration of the test.

The FSCH test is performed in both Level II and Level III performance prediction to determine the complex shear modulus. The procedure for conducting this test is described in AASHTO TP7 (AASHTO 1995).

Table 2.15 Frequency Sweep at Constant Height Test Parameters

Analysis Level	Temperature (^{o}C)
II	T_{eff}(PD) T_{eff}(FC)
III	4 20 40

2.7.3.7 Indirect Tension Test

The indirect tension test (IDT) is performed to evaluate tensile strength and tensile strain at failure of asphalt concrete. The test is performed using an indirect tensile tester which applies a single or repeated sinusoidal vertical compressive load along the diametral plane of a cylindrical specimen. As a result, a relatively uniform tensile stress develops perpendicular to the direction of applied load which ultimately causes the sample to split along the vertical diameter. Stress states of the IDT test are illustrated in Figure 2.47. Strain is measured by strain gauges mounted along and across the diametral axis, as illustrated in Figure 2.48.

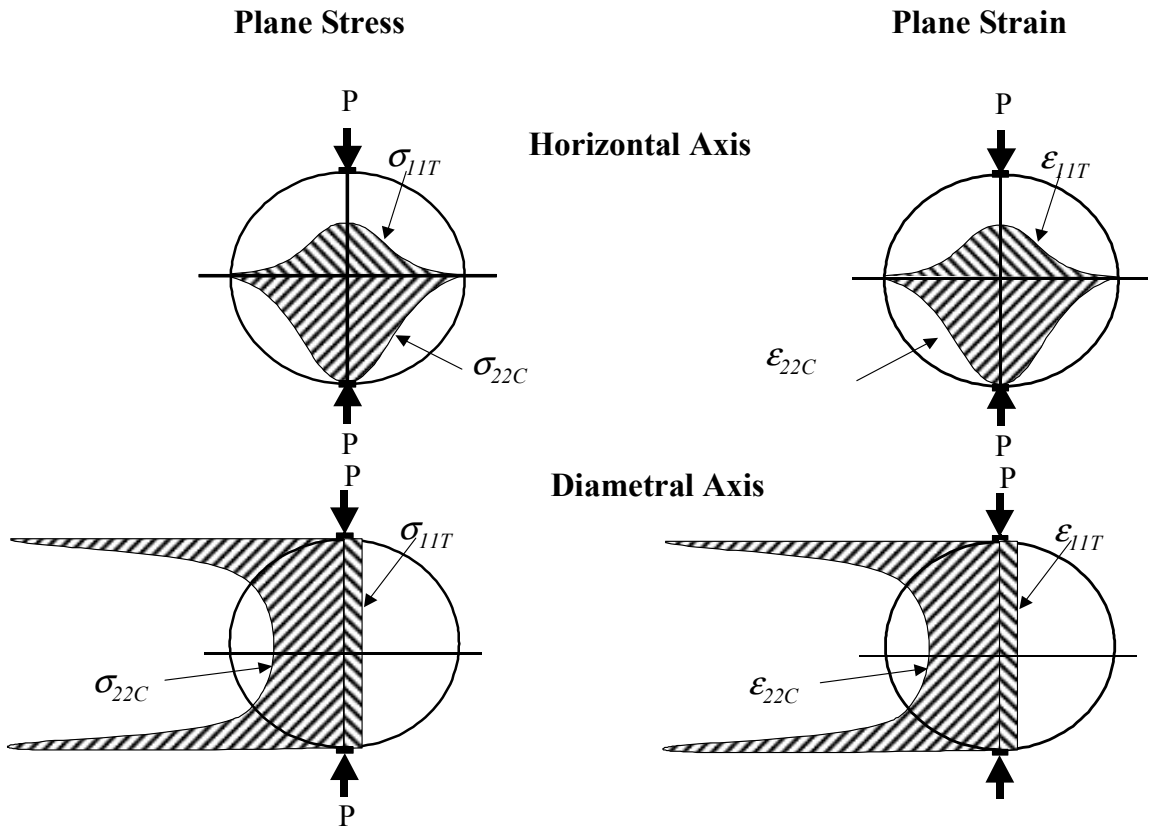

Figure 2.47 Indirect Tension Test Stress States

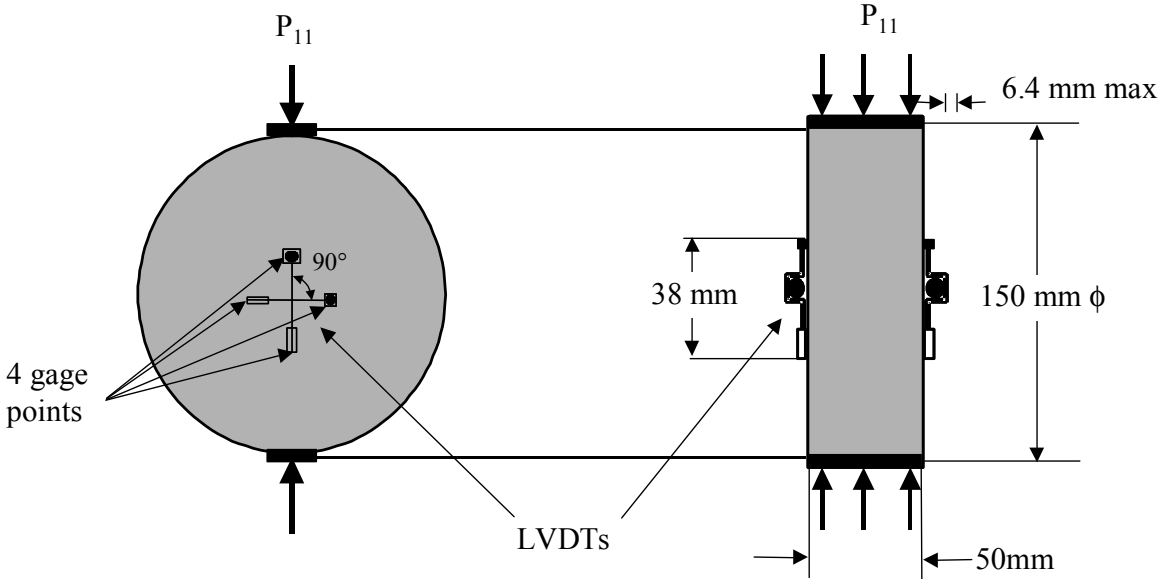

Figure 2.48 Indirect Tension Test Strain Gauge Locations

The IDT is used in Superpave™ performance prediction to perform both low temperature cracking analysis and fatigue cracking analysis. The IDT creep compliance and strength test is used for low temperature thermal cracking analysis. The creep phase involves applying a fixed magnitude load to the specimen to produce between 50 and 750 horizontal micro strain over 100 seconds. The load is then increased at a rate of 12.5 mm per minute until the sample fails. The test temperature depends on the level of performance prediction. The creep compliance and strength test is used in Level II and Level III performance prediction. The procedure for conducting these tests is described in AASHTO TP9 (AASHTO 1995) and ASTM D4123 (ASTM 1996).

Tensile strength is often used to determine the water susceptibility of mixes by performing the test before and after water conditioning of specimens. Tensile strain at failure is useful in predicting the mix thermal cracking potential. The procedure for conducting the IDT test is described in AASHTO TP9 (AASHTO 1995) and ASTM D4123 (ASTM 1996).

Limitations of the IDT include (Brown and Foo 1991, Kim *et al*. 1992, Tayebali et al 1995):

- The stress states developed during IDT testing may not be appropriate for testing of particulate composite materials such as asphalt concrete;
- The test is cumbersome to perform;
- There is wide variability in Poisson's ratio and dynamic modulus results even though the test simulates pavement loading reasonably well; and
- The test cannot obtain Poisson's ratio accurately from the horizontal and vertical deformations.

2.8 Post-SHRP Characterization

Conventional asphalt concrete mix testing, such as the Hveem and Marshall methods lack of multi-axial traction states and repeated loads and are therefore not representative of field state conditions. It is therefore difficult to use the results of these tests for performance prediction or structural design.

Mechanistic testing employs the laws of thermodynamics and primary responses, such as stress and strain, in the pavement structure. However, the determination of these parameters can require extensive laboratory testing and/or precise field measurements, which is not always practical or timely (SHRP-A-415 1994). In addition, stress conditions from traffic loading are more complicated than stress conditions provided by currently employed test configurations. The need has been identified to develop a mechanistic based asphalt concrete performance test procedure that is able to accurately reproduce *in situ* pavement axial stress, confinement stress, and temperature conditions in order to obtain accurate stress and strain relations for pavement performance prediction (Brown 1976, Croney 1977, Witczak 2003).

2.8.1 AASHTO 2002

The 2002 edition is the most recent version of the AASHTO Design Guide. Previous AASHTO design guides have been empirically based, resulting in inaccurate flexible pavement design equations (Baladi and Thomas 1994). The pavement design methodology has been updated to employ mechanistic principles in order to increase the efficiency of the use of pavement materials, increase pavement design reliability, improve pavement performance, and reduce life cycle costs (AASHTO 2004).

Materials characterization guidelines will be provided to help asphalt concrete designers determine the appropriate material properties as inputs for the analysis portion of the design process. These material properties fall into the following categories:

- Pavement response model material inputs;
- Materials-related pavement distress criteria; and
- Other materials properties.

Pavement response model inputs include moduli and phase angle. Although Poisson's ratio is a major contributor to material behaviour, it is not included in AASHTO 2002. Materials-related pavement distress criteria are usually related to a measure of material strength such as modulus of rupture, shear strength, or compressive strength, or are related to a materialization of the actual distress effect such as permanent deformation.

2.8.2 Triaxial Frequency Sweep Testing

Given the inherent limitations of SHRP Level II and III mix testing protocols, SHRP Level II and III laboratory testing is not always practical and timely for performing hot mix asphalt concrete mix designs. The triaxial frequency sweep test is being developed as a mechanistic based, cost effective, and time efficient method for determining mechanistic engineering material properties of asphalt concrete for a range of field state conditions.

The rapid triaxial test (RaTT) cell, illustrated in Figure 2.49 and Figure 2.50, uses pneumatic pressure in a rubber membrane to apply a confining pressure to the sample while a sinusoidal load is applied vertically. Strains in the sample are monitored throughout the test using two vertically-mounted LVDTs and four radially-mounted LVDTs (Berthelot 1999). Feedback-controlled multi-axial measurements taken during testing are essential in accurately characterizing the mechanistic continuum performance characteristics of asphalt concrete over a range of field state conditions.

Based on engineering first principles, the RaTT can accurately reproduce field state conditions. The sinusoidal loading reasonably simulates the rolling wheel action experienced by the pavement in the field (Crockford *et al.* 2002, Anthony and Berthelot 2004). Confining pressure allows close duplication of pavement service stress states in addition to preventing premature sample failure (Brown *et al.* 2001). Both the vertical and confining pressures can be user defined, allowing for characterization of a broad range of field state conditios. The vertical sinusoidal load frequency can be varied allowing simulation of a range of traffic speeds. The test temperature can also be varied to accommodate a range of service temperatures.

Figure 2.49 Rapid Triaxial Test Cell Raised Above Asphalt Concrete Sample

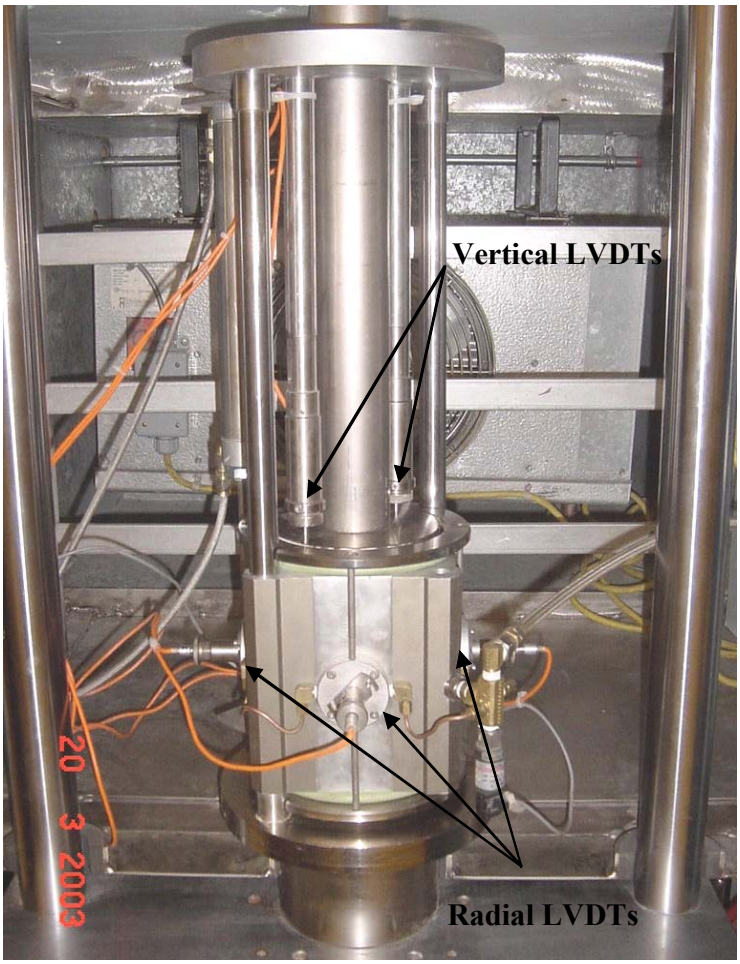

Figure 2.50 Rapid Triaxial Test Cell Lowered Over Asphalt Concrete Sample

The RaTT apparatus also has the ability to produce stress reversal under dynamic loading in the asphalt concrete sample. Moving wheel loads create a stress reversal, or areas in extension, in the asphalt concrete layer (SHRP-A-357 1993), as illustrated in Figure 2.51. The constant confining pressure in the RaTT creates a stress reversal in the asphalt concrete sample during the periods in the sinusoidal loading when the axial stress is less than the confining stress (Berthelot *et al.* 1999). Stress reversal cannot be obtained with normal triaxial testing in either confined or unconfined mode. (Carpenter and Vavrik 2001)

The RaTT apparatus is design to employ 150 mm diameter by 150 mm tall samples SHRP gyratory compacted samples. Since Superpave™ Level I also uses 150 mm by 150 mm samples, the samples can be tested in the RaTT after Level I volumetric analysis. In addition, RaTT samples are not cut and/or glued to end platens. The result

is significantly reduced sample preparation time relative to Level II and III characterization. Eliminating the need for saw cutting and/or gluing the sample also eliminates disturbance of the sample, improving the reliability of the characterization results. RaTT frequency sweep characterization could therefore compliment the SHRP gyratory compactor as a mechanistic characterization tool in the Superpave™ Level I mix design method.

St. Venant's continuum material mechanistic characterization principles (Malvern 1969) greatly simplify field equations for the conservation of linear momentum, conservation of angular momentum, and entropy inequality, in turn simplifying the amount of data analysis required. A major benefit of the RaTT is that is was designed as a continuum mechanics test based on St. Venant's principles of continuum mechanics, which are (Berthelot 2003):

- The stress-strain field in the sample must be uniform;
- The specimen size must be at least two to three times larger than the largest particle size contained in the material;
- Thermal gradients in the sample must be eliminated;
- The applied load rate should be much slower than the natural frequency of the material;
- Body forces (creep) in the specimen must be eliminated;
- Heat sources in the specimen must be eliminated; and
- Inertial effects must be eliminated.

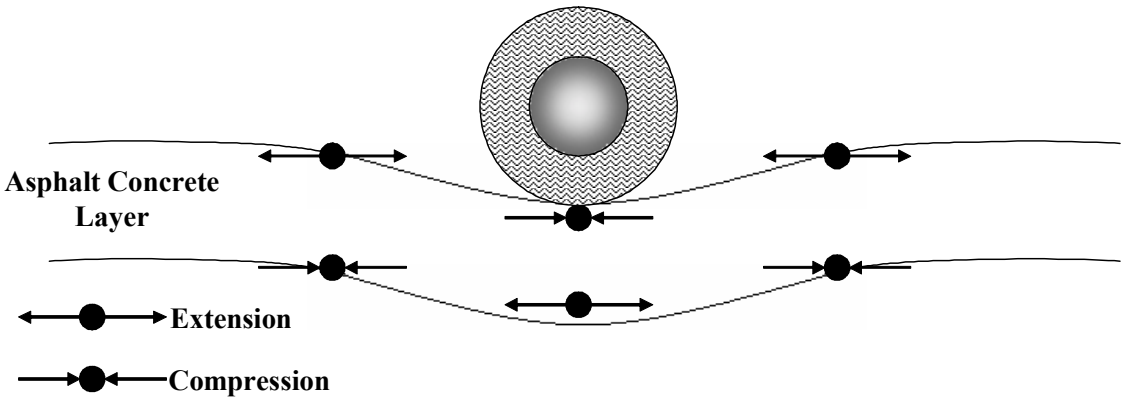

Figure 2.51 Cross Section of Stress Reversal in Flexible Pavement Wheel Path

In the RaTT all vertical surfaces are radially confined and vertical loading is applied over the entire horizontal surface, creating a uniform stress-strain field. Many Superpave™ performance tests involve gluing of samples to end platens, inducing stress-strain gradients and shear effects. The large size of the gyratory compacted samples allows the samples to be two to three times larger than the largest aggregate size contained within the sample. Superpave™ performance tests, on the other hand, employ saw-cut gyratory compacted samples, resulting in samples that are too small relative to the largest aggregate size. The RaTT can be placed in an environmental chamber, as illustrated in Figure 2.52, to eliminate temperature gradients in the sample during testing. The natural frequency of solid materials, including asphalt concrete, is much higher than the maximum test frequency of 10.0 Hz. The sample size and test cell configuration does not impose body forces or inertial effects on the sample. Asphalt concrete samples do not contain internal heat sources when brought to temperature equilibrium. Therefore, the RaTT obeys St. Venant's principles.

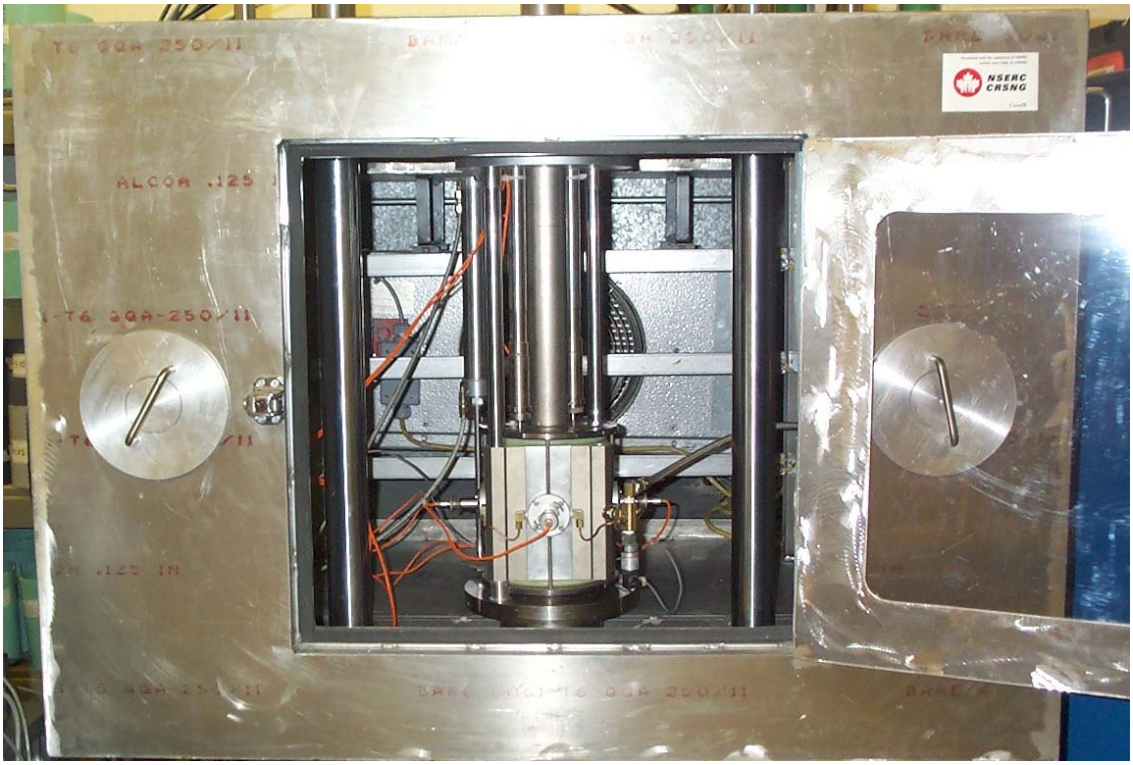

Figure 2.52 Triaxial Frequency Sweep Cell Inside of an Environmental Chamber

The RaTT test apparatus software uses measured deflections to calculate strains and engineering material properties as a function of magnitude of axial stress, application rate of axial stress, and magnitude of confining stress. Material properties can then be employed to characterize the behaviour of the asphalt concrete samples. Because the material properties determined from triaxial frequency sweep characterization are mechanistically based, they may be used as inputs for permanent deformation performance prediction and road structural models (Berthelot *et al.* 1999). RaTT material properties obtained include:

- Dynamic modulus;
- Phase angle; and
- Poisson's ratio.

Past research has found triaxial frequency sweep characterization in the RaTT to be a significant improvement over traditional empirical as well as mechanistic-empirical characterization methods. Marshall asphalt concrete characterization results have been found to be relatively repeatable but insensitive to different types of mixes. Hveem characterization has been found to be somewhat more repeatable and more sensitive than Marshall characterization. SHRP performance tests were found to have very poor repeatability and sensitivity equal to or poorer than Marshall and Hveem. RaTT frequency sweep asphalt concrete characterization results have been found to have repeatability comparable to the Hveem and Marshall methods, but the sensitivity to different mixes was found to be much higher than SHRP performance tests. (Berthelot 1999)

Triaxial frequency sweep testing in the RaTT may be a feasible addition to the SHRP Level I volumetric mix design as a reliable, fast, and economical performance verification test able to measure the fundamental properties of asphalt concrete. Research has determined that the RaTT is suitable for laboratory testing in addition to quality control in the field (Berthelot *et al.* 1997).

2.9 Summary

This chapter has summarized hot mix asphalt concrete distresses, conventional physical properties used for mix design, and several conventional mix design methods. Elastic and inelastic mechanistic material behaviour was also summarized.

Table 2.16 summarizes behaviour of asphalt concrete as influenced by an increase in asphalt cement viscosity, VTM, VMA, VFA, dynamic modulus, phase angle, and Poisson's ratio.

Table 2.16 Effect of Changing Properties on Asphalt Concrete Behaviour

Asphalt Concrete Property	Effect of Increased Property Value on Asphalt Concrete Performance			
	Fracture	**Permanent Deformation**	**Mix Durability**	**Structural**
Asphalt Cement Viscosity	Increase	Decrease	Minimal impact	Increase
Voids in Total Mix	Increase	Increase (shoving and consolidation)	Decrease	Decrease
Voids in Mineral Aggregate	Increase	Increase (shoving and consolidation)	Decrease	Decrease
Voids Filled with Asphalt	Increase	Increase (shoving) Decrease (consolidation)	Increase	Decrease
Dynamic Modulus	Increase	Decrease	N/A	Increase
Phase Angle	Decrease	Increase	N/A	Decrease
Poisson's Ratio	Decrease	Increase	N/A	Decrease

Traditional phenomenological-empirical mix design methods, such as Hveem and Marshall, were concluded to have several limitations including:

- The results are dependent upon the test apparatus configuration and therefore do not characterize the material's fundamental thermomechanical behaviour which is directly related to damage prediction; and
- The traffic field state loadings and material conditions under which the mix design methods were developed have changed.

It was established that recent advances in asphalt concrete mix designs, such as the SHRP Superpave™ method, are an improvement over traditional empirical methods. However, SHRP performance tests lack accuracy and efficiency.

Mechanistic testing employs the laws of thermodynamics and primary responses, such as stress and strain, in the pavement structure. The laws of thermodynamics are universal for all materials and do not change over time, allowing for continual modifications to performance models and changing pavement conditions. However, the determination of these parameters can require extensive laboratory testing which is not always practical or timely. Stress conditions from traffic loading are more complicated than stress conditions provided by currently employed test configurations. The need has been identified to develop a mechanistic asphalt concrete performance test procedure that is able to characterize asphalt mixes across pavement field state conditions.

Mechanistic characterization of a viscoelastic material, such as asphalt concrete, requires Poisson's ratio, a modulus such as dynamic modulus, and a time-dependent term such as phase angle to describe the fundamental mechanistic material behaviour.

Triaxial frequency sweep characterization in the rapid triaxial tester (RaTT) was introduced as a mechanistic based asphalt concrete characterization tool. The RaTT uses feedback-controlled multi-axial measurements made directly on the sample to calculate material properties including dynamic modulus, Poisson's ratio, and phase angle. The RaTT obeys the laws of mechanistic continuum mechanics testing. Because the RaTT is time efficient, RaTT may be a practical addition to the SHRP Superpave™ Level I volumetric analysis as a simple performance verification test.

In addition, the RaTT provides fundamental mechanistic material constitutive relations that can be used to specify road materials based on fundamental performance related behaviour, as well as encode fundamental material properties into a road structural model for structural design and analysis purposes. The RaTT apparatus can provide mechanistic based material properties in a time efficient and pragmatic framework required for mix design purposes.

3.0 CONVENTIONAL HOT MIX ASPHALT CONCRETE LABORATORY CHARACTERIZATION

The asphalt concrete samples used in this research were designed based on the COS Type A1 asphalt concrete mix design specifications (City of Saskatoon 2000). COS Type A1 is dense graded hot mix asphalt concrete typically used for high traffic volume urban roads. The asphalt concrete mix design results obtained were compared to DHT Type 71 specifications. DHT Type 71 is a dense-graded mix typically used for paving highways in Saskatchewan. Three different aggregate blend gradations were investigated.

Since both the COS and DHT employ the Marshall mix design method, the Marshall mix design method was employed to determine the asphalt concrete mix designs for each aggregate blend gradation. In addition, SHRP gyratory compaction was employed to evaluate asphalt concrete mix design volumetric parameters for each aggregate blend gradation.

3.1 Asphalt Cement Binder Characterization Results

Primary asphalt concrete pavements on Saskatchewan high traffic arterial highways are typically constructed using 150-200A penetration grade asphalt cement. Therefore, 150-200A grade asphalt cement was employed in this research. Penetration and absolute viscosity tests were performed on the asphalt cement as specified in ASTM D5 (ASTM 1996) and ASTM D2171 (ASTM 1996), respectively, to verify the asphalt cement grade. The penetration was determined to be 155 dmm. The absolute viscosity was determined to be 95.8 Pa.s. The penetration and viscosity results fell within acceptable limits and are illustrated with respect to the CGSB specification limits in Figure 3.1.

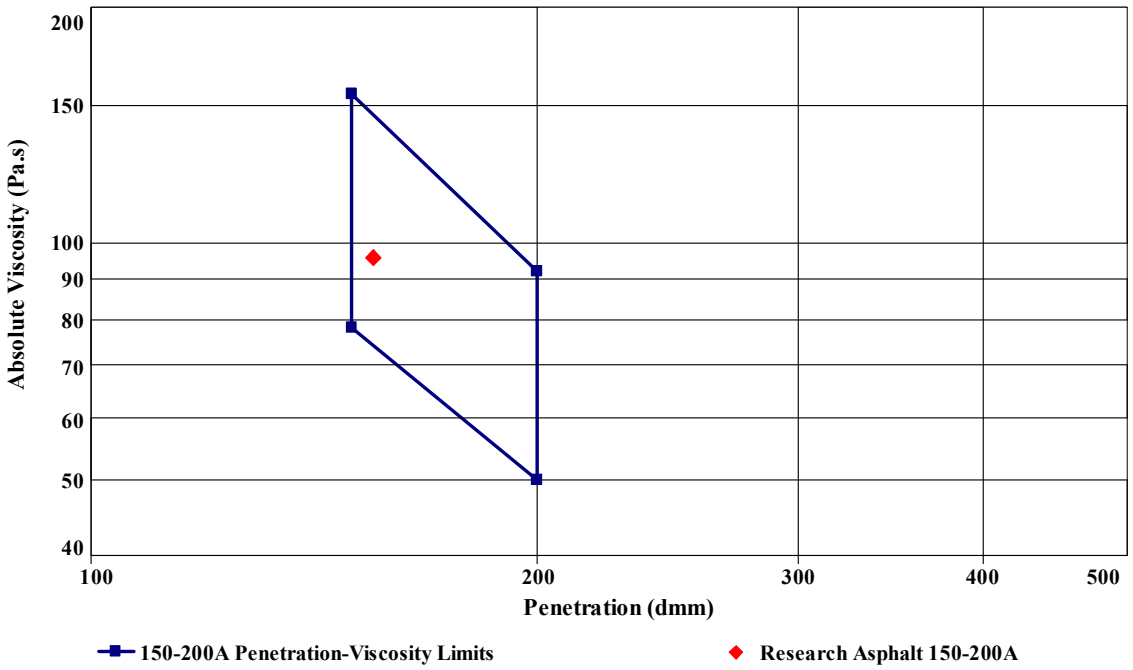

Figure 3.1 150-200A Asphalt Cement Absolute Viscosity and Penetration Results

3.2 Stockpile Aggregate Properties

The aggregate used in this research was obtained from an aggregate pit near Highway 16, approximately 40 kilometres west of the City of Saskatoon. The stockpile aggregate types sampled include:

- 3/4 inch;
- 5/8 inch;
- 1/2 inch;
- Fine crush;
- Blend sand; and
- Natural fines.

The gradation of each stockpile aggregate type is summarized in Table 3.1 and illustrated in Figure 3.2. The stockpile aggregate properties are summarized in Table 3.2 and Table 3.3. All COS Type A1 and DHT Type 71 aggregate specifications were met except for the sand equivalence value for blend sand. However, when combined in each of the three research blend gradation proportions discussed subsequently, the resulting

sand equivalence value met the minimum 45 percent required by COS Type A1 and DHT Type 71 mix specifications.

Table 3.1 Stockpile Aggregate Gradations

Sieve Size (mm)	Percent Passing by Weight					
	3/4 Inch	5/8 Inch	1/2 Inch	Fine Crush	Blend Sand	Natural Fines
25.0	100.0	100.0	100.0	100.0	100.0	100.0
20.0	97.63	100.0	100.0	100.0	100.0	100.0
16.0	66.65	99.7	100.0	100.0	100.0	100.0
12.5	36.3	90.6	100.0	100.0	100.0	100.0
9.00	10.1	45.0	99.8	100.0	99.8	98.7
5.00	1.4	7.4	95.4	99.5	95.4	92.0
2.00	0.7	0.7	76.3	62.1	76.3	76.6
0.900	0.7	0.77	38.4	38.7	38.4	59.6
0.400	0.6	0.6	12.9	26.4	12.9	43.7
0.160	0.5	0.6	4.5	14.9	4.5	27.7
0.071	0.4	0.5	3.8	9.9	3.8	21.0

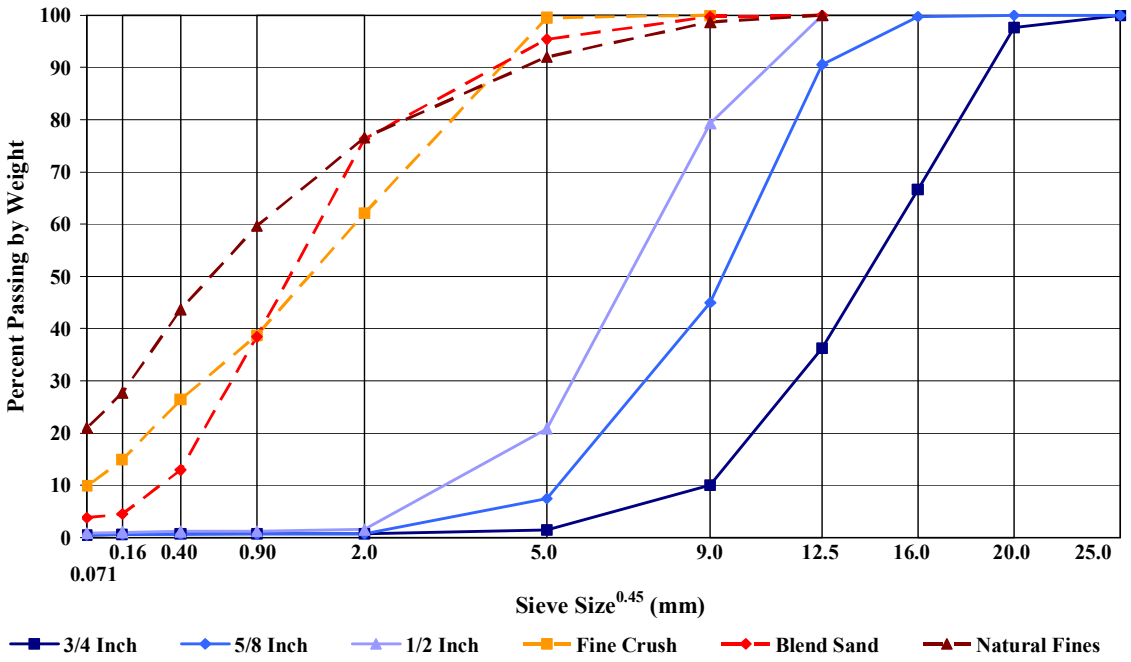

Figure 3.2 Stockpile Aggregate Gradations

Table 3.2 Stockpile Aggregate Properties

Aggregate Type	Sand Equivalence	Organic Content (%)
3/4 Inch	---	0.0
5/8 Inch	---	0.0
1/2 Inch	---	0.0
Fine Crush	73.9	0.0
Blend Sand	23.1	0.0
Natural Fines	58.3	0.0

Table 3.3 Stockpile Aggregate Properties

Aggregate Type	Coarse Aggregate Angularity (% Minimum)		Fine Aggregate Angularity (% Minimum)	Manufactured Fines (% Passing 5.0mm Sieve)
	One or More Fractured Faces	Two or More Fractured Faces		
3/4 Inch	85.1	80.5	---	---
5/8 Inch	90.4	82.9	---	---
1/2 Inch	97.5	94.7	---	95.4
Fine Crush	---	---	39.0	99.5
Blend Sand	---	---	35.7	---
Natural Fines	---	---	44.6	---

All aggregate types except for blend sand met the Superpave™ sand equivalence specifications. However, when combined in each of the three research blend gradation proportions discussed subsequently, the resulting sand equivalence met the minimum 40 percent Superpave™ specification. All coarse aggregate types met coarse aggregate angularity requirements. Natural fines met the minimum fine aggregate angularity specifications, but blend sand and fine crush did not. However, when combined in each of the three research blend gradation proportions discussed subsequently, the resulting fine aggregate angularity met the minimum 40 percent specification.

3.3 Research Mix Blend Gradations

The six stockpile aggregate types were combined to create three different research mix aggregate blend gradations based on the COS Type A1 gradation limits. The resulting individual stockpile aggregate type proportions are summarized in Table

3.4. The research mix blends were chosen so that the fine blend gradation followed the top limit of the gradation envelope, the middle blend was in the middle or the maximum density range of the gradation envelope, and the coarse blend followed the bottom limit of the gradation envelope, as summarized in Table 3.5 and illustrated in Figure 3.3. It should be noted that the fine and coarse blend gradations fell slightly outside of the COS Type A1 gradation envelope which is common with COS asphalt concrete mix gradations.

Table 3.4 Stockpile Aggregate Blend Proportions

Aggregate Type	Percent		
	Fine Blend	Middle Blend	Coarse Blend
3/4 Inch	15	28	35
5/8 Inch	11	7	10
1/2 Inch	8	9	8
Fine Crush	21	21	21
Blend Sand	33	27	26
Natural Fines	12	8	0

Table 3.5 COS Type A1 Gradation Specifications and Research Mix Blend Gradations

Sieve Size (mm)	Percent Passing by Weight				
	Minimum	Maximum	Fine Blend	Middle Blend	Coarse Blend
20.0	100	100	100.0	100.0	100.0
16.0	93	100	99.6	99.3	99.2
12.5	88	95	95.0	90.6	88.3
9.00	78	86	89.4	81.5	76.7
5.00	65	76	78.5	68.8	61.2
2.00	48	59	66.3	57.0	48.8
0.900	32	54	47.8	40.2	33.4
0.400	22	42	28.3	23.7	18.6
0.160	3	10	15.3	12.9	9.3
0.071	2	5	8.2	6.9	4.7

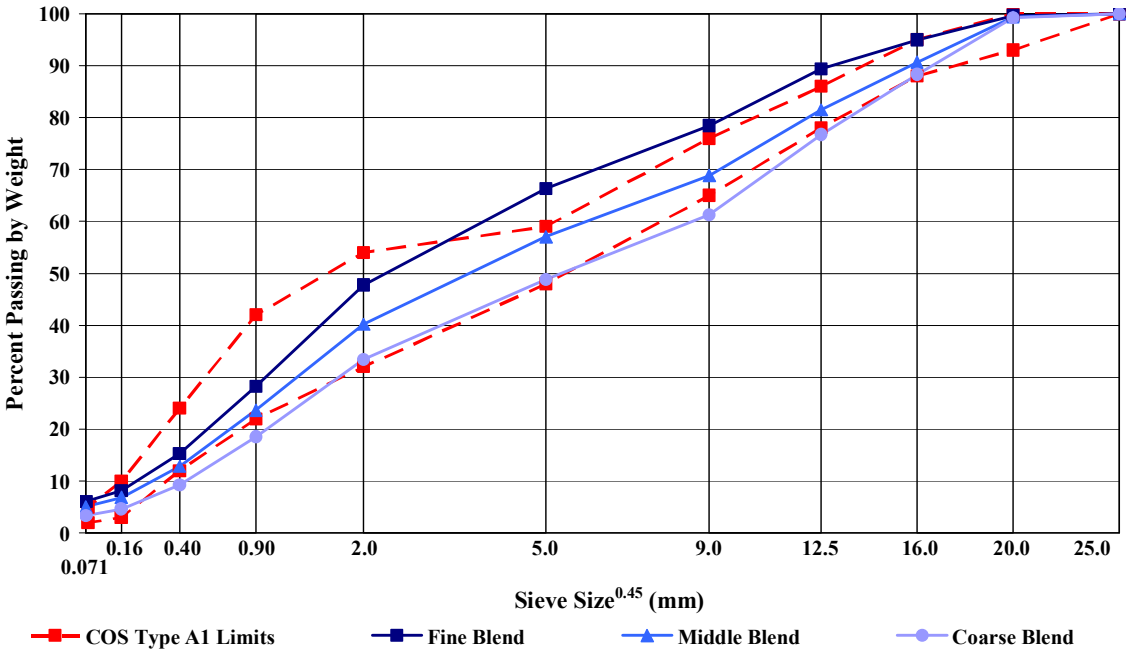

Figure 3.3 COS Type A1 Gradation Envelope and Research Mix Blend Gradations

Although the three research mix blend gradations were based on the COS Type A1 gradation envelope, the gradations also fell in approximately the top, middle, and bottom of the DHT Type 71 gradation envelope, as summarized in Table 3.6 and illustrated in Figure 3.4.

Table 3.6 DHT Type 71 Gradation Specifications and Research Mix Blend Gradations

Sieve Size (mm)	Percent Passing by Weight				
	Minimum	Maximum	Fine Blend	Middle Blend	Coarse Blend
18.0	100	100	---	---	---
16.0	100	100	99.6	99.3	99.2
12.5	78	98	95.0	90.6	88.3
9.00	66	90	89.4	81.5	76.7
5.00	46	72	78.5	68.8	61.2
2.00	23	51	66.3	57.0	48.8
0.900	15	37	47.8	40.2	33.4
0.400	10	30	28.3	23.7	18.6
0.160	3	14	15.3	12.9	9.3
0.071	2	9	8.2	6.9	4.7

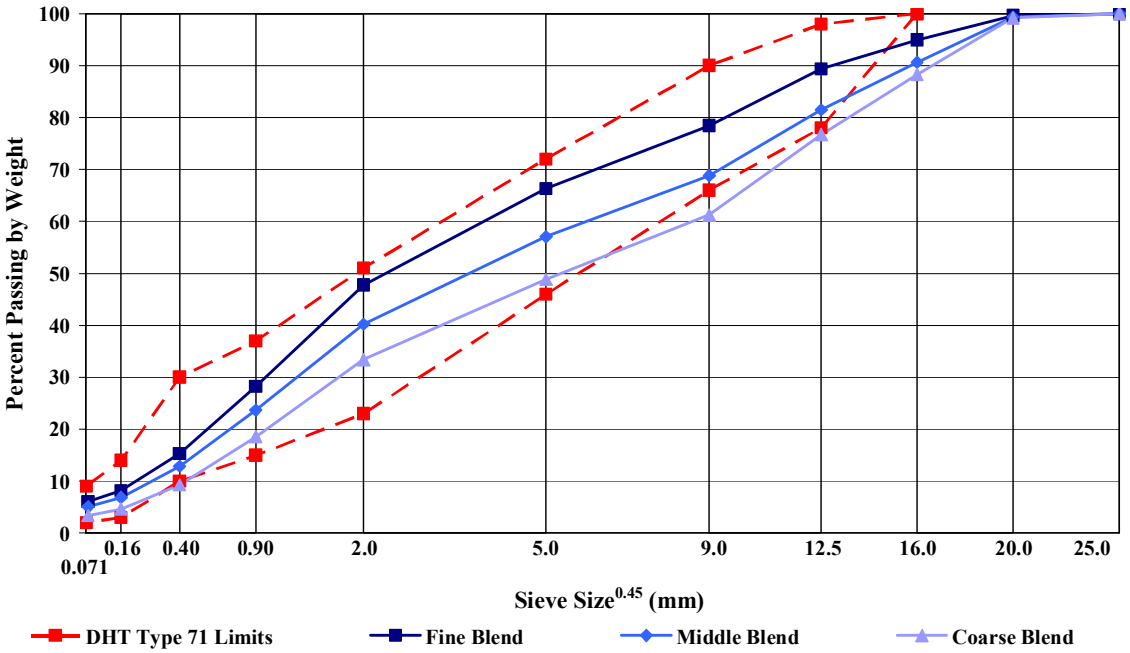

Figure 3.4 DHT Type 71 Gradation Envelope and Research Mix Blend Gradations

The SHRP Superpave™ nominal sizes of the fine, middle, and coarse blend gradations were 9.5 mm, 9.5 mm, and 12.5 mm, respectively. Figure 3.5 illustrates the three research mix blend gradations with respect to the SHRP 12.5 mm nominal size gradation specifications. The gradation limits were not tabulated due to the use of different sieve sizes for SHRP and COS mix design specifications. It can be seen that none of the three research blend mixes satisfied the SHRP gradation specifications. The fine and middle blends passed through the restricted zone, and all three blend gradations passed below the 12.5 mm control point.

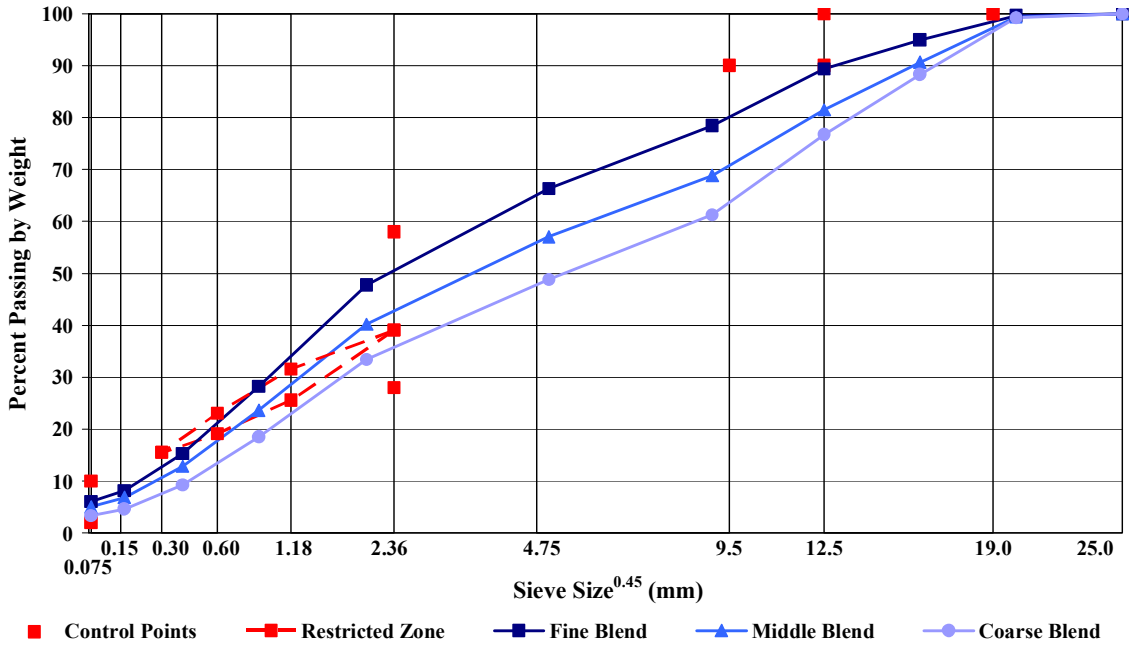

Figure 3.5 SHRP 12.5 mm Nominal Size Gradation Specifications and Research Mix Blend Gradations

3.4 Marshall Mix Analysis

Asphalt concrete on Saskatchewan high traffic arterial highways is typically designed using the 75 blow Marshall mix design method. Therefore, 75 blow Marshall mix designs were performed as specified in ASTM 1559 (ASTM 1996) for the fine, middle, and coarse blend gradations. Each mix design consisted of two repeat samples compacted at 4.0, 4.5, 5.0, 5.5, 6.0, and 6.5 percent asphalt cement content by weight of dry aggregate. During sample preparation, the fine blend sample containing 4.0 percent asphalt was found to be too "dry" and did not provide a visually acceptable continuum sample. Similarly, the coarse blend sample containing 6.5 percent asphalt was found to be too "wet". Therefore the data for these samples were not included in the analysis.

Volumetric measurements were performed on each compacted Marshall sample as specified in ASTM 2726 (ASTM 1996). Rice maximum theoretical specific gravity tests were performed as specified in ASTM D2041 (ASTM 1996) to determine the maximum density of each asphalt content of each blend gradation. Rice maximum theoretical specific gravity values are independent of compaction method; therefore, the same values were used for both the Marshall and SHRP gyratory mix designs. The

VTM, VMA, and VFA values were determined as specified in ASTM D3203 (ASTM 1996) and were plotted versus the two repeat samples to determine the value of each asphalt content. The Marshall volumetric results are summarized in Table 3.7 and illustrated in Figure 3.6 through Figure 3.9. Marshall stability and flow testing was performed on each sample as specified in ASTM 1559 (ASTM 1996), and the results are summarized in Table 3.7 and illustrated in Figure 3.10 and Figure 3.11.

The Marshall fine blend increased in density with increasing asphalt content. The middle blend increased in density with increasing asphalt content, but peaked at 6.0 percent asphalt content and subsequently decreased. The coarse blend increased in density with increasing asphalt content. These trends may indicate as asphalt content increases, there is increased lubrication between the aggregate particles, allowing aggregate to move easier in the mould during compaction, therefore increasing sample density.

The Marshall samples were found to decrease in VTM with increasing asphalt content for all three blend gradations. However, the VTM of the middle blend seemed to plateau between 5.0 percent and 6.5 percent asphalt content. These trends may indicate that as asphalt content increases there are less air voids in the sample to allow for asphalt cement expansion at high temperatures, decreasing stone-on-stone contact and therefore decreasing rutting resistance. In addition, the high VTM at lower asphalt contents may indicate excessive air voids and therefore a mix that may experience consolidation rutting under traffic loading.

The Marshall samples generally produced constant VMA values for asphalt contents for all three blend gradations except for the middle blend at 6.5 percent asphalt content which increased. There was no consistent VMA trend with respect to asphalt content.

Table 3.7 Marshall Mix Design Volumetric and Stability Results

	Blend Gradation	Percent Asphalt Content					
		4.0	4.5	5.0	5.5	6.0	6.5
Maximum Density (kg/m³)	Fine	---	2508	2451	2453	2387	2359
	Middle	2462	2432	2390	2421	2422	2363
	Coarse	2470	2455	2440	2424	2373	---
Density (kg/m³)	Fine	---	2287	2292	2321	2339	2347
	Middle	2317	2329	2360	2371	2385	2315
	Coarse	2290	2326	2312	2330	2347	---
VTM (%)	Fine	---	8.8	6.5	5.4	2.0	0.5
	Middle	5.9	4.2	1.2	2.1	1.5	2.0
	Coarse	7.3	5.3	5.2	3.9	1.1	---
VMA (%)	Fine	---	16.7	16.9	16.3	16.1	16.2
	Middle	15.7	15.7	15.0	15.1	15.0	18.0
	Coarse	17.0	16.2	17.1	16.9	16.7	---
VFA (%)	Fine	---	47.1	61.8	67.1	87.6	97.0
	Middle	62.5	73.1	92.1	86.4	89.9	89.4
	Coarse	57.2	67.3	69.4	77.0	93.6	---
Stability (kN)	Fine	---	3.6	3.1	3.0	3.9	3.6
	Middle	3.4	3.3	4.8	3.9	3.1	3.1
	Coarse	2.6	2.5	1.9	2.9	2.1	---
Flow (mm)	Fine	---	1.5	2.0	1.9	1.8	2.2
	Middle	1.7	2.0	1.9	1.7	2.0	1.9
	Coarse	2.7	2.5	1.6	2.5	2.2	---

The Marshall samples increased in VFA with increasing asphalt content for all three blend gradations. However, the middle blend VFA peaked at 5.0 percent asphalt content. These trends may indicate that as asphalt content increases the percent of the VMA filled with asphalt cement may be excessive and not allowing for asphalt cement expansion at high temperatures and therefore decreasing rutting resistance. In addition, the lower VFA at lower asphalt contents may result in insufficient asphalt cement film thickness on the aggregate, resulting in increased oxidation and therefore a brittle mix, therefore decreasing fracture toughness of the mix.

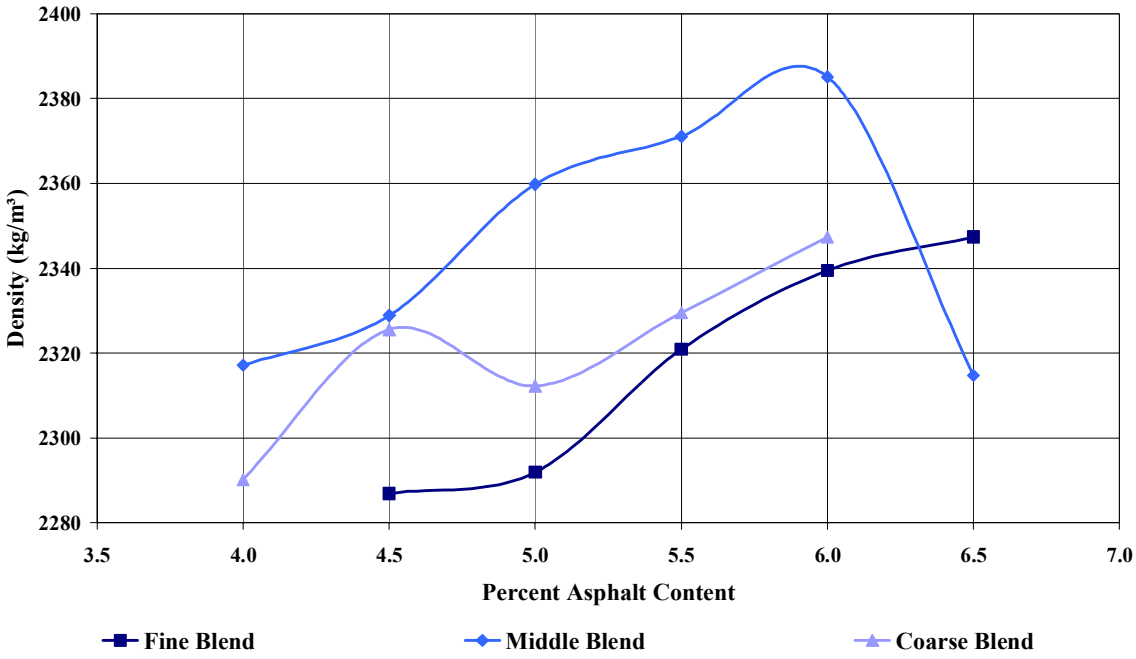

Figure 3.6 75 Blow Marshall Density

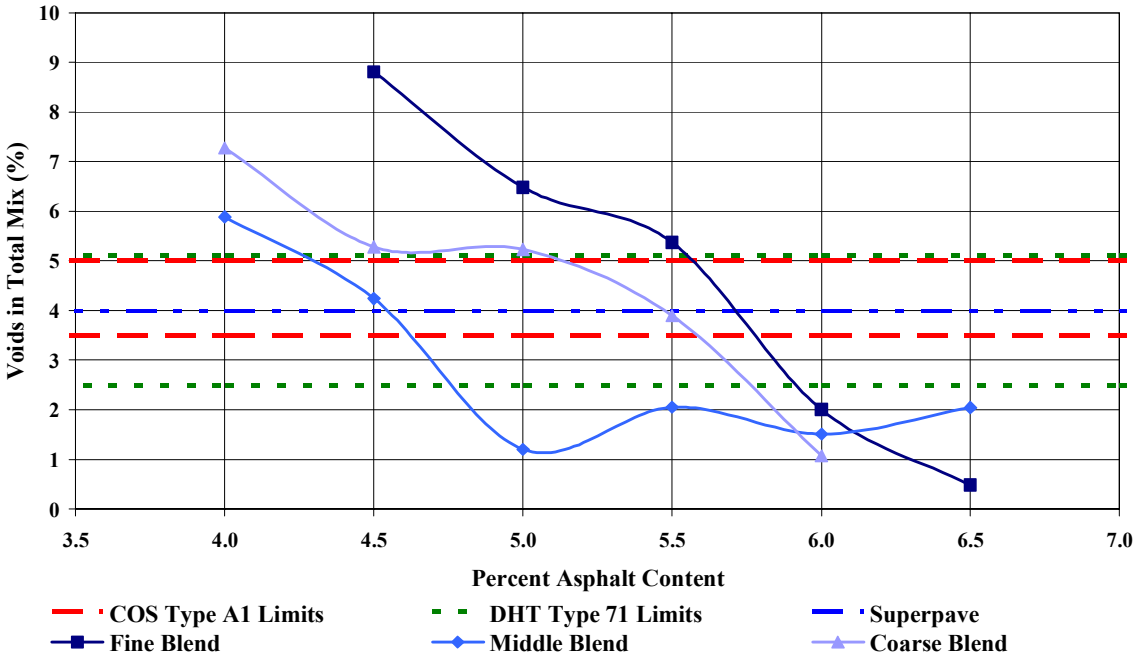

Figure 3.7 75 Blow Marshall VTM

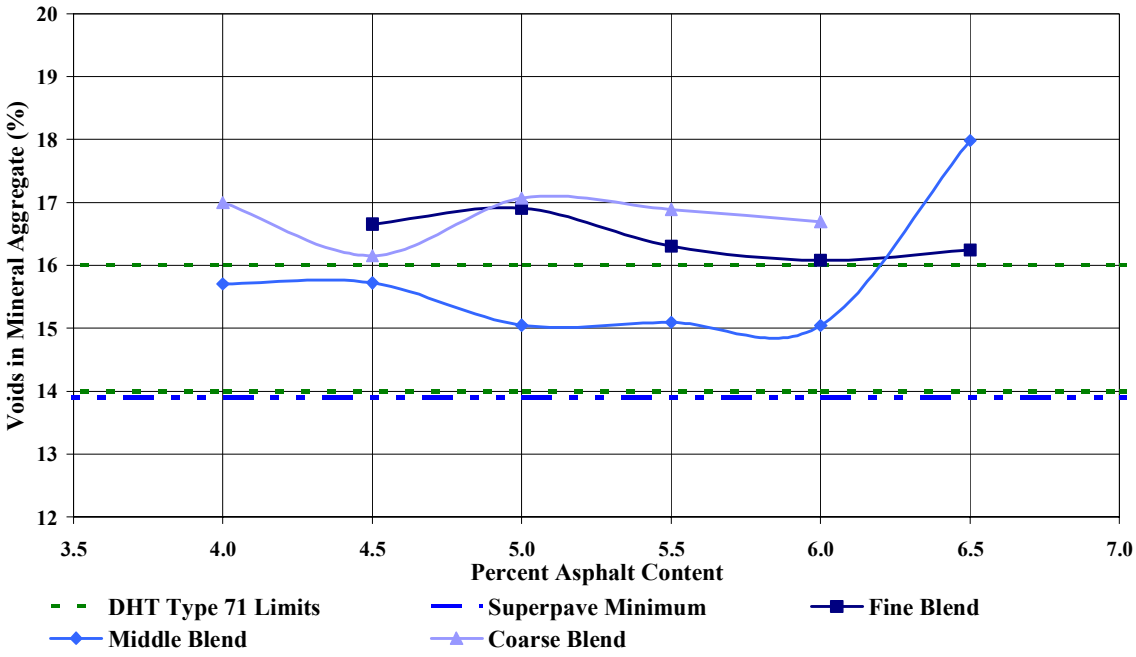

Figure 3.8 75 Blow Marshall VMA

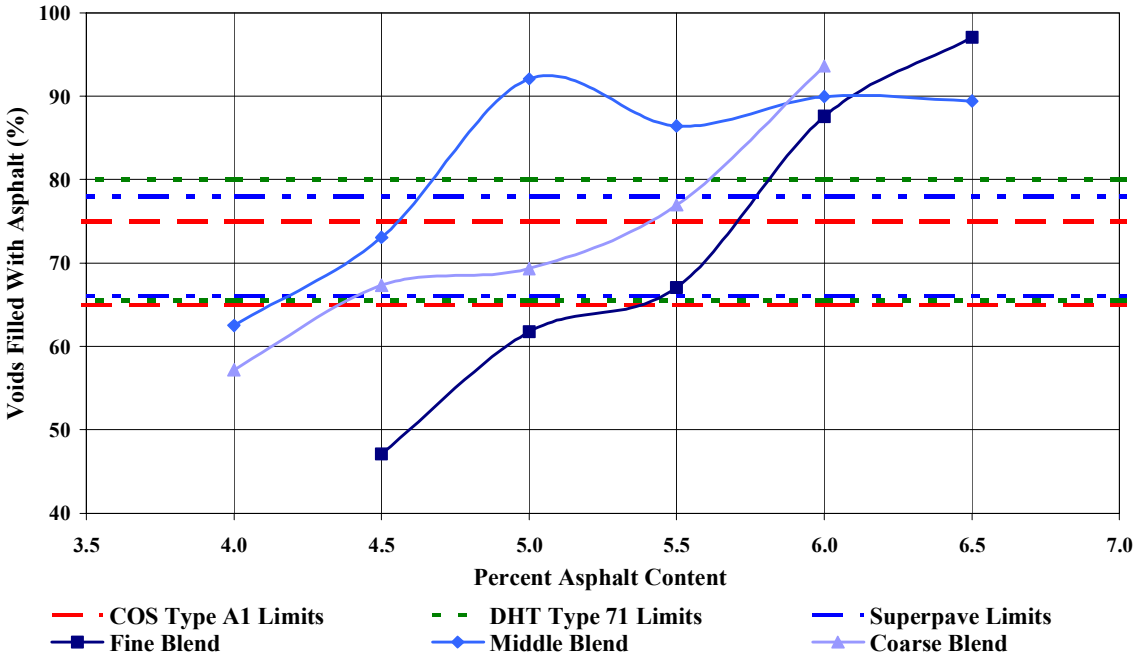

Figure 3.9 75 Blow Marshall VFA

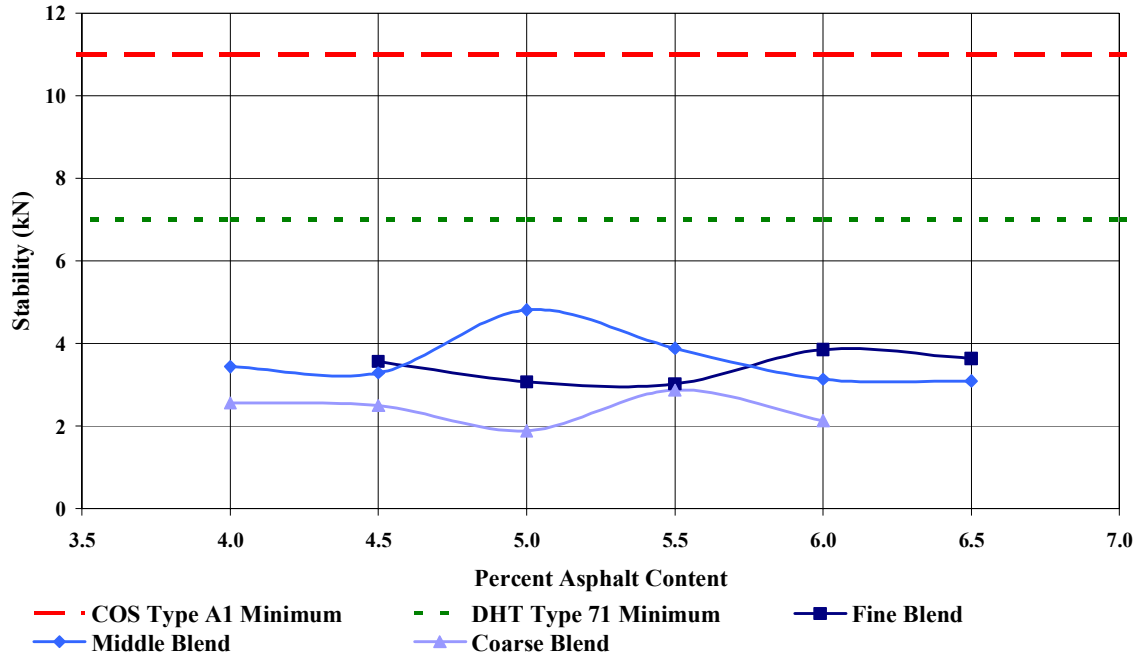

Figure 3.10 75 Blow Marshall Stability

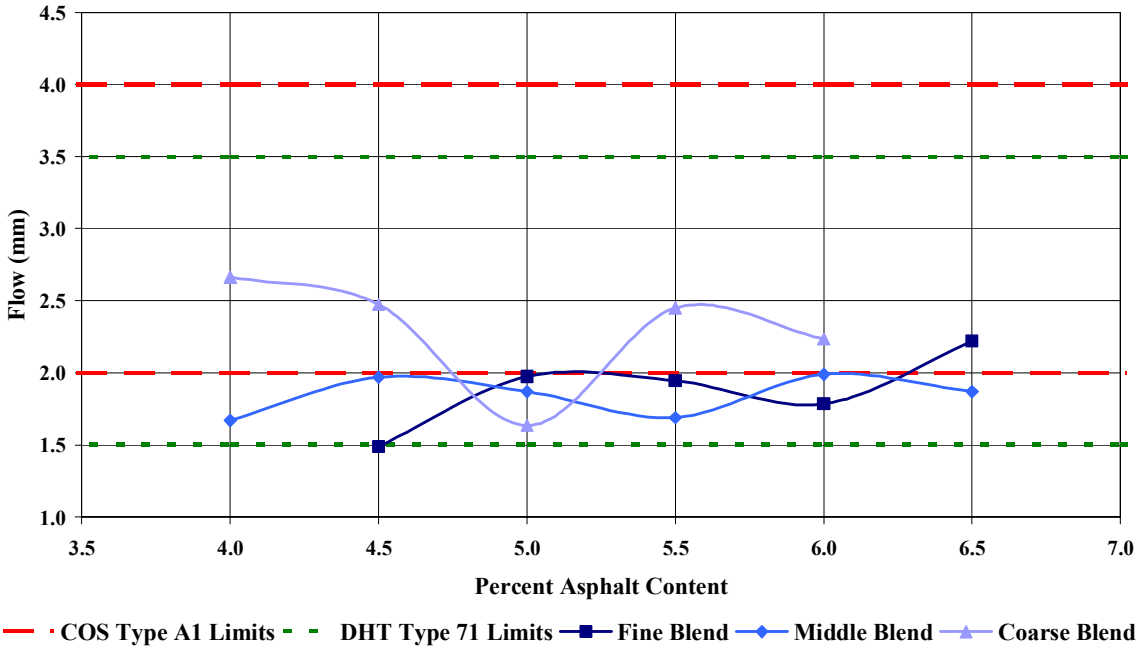

Figure 3.11 75 Blow Marshall Flow

The fine blend Marshall stability peaked at 6.0 percent asphalt content, the middle blend peaked at 5.0 percent asphalt content, while the coarse blend peaked at 5.5 percent asphalt content. Based on the premise that a higher Marshall stability value will result in a stronger asphalt concrete mix in the field, these trends may indicate that the asphalt cement content for optimum performance in the field would be that which yields the highest Marshall stability. It should be noted that none of the blend gradations met stability requirements. This may be due to the roundness of the coarse aggregate, although coarse aggregate angularity specifications were satisfied.

No clear Marshall flow trend with respect to asphalt content was apparent for any of the blend gradations. This may be a result of not using anti-strip in the mixes.

3.5 SHRP Superpave^{TM} Level I Gyratory Mix Analysis

A mix analysis was performed using SHRP Superpave^{TM} Level I gyratory compaction protocols for the fine, middle, and coarse blend gradations. Specimen preparation and gyratory compaction was performed as specified in AASHTO TP4 (AASHTO 1995). Bulk specific gravity and VTM compaction profiles of the gyratory compacted samples are illustrated in Appendix A. The traffic level for this research was 3 million ESALs and the high air temperature for Saskatchewan was less than 39^{o}C. Therefore, N_{ini}, N_{des}, and N_{max} used in the experimental design were 8, 96, and 152 gyrations, respectively, as shown in Table 2.9.

Due to the preliminary nature of this research and material constraints, each Superpave^{TM} mix design consisted of only one repeat gyratory compacted sample at 4.0, 4.5, 5.0, 5.5, 6.0, and 6.5 percent asphalt content by weight of dry aggregate. During sample preparation, the fine blend sample containing 4.0 percent asphalt was found to be too “dry” and did not provide a visually acceptable continuum sample. Similarly, the coarse blend sample containing 6.5 percent asphalt was found to be too “wet”. Therefore the data for these samples were not included in the analysis.

3.5.1 Density

Table 3.8 summarizes the density results of the three blend gradations for the gyratory compacted samples. Figure 3.12 through Figure 3.14 illustrate the density results of the SHRP gyratory compacted samples with respect to the Marshall samples.

Table 3.8 Superpave™ Mix Design Density Results

	Blend Gradation	Percent Asphalt Content					
		4.0	4.5	5.0	5.5	6.0	6.5
Density at N_{ini} (kg/m³)	**Fine**	---	2111	2106	2115	2119	2151
	Middle	2094	2114	2130	2142	2164	2149
	Coarse	2131	2106	2133	2157	2144	---
% of Maximum Density at N_{ini}	**Fine**	---	0.85	0.87	0.87	0.90	0.92
	Middle	0.87	0.89	0.91	0.90	0.91	0.92
	Coarse	0.88	0.88	0.90	0.91	0.92	---
Density at N_{des} (kg/m³)	**Fine**	---	2275	2270	2292	2292	2328
	Middle	2255	2294	2305	2321	2366	2347
	Coarse	2295	2274	2305	2344	2323	---
% of Maximum Density at N_{des}	**Fine**	---	0.96	0.96	0.97	0.96	0.98
	Middle	0.93	0.95	0.95	0.96	0.97	0.97
	Coarse	0.95	0.95	0.96	0.97	0.96	---
Density at N_{max} (kg/m³)	**Fine**	---	2299	2298	2318	2319	2353
	Middle	2280	2325	2330	2346	2392	2374
	Coarse	2319	2301	2332	2370	2352	---
% of Maximum Density at N_{max}	**Fine**	---	0.93	0.95	0.96	0.98	1.00
	Middle	0.94	0.98	0.99	0.99	1.00	1.00
	Coarse	0.96	0.96	0.98	1.00	1.00	---

The density trends of the Marshall and SHRP gyratory compacted samples were similar with respect to asphalt content for all blend gradations. The gyratory density trends of N_{des} and N_{max} were similar to each other, with the density at N_{max} being higher than at N_{des} for all blend gradations. This would be expected given that the same sample will have been subjected to more gyrations at N_{max} than N_{des}, therefore the sample will have a higher density at N_{max}.

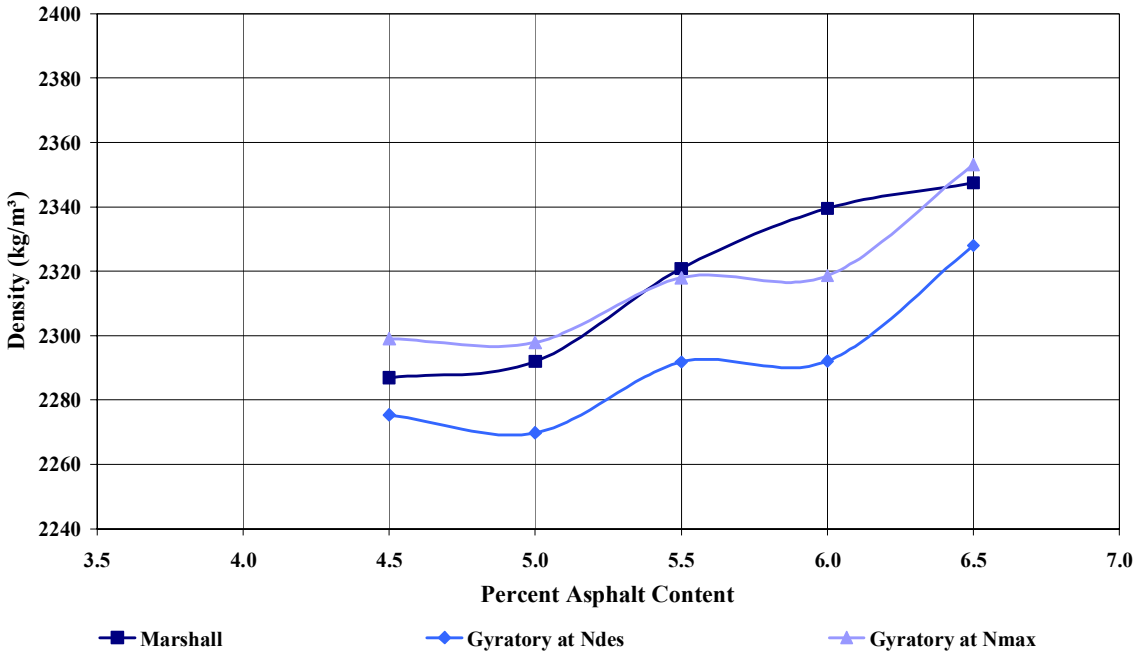

Figure 3.12 Fine Blend 75 Blow Marshall and Superpave™ Density

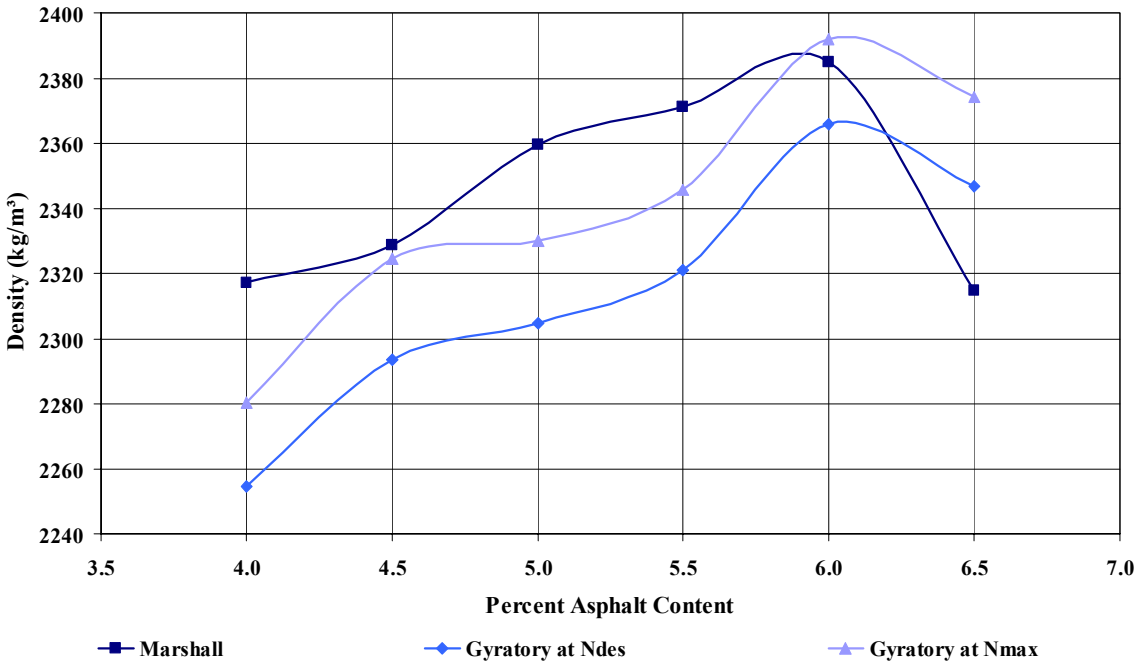

Figure 3.13 Middle Blend 75 Blow Marshall and Superpave™ Density

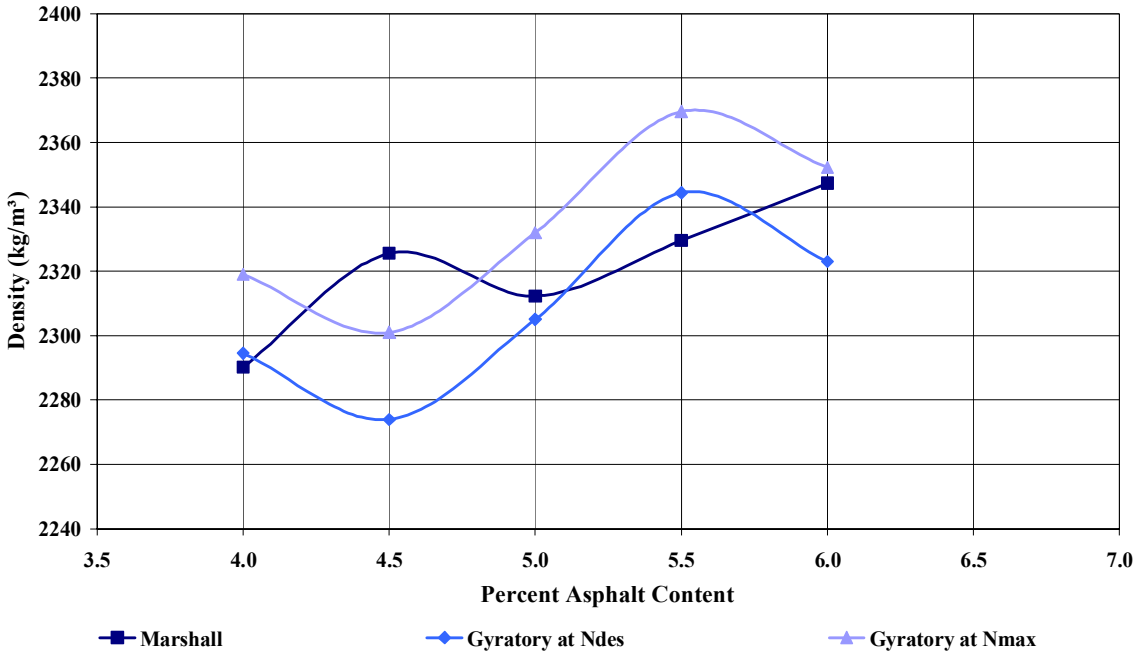

Figure 3.14 Coarse Blend 75 Blow Marshall and Superpave™ Density

The fine blend gyratory compacted samples increased in density with increasing asphalt content. The middle blend gyratory compacted samples increased in density with increasing asphalt content but peaked at 6.0 percent and subsequently decreased. The coarse blend gyratory compacted samples increased in density with increasing asphalt content but peaked at 5.5 percent asphalt content and subsequently decreased. The decrease in density of the middle and coarse blend gradations may be an indication of excessive asphalt content, filling the VMA with lower-density asphalt cement instead of higher density aggregate.

To illustrate the variation in mix density as the aggregate gradation deviates from the maximum density line, the density of the three mixes was compared at 6.0 percent asphalt content. An asphalt content of 6.0 percent was chosen since this produced the maximum density for the middle blend, which was the closest of the three aggregate blends to the maximum density line.

When the density of each mix was compared at 6.0 percent asphalt content, as illustrated in Figure 3.15, it is clear that the middle blend had a higher density than the fine and coarse blends. Therefore, the closer the aggregate blend gradation is to the

maximum density line, the higher the density of the compacted sample. As the aggregate gradation moves away from the maximum density line, the mix becomes more "open", resulting in a lower density. The middle blend had the highest density and the fine blend had the lowest density for both the Marshall and gyratory samples. However, the density of the fine blend gyratory sample was lower than for the fine blend Marshall. This trend was not expected, given the higher compactive shear effort and particle reorientation in the gyratory compactor relative to the Marshall impact hammer, which should increase sample compaction and therefore increase density.

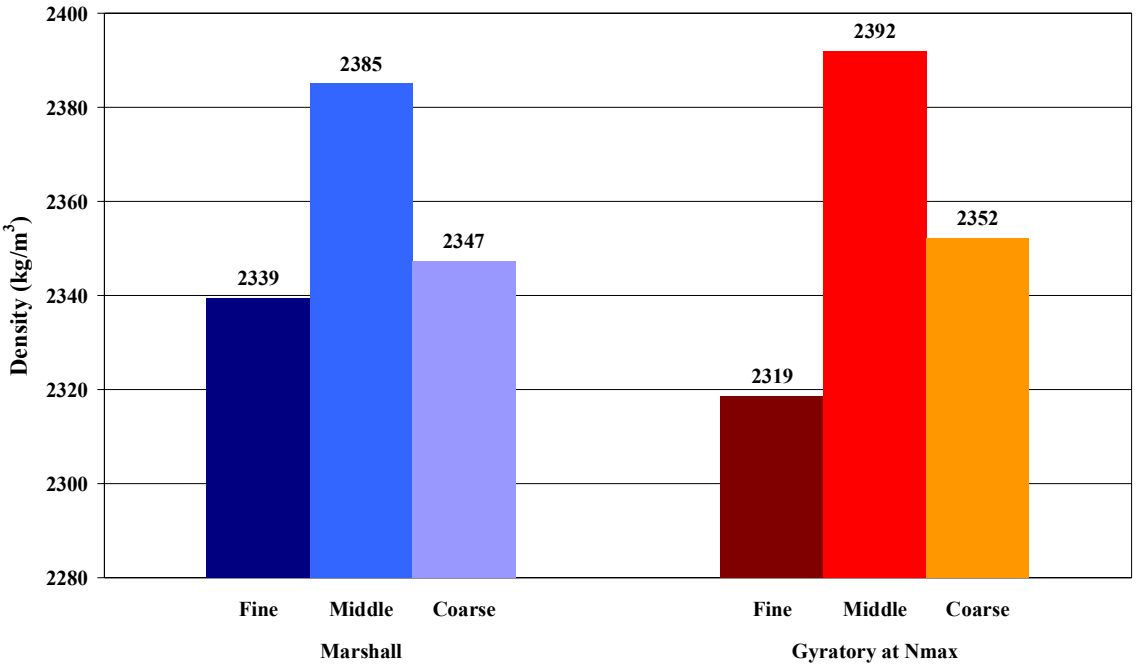

Figure 3.15 Density at 6.0 Percent Asphalt Content

3.5.2 Voids in the Total Mix

Table 3.9 summarizes the VTM results of the three blend gradations for the gyratory compacted samples at N_{ini}, N_{des}, and N_{max}. The VTM compaction profiles of the gyratory compacted samples are illustrated in Appendix B. Figure 3.16 through Figure 3.18 illustrate the VTM results of the three blend gradations from both the Marshall and SHRP gyratory mix designs. As seen in Table 3.9, all gyratory samples met the minimum 11.0 percent VTM requirement at N_{ini} except for the fine blend at 6.5

percent asphalt content, the middle blend at 6.0 and 6.5 percent, and the coarse blend at 6.0 percent.

The gyratory compacted samples had decreasing VTM with increasing asphalt content for all three blend gradations, except for the middle blend which plateaued between 5.0 percent and 5.5 percent asphalt content. There was a general correlation between the decreasing VTM with increasing asphalt content of the Marshall and gyratory samples for each blend gradation. However, it should be noted that the VTM values were lower for the Marshall samples than the gyratory samples. This trend was not expected, given the higher compactive shear effort and particle reorientation in the gyratory compactor relative to the Marshall impact hammer which should increase sample compaction and therefore decrease VTM.

The gyratory VTM trends of N_{des} and N_{max} were consistently similar, with the VTM at N_{des} being consistently higher than at N_{max} for all blend gradations. This would be expected given that the same sample will have been subjected to more gyrations at N_{max} than N_{des}, therefore the sample will have lower VTM at N_{max}.

Table 3.9 Superpave™ Mix Design VTM Results

	Blend Gradation	Asphalt Content (%)					
		4.0	**4.5**	**5.0**	**5.5**	**6.0**	**6.5**
VTM at N_{ini} (%)	**Fine**	---	15.8	14.1	13.7	11.2	9.4
	Middle	15.0	13.1	10.8	11.5	10.6	10.4
	Coarse	13.7	14.2	12.6	11.0	10.0	---
VTM at N_{des} (%)	**Fine**	---	9.3	7.4	6.6	4.0	2.0
	Middle	8.4	5.7	3.5	4.1	2.3	2.2
	Coarse	7.1	7.4	5.5	3.3	2.5	---
VTM at N_{max} (%)	**Fine**	---	8.3	6.2	5.5	2.9	0.9
	Middle	7.4	4.4	2.4	3.1	1.2	1.0
	Coarse	6.1	6.3	4.4	2.2	1.3	---

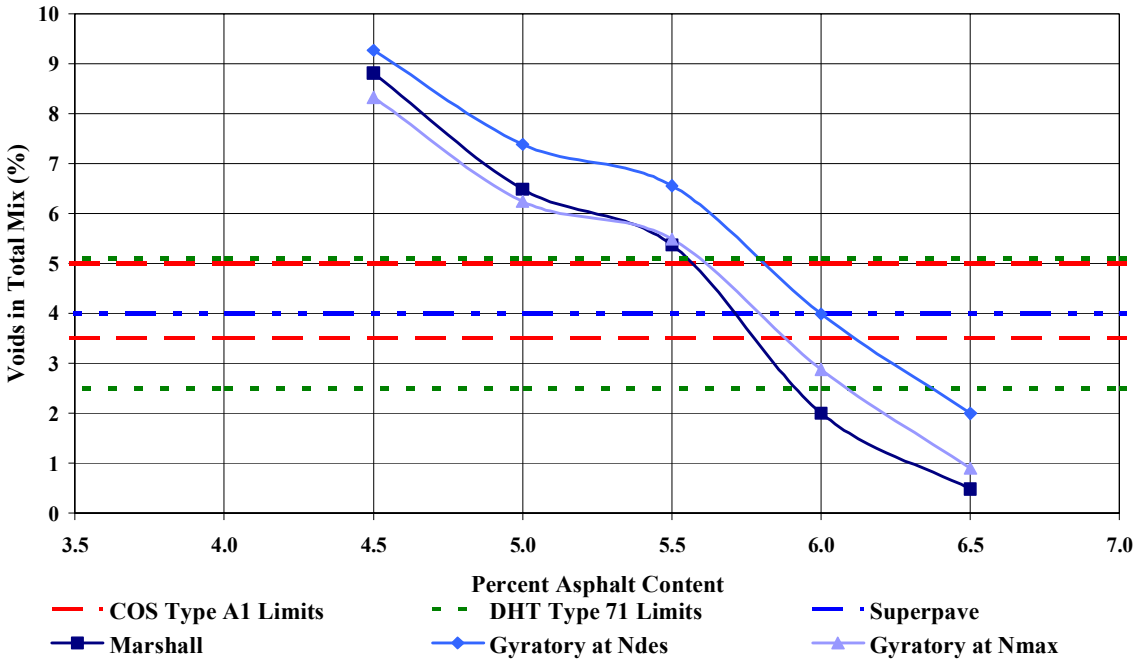

Figure 3.16 Fine Blend 75 Blow Marshall and Gyratory VTM

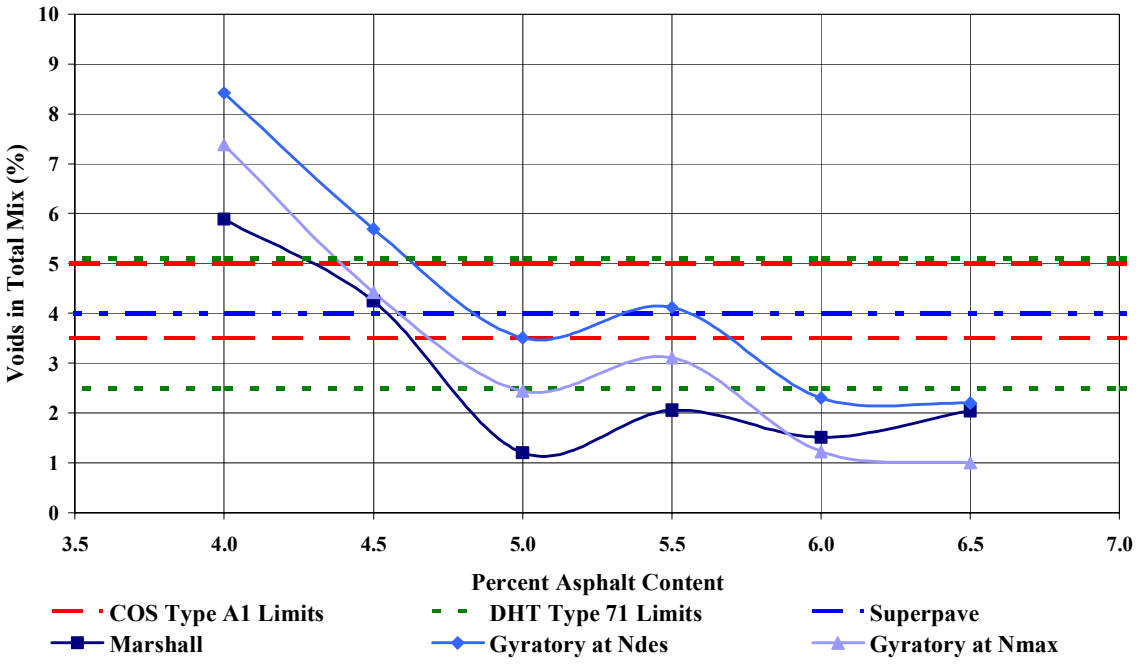

Figure 3.17 Middle Blend 75 Blow Marshall and Gyratory VTM

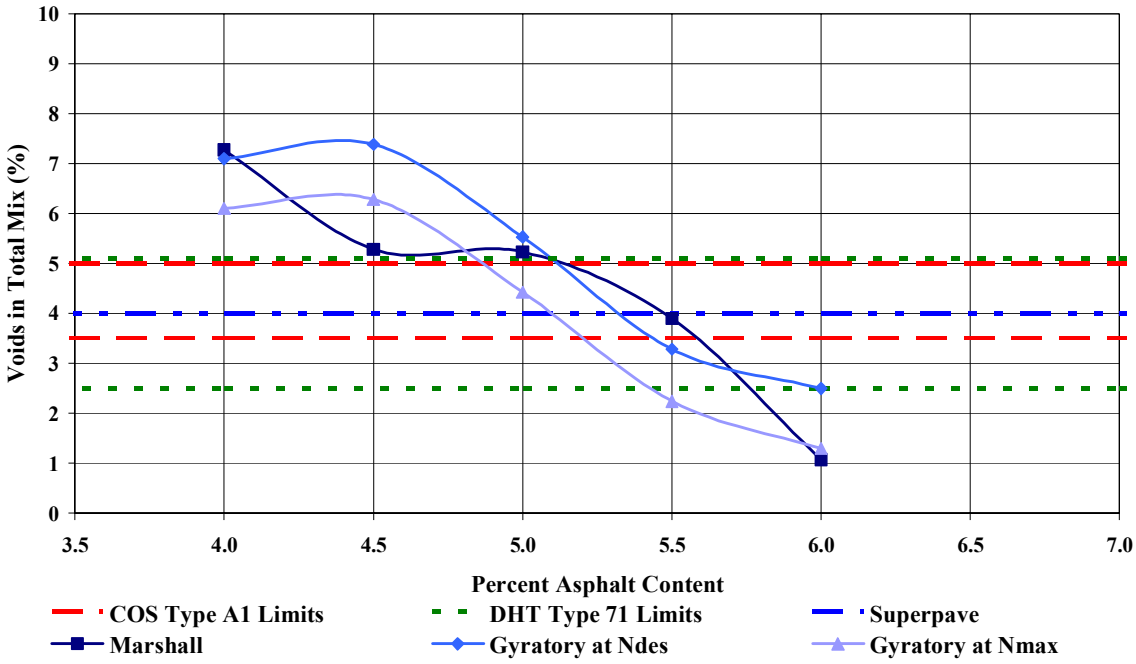

Figure 3.18 Coarse Blend 75 Blow Marshall and Gyratory VTM

Figure 3.19 through Figure 3.21 illustrate the range of asphalt contents that met DHT, COS, and Superpave™ VTM specifications for the fine, middle, and coarse blend gradations. The fine blend Marshall mix design met the DHT VTM criteria between 5.4 and 6.0 percent asphalt content, met the COS criteria between 5.4 and 5.8 percent, and met the Superpave™ criteria at 5.7 percent. The fine blend gyratory mix design at N_{des} met the DHT VTM criteria between 5.7 and 6.3 percent asphalt content, met the COS criteria between 5.7 and 6.1 percent, and met the Superpave™ criteria at 4.9 percent. The fine blend gyratory mix design at N_{max} met the DHT VTM criteria between 5.4 and 6.1 percent asphalt content, met the COS criteria between 5.4 and 5.8 percent, and met the Superpave™ criteria at 5.7 percent.

The middle blend Marshall mix design met the DHT VTM criteria between 4.2 and 4.9 percent asphalt content, met the COS criteria between 4.2 and 4.6 percent, and met the Superpave™ criteria at 4.6 percent. The middle blend gyratory mix design at N_{des} met the DHT VTM criteria between 4.9 and 5.8 percent asphalt content, met the COS criteria between 4.5 and 5.5 percent, and met the Superpave™ criteria at 5.3 percent. The middle blend gyratory mix design at N_{max} met the DHT VTM criteria

between 4.5 and 5.4 percent asphalt content, met the COS criteria between 4.5 and 5.1 percent, and met the Superpave™ criteria at 4.9 percent.

The coarse blend Marshall mix design met the DHT VTM criteria between 4.8 and 5.8 percent asphalt content, met the COS criteria between 4.8 and 5.6 percent, and met the Superpave™ criteria at 5.5 percent. The coarse blend gyratory mix design at N_{des} met the DHT VTM criteria between 4.9 and 5.8 percent asphalt content, met the COS criteria between 4.5 and 5.5 percent, and met the Superpave™ criteria at 5.4 percent. The coarse blend gyratory mix design at N_{max} met the DHT VTM criteria between 4.8 and 5.5 percent asphalt content, met the COS criteria between 4.8 and 5.2 percent, and met the Superpave™ criteria at 5.1 percent.

The trends in asphalt content that meet VTM specifications indicate that the fine blend requires a higher asphalt cement content than the middle and coarse blends in order to meet volumetric specifications. This correlates with empirical mix design inference, however would have to be confirmed with repeat testing.

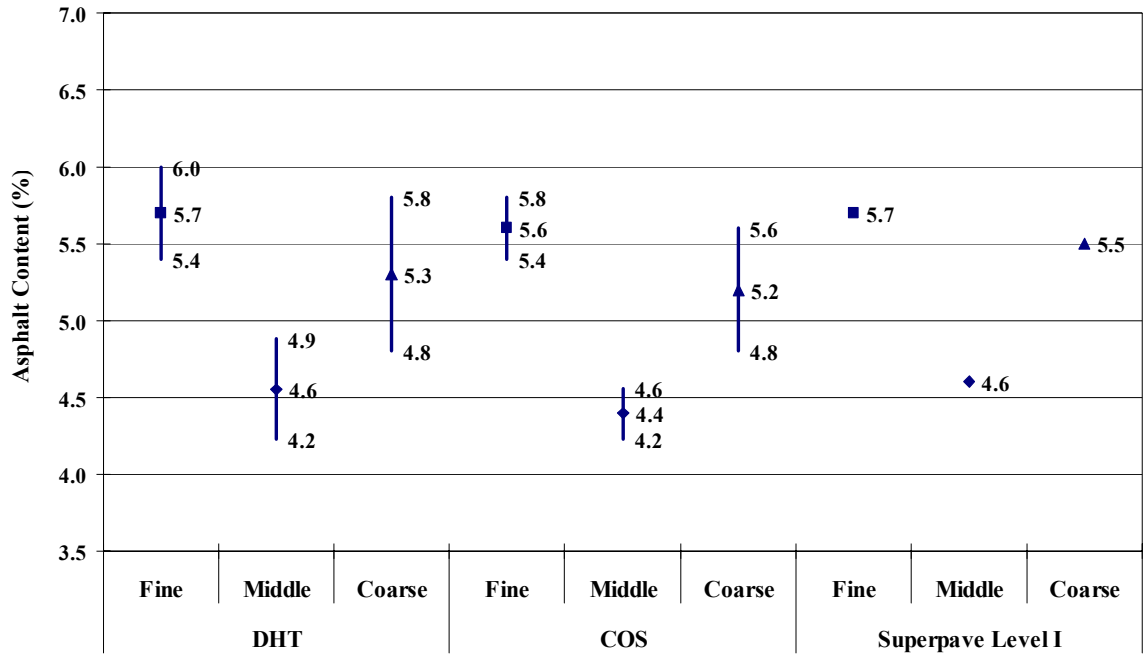

Figure 3.19 75 Blow Marshall Asphalt Content Ranges for Acceptable VTM Specifications

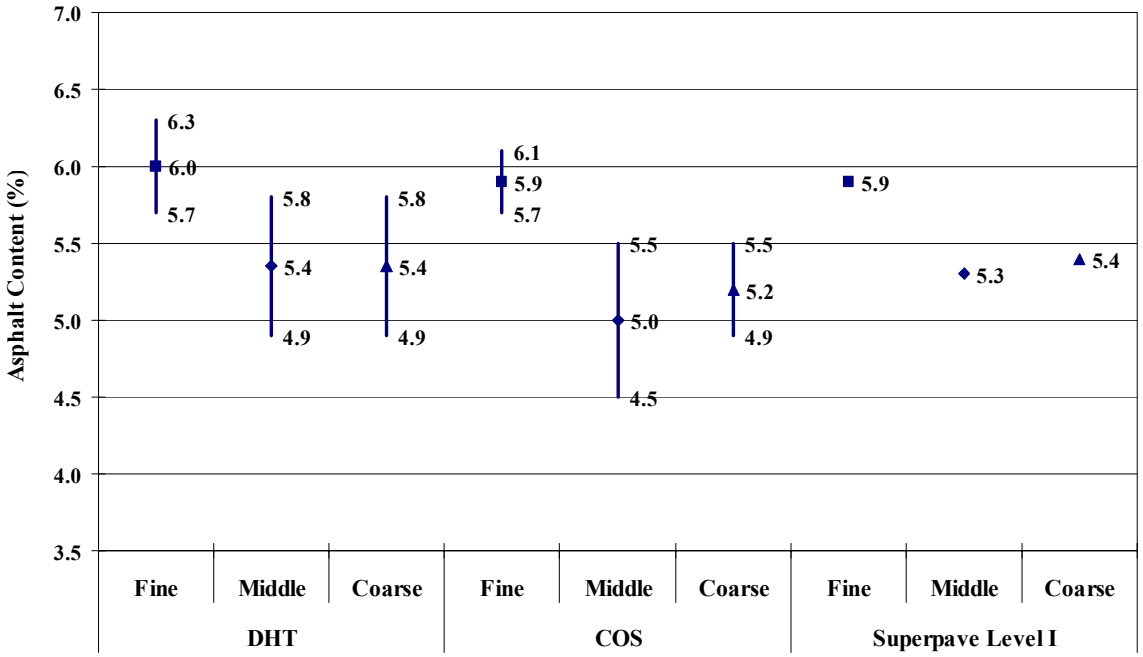

Figure 3.20 Superpave™ Asphalt Content Ranges for Acceptable VTM Specifications at N_{des}

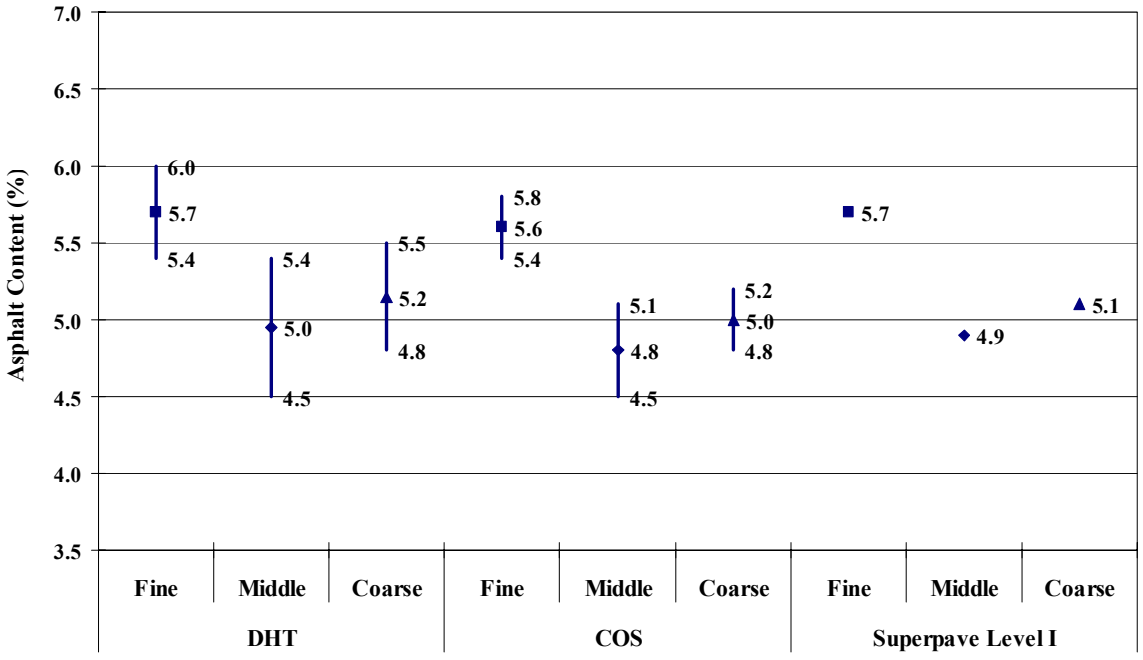

Figure 3.21 Superpave™ Asphalt Content Ranges for Acceptable VTM Specifications at N_{max}

The coarse blend Marshall samples met VTM requirements for a wider range of asphalt contents relative to the fine and middle blends. As this was not observed in the gyratory samples, this could have been caused by insufficient volume in the 102 mm Marshall mould to allow the coarse aggregate particles to become re-orientated, resulting in large void spaces which needed to be filled with asphalt cement to decrease the VTM to meet specifications. It is suspected that this trend was not apparent with the gyratory samples since the gyratory compactor had more ability to knead the aggregate into place in the larger 150 mm mould. This trend was observed to be consistent with other research (Carlberg 2003).

The acceptable range of asphalt contents of the Superpave^{TM} gyratory compacted samples were generally higher than the range in the Marshall compacted samples. This trend was unexpected since the nature of compaction in the gyratory compactor should increase compaction of the aggregate skeleton relative to the Marshall hammer, requiring less asphalt cement to fill the VMA to meet VTM requirements.

The acceptable asphalt content range for the gyratory compacted samples for VTM specifications was observed to be lower for N_{max} than N_{des}. The relatively large decrease in VTM from N_{des} to N_{max} may be an indication that the mixes would collapse under shear loading in the field.

The acceptable range in asphalt cement contents for the middle blend were typically lower or equal to the acceptable asphalt contents for the fine and coarse blends. This could have been due to the uniform gradation of the middle blend relative to the fine and coarse blends.

The asphalt content ranges for acceptable VTM specifications ranged from 0.6 to 1.2 percent lower for the middle blend relative to the fine and coarse blend gradations for the Marshall samples, compared to 0.1 to 0.9 percent lower for the SHRP Superpave^{TM} gyratory samples compacted to N_{max}. Therefore, the Marshall samples appeared to be more responsive to changes in the blend gradations than the gyratory compacted samples.

3.5.3 Voids in the Mineral Aggregate

Table 3.10 summarizes the VMA results of the three blend gradations for the gyratory compacted samples at N_{des} and N_{max}. Figure 3.22 through Figure 3.24 illustrate the VMA results of the three blend gradations from the Marshall and gyratory mix designs. The Marshall VMA values were higher than gyratory VMA values, which was likely a result of kneading compaction by the gyratory compactor. Other research has also indicated that a sample compacted with the gyratory compactor has a lower VMA than the same sample compacted with a Marshall impact compactor (D'Angelo *et al.* 1995, Carlberg 2003).

The gyratory compacted samples decreased in VMA with increasing asphalt content for all three blend gradations. The coarse blend Marshall and gyratory VMA trends were dissimilar in that the Marshall VMA dipped at 4.5 percent asphalt content while the gyratory VMA peaked at 4.5 percent. The gyratory VMA trends at N_{des} and N_{max} were similar, with the VMA at N_{des} being higher than at N_{max} for all blend gradations, as would be expected due to the increased compaction and therefore decreased voids.

Table 3.10 Gyratory Mix Design VMA Results

	Blend Gradation	Asphalt Content (%)					
		4.0	4.5	5.0	5.5	6.0	6.5
VMA at N_{des} (%)	Fine	---	13.2	13.4	12.6	12.6	11.2
	Middle	14.6	13.1	12.7	12.1	10.4	11.1
	Coarse	13.4	14.2	13.0	11.5	12.4	---
VMA at N_{max} (%)	Fine	---	11.1	11.2	10.4	10.4	9.5
	Middle	12.1	10.1	10.1	9.4	8.3	8.7
	Coarse	10.8	10.8	9.6	8.6	9.4	---

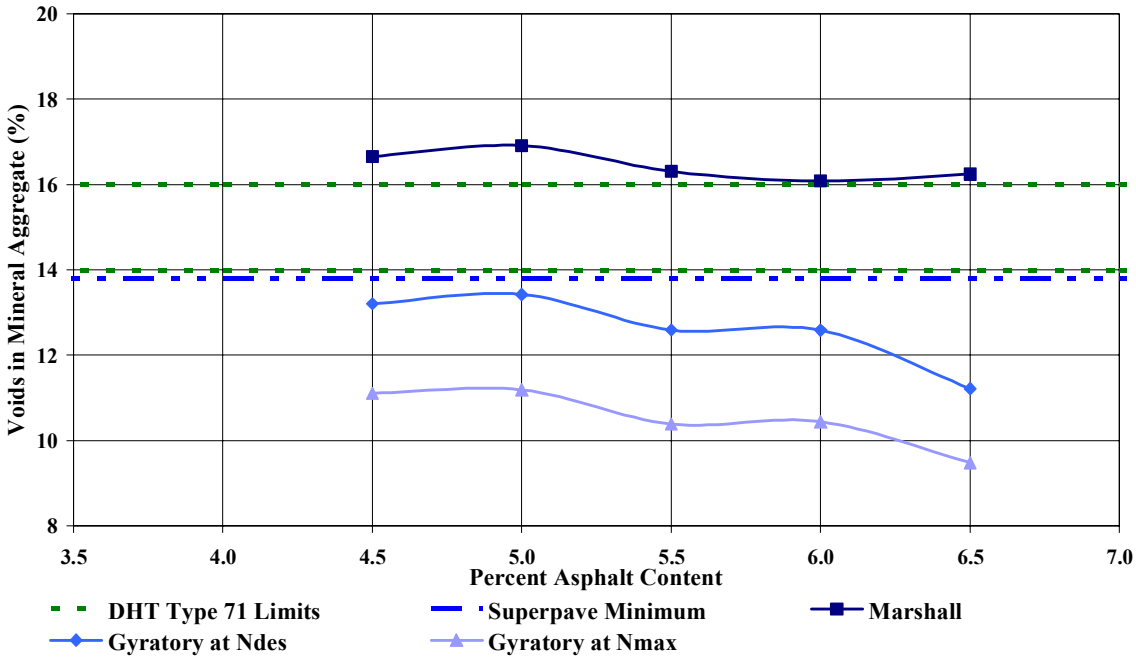

Figure 3.22 Fine Blend 75 Blow Marshall and Superpave™ VMA

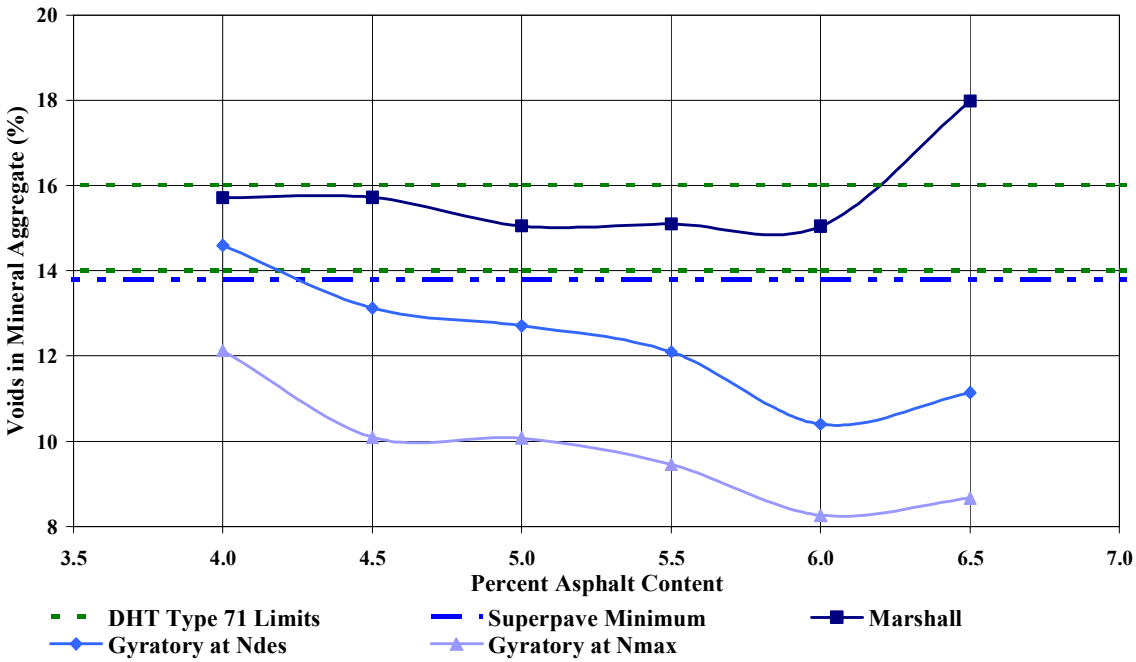

Figure 3.23 Middle Blend 75 Blow Marshall and Superpave™ VMA

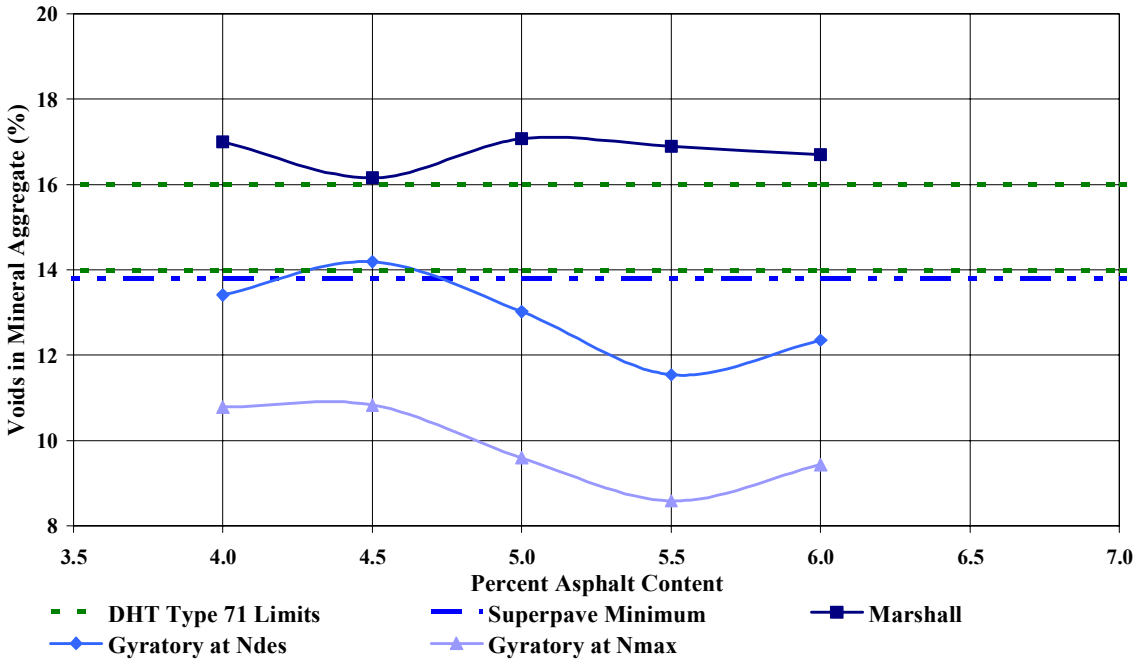

Figure 3.24 Coarse Blend75 Blow Marshall and Superpave™ VMA

Figure 3.25 and Figure 3.26 illustrate the range of asphalt contents that met DHT and Superpave™ VMA specifications for the fine, middle, and coarse blend gradations.

The fine blend Marshall mix design VMA values were too high to meet the DHT VMA criteria. However, they did meet the Superpave™ criteria between 4.5 and 6.5 percent. The fine blend gyratory mix design VMA values at N_{des} were too low to meet the DHT VMA criteria. However, they did meet the Superpave™ criteria between 4.0 and 5.0 percent asphalt content. The fine blend gyratory mix design VMA values at N_{max} were too low to meet either the DHT or the Superpave™ VMA criteria.

The middle blend Marshall mix design met the DHT VMA criteria between 4.0 and 6.2 percent asphalt content and met the Superpave™ criteria between 4.0 and 6.5 percent. The middle blend gyratory mix design at N_{des} met the DHT VMA criteria between 4.0 and 4.1 percent asphalt content and met the Superpave™ criteria between 4.0 and 4.5 percent. The middle blend gyratory mix design VMA values at N_{max} were too low to meet either the DHT or the Superpave™ VMA criteria.

The coarse blend Marshall mix design VMA values were too low to meet the DHT VMA criteria. However, the coarse blend did meet the Superpave™ criteria between 4.5 and 6.5 percent asphalt content. The coarse blend gyratory mix design VMA values at N_{des} were too low to meet the DHT VMA criteria. However the coarse blend did meet the Superpave™ criteria between 4.0 and 5.0 percent asphalt content. The coarse blend gyratory mix design VMA values at N_{max} were too low to meet either the DHT or the Superpave™ VMA criteria.

The asphalt content ranges which met acceptable VMA criteria were observed to be much wider than the VTM criteria, indicating that VMA may be an easier specification to meet than VTM. The VMA of the gyratory samples at N_{max} did not meet volumetric specifications likely due to the increased compaction relative to N_{des}. This may indicate that the mixes would collapse under heavy loading in the field or in urban traffic field state loadings. These results concur with empirical asphalt mix performance.

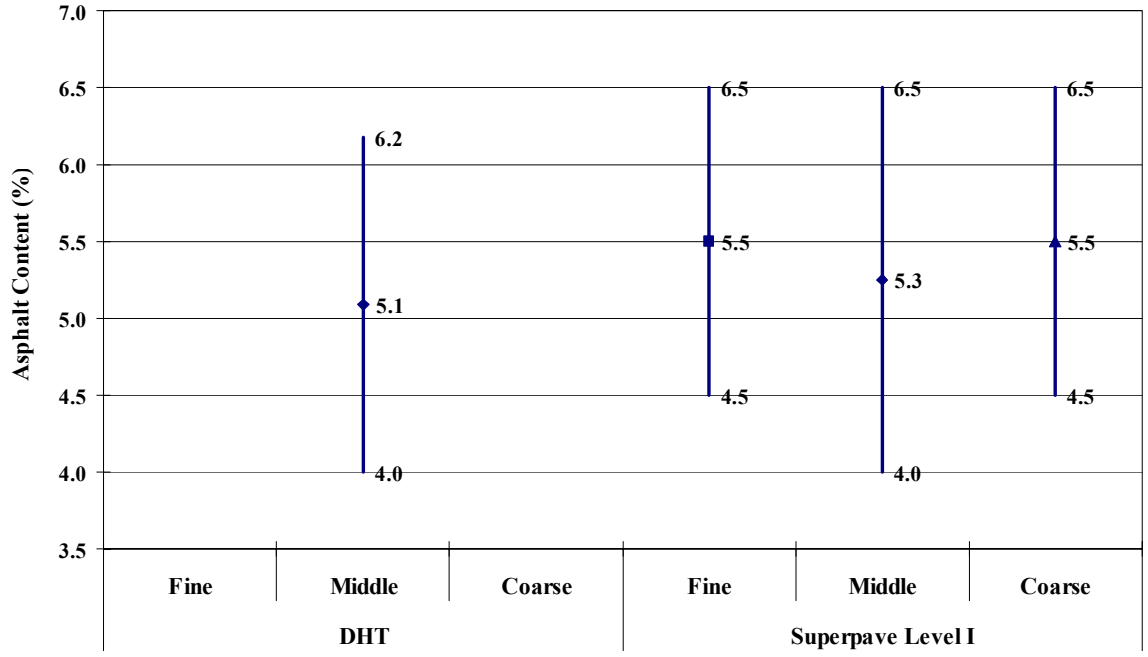

Figure 3.25 75 Blow Marshall Asphalt Content Ranges for Acceptable VMA Specifications

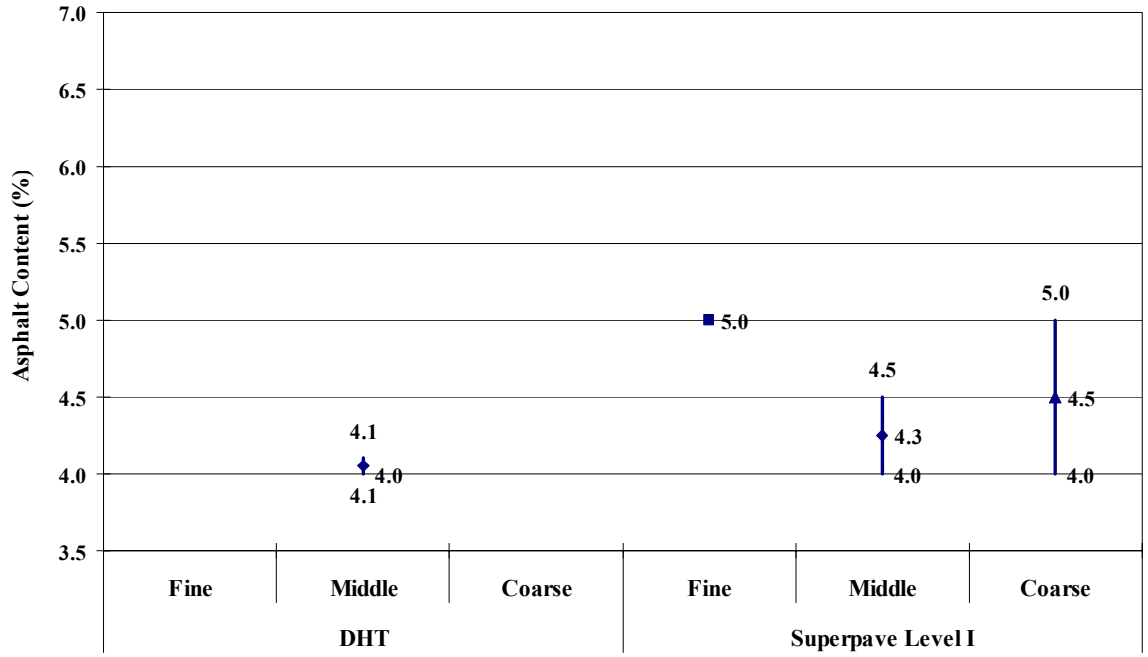

Figure 3.26 Superpave^{TM} Asphalt Content Ranges for Acceptable VMA Specifications at N_{des}

3.5.4 Voids Filled with Asphalt

Table 3.11 summarizes the gyratory VFA results at N_{des} and N_{max}. Figure 3.27 through Figure 3.29 illustrate the VFA results of the three blend gradations from both the Marshall and SHRP gyratory mix designs.

The Marshall and gyratory samples were observed to have similar trends in VFA with respect to asphalt content for all blend gradations. High VFA at high asphalt contents may indicate excessive asphalt content, filling too much of the VMA, resulting in excessive film thickness, decreasing interparticle friction and therefore reduced the strength of the mix.

The Marshall VFA results were observed to be higher than the gyratory VFA results. This was unexpected since the nature of compaction in the gyratory compactor should increase compaction of the aggregate skeleton relative to the Marshall hammer, resulting in lower VMA and therefore higher VFA. Further investigation into the mix aggregate skeleton would have to be performed using several repeat samples before conclusions may be made between the two compaction methods.

The gyratory VFA trends at N_{des} and N_{max} were similar with respect to asphalt content, with the VFA at N_{des} being higher than at N_{max} at lower asphalt contents and the VFA at N_{max} lower than N_{des} at higher asphalt contents for the middle and coarse blend gradations. This trend is likely due to discrepancy in the measurement apparatus.

Table 3.11 Gyratory Mix Design VFA Results

	Blend Gradation	Asphalt Content (%)					
		4.0	4.5	5.0	5.5	6.0	6.5
VFA at N_{des} (%)	Fine	---	29.8	45.0	47.9	68.3	82.4
	Middle	42.3	56.7	72.4	66.0	77.9	80.5
	Coarse	47.1	48.0	57.5	71.6	79.7	---
VFA at N_{max} (%)	Fine	---	25.0	44.2	47.1	72.4	90.4
	Middle	39.2	56.2	75.8	67.1	85.2	88.1
	Coarse	43.4	42.0	53.9	73.9	86.4	---

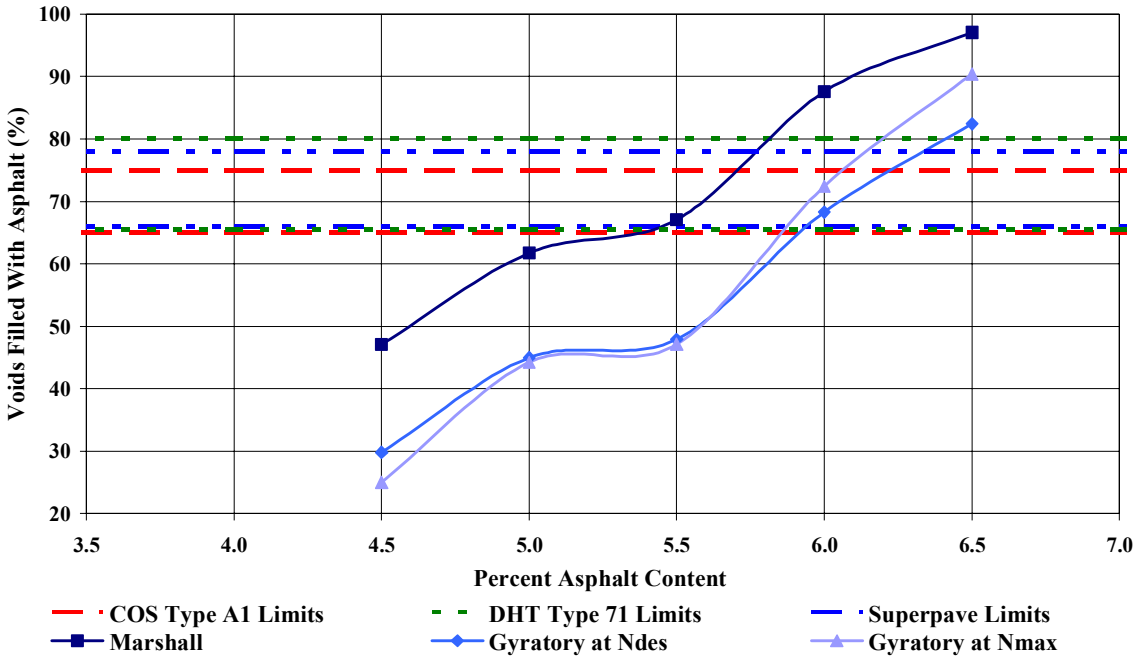

Figure 3.27 Fine Blend 75 Blow Marshall and Superpave™ VFA

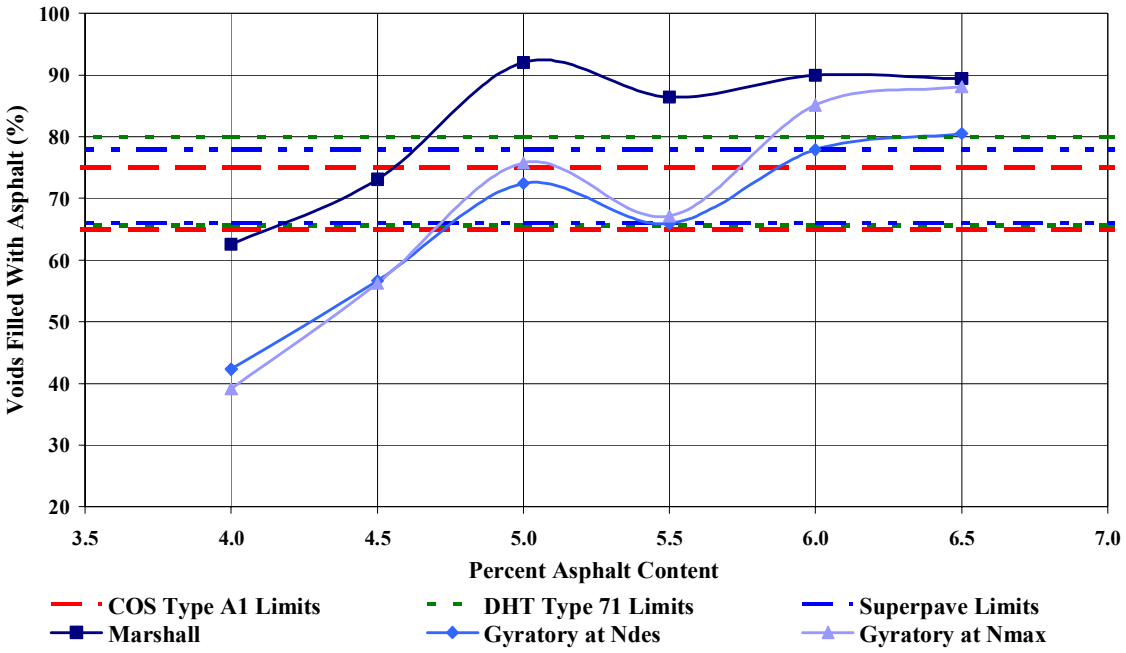

Figure 3.28 Middle Blend 75 Blow Marshall and Superpave™ VFA

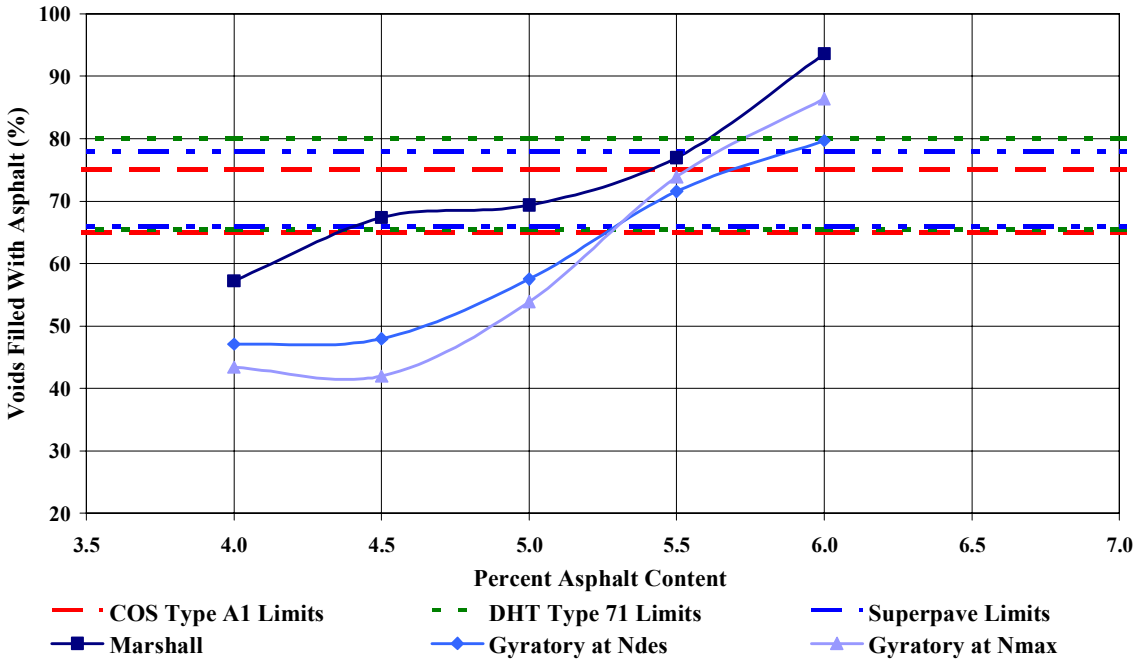

Figure 3.29 Coarse Blend 75 Blow Marshall and Superpave™ VFA

Figure 3.30 through Figure 3.32 illustrate the range of asphalt cement contents that met DHT, COS, and Superpave™ VFA specifications for the fine, middle, and coarse blend gradations.

The fine blend Marshall mix design met the DHT VFA criteria between 5.2 and 5.8 percent asphalt content, met the COS criteria between 5.2 and 5.6 percent, and met the Superpave™ criteria between 5.2 and 5.7 percent. The fine blend gyratory mix design at N_{des} met the DHT VFA criteria between 5.8 and 6.4 percent asphalt content, met the COS criteria between 5.8 and 6.2 percent, and met the Superpave™ criteria between 5.8 and 6.4 percent. The fine blend gyratory mix design at N_{max} met the DHT VFA criteria between 5.7 and 6.0 percent asphalt content, met the COS criteria between 5.7 and 6.1 percent, and met the Superpave™ criteria between 5.7 and 6.2 percent.

The middle blend Marshall mix design met the DHT VFA criteria between 4.1 and 4.6 percent asphalt content, met the COS criteria between 4.1 and 4.5 percent, and met the Superpave™ criteria between 4.1 and 4.6 percent. The middle blend gyratory mix design at N_{des} met the DHT VFA criteria between 5.1 and 5.9 percent asphalt content, met the COS criteria between 5.1 and 5.6 percent, and met the Superpave™ criteria between 5.1 and 6.1 percent. The middle blend gyratory mix design at N_{max} met the DHT VFA criteria between 5.0 and 5.7 percent asphalt content, met the COS criteria between 5.0 and 5.5 percent, and met the Superpave™ criteria between 5.0 and 5.8 percent.

The coarse blend Marshall mix design met the DHT VFA criteria between 4.5 and 5.4 percent asphalt content, met the COS criteria between 4.5 and 5.1 percent, and met the Superpave™ criteria between 4.5 and 5.3 percent. The coarse blend gyratory mix design at N_{des} met the DHT VFA criteria between 5.3 and 5.9 percent asphalt content, met the COS criteria between 5.3 and 5.7 percent, and met the Superpave™ criteria between 5.3 and 5.9 percent. The coarse blend gyratory mix design at N_{max} met the DHT VFA criteria between 5.3 and 5.7 percent asphalt content, met the COS criteria between 5.3 and 5.6 percent, and met the Superpave™ criteria between 5.3 and 5.5 percent.

The asphalt cement content ranges that met VFA requirements for the Marshall mix designs were observed to be lower than the asphalt content ranges for the gyratory mix designs. This trend was unexpected since the nature of compaction in the gyratory compactor should increase compaction of the aggregate skeleton relative to the Marshall hammer, requiring less asphalt cement to fill the VMA to meet VFA requirements.

The acceptable asphalt cement content ranges were consistently lower at N_{max} than at N_{des} for the gyratory compacted samples, as would be expected due to the increased compaction, therefore less asphalt cement is required to fill the VMA to meet VFA requirements.

Similar to the VTM specifications, the acceptable asphalt contents for the middle blend were typically lower or equal to the acceptable asphalt contents for the fine and coarse blends. Similarities between the asphalt content ranges which met VTM and VFA specifications were expected since VFA is calculated based on VTM. The trend of acceptable asphalt contents was opposite to the density trends at 6.0 percent asphalt content, illustrating that the mixes which deviated from the maximum density line were more "open" and required higher asphalt contents to fill the voids in order to meet VFA specifications.

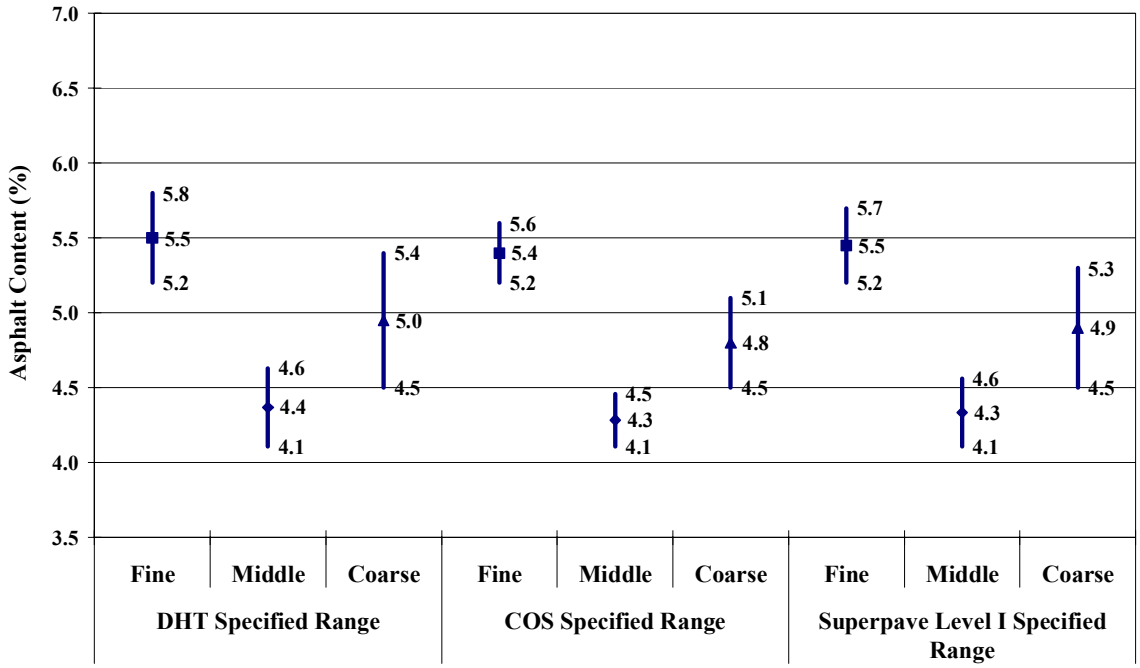

Figure 3.30 75 Blow Marshall Asphalt Content Ranges for Acceptable VFA Specifications

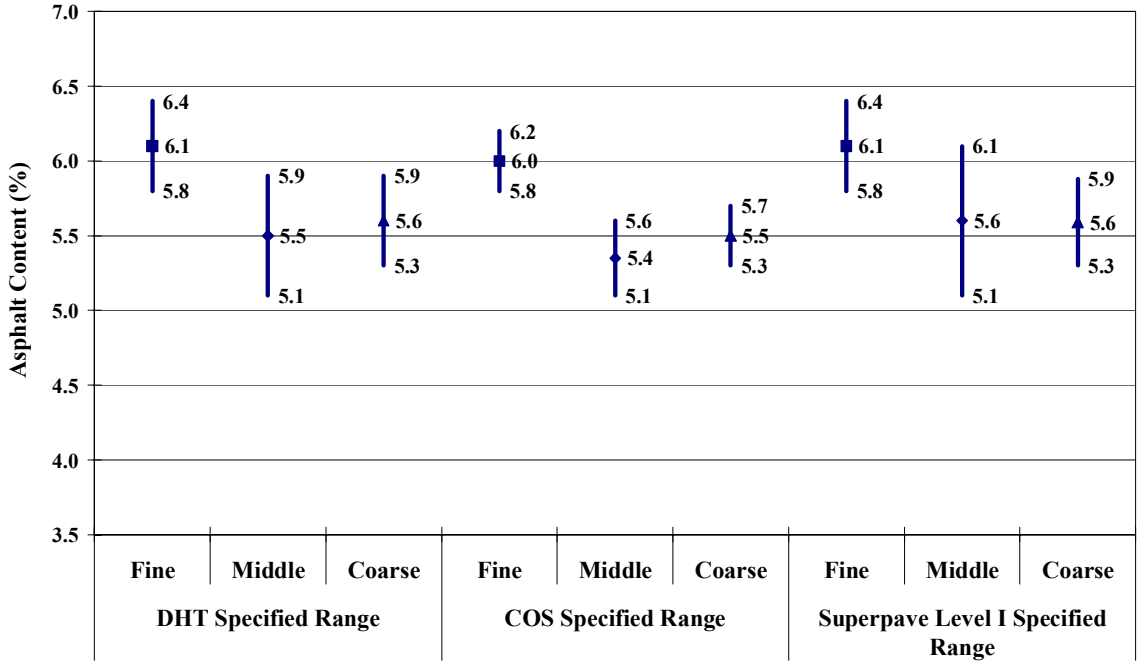

Figure 3.31 Superpave™ Asphalt Content Ranges for Acceptable VFA Specifications at N_{des}

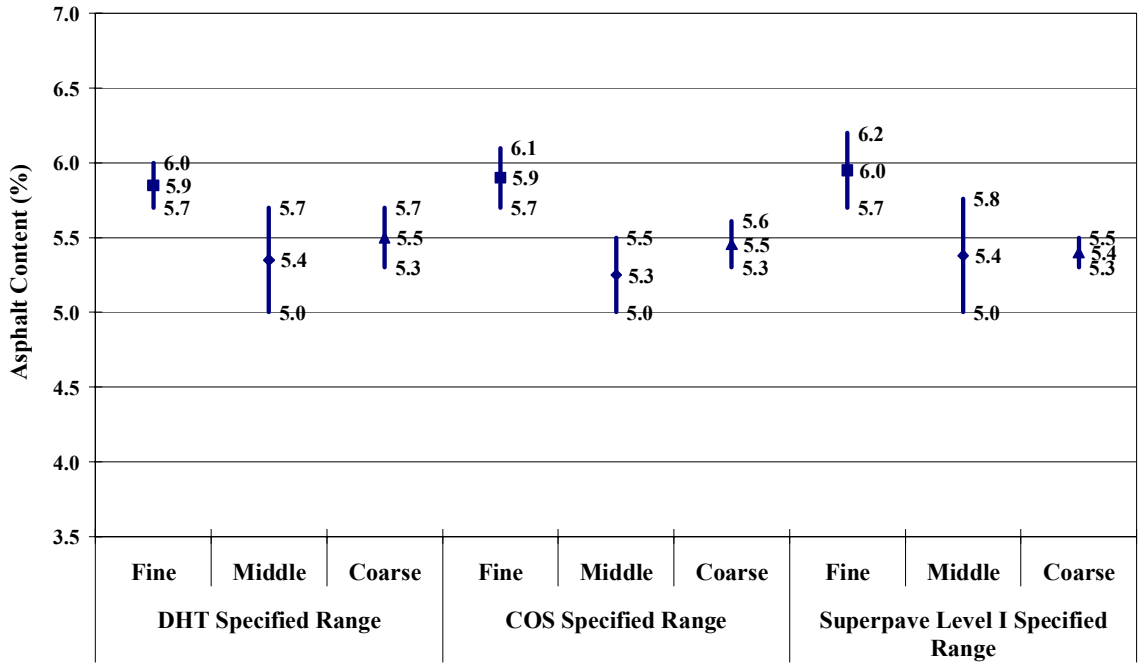

Figure 3.32 Superpave™ Asphalt Content Ranges for Acceptable VFA Specifications at N_{max}

The coarse blend Marshall samples met VFA requirements for a wider range of asphalt contents than the fine and middle blends. As this was not observed in the gyratory samples, this could have been caused by insufficient volume in the 102 mm Marshall mould to allow the coarse aggregate particles to become re-orientated resulting in large void spaces which needed to be filled with asphalt cement to increase the VFA to meet specifications. It is suspected that this trend was not apparent with the gyratory samples since the gyratory compactor had more ability to knead the aggregates into place in the larger 150 mm mould. This trend was consistent with other research (Carlberg 2003).

Based on VFA, the variation in acceptable asphalt contents between the three mix blend gradations is more pronounced for the Marshall samples than for the gyratory samples. Therefore, the Marshall samples appear to be more responsive to changes in the blend gradations than the gyratory compacted samples.

3.6 Summary

This chapter has presented the hot mix asphalt concrete mix types, aggregate and asphalt cement specifications, and compacted mix volumetric specifications employed in this research. Three hot mix asphalt concrete blends with different aggregate gradations were developed based on City of Saskatoon Type A1 and Saskatchewan Department of Highways and Transportation Type 71 dense graded asphalt concrete mixes. Marshall and SHRP gyratory compaction mix design methods were performed for each blend gradation. Volumetric analysis was performed on all asphalt contents for each blend gradation. The range of asphalt contents which met volumetric specifications was determined for each blend gradation.

Marshall stability requirements were not met, which may be due to the roundness of the coarse aggregate, although coarse aggregate angularity specifications were satisfied.

The asphalt contents corresponding to road agency volumetric specifications of the gyratory compacted samples were generally higher than for the Marshall compacted samples. This trend was unexpected since the nature of compaction in the gyratory compactor should increase compaction of the aggregate skeleton relative to the Marshall hammer, requiring less asphalt cement to fill the VMA to meet VTM requirements.

The Marshall VTM results were lower than the SHRP gyratory VTM results. The Marshall VFA results were higher than the SHRP gyratory VFA results. This was unexpected, given the higher compactive shear effort and particle reorientation in the gyratory compactor relative to the Marshall impact hammer which should increase sample compaction and therefore decrease VTM and increase VFA.

The asphalt content ranges for acceptable VTM and VFA specifications was observed to be higher for Marshall compacted samples relative to SHRP gyratory compacted samples. The decreased amount of asphalt cement in the coarse blend relative to the fine blend concurs with field experience. Mixes with lower asphalt cement content tend to be more stable relative to mixes with excessive asphalt cement contents. If an asphalt concrete mix is determined to be too dry, it may be flushed for

increased climatic durability. However, the only recourse for a pavement with excessive asphalt cement content is removal of the pavement. In addition mixes with lower asphalt cement content are more economical since asphalt cement is the most expensive component of asphalt concrete.

4.0 TRIAXIAL FREQUENCY SWEEP CHARACTERIZATION OF HOT MIX ASPHALT CONCRETE

This chapter presents the results of the triaxial frequency sweep characterization in the RaTT of typical Saskatchewan asphalt concrete mix types asphalt cement contents for typical traffic loads, traffic speeds, and temperatures. The primary mix design parameters were deviatoric stress state, frequency, and asphalt cement content. The secondary design parameter was temperature, and was employed to identify the variability of the primary design parameters. The material properties determined from the RaTT and their acceptable ranges that met COS, DHT, and SHRP Superpave^{TM} volumetric specifications were compared. The trends in the material properties were analyzed to evaluate the use of triaxial frequency sweep characterization in dense graded asphalt concrete mix designs.

4.1 Triaxial Frequency Sweep Characterization

Each gyratory compacted sample was subjected to triaxial frequency sweep characterization in the RaTT. Each sample was subjected to five loading frequencies at five traction magnitudes as summarized in Table 4.1 and Table 4.2 and illustrated in Figure 4.1.

The triaxial frequency sweep characterization performed in this research took approximately 30 minutes for each samples including five loading frequencies, five traction states, and inserting and removing the sample from the RaTT. The short test time allowed frequency sweep testing to be performed for one mix design at two test temperatures in the same day, making it feasible to addition the Superpave^{TM} Level I mix design volumetric analysis as a simple performance verification test.

Table 4.1 Triaxial Frequency Sweep Load Frequencies

Frequency Order	Axial Loading Frequency (Hz)
1	10.0
2	5.0
3	1.0
4	0.5
5	0.125

Table 4.2 Applied Triaxial Frequency Sweep Traction Magnitudes

Traction State Order	Maximum Axial Traction (kPa)	Minimum Axial Traction (kPa)	Confining Traction (kPa)	Resulting Deviatoric Stress (kPa)
1	200	50	50	150
2	300	75	75	225
3	400	100	100	300
4	600	150	150	450
5	800	200	200	600

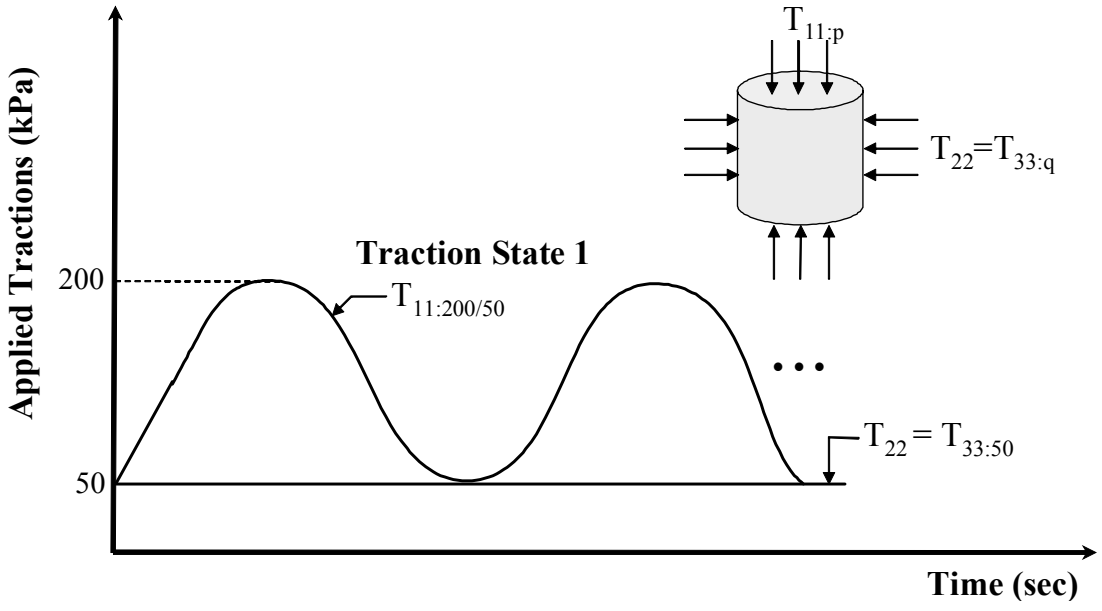

Figure 4.1 Applied Traction Magnitudes and Resulting Stress States

4.2 Analysis of RaTT Material Properties

Dynamic modulus, Poisson's ratio, and phase angle were determined from triaxial frequency sweep characterization in the RaTT. Appendix D through Appendix F illustrate the material property results plotted versus deviatoric stress state and versus frequency. It should be noted that the material property results were calculated from samples compacted to N_{max}. The material property results therefore correspond to the theoretical worst case scenario of pavement performance.

4.2.1 Dynamic Modulus

Dynamic modulus values calculated from the RaTT software are summarized in Table 4.3 and illustrated in Figure 4.2 and Figure 4.3. Dynamic modulus results plotted versus frequency and versus deviatoric stress state are illustrated in Appendix D.

Dynamic modulus plotted versus asphalt content is illustrated in Figure 4.3. As hypothesized, dynamic modulus was found to be higher at 25°C than at 60°C for all blend gradations. Based on the difference in dynamic modulus at 25°C and 60°C, asphalt concrete was found to behave differently depending on temperature. Therefore the range of service temperatures may be a necessary input when designing asphalt concrete. As also hypothesized, dynamic modulus decreased with increasing asphalt content for all blend gradations at both 25°C and 60°C.

The coarse blend exhibited the highest dynamic modulus at 25°C, indicating a stiffer mix, perhaps due to the higher proportion of coarse aggregate in the coarse blend gradation. The three blend gradations could not be differentiated at 60°C.

Table 4.3 Dynamic Modulus Results at 25°C and 60°C

Asphalt Content (%)	Blend Gradation	Dynamic Modulus (MPa)	
		25° C	60° C
4.0	Fine	---*	---*
	Middle	1219	580
	Coarse	1157	604
4.5	Fine	1293	501
	Middle	1236	531
	Coarse	1166	509
5.0	Fine	1279	475
	Middle	1254	516
	Coarse	1228	473
5.5	Fine	1241	457
	Middle	1179	462
	Coarse	1101	309
6.0	Fine	1220	455
	Middle	1241	342
	Coarse	1182	493
6.5	Fine	1227	403
	Middle	1057	339
	Coarse	---*	---*

* - Data not included due to inappropriate asphalt cement content for the mix

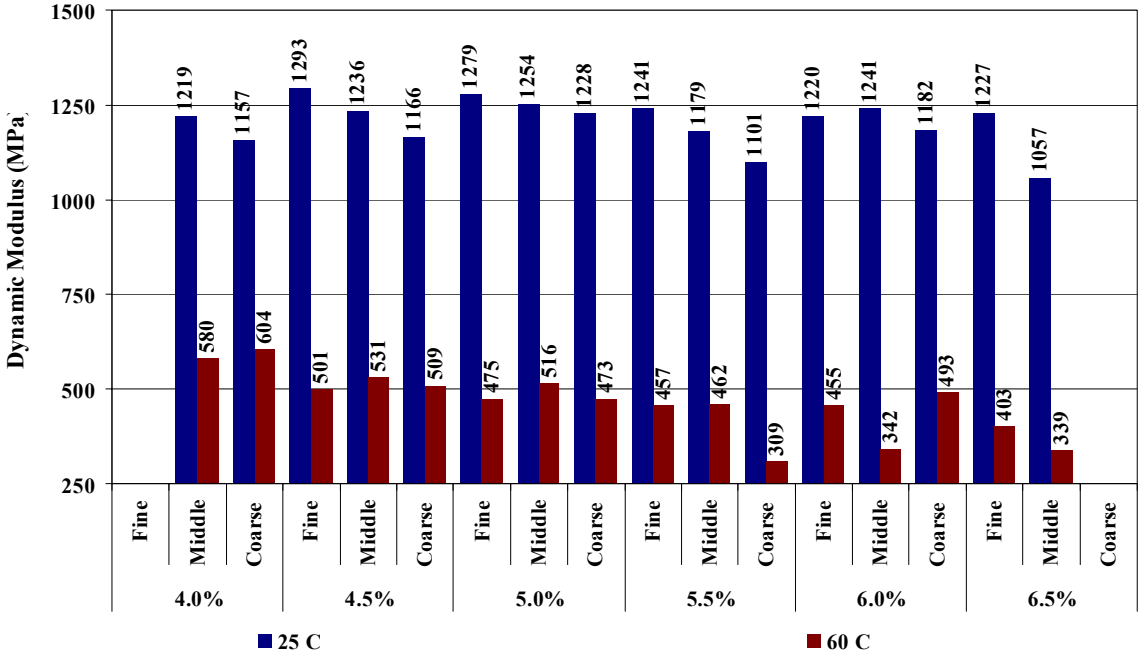

Figure 4.2 Dynamic Modulus Results at 25°C and 60°C

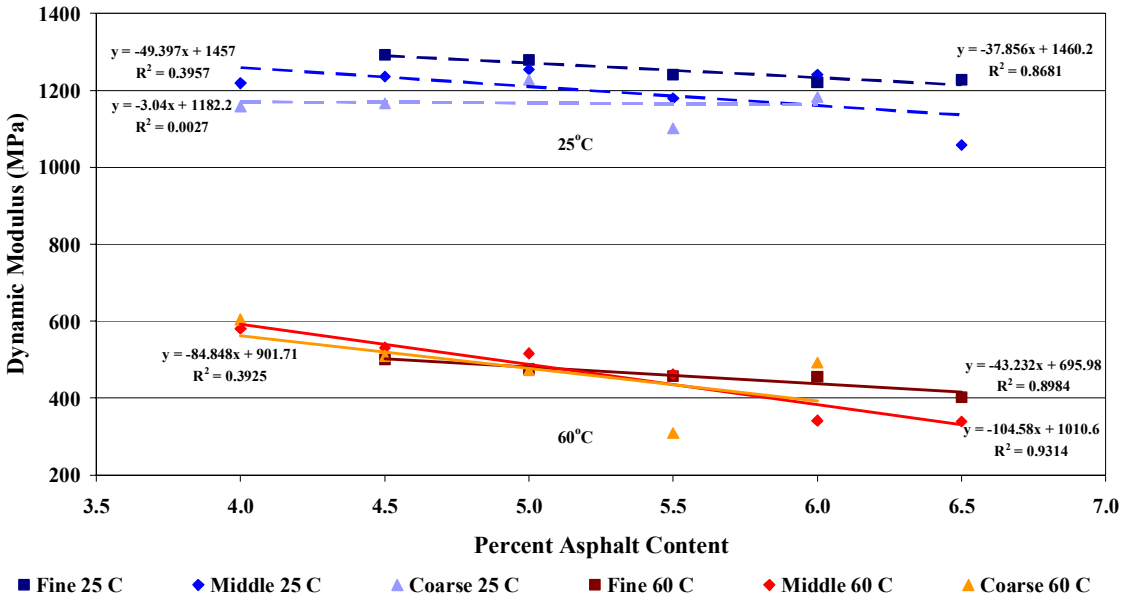

Figure 4.3 Dynamic Modulus Versus Asphalt Content

Figure 4.4 through Figure 4.9 illustrate the triaxial frequency sweep characterization dynamic modulus results plotted versus frequency and plotted versus deviatoric stress state for all three blend gradations at 25°C and 60°C. When plotted versus frequency at 25°C, dynamic modulus ranged from 903 MPa to 1635 MPa, from 775 MPa to 1561 MPa, and from 847 MPa to 1528 MPa for the fine, middle, and coarse blends, respectively. At 60°C dynamic modulus ranged from 263 MPa to 723 MPa, from 228 MPa to 828 MPa, and from 293 MPa to 883 MPa for the fine, middle, and coarse blends, respectively. When plotted versus deviatoric stress state at 25°C, dynamic modulus ranged from 708 MPa to 1820 MPa, from 606 MPa to 1847 MPa, and from 625 MPa to 1764 MPa for the fine, middle, and coarse blends, respectively. At 60°C dynamic modulus ranged from 339 MPa to 604 MPa, from 250 MPa to 737 MPa, and from 406 MPa to 788 MPa for the fine, middle, and coarse blends, respectively.

In order to best fit the dynamic modulus results, linear trend lines were fitted through the results plotted versus deviatoric stress state and power law trend lines were fitted through the results plotted versus frequency as illustrated in Figure 4.4 through Figure 4.9. Linear trend line equations have the form:

$$y = mx + b \quad \textbf{(4.1)}$$

Where:

y = Value on the vertical axis;

m = Slope of the trend line;

x = Value of the horizontal axis; and

b = Intercept of the trend line on the vertical axis.

Power law trend line equations have the form:

$$y = \alpha x^{\beta} \quad \textbf{(4.2)}$$

Where:

α = Curvature of the trend line; and

β = Powerlaw exponent.

The slope and intercept values of the linear trend lines and α and β values of the power law trend lines are illustrated in Appendix C.

Dynamic modulus was found to increase with increasing deviatoric stress state for all blend gradations at 25°C and 60°C, as illustrated in Figure 4.4 through Figure 4.6. This could be because higher stress states mobilized more asphalt cement molecular resistance, especially at lower temperatures, increasing dynamic modulus. The linear trend line slopes became smaller as asphalt content increased for all three blend gradations and two test temperatures, and the slope and were higher at 25°C than 60°C. These trends may be due to the lubrication effect of the asphalt cement on the aggregate skeleton. The trend line intercepts remained relatively constant at 25°C and 60°C, with the intercepts being larger at 25°C than 60°C. Dynamic modulus was found to be linear when plotted versus deviatoric stress state.

Dynamic modulus was found to increase with increasing frequency for each blend gradation at 25°C and 60°C, as illustrated in Figure 4.7 through Figure 4.9. The power law trend line α values decreased as asphalt content increased at both 25°C and 60°C, but were higher at 25°C than 60°C. Therefore, the dynamic modulus for each blend gradation increased at a faster rate at 25°C than at 60°C. This is a logical trend given the decreased influence of asphalt binder at 60°C relative to 25°C. The β values

were higher at 25°C than 60°C indicating a relatively large increase in dynamic modulus as frequency increased at 25°C and a relatively constant dynamic modulus versus frequency at 60°C. The difference in dynamic modulus at low and high frequencies is an indication that asphalt concrete behaves differently at different traffic speeds.

Nonlinearity was observed in the dynamic modulus when plotted versus frequency from 0.125 Hz through approximately 2 Hz for all blend gradations. Linearity was observed from approximately 2 Hz through 10 Hz. Therefore RaTT characterization identified asphalt concrete behaviour as nonlinear.

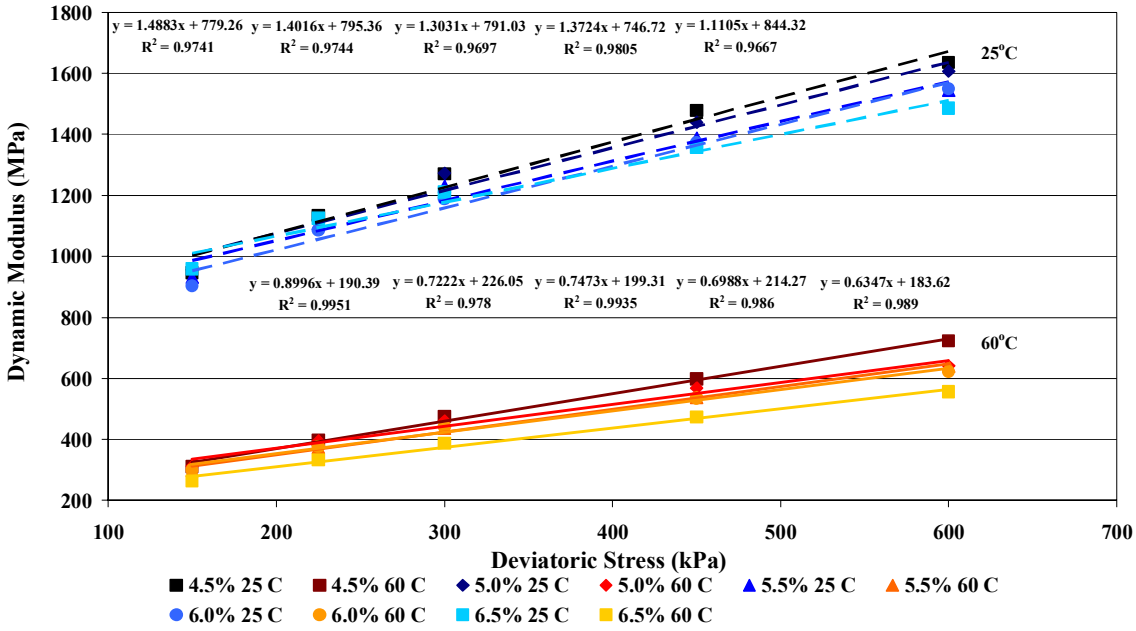

Figure 4.4 Fine Blend Dynamic Modulus Plotted versus Deviatoric Stress State

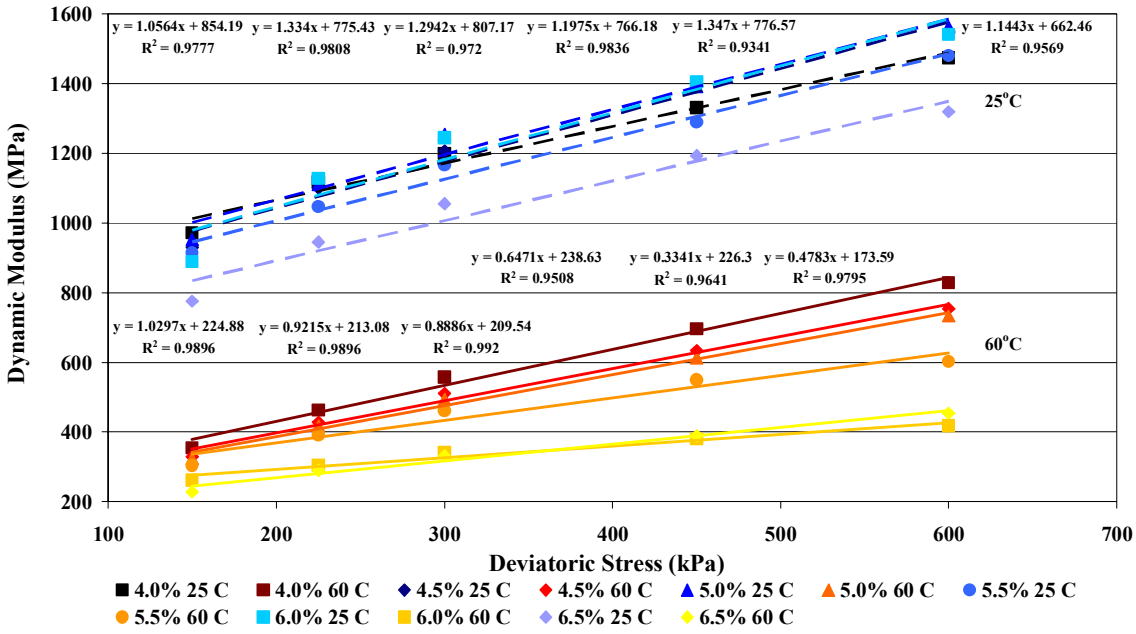

Figure 4.5 Middle Blend Dynamic Modulus Plotted versus Deviatoric Stress State

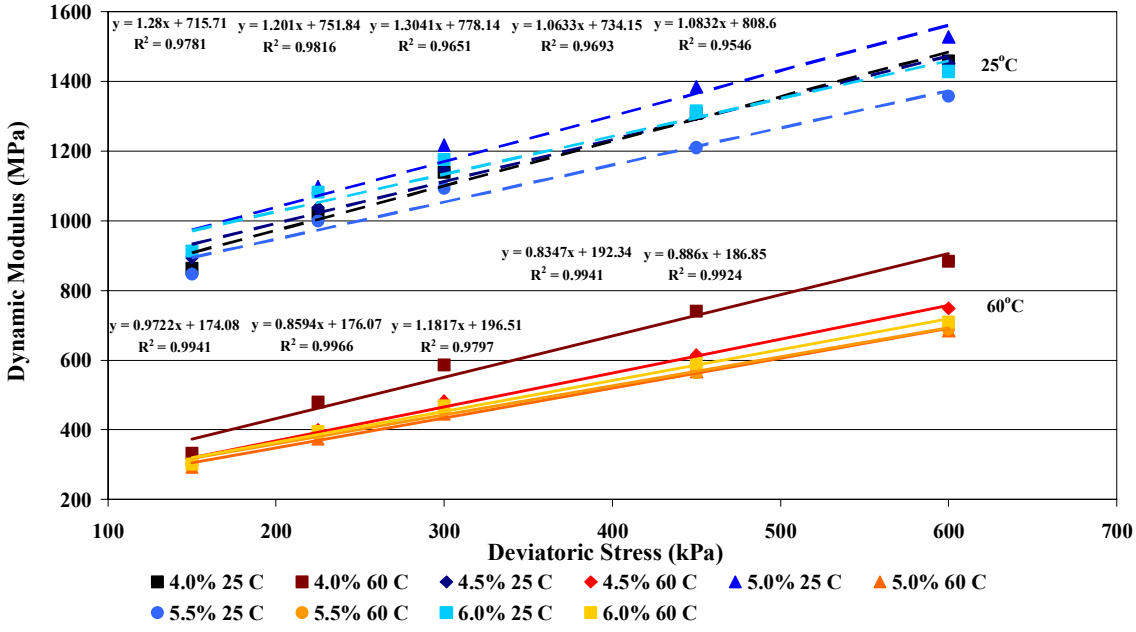

Figure 4.6 Coarse Blend Dynamic Modulus Plotted versus Deviatoric Stress State

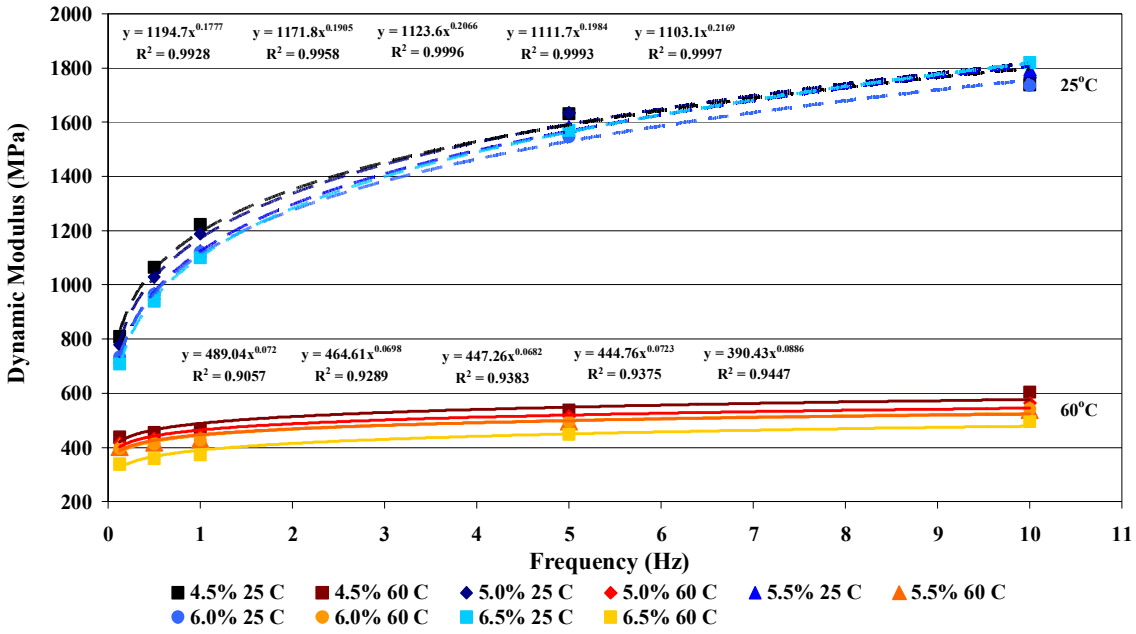

Figure 4.7 Fine Blend Dynamic Modulus Plotted versus Frequency

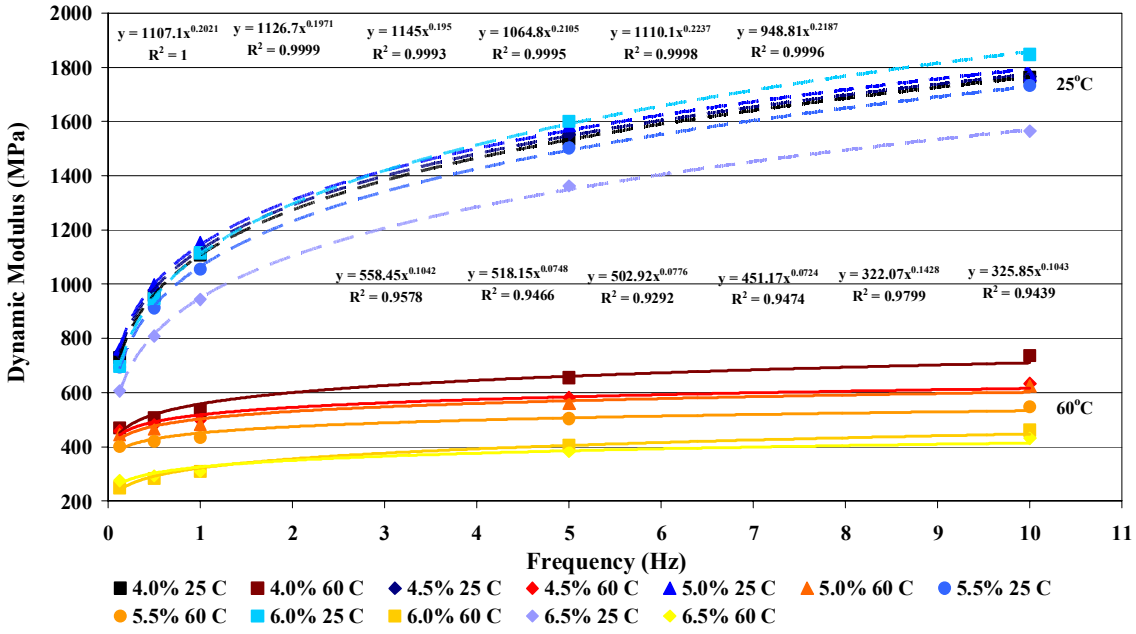

Figure 4.8 Middle Blend Dynamic Modulus Plotted versus Frequency

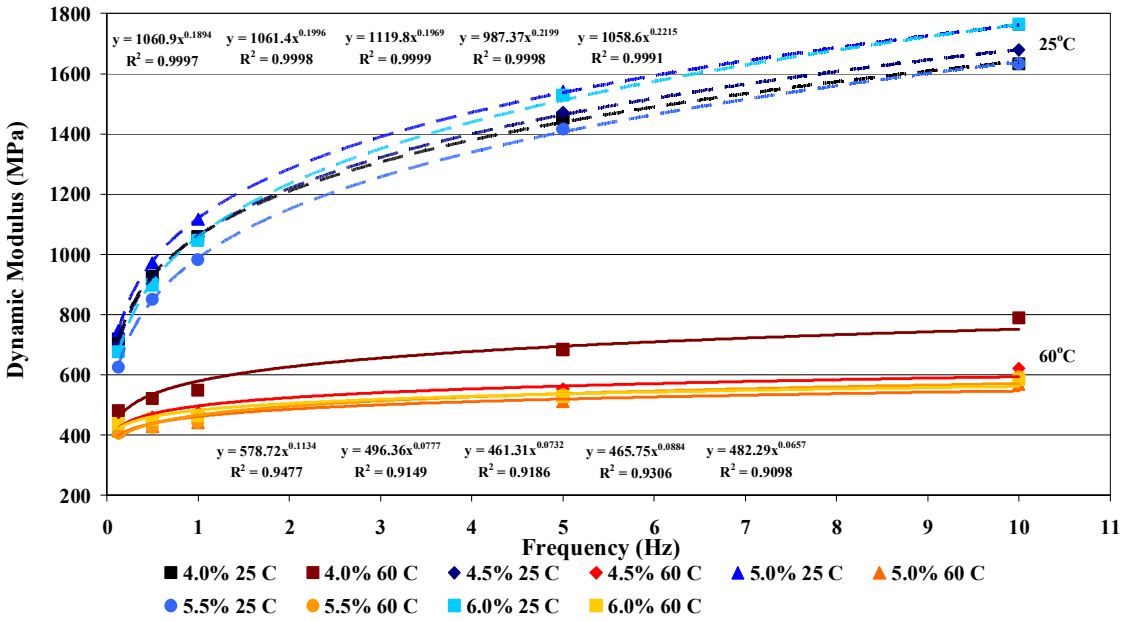

Figure 4.9 Coarse Blend Dynamic Modulus Plotted versus Frequency

4.2.2 Poisson's Ratio

Poisson's ratio values calculated from the triaxial frequency sweep software plotted versus deviatoric stress state and frequency are summarized in Table 4.4 and illustrated in Figure 4.10 and Figure 4.11. Poisson's ratio results plotted versus deviatoric stress state and plotted versus frequency are illustrated in Appendix E.

As illustrated in Figure 4.11, Poisson's ratio increased with increasing asphalt content for all three blend gradations at both 25°C and 60°C. The increasing trend could be a result of decreased aggregate interlock due to higher asphalt cement volume. As hypothesized, Poisson's ratio was found to be higher at 60°C than at 25°C for each blend gradation. It should be noted that the Poisson's ratio for the coarse blend at 4.0 percent asphalt content at 60°C was inexplicably lower than all other samples at 60°C. Based on the difference in Poisson's ratio at 25°C and 60°C, asphalt concrete was found to behave differently depending on temperature. Therefore the range of service temperatures may be a necessary input when designing asphalt concrete.

Table 4.4 Poisson's Ratio Results at 25°C and 60°C

Asphalt Content (%)	Blend Gradation	25° C	60° C
4.0	Fine	---*	---*
	Middle	0.22	0.45
	Coarse	0.23	0.24
4.5	Fine	0.20	0.42
	Middle	0.25	0.49
	Coarse	0.25	0.51
5.0	Fine	0.27	0.45
	Middle	0.29	0.44
	Coarse	0.33	0.47
5.5	Fine	0.29	0.51
	Middle	0.32	0.50
	Coarse	0.33	0.58
6.0	Fine	0.30	0.47
	Middle	0.32	0.60
	Coarse	0.28	0.44
6.5	Fine	0.32	0.57
	Middle	0.32	0.57
	Coarse	---*	---*

* - Data not included due to inappropriate asphalt cement content for the mix

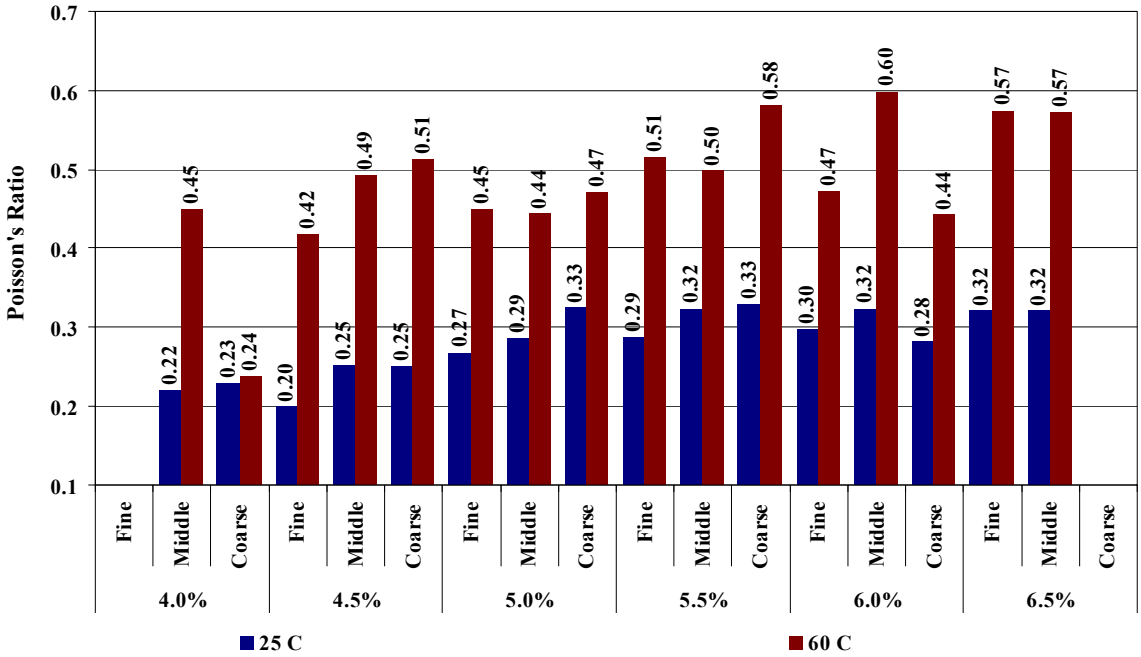

Figure 4.10 Poisson's Ratio Results at 25°C and 60°C

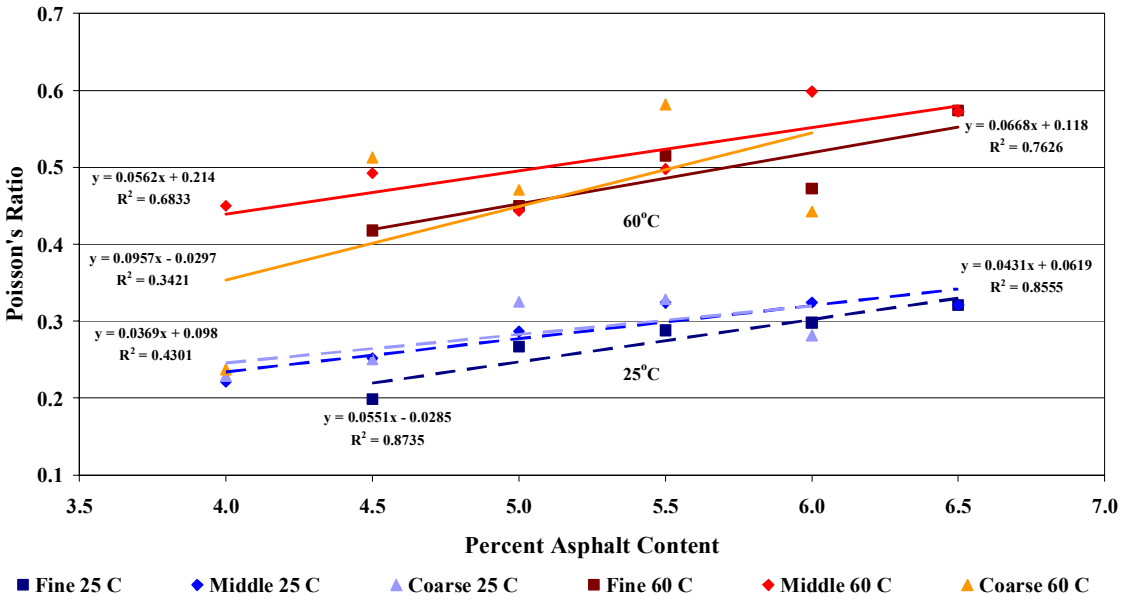

Figure 4.11 Poisson's Ratio Results at 25°C and 60°C

Figure 4.12 through Figure 4.17 illustrate triaxial frequency sweep characterization Poisson's ratio results plotted versus frequency and plotted versus deviatoric stress state for all three blend gradations at 25°C and 60°C. When plotted versus frequency, Poisson's ratio ranged from 0.08 to 0.36, from 0.16 to 0.38, and from 0.19 to 0.36 for the fine, middle, and coarse blends, respectively, at 25°C. Poisson's ratio ranged from 0.39 to 0.60, from 0.39 to 0.62, and from 0.19 to 0.58 for the fine, middle, and coarse blends, respectively, at 60°C. When plotted versus deviatoric stress state, Poisson's ratio ranged from 0.17 to 0.36, from 0.19 to 0.37, and from 0.20 to 0.37 for the fine, middle, and coarse blends, respectively, at 25°C. Poisson's ratio ranged from 0.40 to 0.58, from 0.41 to 0.61, and from 0.21 to 0.58 for the fine, middle, and coarse blends, respectively, at 60°C.

Linear trend lines were fitted through the results plotted versus deviatoric stress state and plotted versus frequency. The slope and intercept values of the linear trend lines are illustrated in Appendix C.

Poisson's ratio was found to increase with increasing deviatoric stress at 25°C and was found to typically decrease with increasing deviatoric stress at 60°C for all blend gradations, as illustrated in Figure 4.12 through Figure 4.14. However, there was

no identifiable Poisson's ratio trend in the linear trend line slopes. The linear trend line intercepts increased as asphalt content increased for each blend gradation at both 25°C and 60°C. This may be due to increased lubrication between the aggregate particles as asphalt content increases, allowing aggregate to dilate easier. The intercepts were lower at 25°C than 60°C, but had no identifiable trend with respect to asphalt content.

Poisson's ratio was found to increase with increasing axial loading frequency for each blend gradation at 25°C and 60°C, as illustrated in Figure 4.15 through Figure 4.17. The linear trend line slopes were similar at 25°C and 60°C with no identifiable Poisson's ratio trend with asphalt content. The trend line intercepts increased as asphalt content increased for each blend gradation at both 25°C and 60°C. The intercepts were lower at 25°C than 60°Cults. Poisson's ratio was found to be linear when plotted versus frequency.

Poisson's ratio results were not grouped together as closely at each test temperature as the dynamic modulus or phase angle results. This is likely due to the high responsiveness of the RaTT's radial LVDTs, resulting in Poisson's ratio being difficult to measure accurately. Decreasing the sensitivity of the radial LVDTs may be an area of improvement to the RaTT.

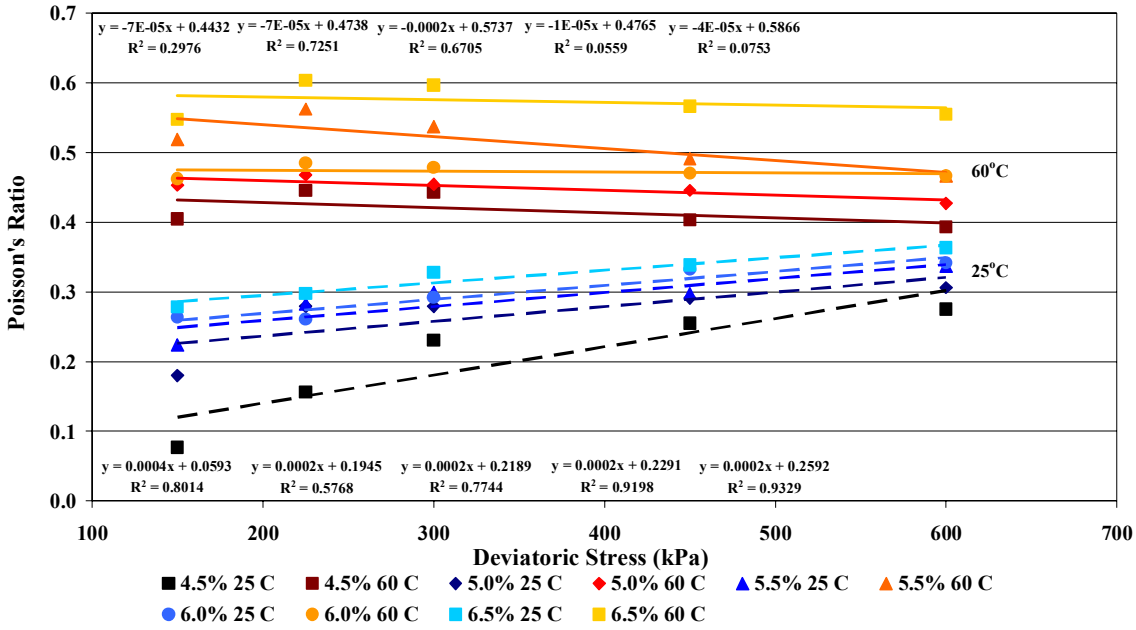

Figure 4.12 Fine Blend Poisson's Ratio Plotted versus Deviatoric Stress State

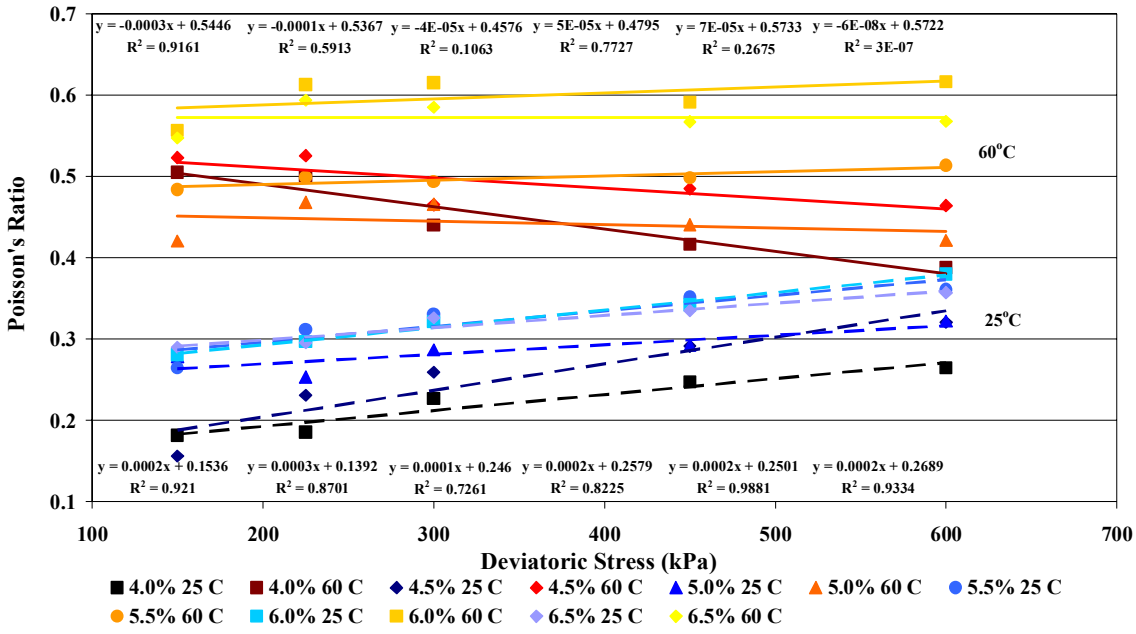

Figure 4.13 Middle Blend Poisson's Ratio Plotted versus Deviatoric Stress State

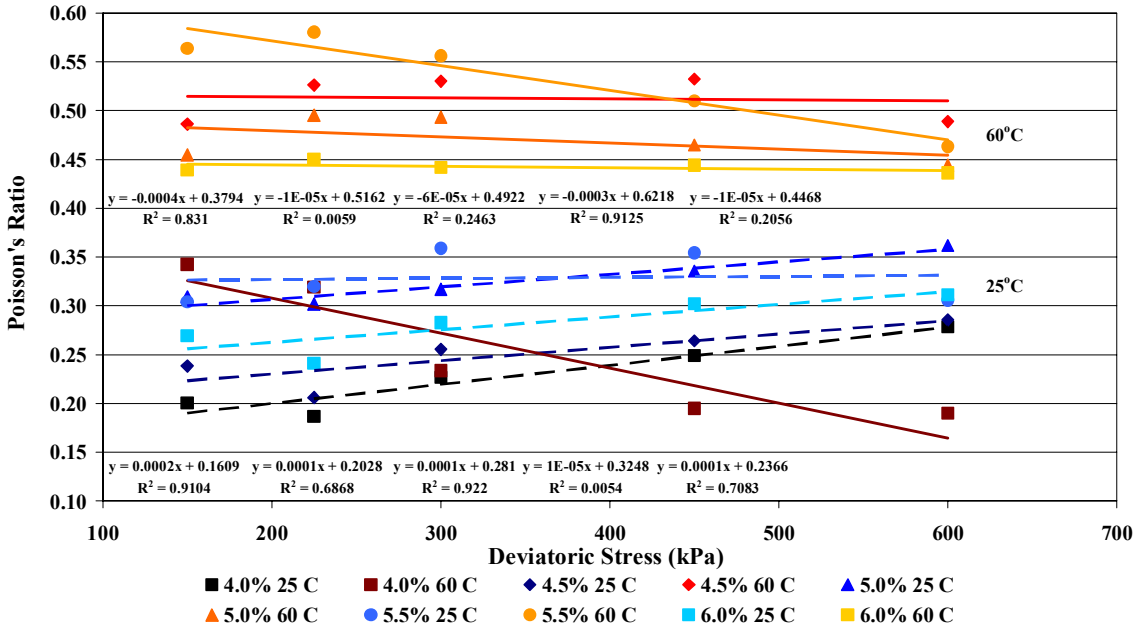

Figure 4.14 Coarse Blend Poisson's Ratio Plotted versus Deviatoric Stress State

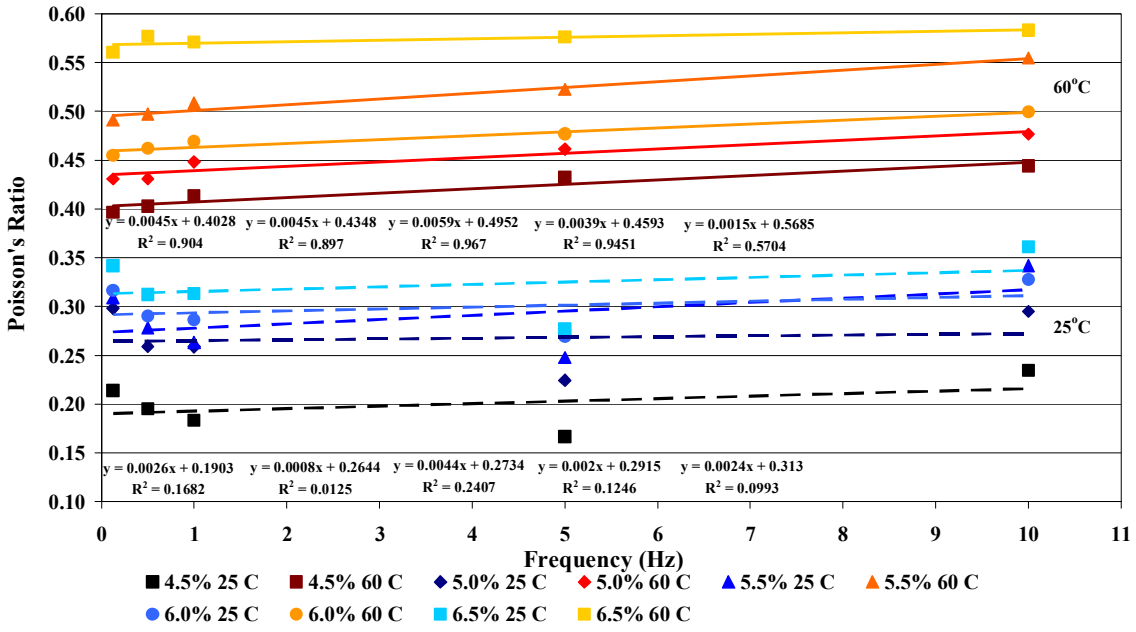

Figure 4.15 Fine Blend Poisson's Ratio Plotted versus Frequency

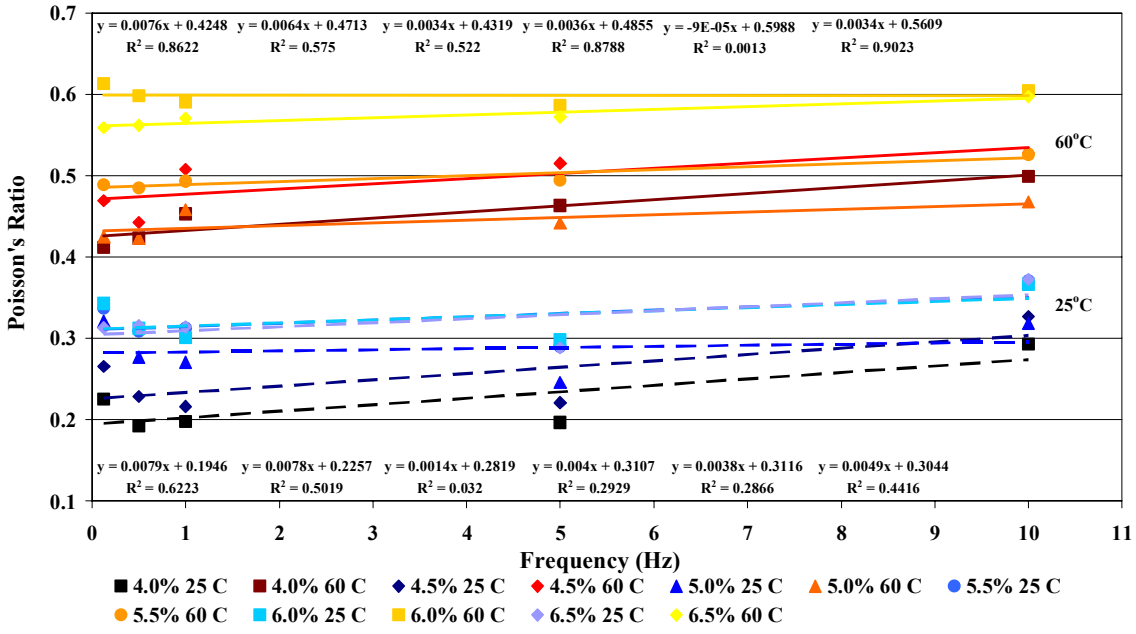

Figure 4.16 Middle Blend Poisson's Ratio Plotted versus Frequency

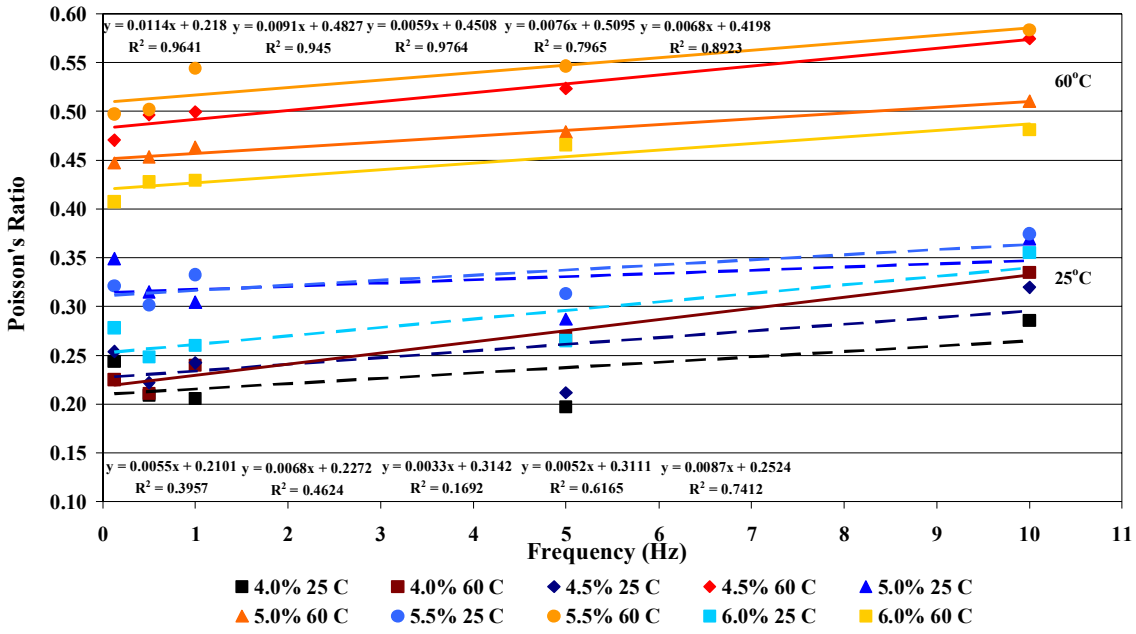

Figure 4.17 Coarse Blend Poisson's Ratio Plotted versus Frequency

4.2.3 Phase Angle

Phase angle values calculated from the triaxial frequency sweep characterization plotted versus deviatoric stress state and frequency are summarized in Table 4.5 and illustrated in Figure 4.18 and Figure 4.19. Phase angle results plotted versus deviatoric stress state and plotted versus frequency are illustrated in Appendix F.

As hypothesized, phase angle was found to be lower at 60°C than at 25°C for each blend gradation, as illustrated in Figure 4.19. Phase angle had an increasing trend with increasing asphalt content at 25°C but no clear trend was observed at 60°C. The increasing trend at 25°C could be a result of increased asphalt cement volume resulting in a larger proportion of viscous material in the asphalt concrete sample. Based on the difference in phase angle at 25°C and 60°C, asphalt concrete was found to behave differently depending on temperature. Therefore the range of service temperatures may be a necessary input when designing asphalt concrete.

It is interesting to note that the phase angle for all three blends was similar at 25°C and at 60°C at approximately 5.25 percent asphalt content.

Table 4.5 Phase Angle Results at 25°C and 60°C

Asphalt Content (%)	Blend Gradation	Phase Angle (Degrees)	
		25° C	60° C
4.0	Fine	---*	---*
	Middle	22.0	19.9
	Coarse	20.2	20.0
4.5	Fine	22.0	18.4
	Middle	21.0	18.8
	Coarse	20.9	18.9
5.0	Fine	22.1	19.1
	Middle	21.4	18.3
	Coarse	20.8	18.9
5.5	Fine	22.5	19.2
	Middle	21.8	18.6
	Coarse	23.1	19.8
6.0	Fine	22.0	19.1
	Middle	23.1	19.2
	Coarse	23.2	18.1
6.5	Fine	22.9	19.7
	Middle	23.1	18.6
	Coarse	---*	---*

* - Data not included due to inappropriate asphalt cement content for the mix

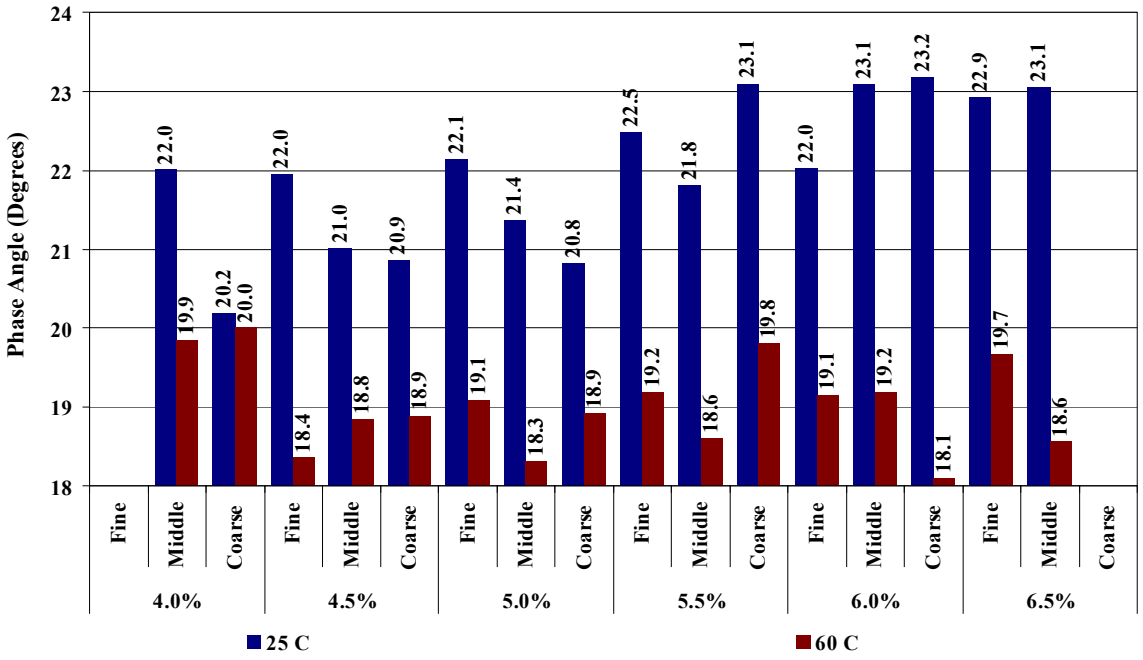

Figure 4.18 Phase Angle Results at 25°C and 60°C

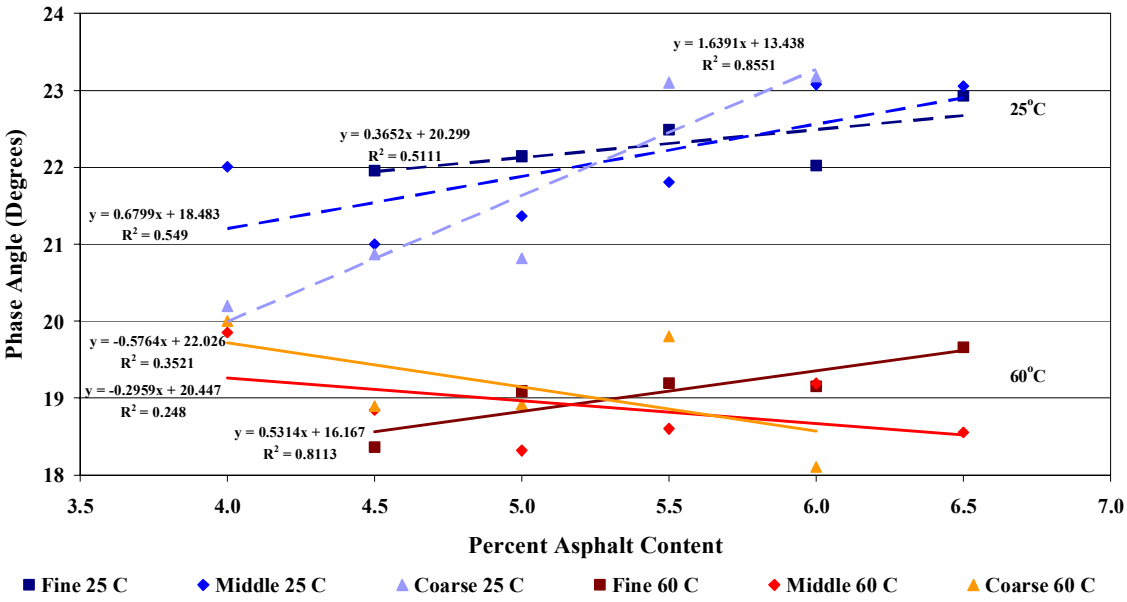

Figure 4.19 Phase Angle Results at 25°C and 60°C

Figure 4.20 through Figure 4.25 illustrate the triaxial frequency sweep characterization phase angle results plotted versus frequency and plotted versus deviatoric stress state for all three blend gradations at 25°C and 60°C. When plotted versus frequency, phase angle ranged from 20.9 degrees to 25.3 degrees, from 20.1 degrees to 24.2 degrees, and from 19.5 degrees to 25.0 degrees for the fine, middle, and coarse blends, respectively, at 25°C. Phase angle ranged from 16.6 degrees to 21.0 degrees, from 16.6 degrees to 21.3 degrees, and from 16.3 degrees to 21.9 degrees for the fine, middle, and coarse blends, respectively, at 60°C. When plotted versus deviatoric stress state, phase angle ranged from 20.2 degrees to 24.3 degrees, from 19.5 degrees to 24.6 degrees, and from 17.2 degrees to 24.8 degrees for the fine, middle, and coarse blends, respectively, at 25°C. Phase angle ranged from 14.9 degrees to 24.0 degrees, from 14.8 degrees to 24.7 degrees, and from 15.0 degrees to 24.8 degrees for the fine, middle, and coarse blends, respectively, at 60°C.

Linear trend lines were fitted through the results plotted versus deviatoric stress state and power law trend lines were fitted through the results plotted versus frequency. The slope and intercept values of the linear trend lines and the α and β values for the power law trend lines are summarized and illustrated in Appendix C.

Phase angle was found to decrease with increasing deviatoric stress state at 25°C and 60°C for each blend gradation, as illustrated in Figure 4.20 through Figure 4.22. This could be because higher stress states mobilized more asphalt cement molecular resistance, especially at lower temperatures, decreasing phase angle. The linear trend line slopes were found to be similar for all blend gradations at 25°C and 60°C, but had no trend with respect to asphalt content. The trend line intercepts were slightly higher at 25°C than 60°C for all blend gradations, but had no trend with respect to asphalt content.

Phase angle was found to decrease with increased load frequency at 25°C but was found to increase with increased frequency at 60°C for each blend gradation, as illustrated in Figure 4.23 through Figure 4.25. Phase angle plateaued with increasing frequency indicating a shift from material behaviour depending on temperature to depending on load frequency. Phase angle at 25°C and at 60°C crossed over each other at frequency ranges of approximately 2 to 6 Hz. The difference in phase angle at low and high frequencies is an indication that asphalt concrete behaves differently at different traffic speeds. Therefore, traffic speed may be a necessary input when designing asphalt concrete.

Since phase angle is between 0 and 90 degrees for all blend gradations, the asphalt concrete samples employed in this research are viscoelastic materials. Therefore RaTT characterization identified asphalt concrete behaviour as viscoelastic.

Nonlinearity was observed in the phase angle results from 0.125 Hz through approximately 2 Hz to 6 Hz, and linearity was observed from approximately 2 Hz to 6 Hz through 10 Hz. Therefore RaTT characterization identified asphalt concrete behaviour as nonlinear.

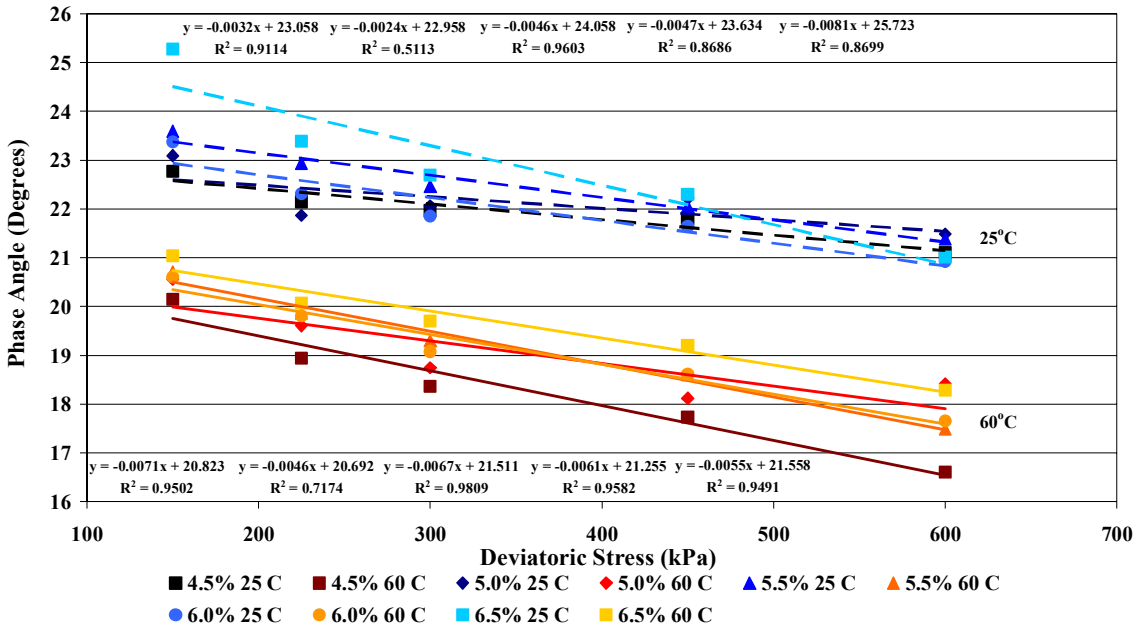

Figure 4.20 Fine Blend Phase Angle Plotted versus Deviatoric Stress State

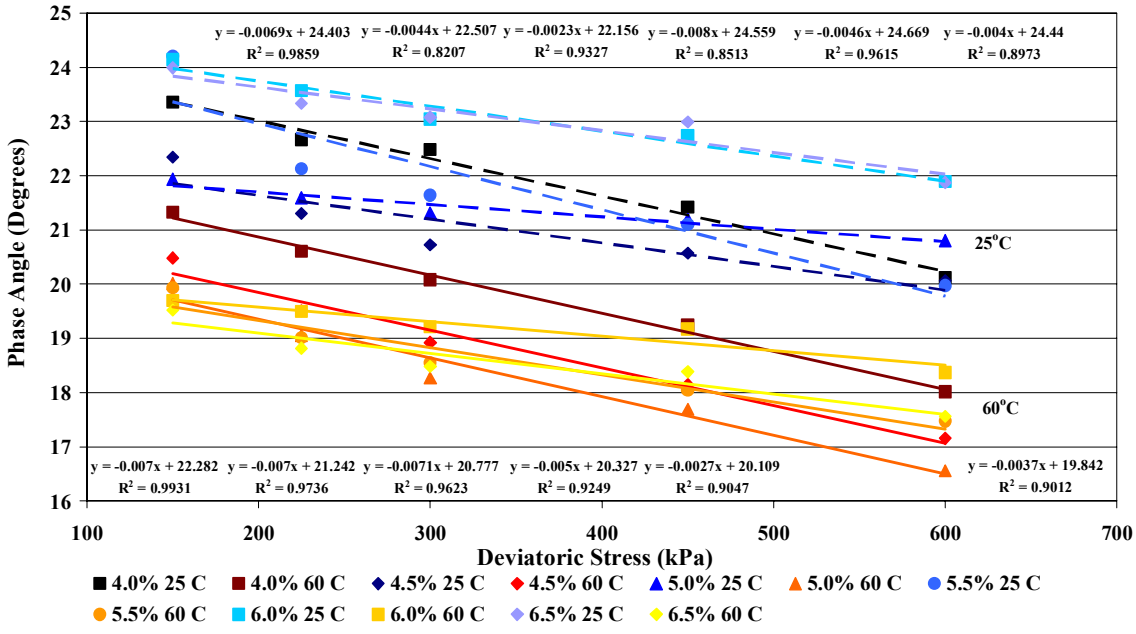

Figure 4.21 Middle Blend Phase Angle Plotted versus Deviatoric Stress State

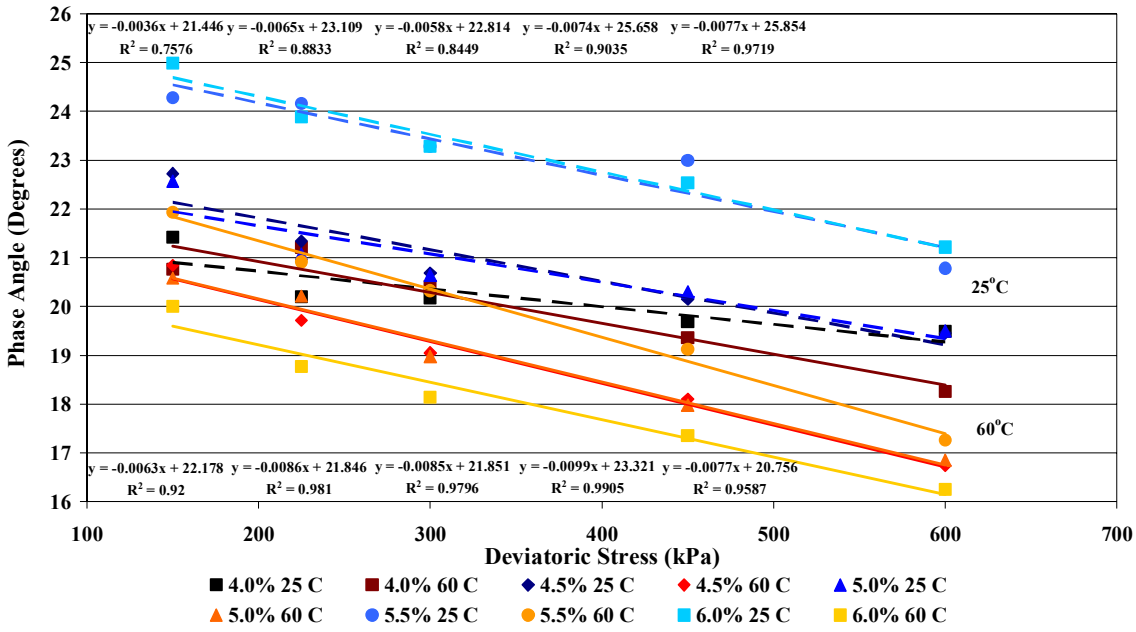

Figure 4.22 Coarse Blend Phase Angle Plotted versus Deviatoric Stress State

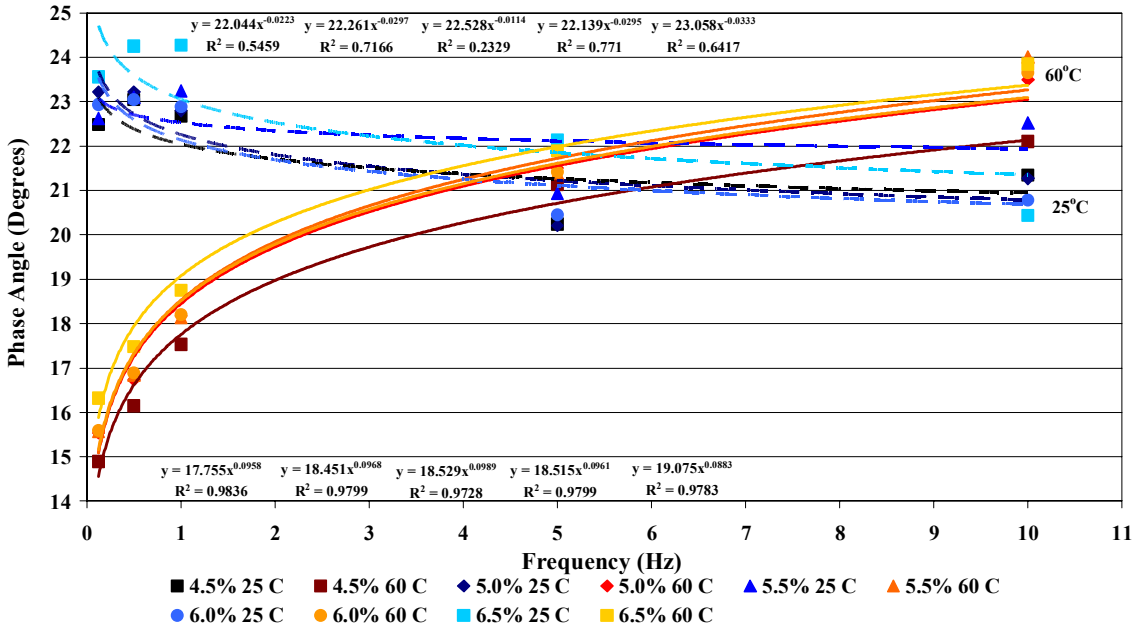

Figure 4.23 Fine Blend Phase Angle Plotted versus Frequency

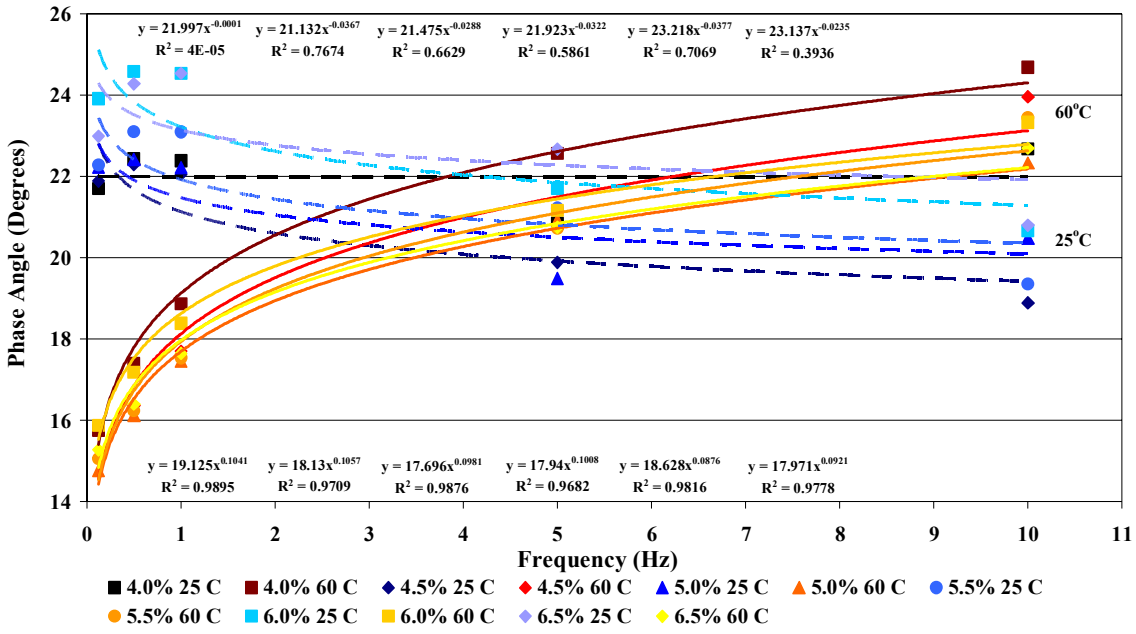

Figure 4.24 Middle Blend Phase Angle Plotted versus Frequency

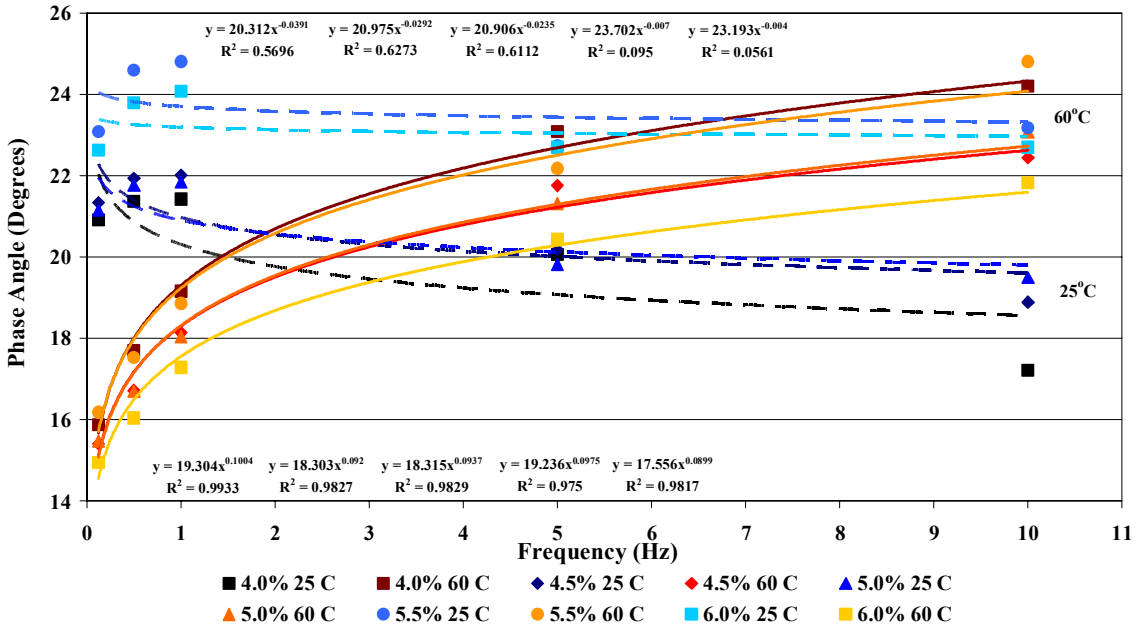

Figure 4.25 Coarse Blend Phase Angle Plotted versus Frequency

4.3 Material Properties Variation With Respect to Mix Design Parameters

In order to identify which mechanistic material properties may be most useful in asphalt concrete mix design, the variation of dynamic modulus, Poisson's ratio, and phase angle with respect to deviatoric stress state, frequency, and asphalt cement content was determined at 25°C and 60°C. The variations of the material properties for each blend gradation are illustrated in Figure 4.26 through Figure 4.28.

For example, dynamic modulus of the middle blend had the highest variation with respect to asphalt cement content at 60°C, increasing by 309 percent through the range of asphalt contents. Phase angle decreased by 86 percent from 150 kPa to 600 kPa deviatoric stress state at 60°C for the middle blend. The primary mix design parameters had the greatest variation with respect to dynamic modulus at both 25°C and 60°C for all blend gradations.

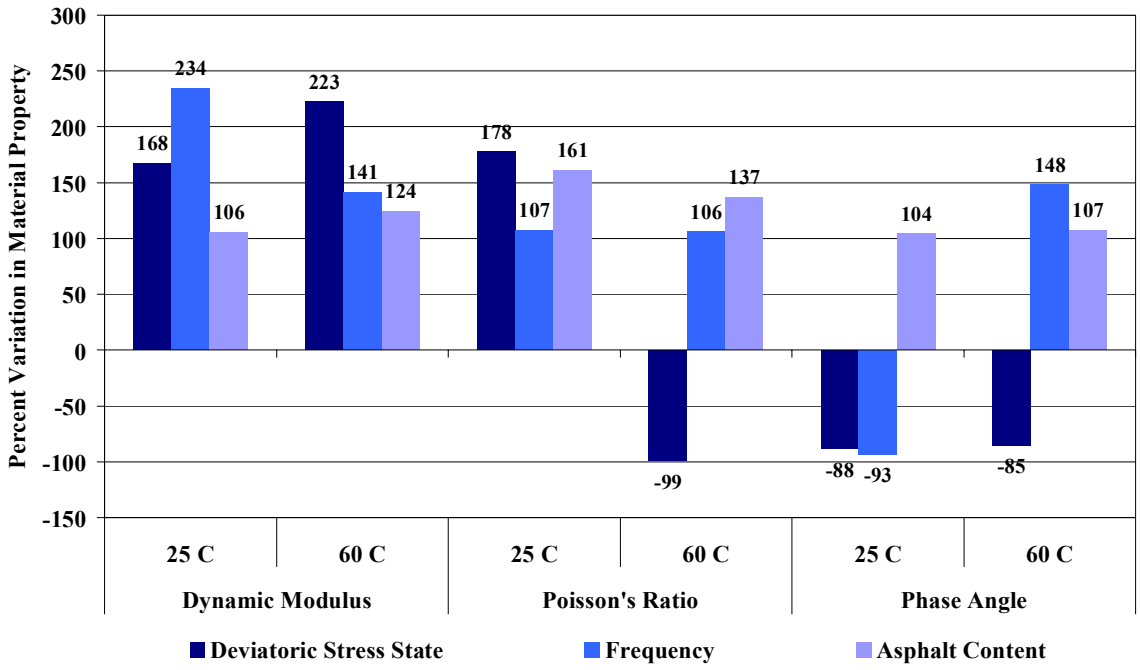

Figure 4.26 Fine Blend Percent Variation in Material Properties for Design Parameters

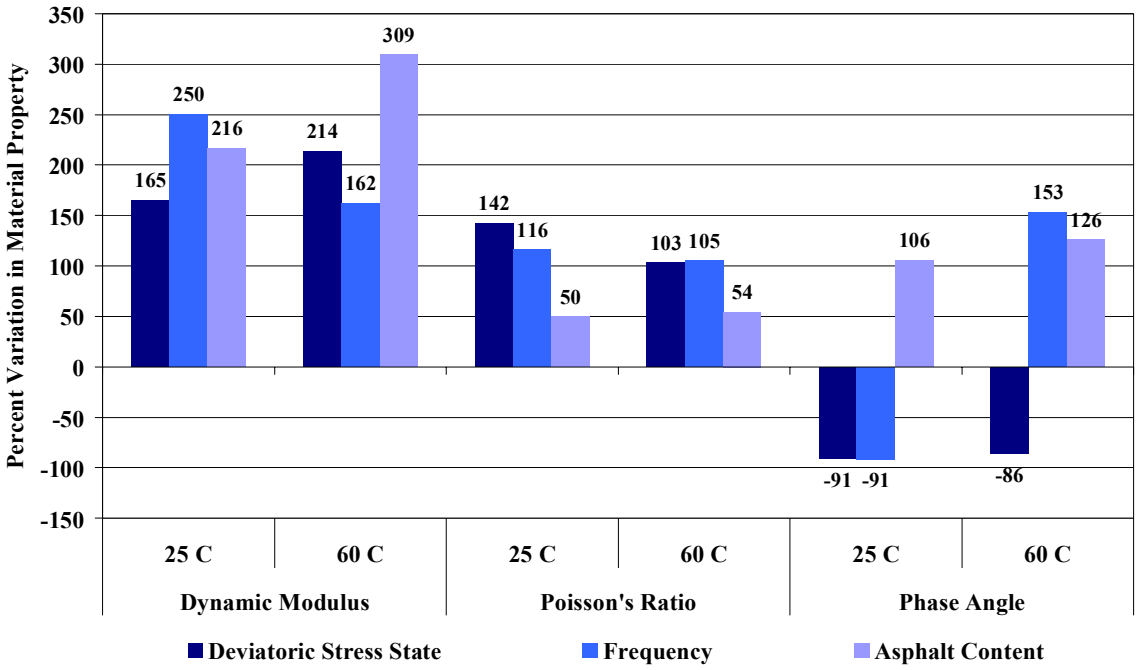

Figure 4.27 Middle Blend Percent Variation in Material Properties for Design Parameters

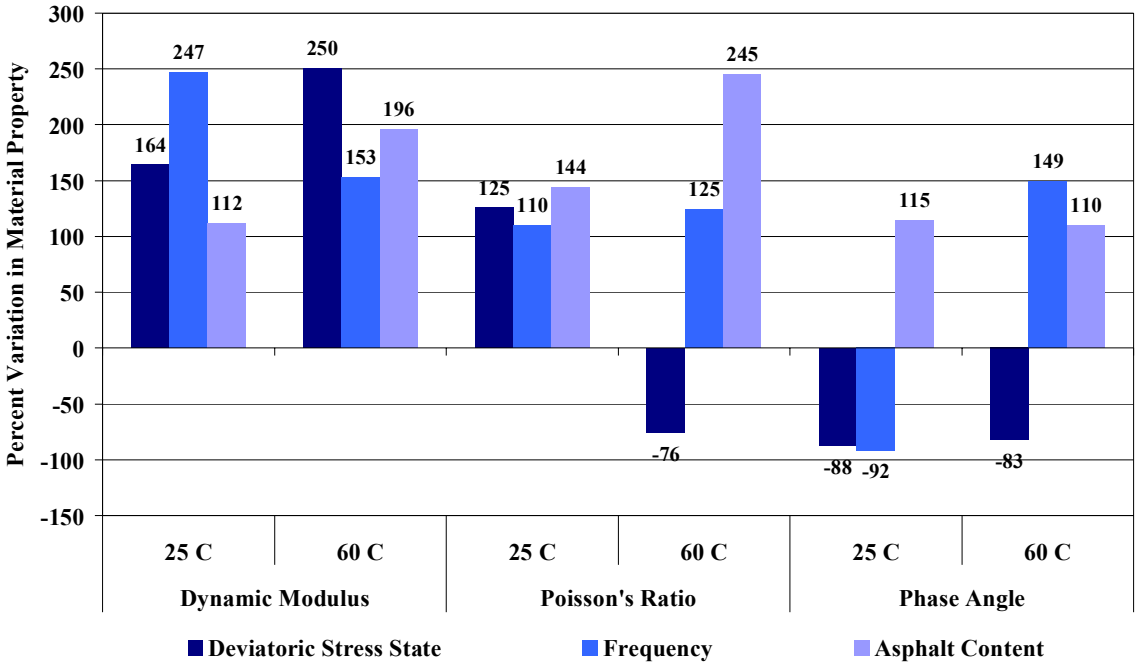

Figure 4.28 Coarse Blend Percent Variation in Material Properties for Design Parameters

The variation of material properties with changing deviatoric stress state, frequency, and asphalt cement content indicates that all three mix design parameters are important factors in asphalt concrete behaviour. An example of load frequency dependence may be 42nd Street in the City of Saskatoon which has extensive rutting only in the areas that experience slow moving traffic. In addition, commercial trucks follow each other closely, submitting the pavement to constant axle loading. This would indicate that load frequency, or traffic speed, and axle load configuration influence pavement performance.

4.3.1 Test Property and Material Ranges Corresponding to Acceptable Volumetric Specifications

In order to compare the Marshall stability and flow results to the material properties obtained from the RaTT, the range of dynamic modulus, Poisson's ratio, and phase angle which corresponded to the range of acceptable volumetric properties which met COS, DHT, and Superpave™ specifications were determined. The test property and material property ranges which corresponded to the asphalt content ranges that met DHT, COS, and Superpave™ volumetric specifications were determined by interpolation. The total range of each property obtained during testing was also determined.

The material property results presented in the following sections are plotted versus both deviatoric stress state and frequency since the range of material properties generally followed the same trends when plotted versus deviatoric stress state as when plotted versus frequency for all volumetric specifications.

4.3.1.1 RaTT Material Property Ranges for VTM Specifications

Figure 4.29 through Figure 4.40 illustrate the mean values of the material property ranges and the ranges relative to the total ranges obtained during triaxial frequency sweep characterization. Appendix G through Appendix I illustrate the material property ranges plotted versus deviatoric stress state and plotted versus

frequency that corresponded to COS, DHT, and Superpave™ specified volumetric ranges.

As illustrated in Figure 4.29 through Figure 4.32, the mean values of the dynamic modulus ranges that met VTM specifications were higher at 25°C than at 60°C when plotted versus both deviatoric stress state and frequency. This trend would be expected given the higher stiffness of asphalt cement at 25°C relative to 60°C. The coarse blend had the lowest mean and the widest range of acceptable values at 25°C and 60°C. The fine and middle blend mean values were similar at 25°C. However, the middle blend had the highest mean at 60°C. Since a high dynamic modulus indicates lower strain in the material, asphalt concrete with a high dynamic modulus should rut less than with a lower dynamic modulus. Therefore, the middle blend was theoretically the best performing mix and the coarse blend was the worst performing mix with respect to dynamic modulus within acceptable VTM specifications.

Since the middle blend had the highest mean dynamic modulus, it would indicate that mixes that follow the maximum density line have more desirable dynamic modulus values than mixes that deviate from the maximum density line for dense graded mixes.

The dynamic modulus ranges for acceptable volumetric requirements were small relative to the total ranges obtained 25°C and 60°C. As a result, when asphalt concrete volumetrics fall outside of specifications, dynamic modulus, and therefore material behaviour, has the potential to be highly variable. It should be noted that there is no range in dynamic modulus for acceptable Superpave™ VTM specifications since the Superpave™ VTM must be 4.0 percent.

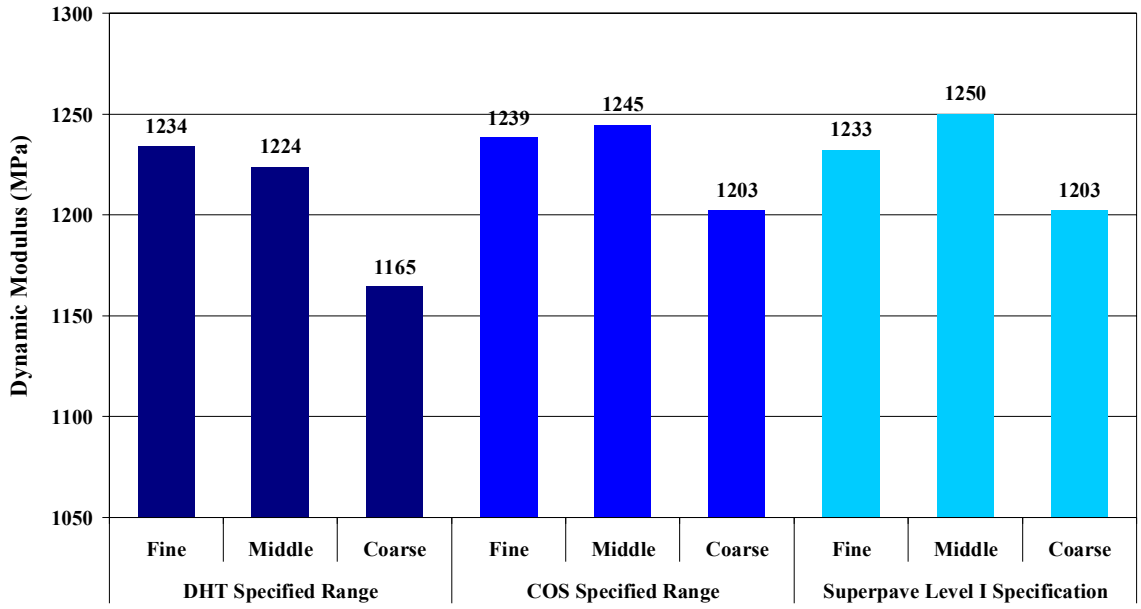

Figure 4.29 Dynamic Modulus Range Mean for Acceptable VTM Specifications at 25°C

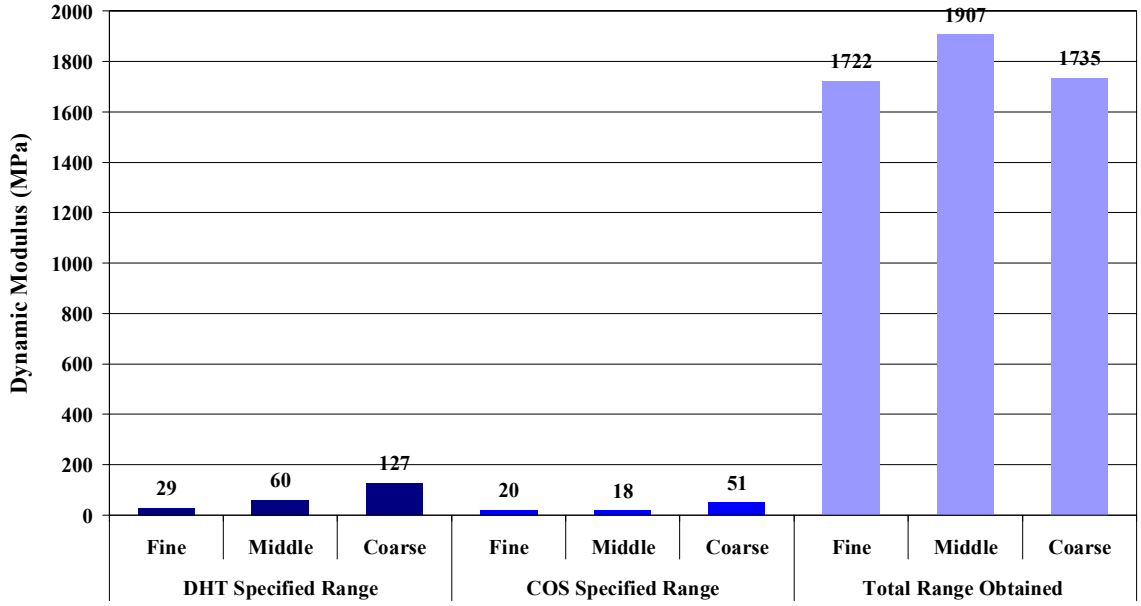

Figure 4.30 Dynamic Modulus Range for Acceptable VTM Specifications Relative to Total Range Obtained at 25°C

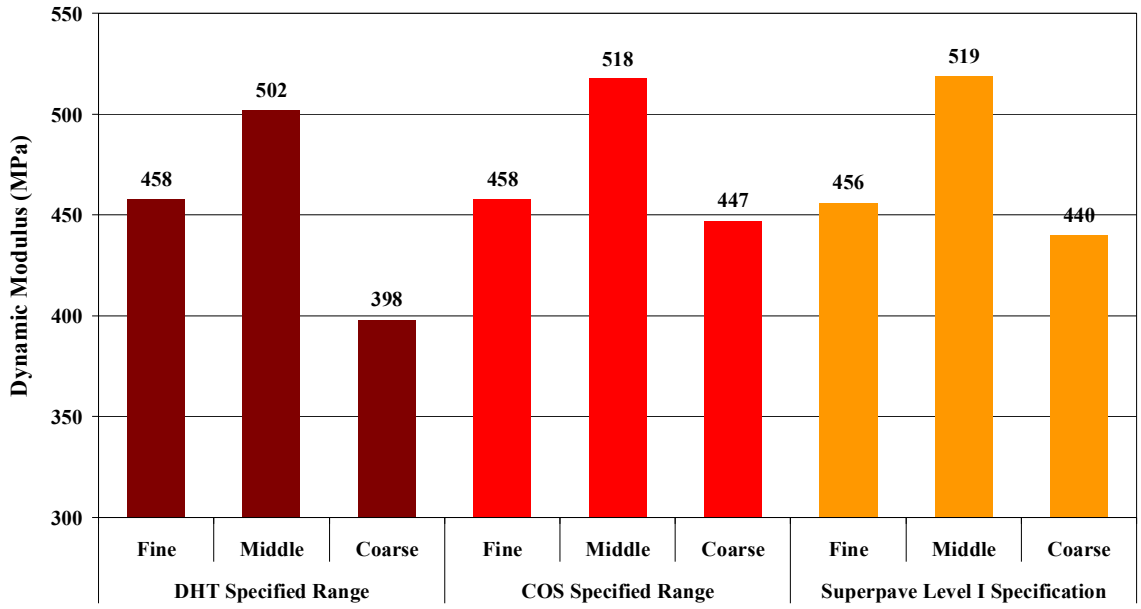

Figure 4.31 Dynamic Modulus Range Mean for Acceptable VTM Specifications at 60°C

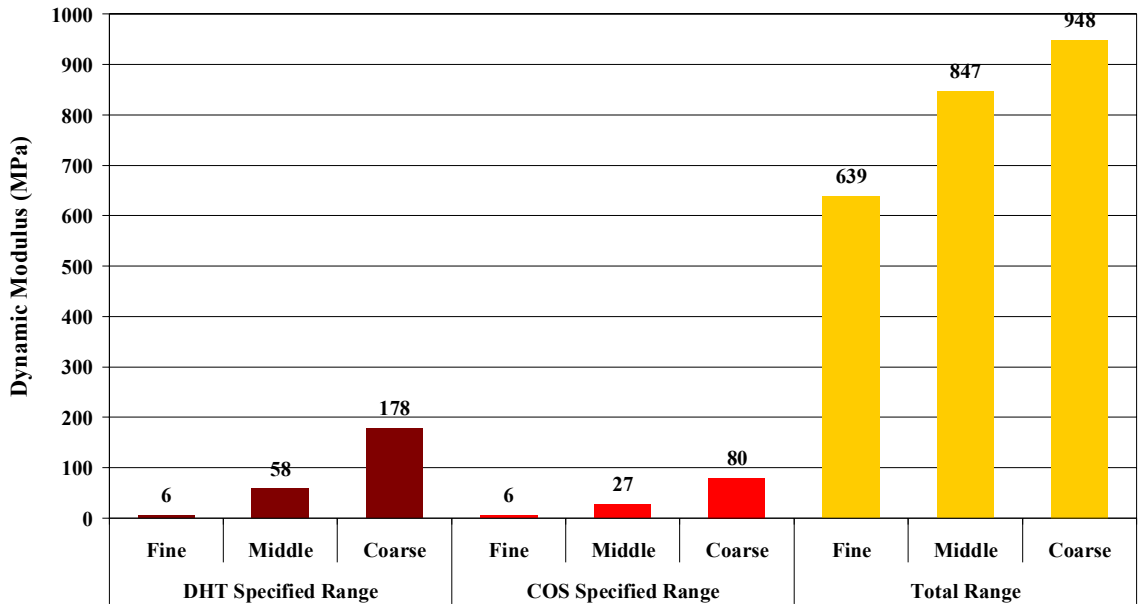

Figure 4.32 Dynamic Modulus Range for Acceptable VTM Specifications Relative to Total Range Obtained at 60°C

As illustrated in Figure 4.33 through Figure 4.36, the mean values of the Poisson's ratio ranges that met VTM specifications were lower at 25°C than at 60°C when plotted versus both deviatoric stress state and frequency. This trend would be expected given the higher stiffness of asphalt cement at 25°C relative to 60°C since stiffer materials will generally have a lower Poisson's ratio than softer materials. The middle blend having the lowest mean values and the coarse blend had the highest mean values at 25°C and 60°C. Since a material with a low Poisson's ratio will dilate less than a material with a higher Poisson's ratio, asphalt concrete with a lower Poisson's ratio will theoretically rut less. Therefore, the middle blend was theoretically the best performing mix at 25°C and 60°C with respect to Poisson's ratio within acceptable VTM specifications.

Since the middle blend had the lowest mean Poisson's ratio, it would indicate that mixes that follow the maximum density line have more desirable Poisson's ratio values than mixes that deviate from the maximum density line for dense graded mixes.

The Poisson's ratio ranges for acceptable volumetric requirements were small relative to the total ranges obtained 25°C and 60°C. As a result, when asphalt concrete volumetrics fall outside of specifications, Poisson's ratio, and therefore material behaviour, has the potential to be highly variable.

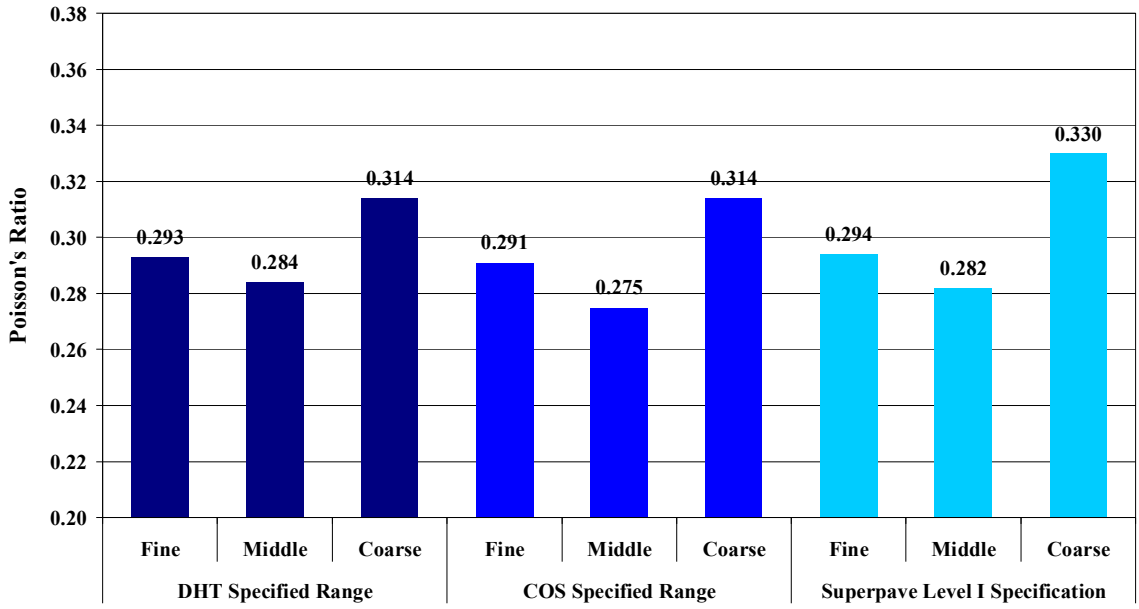

Figure 4.33 Poisson's Ratio Range Mean for Acceptable VTM Specifications at 25°C

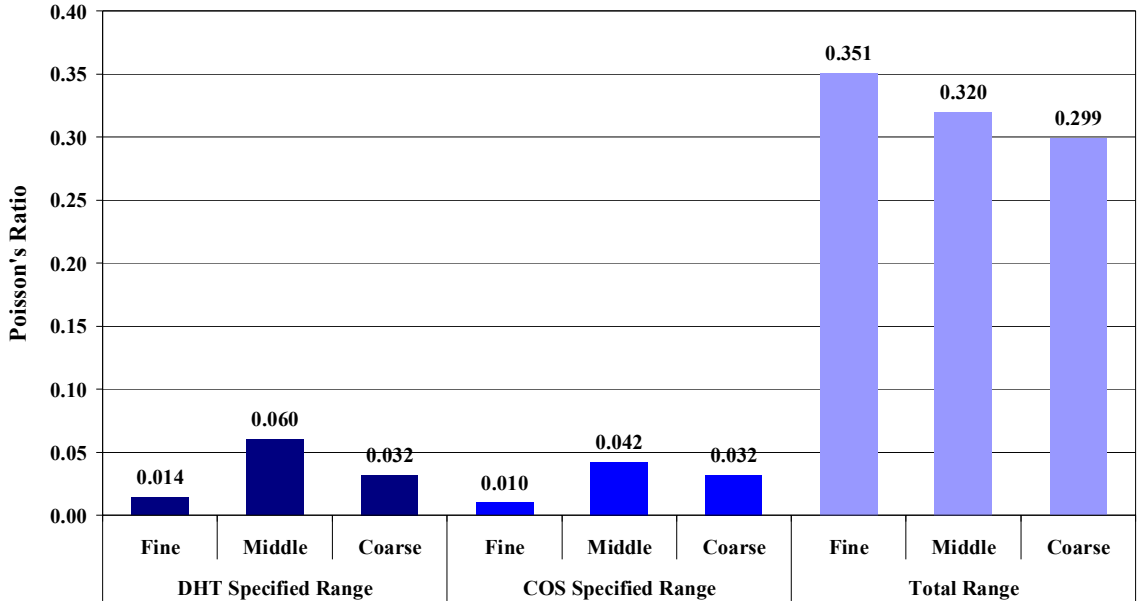

Figure 4.34 Poisson's Ratio Range for Acceptable VTM Specifications Relative to Total Range Obtained at 25°C

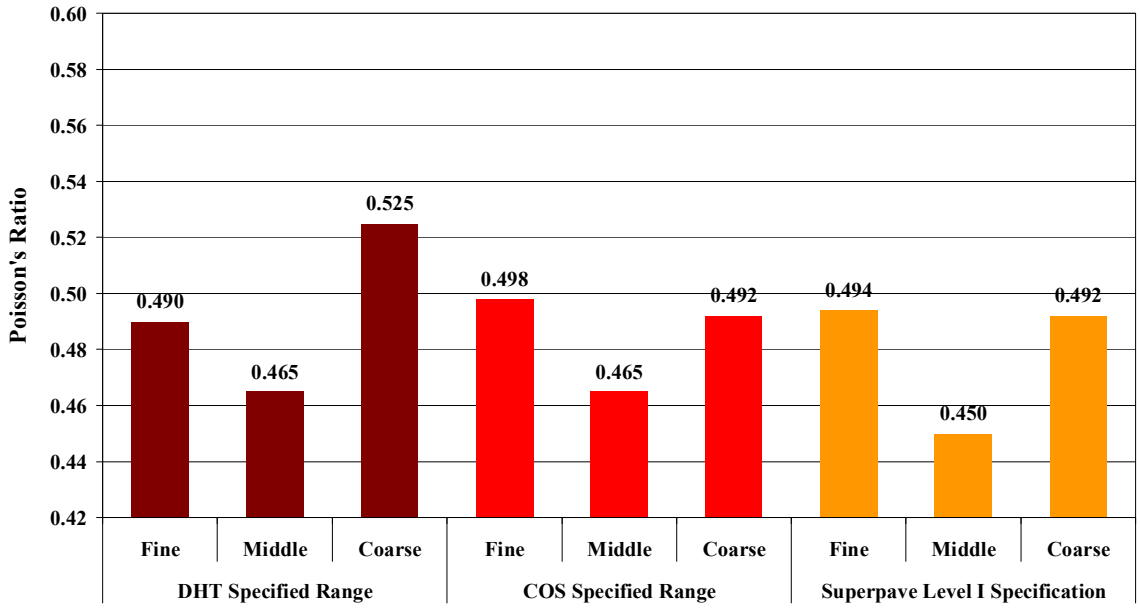

Figure 4.35 Poisson's Ratio Range Mean for Acceptable VTM Specifications at 60°C

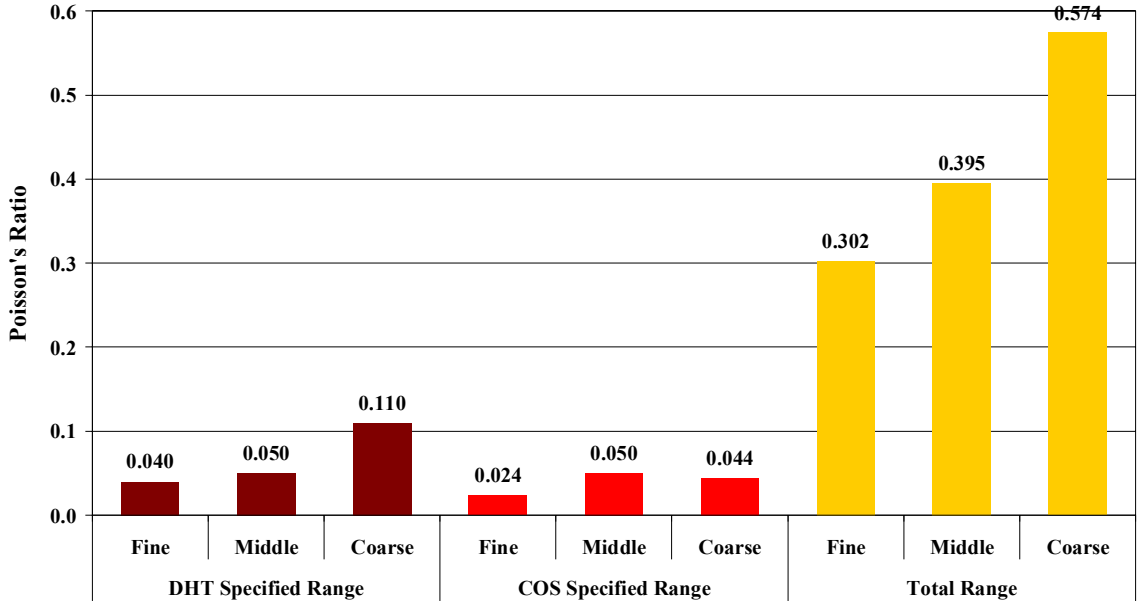

Figure 4.36 Poisson's Ratio Range for Acceptable VTM Specifications Relative to Total Range Obtained at 60°C

As illustrated in Figure 4.37 through Figure 4.40, the mean values of the phase angle ranges that met VTM specifications were higher at 25°C than at 60°C when plotted versus both deviatoric stress state and frequency. This trend would be expected given the decreased effect of asphalt cement and increased effect of the aggregate skeleton on the overall stiffness of the asphalt concrete sample at 60°C relative to 25°C. The middle blend had the lowest mean and the fine blend typically had the highest mean at 25°C and 60°C. Since a material with a lower phase angle has a larger elastic component and a smaller viscous component than a material with a higher phase angle, asphalt concrete with a lower phase angle will theoretically experience more recoverable strain and therefore rut less. Therefore, the middle blend was theoretically the best performing mix at 25°C and 60°C with respect to phase angle within acceptable VTM specifications.

Since the middle blend had the lowest mean phase angle, it would indicate that mixes that follow the maximum density line have more desirable phase angle values than mixes that deviate from the maximum density line for dense graded mixes.

The acceptable phase angle ranges for acceptable volumetric requirements were small relative to the total ranges obtained at 25°C and 60°C. As a result, when asphalt concrete volumetrics fall outside of specifications, phase angle, and therefore material behaviour, has the potential to be highly variable.

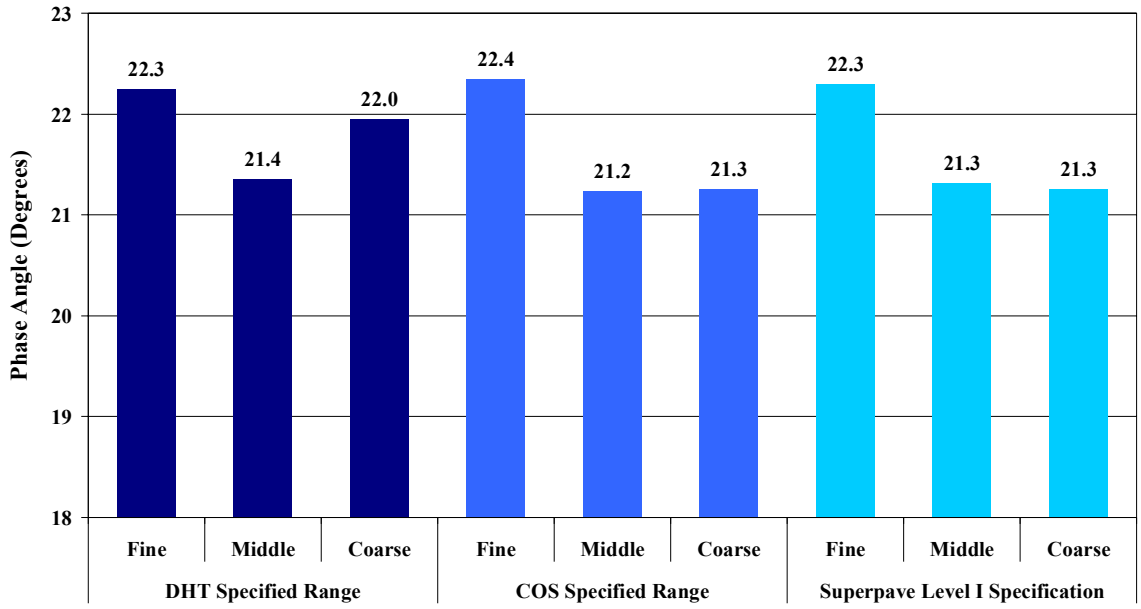

Figure 4.37 Phase Angle Range Mean for Acceptable VTM Specifications at 25°C

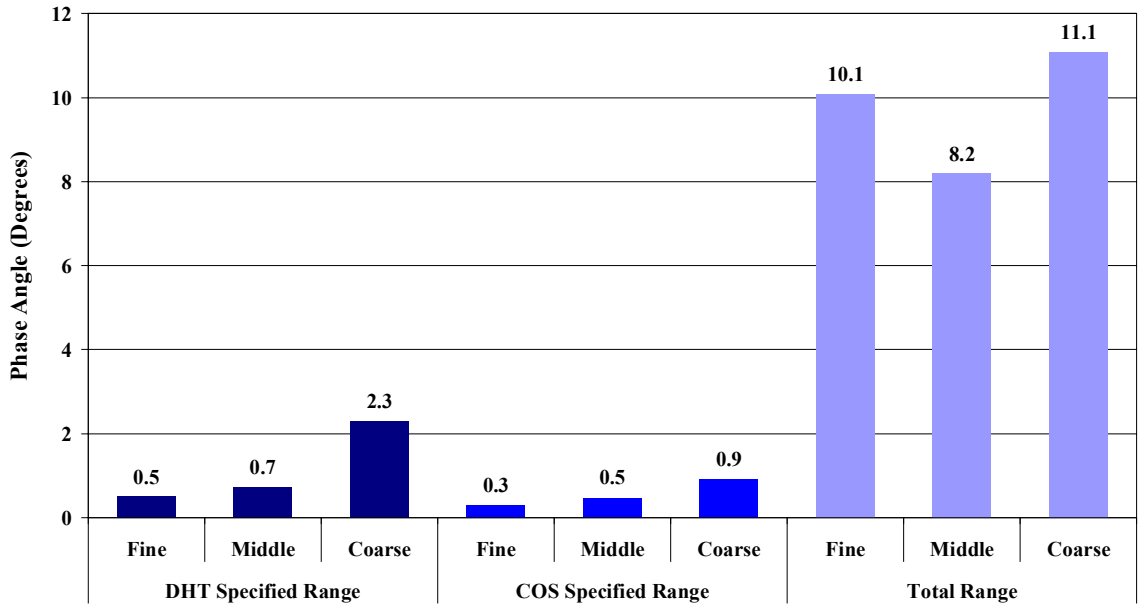

Figure 4.38 Phase Angle Range for Acceptable VTM Specifications Relative to Total Range Obtained at 25°C

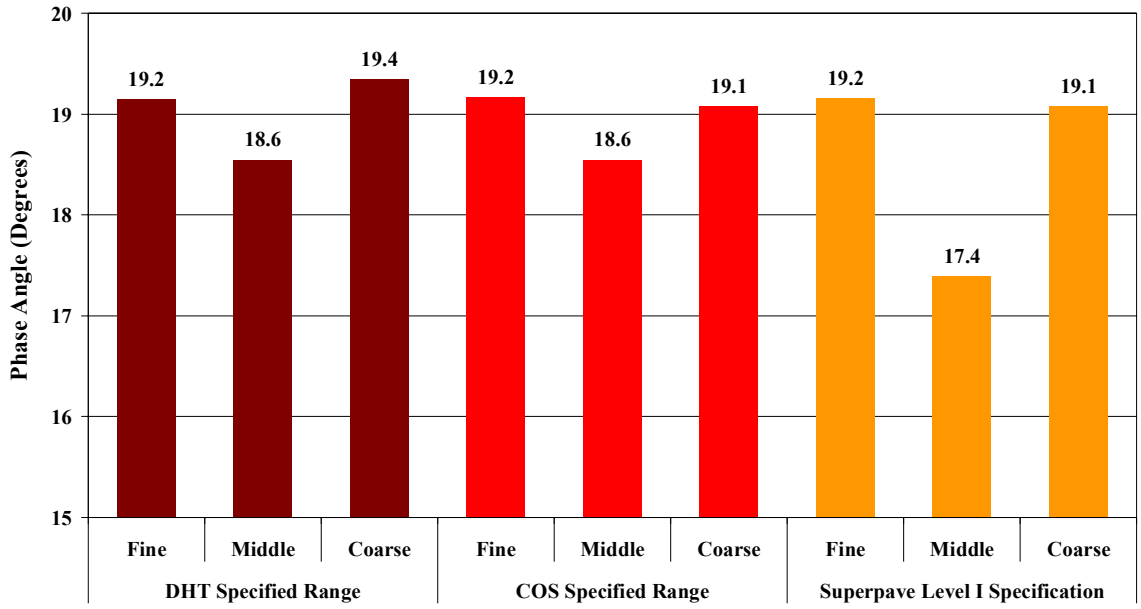

Figure 4.39 Phase Angle Range Mean for Acceptable VTM Specifications at 60°C

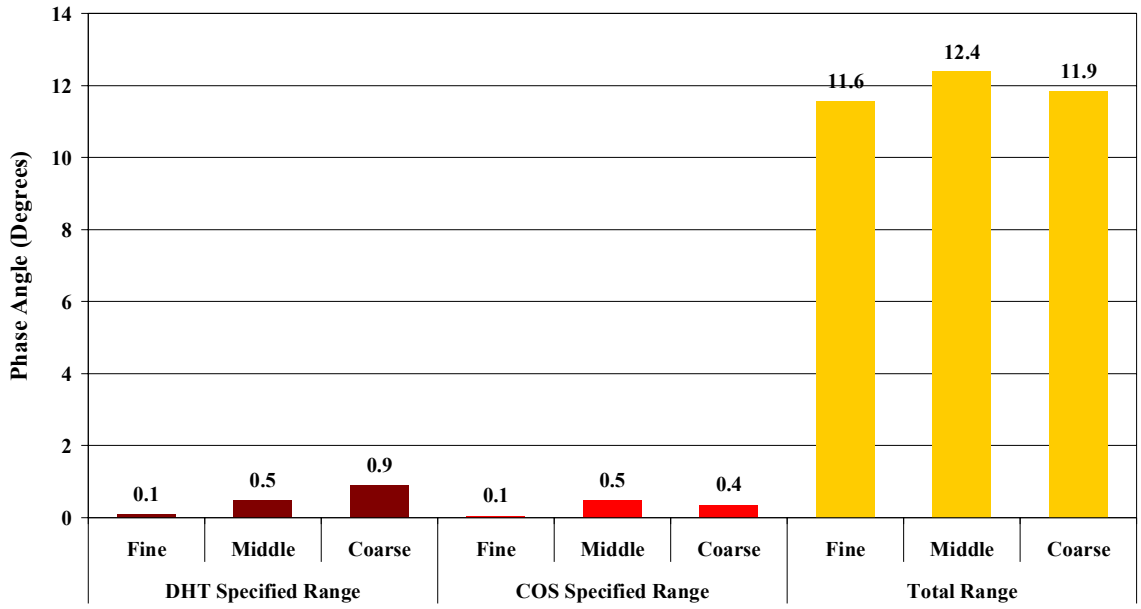

Figure 4.40 Phase Angle Range for Acceptable VTM Specifications Relative to Total Range Obtained at 60°C

4.3.1.2 Marshall Test Property Ranges for VTM Specifications

Figure 4.41 illustrates the Marshall stability and flow mean values corresponding to acceptable VTM ranges. Figure 4.42 illustrates the acceptable ranges relative to the total ranges obtained during testing that corresponded to the asphalt contents which met DHT, COS, and Superpave™ VTM specifications. The acceptable stability and flow ranges were relatively large relative to the total range obtained compared to the material properties presented in the previous section. Therefore, the RaTT material properties had the potential to be more variable when constructed outside of acceptable volumetric properties than for Marshall stability and flow.

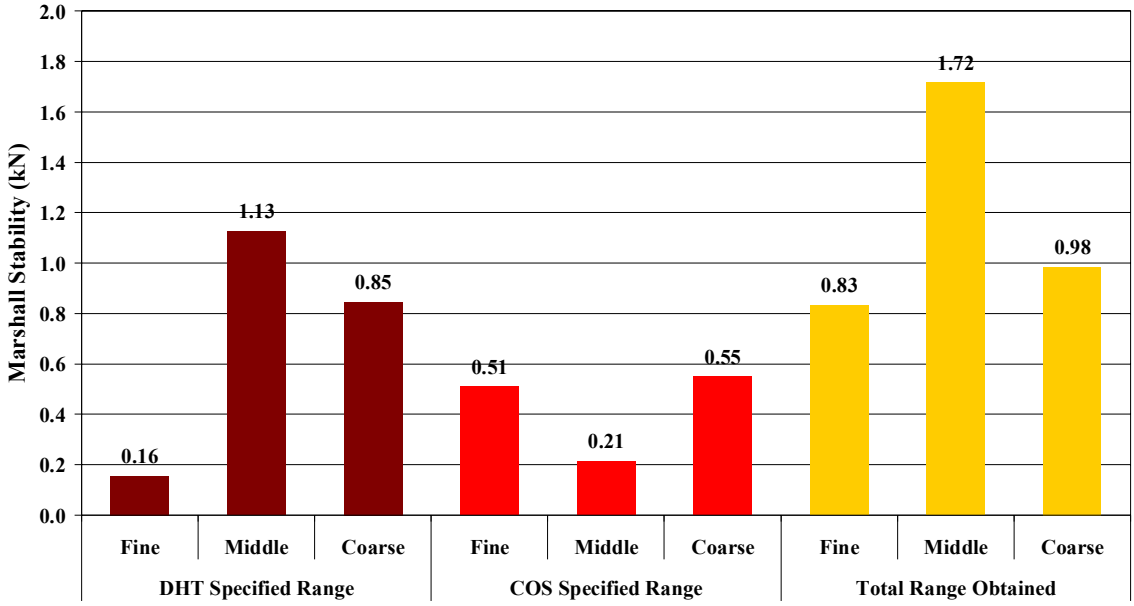

Figure 4.41 Marshall Stability Range for Acceptable VTM Specifications Relative to Total Range Obtained at 60°C

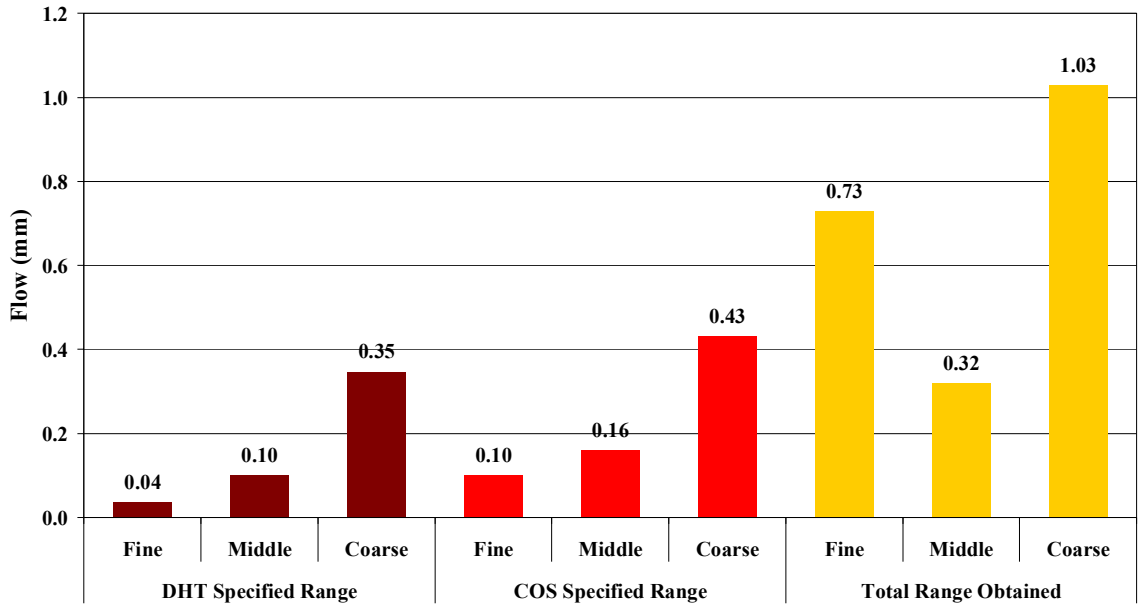

Figure 4.42 Marshall Flow Range for Acceptable VTM Specifications Relative to Total Range Obtained at 60°C

4.3.1.3 RaTT Material Property Ranges for VMA Specifications

Since insufficient samples met VMA requirements, the range of each material property determined from triaxial frequency sweep characterization that corresponded to the asphalt content ranges which met VMA specifications were not illustrated.

4.3.1.4 RaTT Material Property Ranges for VFA Specifications

Since VFA is calculated based on VTM, the material property ranges for VFA specifications are not presented here as they are nearly duplicates of the VTM ranges. In addition, VTM is typically the dominant measurement used in pavement design.

4.4 Post Triaxial Cell Frequency Sweep Volumetrics

Volumetric analysis was repeated on the gyratory compacted samples after triaxial frequency sweep testing to assess the change in volumetric properties as a result of the action of the RaTT. The results of the post-characterization volumetric analysis are summarized in Table 4.6 and Table 4.7 and are illustrated in Figure 4.43 and Figure 4.44.

As summarized in Table 4.6 and illustrated in Figure 4.43, the VTM decreased during characterization in the RaTT for all blend gradations and asphalt contents. The minimum decrease was 0.31 percent and the maximum decrease was 1.43 percent. VTM would be expected to decrease due to consolidation of the asphalt concrete samples during testing.

As summarized in Table 4.7 and illustrated in Figure 4.44, the VFA increased during characterization in the RaTT for all blend gradations and asphalt contents. The minimum increase was 4.8 percent and the maximum increase was 16.6 percent. VFA would be expected to increase due to consolidation of the asphalt concrete samples during testing.

Table 4.6 VTM Before and After RaTT Characterization

		Asphalt Content (%)					
		4.0	**4.5**	**5.0**	**5.5**	**6.0**	**6.5**
Fine Blend	**Initial**	---	8.33	6.24	5.49	2.88	0.90
	After RaTT	---	7.38	5.59	4.40	1.84	0.00
	Change	---	-0.95	-0.66	-1.09	-1.04	-0.90
Middle Blend	**Initial**	7.38	4.42	2.44	3.11	1.23	1.00
	After RaTT	6.49	4.11	1.44	2.01	0.03	0.00
	Change	-0.88	-0.31	-1.00	-1.10	-1.19	-1.00
Coarse Blend	**Initial**	6.10	6.28	4.43	2.24	0.87	---
	After RaTT	5.64	5.54	3.74	0.81	0.30	---
	Change	-0.47	-0.75	-0.69	-1.43	-0.57	---

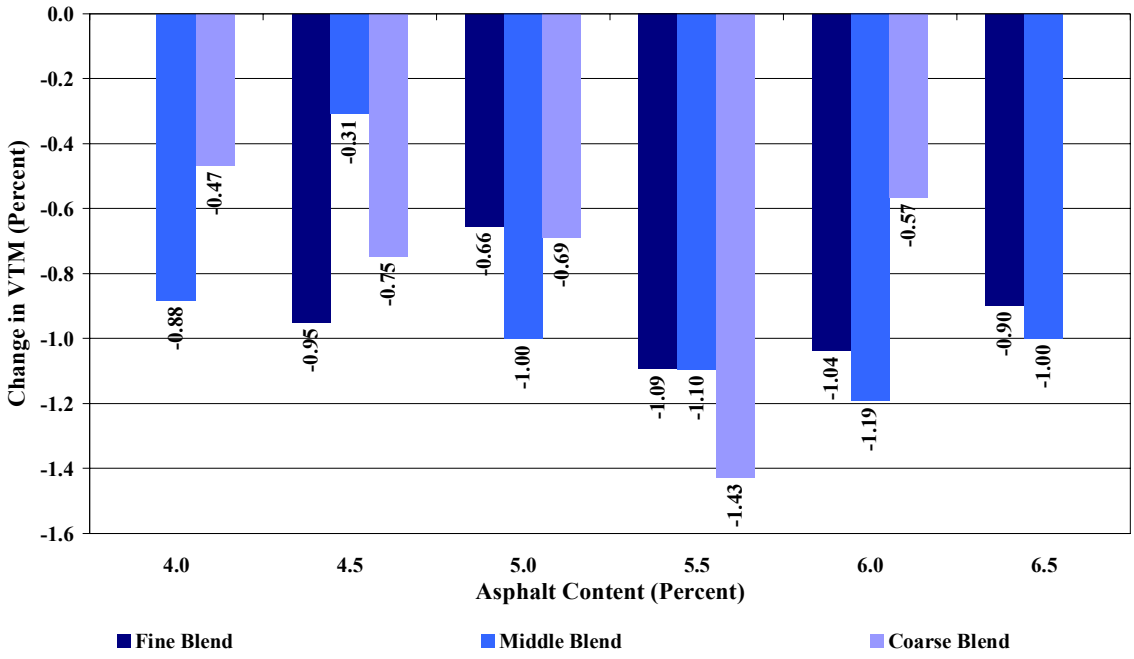

Figure 4.43 VTM Change After RaTT Characterization

Table 4.7 VFA Before and After RaTT Characterization

		Asphalt Content (%)					
		4.0	**4.5**	**5.0**	**5.5**	**6.0**	**6.5**
Fine Blend	**Initial**	---	25.0	44.2	47.1	72.4	90.4
	After RaTT	---	33.8	50.3	57.7	82.5	99.8
	Change	---	8.8	6.0	10.6	10.1	9.4
Middle Blend	**Initial**	39.2	56.2	75.8	67.1	85.2	88.1
	After RaTT	46.2	62.1	85.7	78.8	99.6	99.9
	Change	7.1	5.9	10.0	11.6	14.4	11.8
Coarse Blend	**Initial**	43.4	42.0	53.9	73.9	86.4	---
	After RaTT	48.3	49.8	60.8	90.5	96.8	---
	Change	4.8	7.8	6.9	16.6	10.4	---

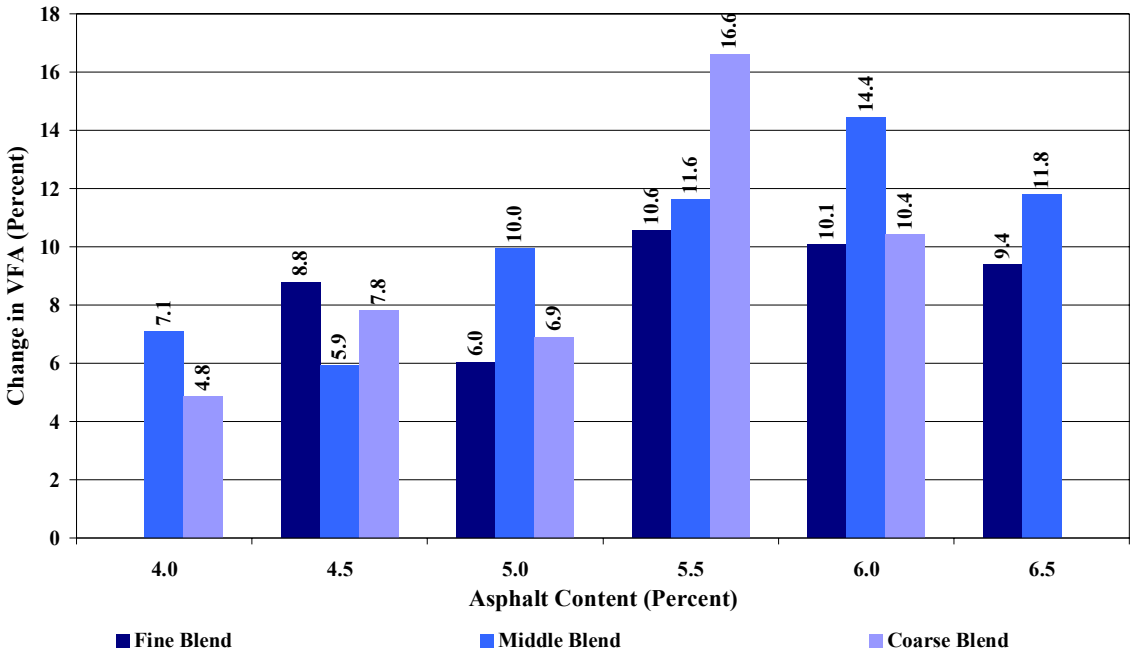

Figure 4.44 VFA Change After RaTT Characterization

4.5 Bauschinger Effect Analysis

A Bauschinger effect analysis was performed to attempt to quantify the effect of stress reversal on asphalt concrete. Figure 4.45 illustrates typical axial micro strain of all deviatoric stress states for 10 Hz at 25°C. The peaks in strain indicate periods in testing when the sample is experiencing compression, and the lows indicate sample extension. The lowest deviatoric stress state, 150 kPa, resulted in the lowest axial strain and the highest deviatoric stress state, 600 kPa, resulted in the highest axial strain, indicating that heavier vehicles will produce higher strains than lighter vehicles. This would be expected since heavy commercial trucks are known to rut pavement more than cars.

Figure 4.46 illustrates typical axial micro strain output for one asphalt concrete sample at 600 kPa deviatoric stress state for 10 Hz at 25°C. Strain tended to increase under repeated loading in compression and decreased in extension, resulting in an increasing difference in compression strain and extension strain with time, known as the Bauschinger effect. The increasing difference between the compression and extension strain with time indicates an increasing strain state, and therefore plastic deformation.

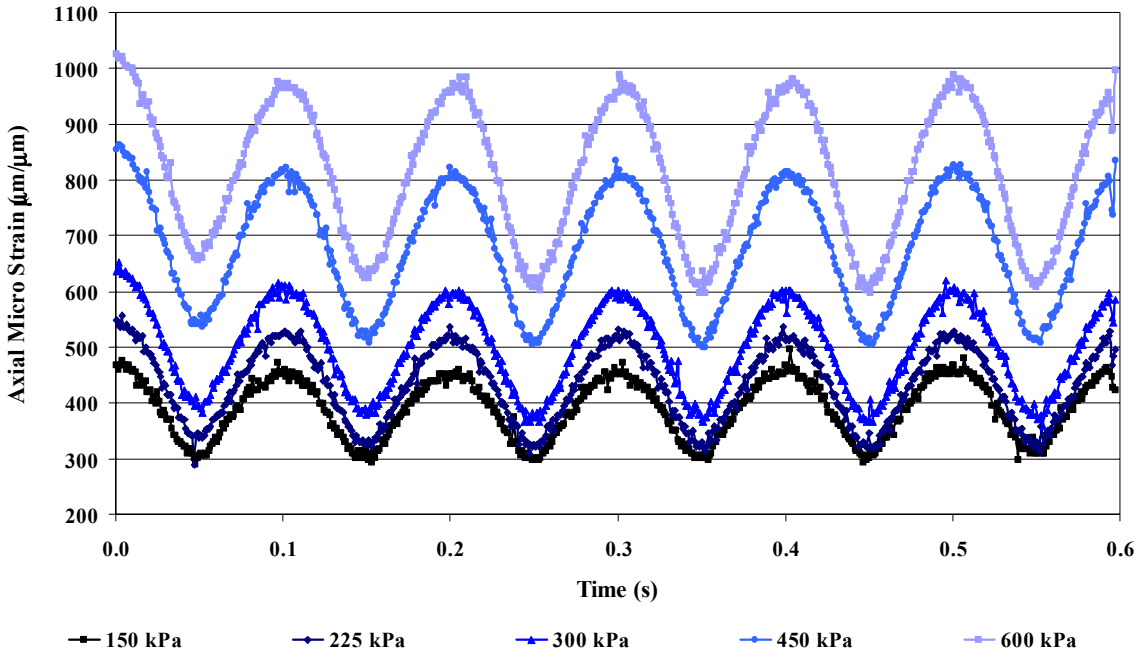

Figure 4.45 Example Triaxial Frequency Sweep Axial Micro Strain Output versus Deviatoric Stress State for 10 Hz at 25°C

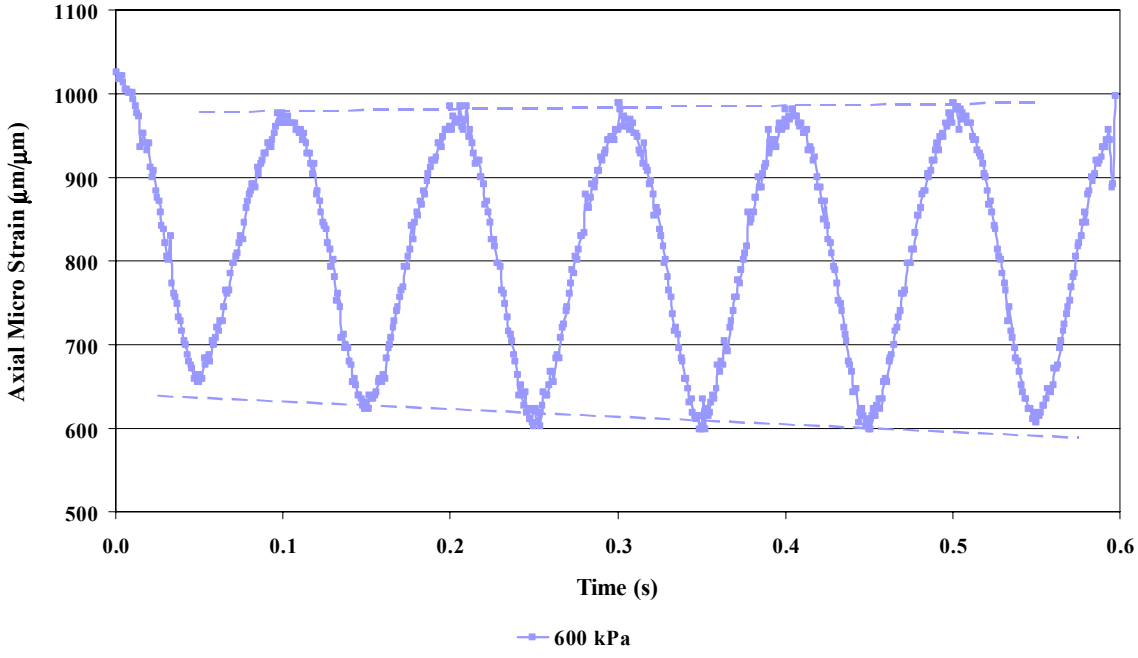

Figure 4.46 Example Triaxial Frequency Sweep Axial Micro Strain Output at 600 kPa for 10 Hz at 25°C

Figure 4.47 through Figure 4.52 illustrate the average slope between the line connecting the compressive peaks and the line connecting the extensive peaks of axial micro strain at 25°C and 60°C plotted versus frequency for all three blend gradations. A positive average slope indicates an increase in plastic strain as the sample experiences the loading cycles, while a decreasing slope indicates a decrease in plastic strain.

Figure 4.47 through Figure 4.52 illustrate the average slope between the line connecting the compressive peaks and the line connecting the extensive peaks of axial micro strain at 25°C and 60°C plotted versus frequency for all three blend gradations. The average slopes were positive for frequencies from 0.125 Hz through 5 Hz but were negative at 10 Hz, indicating less pavement damage at high traffic speeds than for lower speeds. This would be expected since rural highways with high traffic speeds generally rut less than urban intersections with low traffic speeds. The average slopes were largest at 5 Hz and decreased through to 0.125 Hz, perhaps indicating maximum pavement damage at 5 Hz. The reason for the reversal of the average slopes from negative at 10 Hz to positive at 5 Hz can not be fully explained at this time. The average slopes were generally found to be smaller at 25°C than 60°C, indicating increased pavement damage in hot weather. This would be expected since rutting primarily occurs at high temperatures.

The average slope trends were similar for all three blend gradations and the two test temperatures. There was no identifiable trend with asphalt content. 5.0 to 5.5 percent asphalt cement content typically had the lowest average slopes, perhaps indicating a better performing mix. It is interesting to note that 5.0 to 5.5 percent asphalt content is typical of pavements constructed in Saskatchewan.

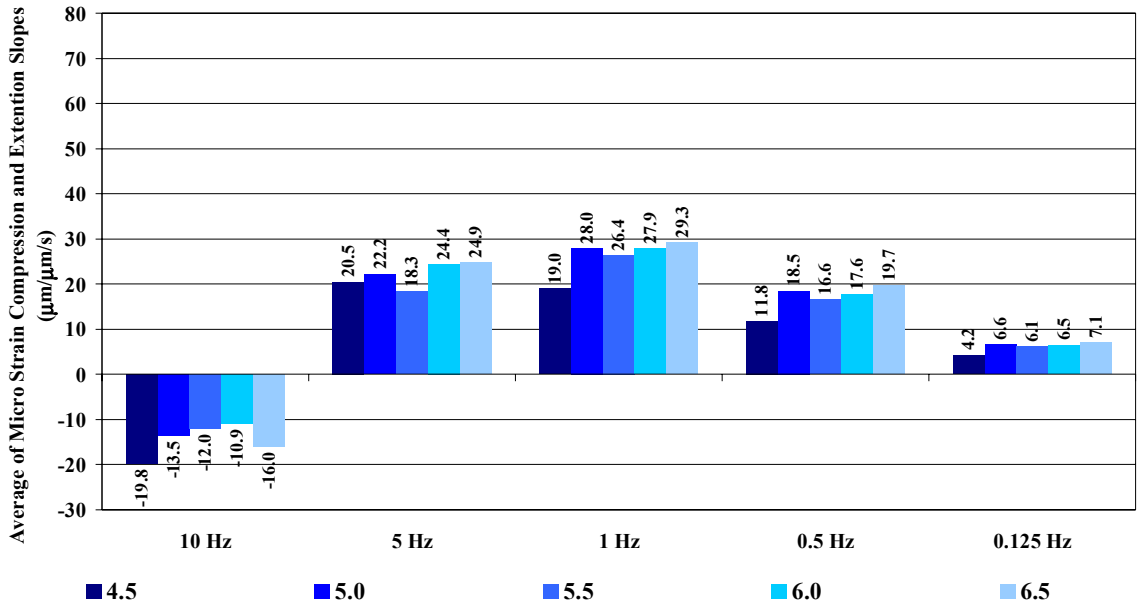

Figure 4.47 Fine Blend Average of Axial Micro Strain Compression and Extension Slopes versus Frequency at 25°C

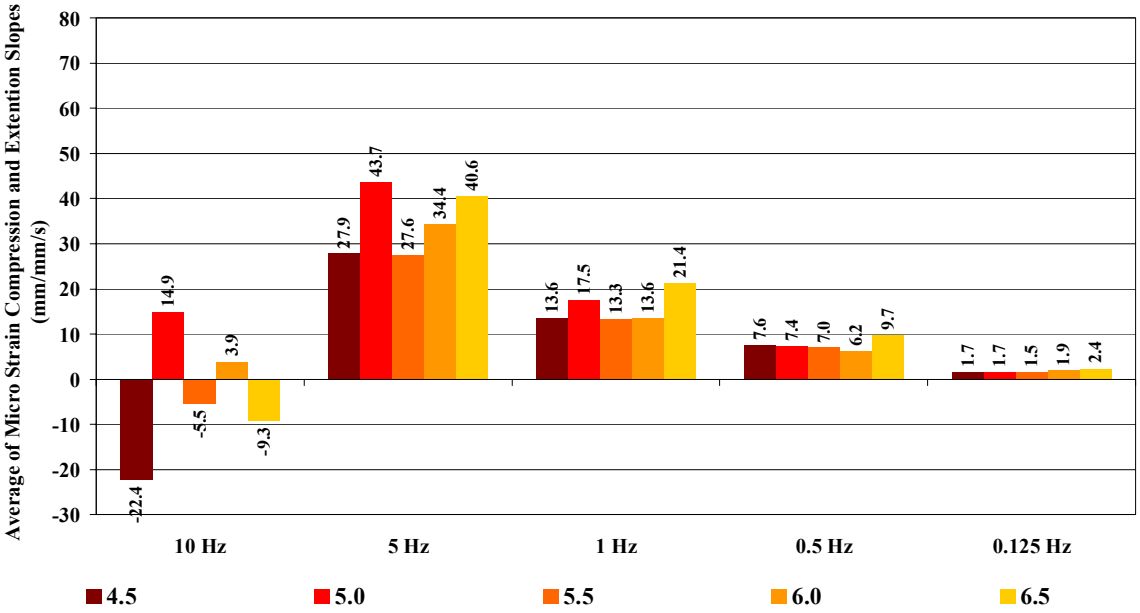

Figure 4.48 Fine Blend Average of Axial Micro Strain Compression and Extension Slopes versus Frequency at 60°C

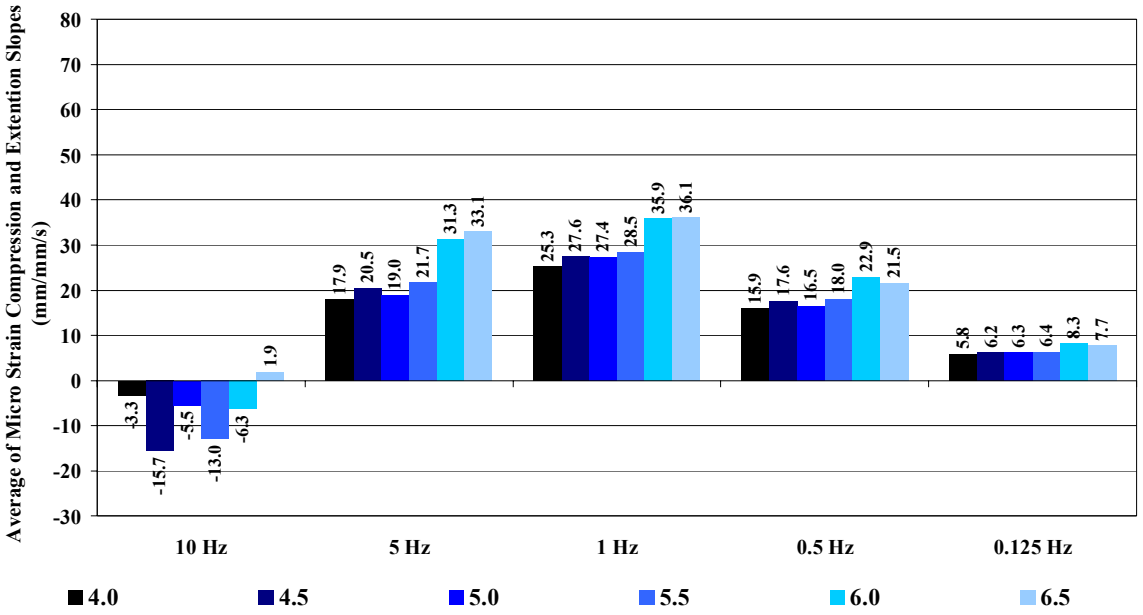

Figure 4.49 Middle Blend Average of Axial Micro Strain Compression and Extension Slopes versus Frequency at 25°C

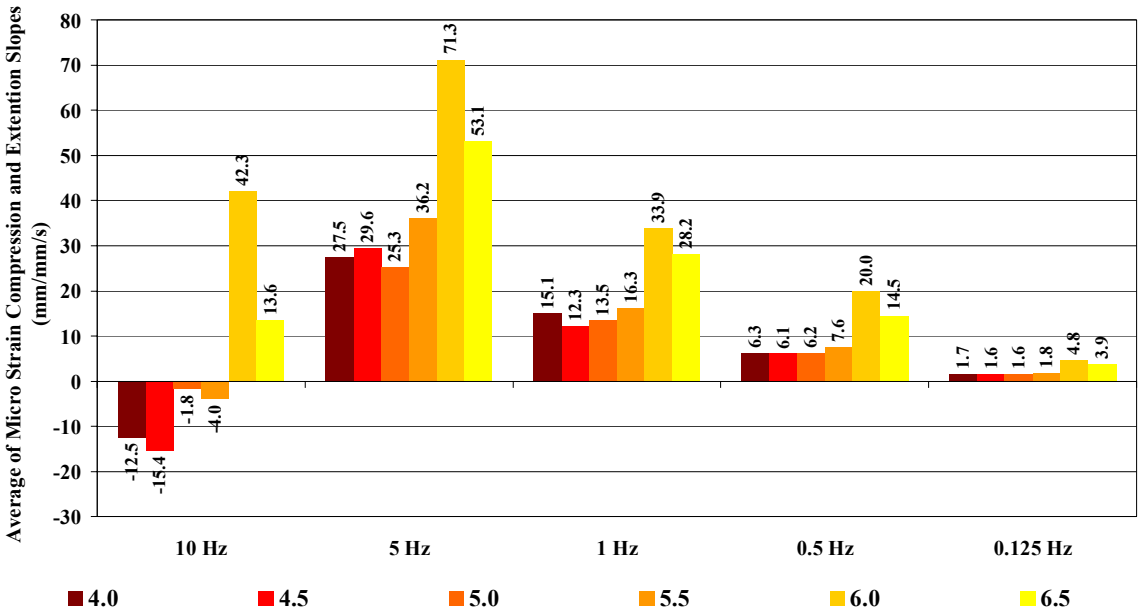

Figure 4.50 Middle Blend Average of Axial Micro Strain Compression and Extension Slopes versus Frequency at 60°C

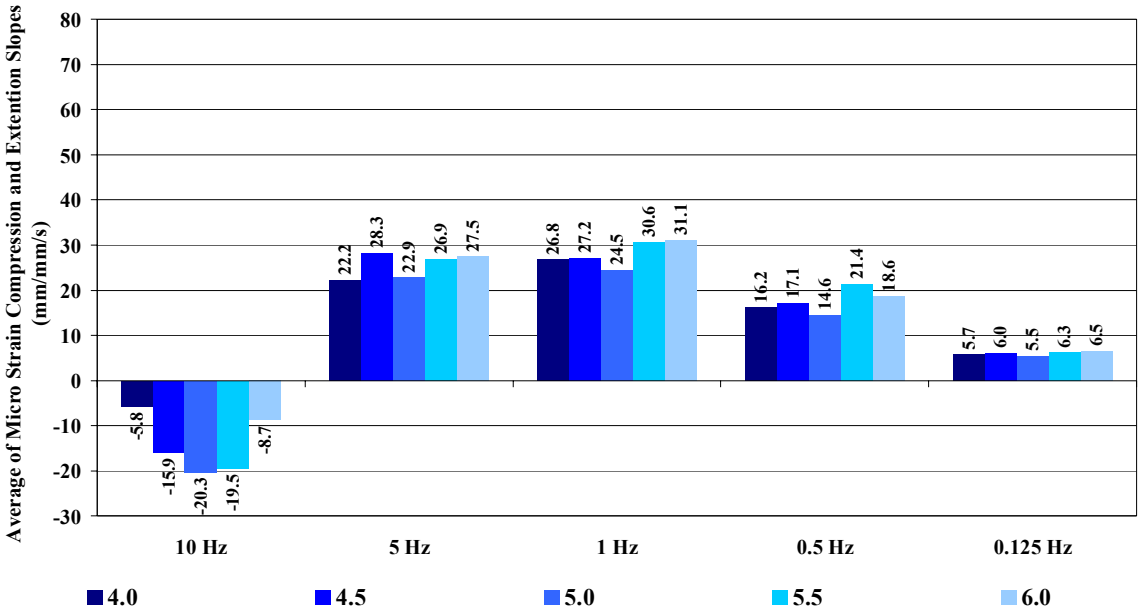

Figure 4.51 Coarse Blend Average of Axial Micro Strain Compression and Extension Slopes versus Frequency at 25°C

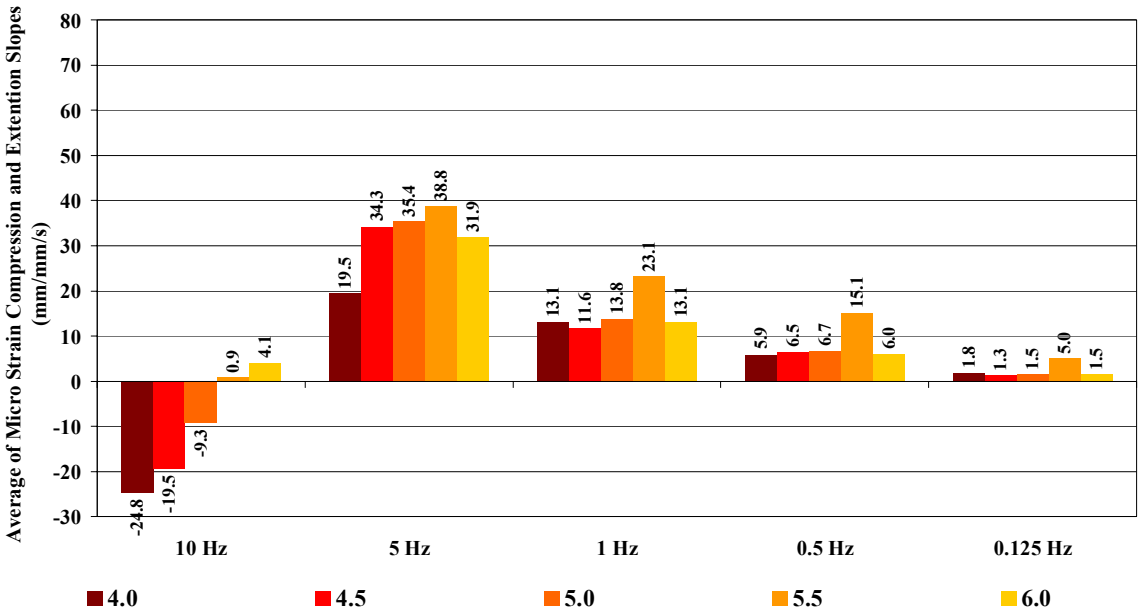

Figure 4.52 Coarse Blend Average of Axial Micro Strain Compression and Extension Slopes versus Frequency at 60°C

Figure 4.53 through Figure 4.58 illustrate slope between the line connecting the compressive peaks and the line connecting the extensive peaks of axial micro strain at 25°C and 60°C plotted versus deviatoric stress state for all three blend gradations.

The average slopes were positive for deviatoric stress states from 150 kPa through 450 kPa, indicating increasing pavement damage at lower traffic loads. The average slopes were both positive and negative at 600 kPa, indicating generally less damage at higher traffic loads. This was not expected since heavy truck loads produce more pavement damage than cars. There was no clear trend with increasing deviatoric stress state, indicating little dependence between the average slope and deviatoric stress state. The average slopes were generally found to be smaller at 25°C than 60°C, indicating increased pavement damage in hot weather. This would be expected since rutting primarily occurs at high temperatures.

The average slope trends were similar for all three blend gradations and the two test temperatures. There was no identifiable trend with asphalt content.

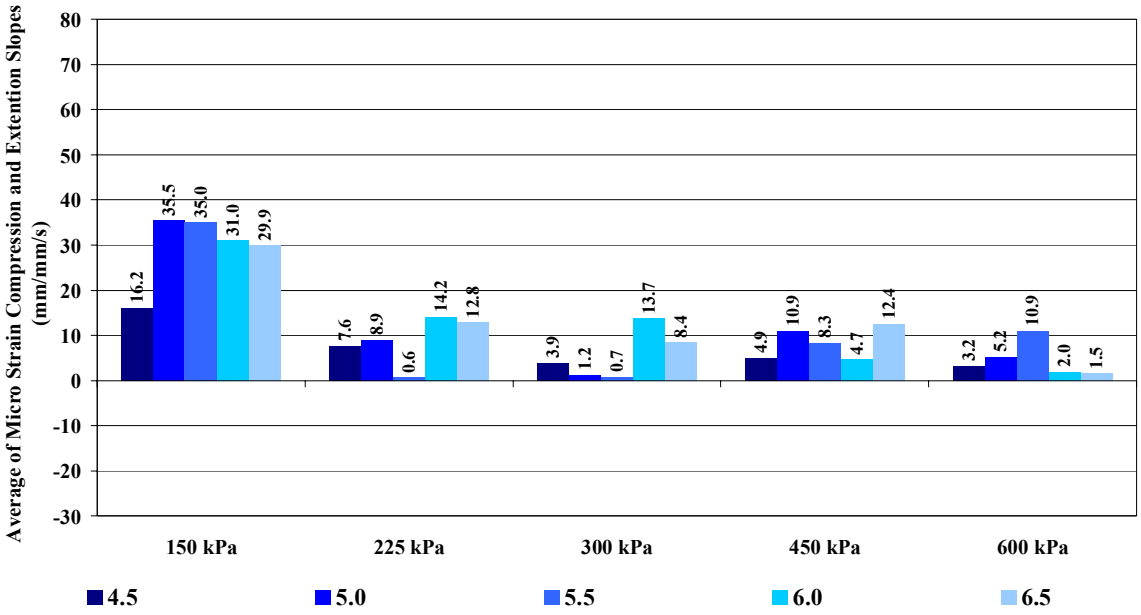

Figure 4.53 Fine Blend Average of Axial Micro Strain Compression and Extension Slopes versus Deviatoric Stress State at 25°C

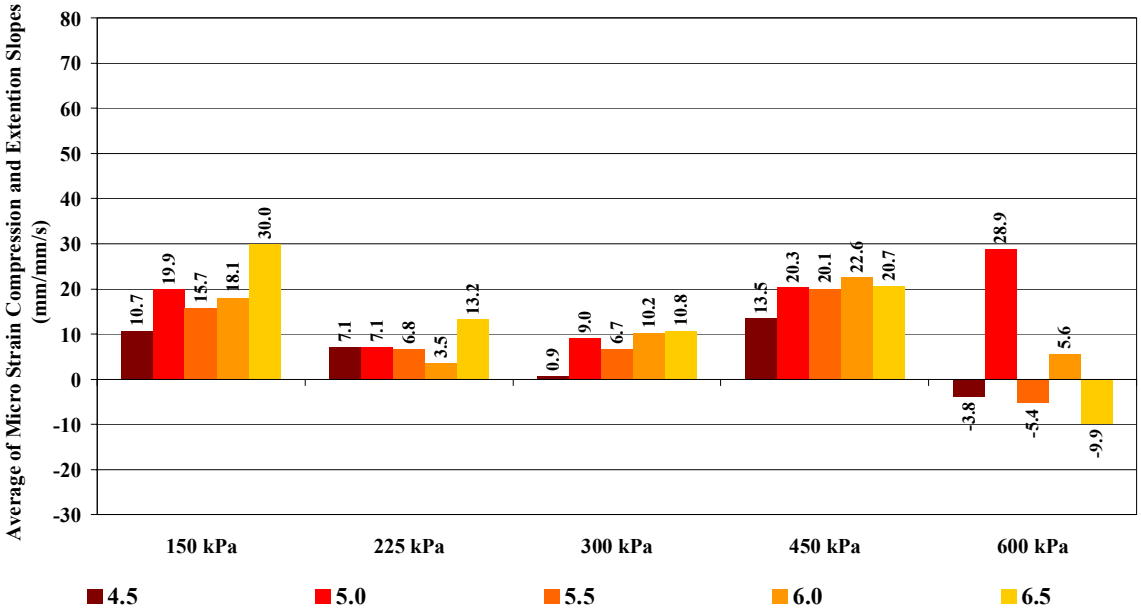

Figure 4.54 Fine Blend Average of Axial Micro Strain Compression and Extension Slopes versus Deviatoric Stress State at 60°C

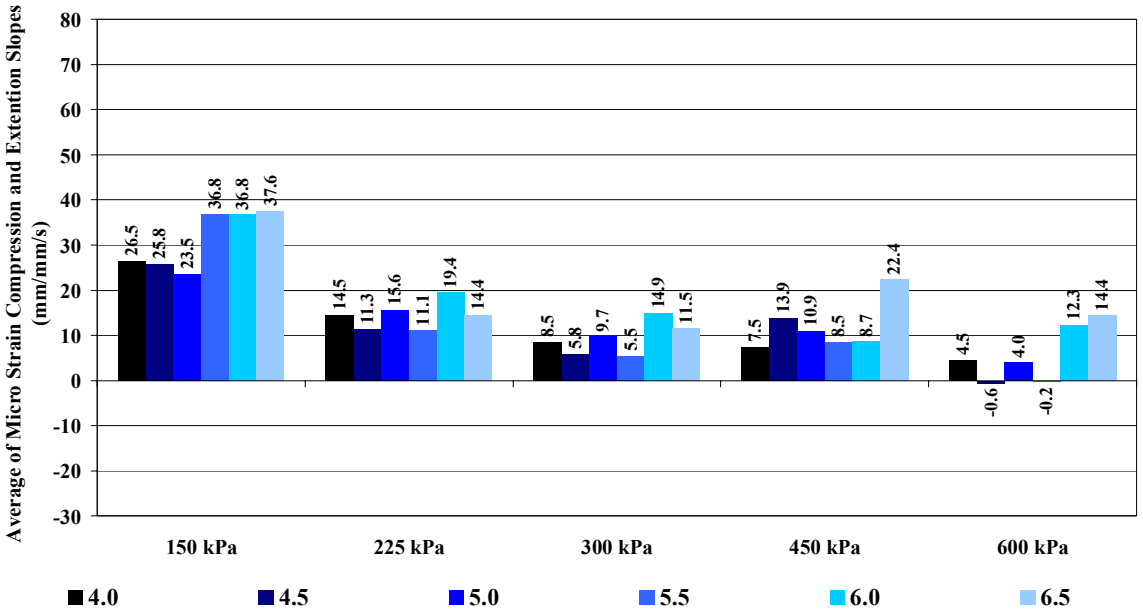

Figure 4.55 Middle Blend Average of Axial Micro Strain Compression and Extension Slopes versus Deviatoric Stress State at 25°C

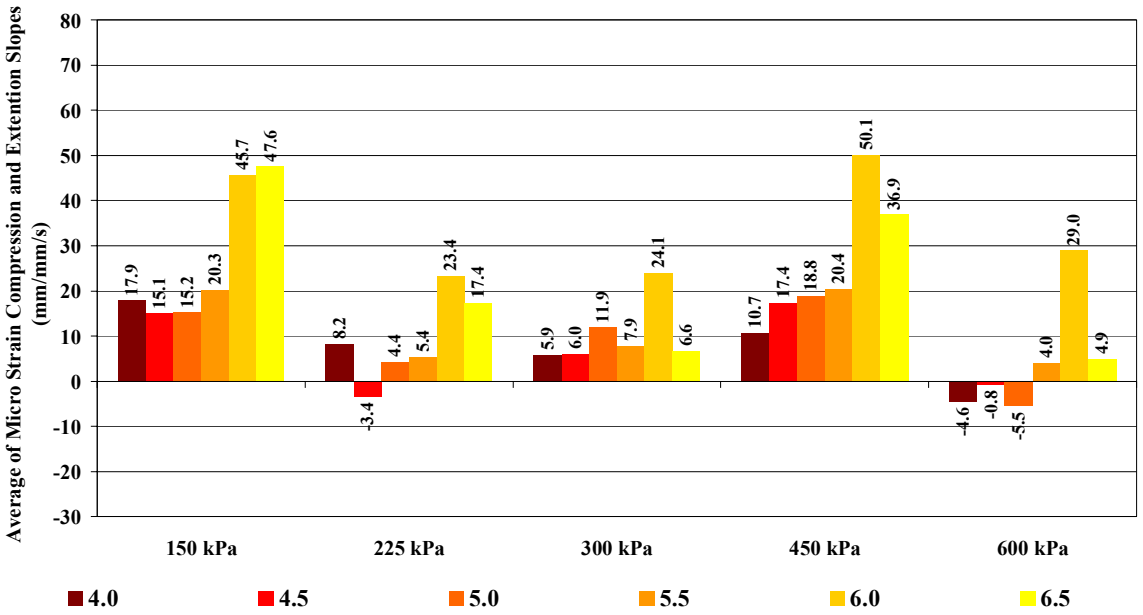

Figure 4.56 Middle Blend Average of Axial Micro Strain Compression and Extension Slopes versus Deviatoric Stress State at 60°C

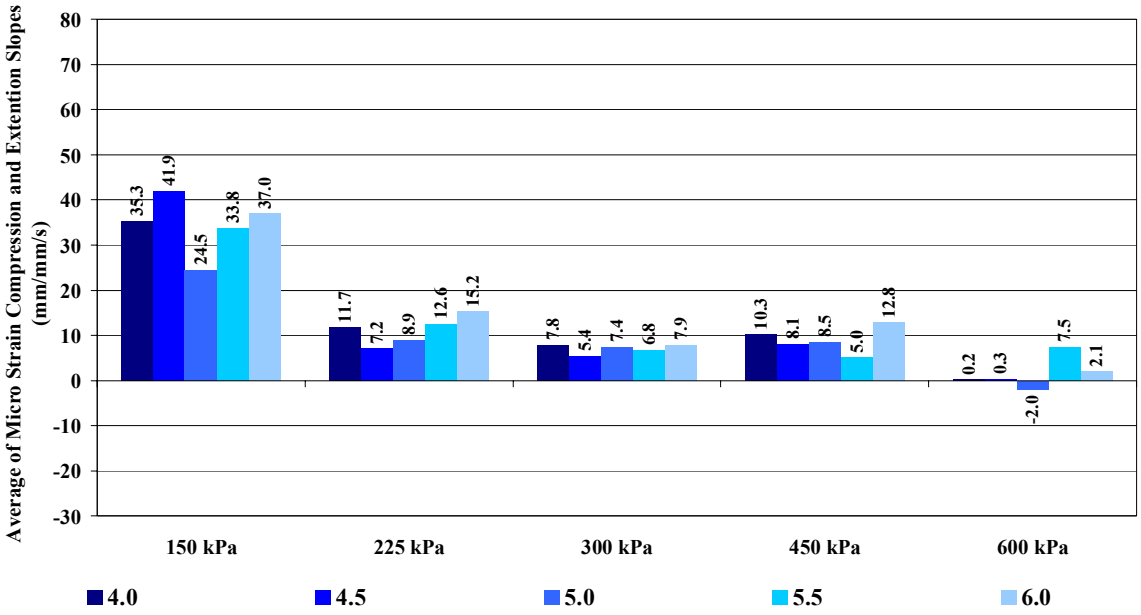

Figure 4.57 Coarse Blend Average of Axial Micro Strain Compression and Extension Slopes versus Deviatoric Stress State at 25°C

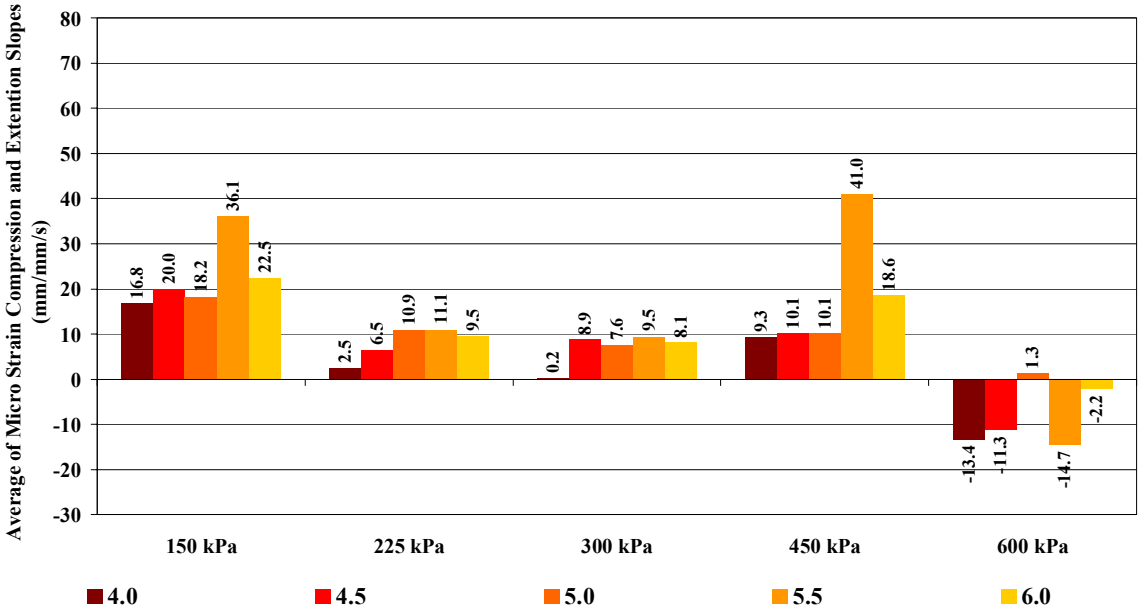

Figure 4.58 Coarse Blend Average of Axial Micro Strain Compression and Extension Slopes versus Deviatoric Stress State at 60°C

Figure 4.59 through Figure 4.64 illustrate the difference in axial compressive strain and axial extensive strain between the first loading cycle to the last loading cycle at 25°C and at 60°C plotted versus frequency for all three blend gradations. An increase in strain difference with time indicates the presence of the Bauschinger effect and therefore an increasing strain state, or increasing plastic deformation, with time. A decrease in strain difference indicates a decreasing strain state, or decreasing plastic deformation, with time.

The strain difference decreased as frequency decreased, indicating less pavement damage at lower traffic speeds. This would not be expected, since more pavement damage typically occurs at urban intersections with low traffic speeds than on highways with high traffic speeds. The strain difference typically increased at 10 Hz and 5 Hz, and typically decreased at 1 Hz, 0.5 Hz, and 0.125 Hz. The strain difference magnitudes were larger at 60°C than at 25°C which may indicate increased pavement damage at higher frequencies at higher service temperatures. This would be expected since rutting primarily occurs at high temperatures.

Strain difference trends were similar for all three blend gradations and the two test temperatures. There was no identifiable trend with asphalt content.

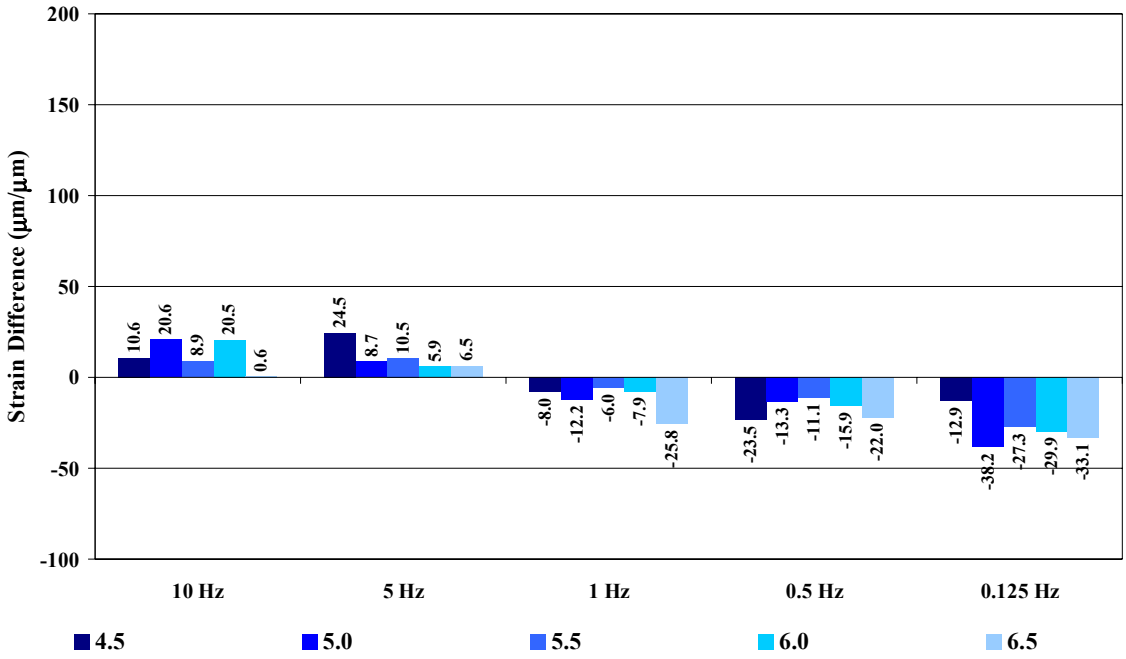

Figure 4.59 Fine Blend Axial Micro Strain Difference Between First and Last Cycle Versus Frequency at 25°C

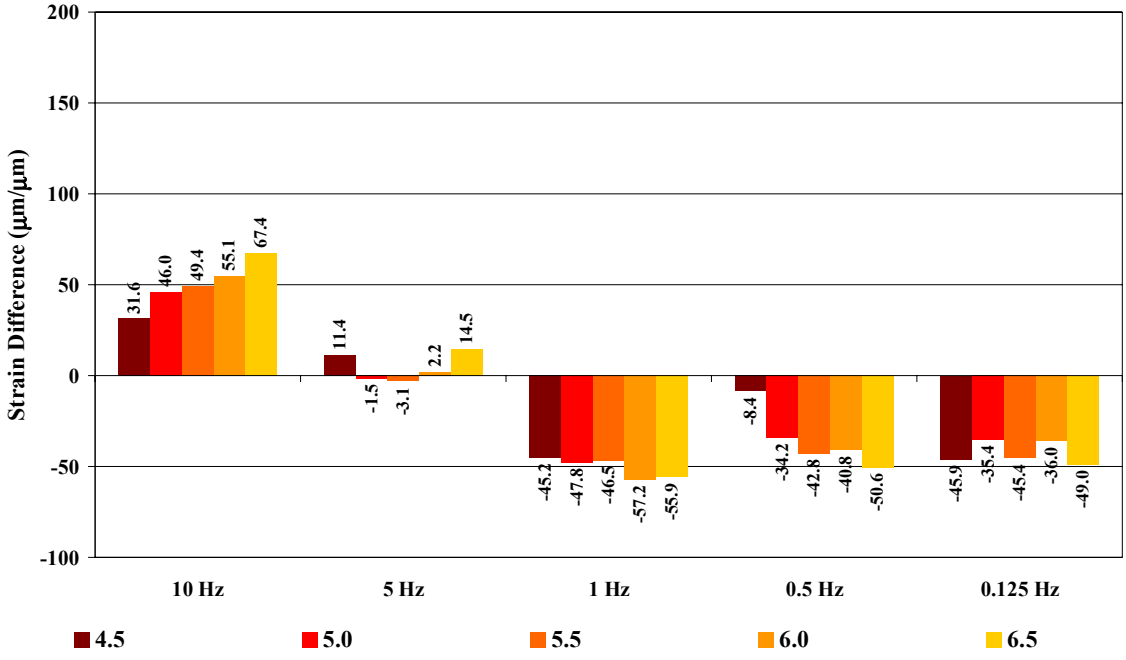

Figure 4.60 Fine Blend Axial Micro Strain Difference Between First and Last Cycle Versus Frequency at 60°C

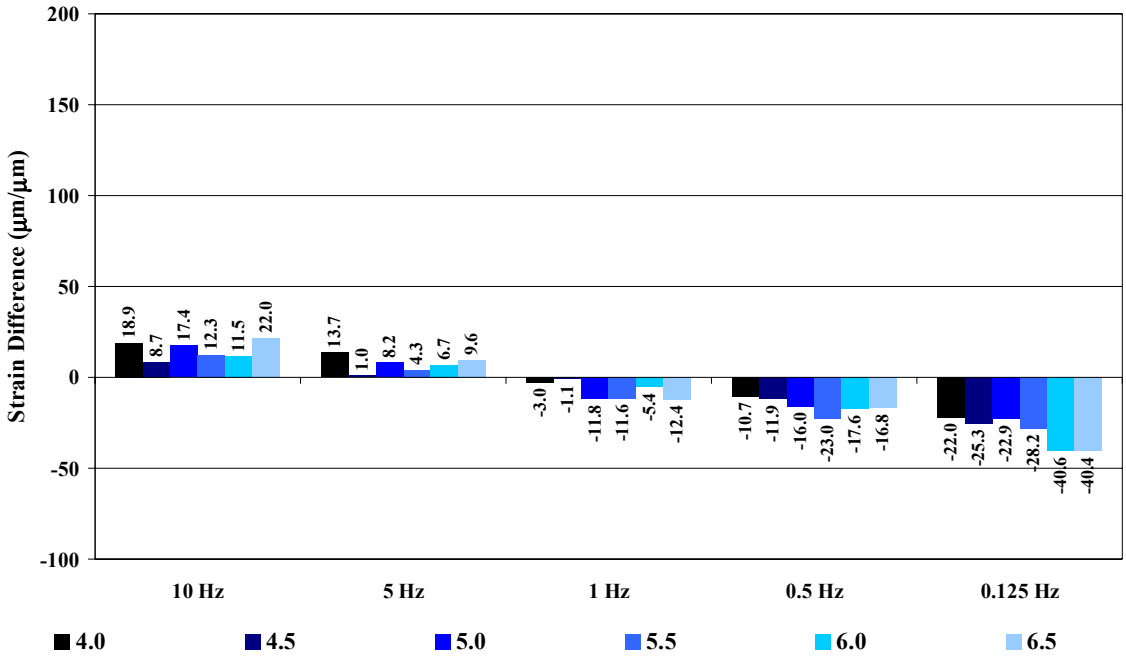

Figure 4.61 Middle Blend Axial Micro Strain Difference Between First and Last Cycle Versus Frequency at 25°C

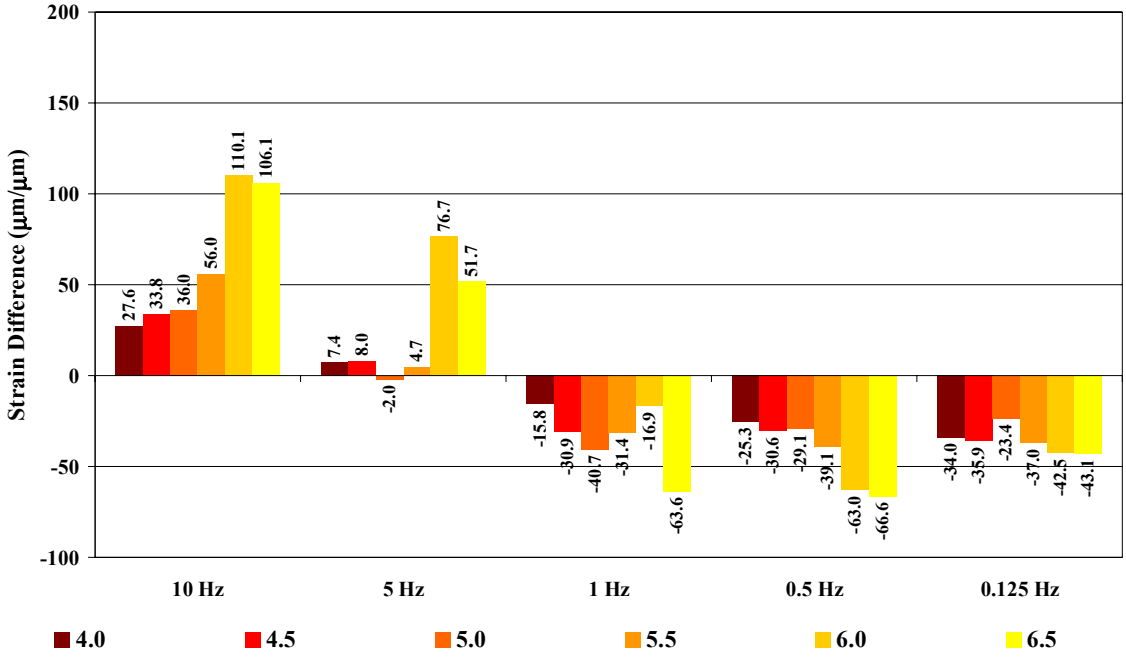

Figure 4.62 Middle Blend Axial Micro Strain Difference Between First and Last Cycle Versus Frequency at 60°C

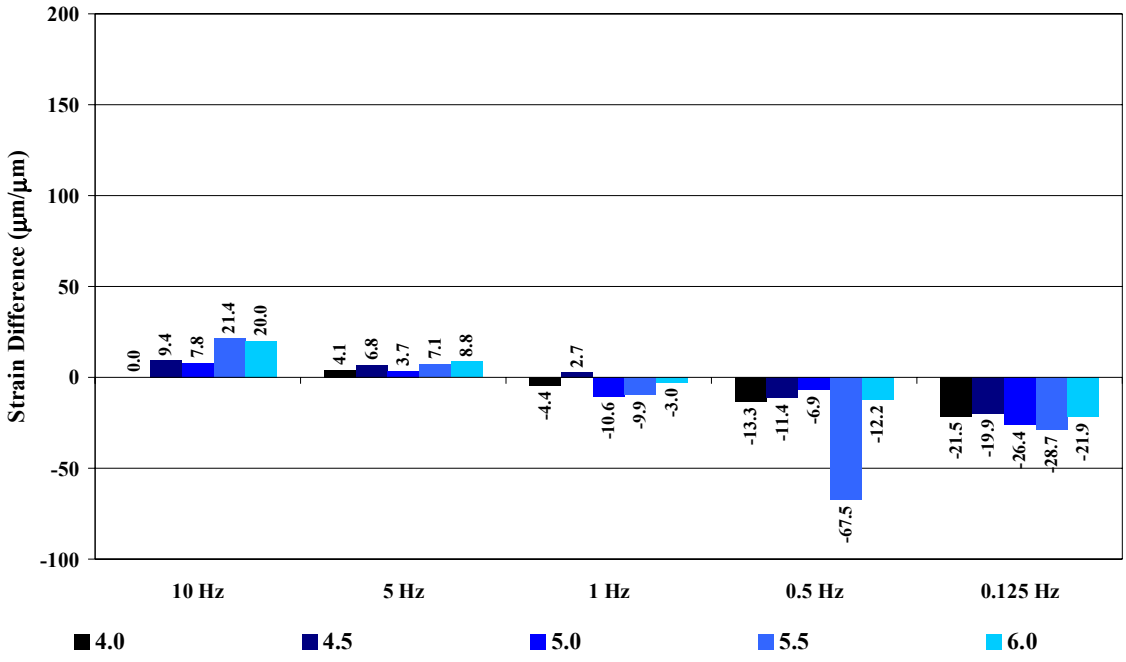

Figure 4.63 Coarse Blend Axial Micro Strain Difference Between First and Last Cycle Versus Frequency at 25°C

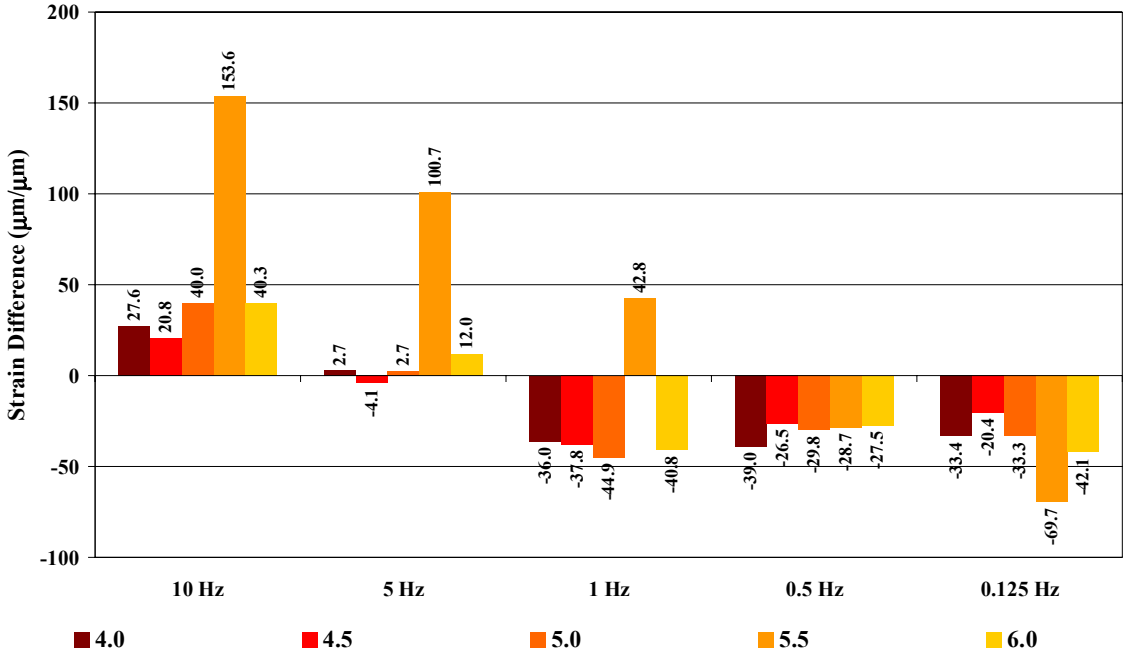

Figure 4.64 Coarse Blend Axial Micro Strain Difference Between First and Last Cycle Versus Frequency at 60°C

Figure 4.65 through Figure 4.70 illustrate the difference in axial compressive strain and axial extensive strain between the first loading cycle to the last loading cycle at 25°C and at 60°C plotted versus deviatoric stress state for all three blend gradations.

The strain difference decreased at 150 kPa through 450 kPa and increased at 600 kPa at 25°C and 60°C. The positive strain difference at the 600 kPa deviatoric stress state indicates damage for heavy traffic loads. This would be expected since heavy truck loads produce more pavement damage than cars. The strain difference magnitudes were larger at 60°C than at 25°C which may indicate increased pavement damage at higher service temperatures. This would be expected since rutting primarily occurs at high temperatures.

At 600 kPa and 60°C, the strain difference of the coarse blend at 5.5 percent asphalt content is many times greater relative to the other asphalt contents, as well as relative to the strain differences of the other blends at all deviatoric stress states. This unusual value may be the result of a software measurement error during characterization.

Strain difference trends were similar for all three blend gradations and the two test temperatures. There was no identifiable trend with asphalt content.

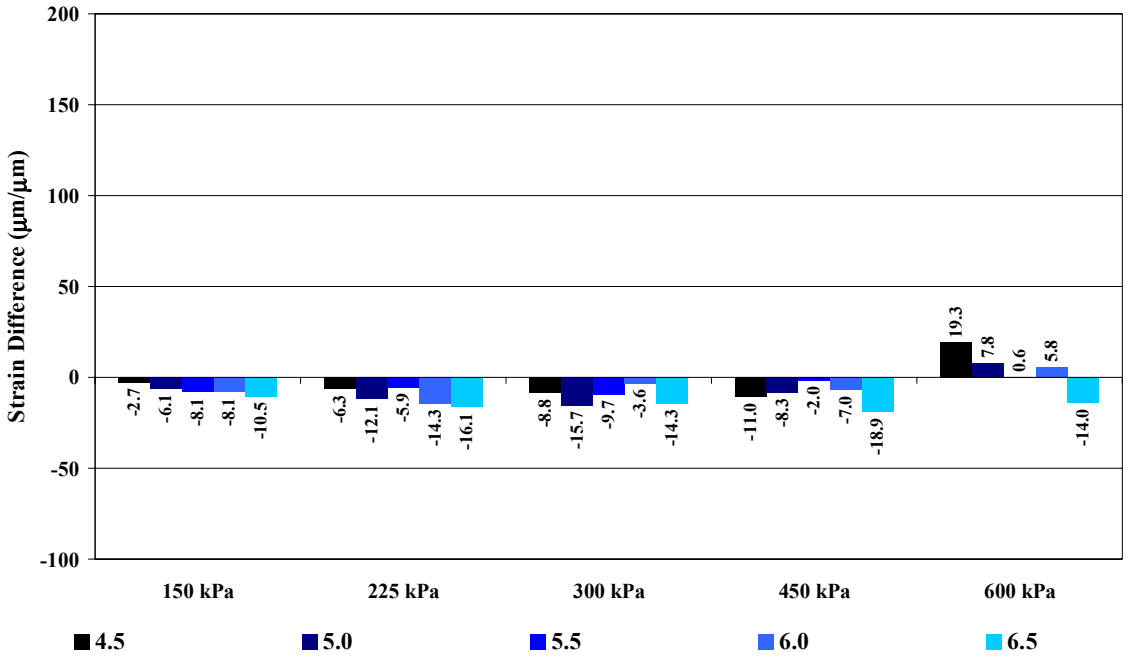

Figure 4.65 Fine Blend Axial Micro Strain Difference Between First and Last Cycle Versus Deviatoric Stress State at 25°C

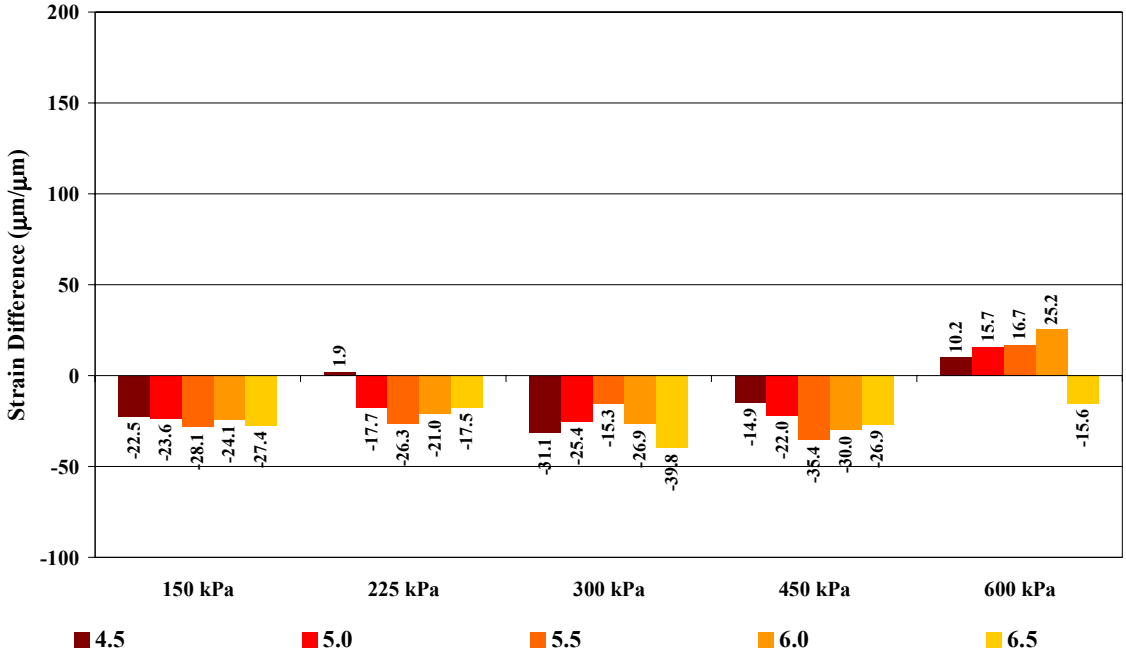

Figure 4.66 Fine Blend Axial Micro Strain Difference Between First and Last Cycle Versus Deviatoric Stress State at 60°C

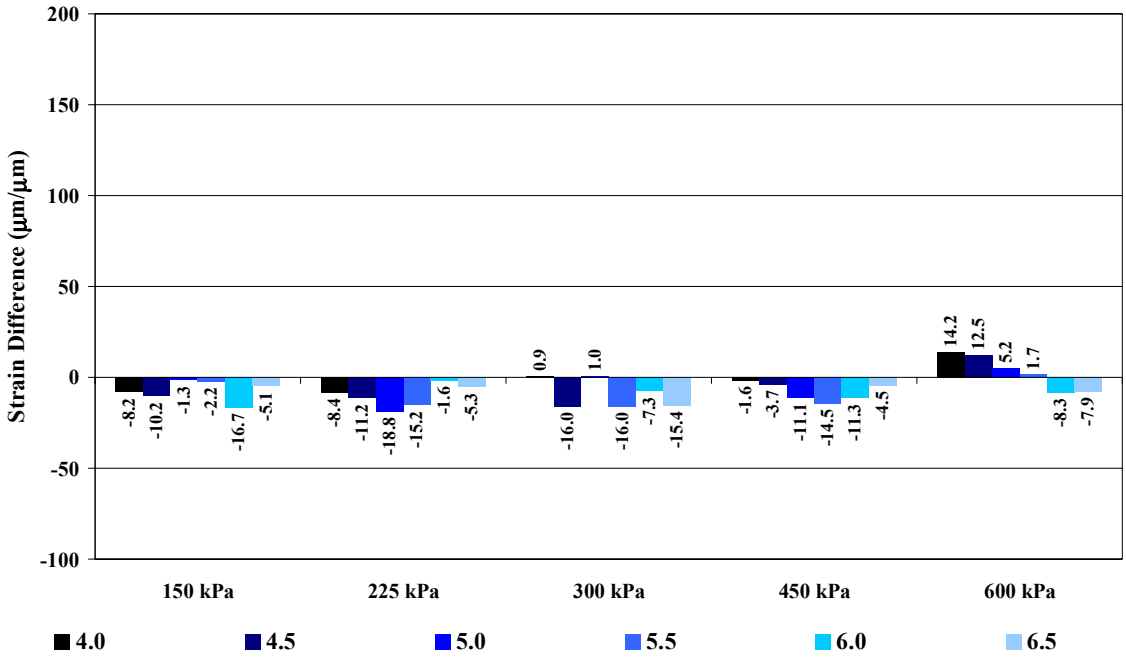

Figure 4.67 Middle Blend Axial Micro Strain Difference Between First and Last Cycle Versus Deviatoric Stress State at 25°C

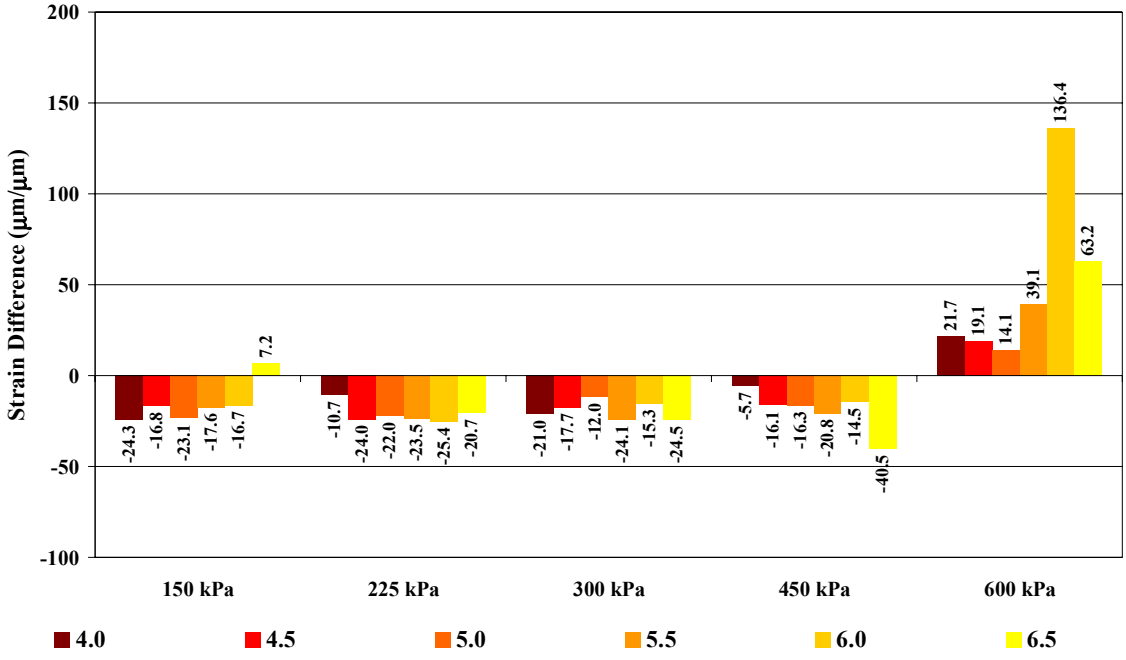

Figure 4.68 Middle Blend Axial Micro Strain Difference Between First and Last Cycle Versus Deviatoric Stress State at 60°C

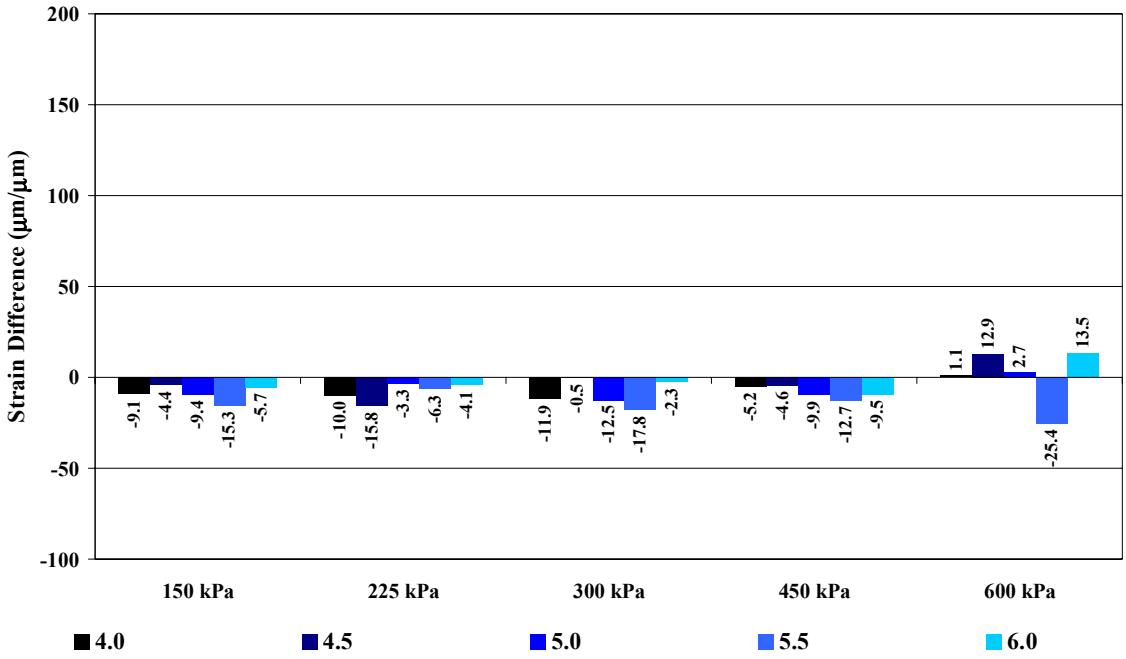

Figure 4.69 Coarse Blend Axial Micro Strain Difference Between First and Last Cycle Versus Deviatoric Stress State at 25°C

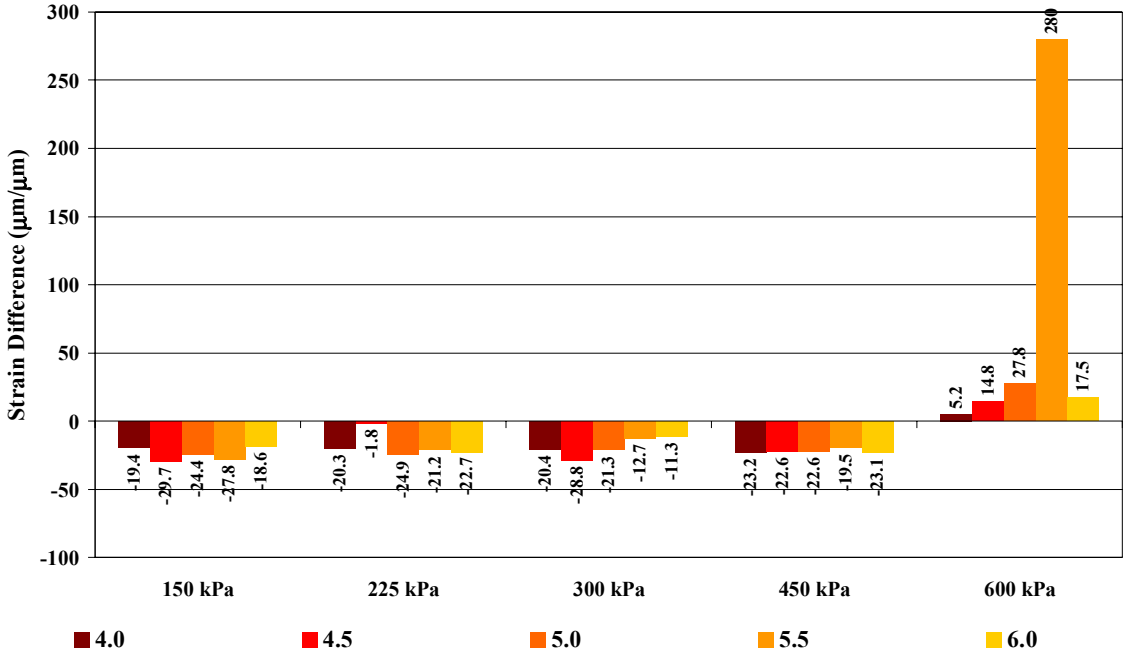

Figure 4.70 Coarse Blend Axial Micro Strain Difference Between First and Last Cycle Versus Deviatoric Stress State at 60°C

4.6 Summary

The SHRP gyratory compacted samples were subjected to triaxial frequency sweep characterization in the RaTT. Each sample was subjected to five loading frequencies at five deviatoric stress states at 25°C and 60°C to simulate a range of field state conditions. Dynamic modulus, Poisson's ratio, and phase angle were determined from RaTT testing.

As hypothesized, dynamic modulus was found to be higher at 25°C than at 60°C for all blend gradations and dynamic modulus decreased with increasing asphalt content for all blend gradations at both 25°C and 60°C. Dynamic modulus was found to increase with increasing deviatoric stress state for all blend gradations at 25°C and 60°C. Dynamic modulus was found to increase with increasing frequency for each blend gradation at 25°C and 60°C, and increased at a faster rate at 25°C than at 60°C. Dynamic modulus was found to be linear when plotted versus deviatoric stress state, and nonlinear when plotted versus frequency.

As hypothesized, Poisson's ratio was found to be higher at 60°C than at 25°C for each blend gradation. Poisson's ratio increased with increasing asphalt content for all three blend gradations at both 25°C and 60°C. Poisson's ratio was found to increase with increasing deviatoric stress at 25°C and was found to decrease with increasing deviatoric stress at 60°C for all blend gradations. Poisson's ratio was found to increase with increasing axial loading frequency for each blend gradation at 25°C and 60°C. Poisson's ratio was found to be linear when plotted versus deviatoric stress state and when plotted versus frequency.

As hypothesized, phase angle was found to be lower at 60°C than at 25°C for each blend gradation. Phase angle increased with increasing asphalt content at 25°C but no clear trend was observed at 60°C. Phase angle was found to decrease with increasing deviatoric stress state at 25°C and 60°C for each blend gradation. Phase angle decreased with increased load frequency at 25°C but increased with increased frequency at 60°C for each blend gradation. Phase angle at 25°C and at 60°C crossed over each other

between approximately 2 to 6 Hz. Phase angle was found to to be linear when plotted versus deviatoric stress state, and nonlinear when plotted versus frequency.

Based on the difference in dynamic modulus, Poisson's ratio, and phase angle between 25°C and 60°C, asphalt concrete was found to behave differently depending on temperature. Therefore service temperatures may be a necessary input when designing asphalt concrete. The difference in dynamic modulus, Poisson's ratio, and phase angle between low and high axial load frequencies is an indication that asphalt concrete behaves differently at different traffic speeds. Therefore, traffic speed may be a necessary input when designing asphalt concrete. Currently, asphalt concrete mix design methods do not take into account traffic speed.

The phase angle indicated that the asphalt concrete mixes considered in this research exhibited viscoelastic behaviour. The nonlinearity of dynamic modulus and phase angle when plotted versus frequency indicated nonlinear material behaviour for all blend gradations. Nonlinearity was observed in the dynamic modulus from 0.125 Hz through approximately 2 Hz, and linearity was observed from approximately 2 Hz through 10 Hz. Nonlinearity was observed in the phase angle results from 0.125 Hz through approximately 2 Hz to 6 Hz, and linearity was observed from approximately 2 Hz to 6 Hz through 10 Hz.

In order to compare the Marshall stability and flow results to the material properties obtained from the RaTT, the range of dynamic modulus, Poisson's ratio, and phase angle which corresponded to the range of acceptable volumetric properties which met COS, DHT, and Superpave™ specifications were determined and compared to the total range of each property obtained during testing. The acceptable stability and flow ranges were relatively large relative to the total range obtained compared to the material properties presented in the previous section. Therefore, the RaTT material properties had the potential to be more variable when constructed outside of acceptable volumetric properties than for Marshall stability and flow. This also illustrates the potential for a large change in mechanistic properties if an asphalt concrete pavement is constructed outside of volumetric specifications.

A Bauschinger effect analysis was performed to attempt to quantify the effect of stress reversal on asphalt concrete. The lowest deviatoric stress state, 150 kPa, resulted in the lowest axial strain and the highest deviatoric stress state, 600 kPa, resulted in the highest axial strain, indicating that heavier vehicles will produce higher strains than lighter vehicles. This would be expected since heavy commercial trucks are known to rut pavement more than cars.

The average slope between the line connecting the compressive peaks and the line connecting the extensive peaks of axial micro strain was determined for all three blend gradations. The average slopes were positive for frequencies from 0.125 Hz through 5 Hz but were negative at 10 Hz, indicating less pavement damage at high traffic speeds than for lower speeds, which would be expected since rural highways with high traffic speeds generally rut less than urban intersections with low traffic speeds. The average slopes were generally found to be smaller at 25^{o}C than 60^{o}C, indicating increased pavement damage in hot weather, which would be expected since rutting primarily occurs at high temperatures.

The average slopes were positive for deviatoric stress states from 150 kPa through 450 kPa, indicating increasing pavement damage at lower traffic loads. The average slopes were both positive and negative at 600 kPa, indicating less damage at higher traffic loads. This was not expected since heavy truck loads produce more pavement damage than cars. The average slopes were generally found to be smaller at 25^{o}C than 60^{o}C, indicating increased pavement damage in hot weather. This would be expected since rutting primarily occurs at high temperatures.

The difference in compressive strain and extensive strain between the first loading cycle and the last loading cycle was determined for all three blend gradations. The strain difference decreased as frequency decreased, indicating less pavement damage at lower traffic speeds. This would not be expected, since more pavement damage typically occurs at urban intersections with low traffic speeds than on highways with high traffic speeds. The strain difference increased at 10 Hz and 5 Hz, and typically decreased at 1 Hz, 0.5 Hz, and 0.125 Hz. The strain difference magnitudes were larger at 60^{o}C than at 25^{o}C which indicating increased pavement damage at higher

frequencies at higher service temperatures. This would be expected since rutting primarily occurs at high temperatures.

The strain difference decreased at 150 kPa through 450 kPa and increased at 600 kPa at 25°C and 60°C. The positive strain difference at the 600 kPa deviatoric stress state indicates damage for heavy traffic loads. This would be expected since heavy truck loads produce more pavement damage than cars. The strain difference magnitudes were larger at 60°C than at 25°C which may indicate increased pavement damage at higher service temperatures. This would be expected since rutting primarily occurs at high temperatures.

5.0 FINDINGS, SUMMARY, AND CONCLUSIONS

Asphalt concrete mix design has historically been based on phenomenological material testing empirically correlated to observed field performance. Saskatchewan road agencies currently employ the phenomenological-empirical Marshall asphalt concrete mix design method. However, empirical mix design methods are based on historic experience and therefore have several inherent limitations when applied to changing field state conditions such as increasing truck traffic, changing materials, and the aged state of road structures.

Mechanistic testing employs the laws of thermodynamics and primary responses, such as stress and strain, in the pavement structure. The need has been identified to develop a mechanistic based asphalt concrete performance test procedure that is able to accurately reproduce *in situ* pavement axial stress, confinement stress, and temperature conditions in order to obtain accurate stress and strain relations for pavement performance prediction (Brown 1976, Croney 1977, Witczak 2003). Mechanistic methods could therefore be highly valuable to pavement engineers when faced with continually changing field state conditions.

The objective of this research was to use material properties obtained from the mechanistic based rapid triaxial tester (RaTT) in conjunction with SHRP gyratory compacted samples for characterizing asphalt concrete mixes for Saskatchewan specified dense graded hot mix asphalt concrete mixes based on typical Saskatchewan asphalt cement contents, traffic loads, traffic speeds, and temperatures. A second objective of this research was to compare the Marshall mix design results to Superpave^{TM} Level I gyratory compaction results and linear viscoelastic material properties obtained from RaTT test results of typical Saskatchewan dense graded asphalt concrete mixes.

Three hot mix asphalt concrete blends were developed based on City of Saskatoon Type A1 and Saskatchewan Department of Highways and Transportation Type 71 dense graded asphalt concrete mixes. Marshall and SHRP gyratory compaction mix design methods were performed for each blend gradation. Mechanistic based characterization was performed on SHRP gyratory compacted asphalt concrete samples in the RaTT. Each sample was subjected to five loading frequencies at five different deviatoric stress states and five frequencies at 25°C and 60°C to simulate a range of field state conditions. Dynamic modulus, Poisson's ratio, and phase angle were determined from RaTT testing.

5.1 Summary

As expected, dynamic modulus was found to be higher at 25°C than at 60°C for all blend gradations and dynamic modulus decreased with increasing asphalt content for all blend gradations at both 25°C and 60°C. Dynamic modulus was found to increase with increasing deviatoric stress state for all blend gradations at 25°C and 60°C. Dynamic modulus was found to increase with increasing frequency for each blend gradation at 25°C and 60°C, and increased at a faster rate at 25°C than at 60°C.

As expected, Poisson's ratio was found to be higher at 60°C than at 25°C for each blend gradation. Poisson's ratio increased with increasing asphalt content for all three blend gradations at both 25°C and 60°C. Poisson's ratio was found to increase with increasing deviatoric stress at 25°C and was found to decrease with increasing deviatoric stress at 60°C for all blend gradations. Poisson's ratio was found to increase with increasing axial loading frequency for each blend gradation at 25°C and 60°C.

As expected, phase angle was found to be lower at 60°C than at 25°C for each blend gradation. Phase angle increased with increasing asphalt content at 25°C but no clear trend was observed at 60°C. Phase angle was found to decrease with increasing deviatoric stress state at 25°C and 60°C for each blend gradation. Phase angle decreased with increased load frequency at 25°C but increased with increased frequency at 60°C for each blend gradation, and crossed over each other between approximately 2 to 6 Hz.

In order to compare the Marshall stability and flow results to the material properties obtained from the RaTT, the range of the material properties which met road agency volumetric specifications were determined and compared to the total range of each property obtained during testing. The acceptable stability and flow ranges were relatively large relative to the total range obtained compared to the material properties presented in the previous section. Therefore, triaxial frequency sweep testing in the RaTT was more responsive to variation in asphalt cement content outside of acceptable ranges of volumetric properties for all blend gradations relative to Marshall stability and flow.

Nonlinearity was observed in the dynamic modulus results from approximately 0.125 Hz through approximately 2 Hz, and linearity was observed from approximately 2 Hz through 10 Hz. Nonlinearity was observed in the phase angle results from approximately 0.125 Hz through approximately 2 Hz, and linearity was observed from approximately 2 Hz to 6 Hz through 10 Hz. The phase angle of all blend gradations indicated that the asphalt concrete mixes considered in this research exhibited viscoelastic behaviour. Therefore, as expected, the RaTT identified asphalt concrete as a nonlinear viscoelastic material.

5.2 Conclusions

Triaxial frequency sweep testing was more responsive to variation in asphalt cement content outside of acceptable ranges of volumetric properties for all blend gradations relative to Marshall stability and flow. In addition, this demonstrated the importance of accurately reproducing field state conditions in the laboratory, because of the variability of material behaviour outside of the acceptable volumetric range.

Dynamic modulus, Poisson's ratio, and phase angle results were in accordance with expected material behaviour, indicating that the RaTT provides reasonable asphalt concrete material properties. Also, the RaTT identified asphalt concrete as a nonlinear viscoelastic material, as expected.

The variation of material properties with changing deviatoric stress state, frequency, and asphalt cement content indicated that deviatoric stress state, frequency, and asphalt cement content are important factors in asphalt concrete behaviour.

Triaxial frequency sweep testing in the RaTT was able to perform triaxial frequency sweep characterization on SHRP gyratory compacted samples for a range of traction states, load frequencies, and temperatures that simulated a range of Saskatchewan field state conditions. Triaxial frequency sweep testing was found to be cost effective, time efficient, and provided mechanistic material constitutive relations that can be employed for inelastic mechanistic mix design and road structural modelling.

Triaxial frequency sweep testing in the RaTT could significantly augment the SHRP Superpave^{TM} Level I asphalt concrete mix design system by providing material properties from SHRP Superpave^{TM} gyratory compacted asphalt concrete samples.

5.3 Future Research

A limitation to this research was the lack of repeat samples required to undertake a statistical analysis. A statistical analysis of mix design properties and design parameters considered in this research may enable determination of the statistical significance of the variation in material properties employed in this research.

Given that viscoplastic permanent deformation in asphalt concrete pavement typically occurs at the pavement surface under high deviatoric stress states and high temperatures, it is recommended that further asphalt concrete mix characterization be performed over the range of acceptable volumetric properties at high deviatoric stress states and high temperatures representative of critical rutting conditions. This may aid in determining the critical combination of factors that result in viscoplastic rutting.

It is recommended that further research be performed to determine the ability of triaxial frequency sweep testing in the RaTT to characterize the behaviour of other asphalt concrete types such as open graded friction course, stone matrix asphalt, polymer modified asphalt cement mixes, different aggregate properties, etc. It also may be beneficial to compare triaxial frequency sweep material constitutive relations to field

performance predictions and structural primary responses of actual field performance of *in situ* pavements.

LIST OF REFERENCES

AASHTO 2004, Development of 2002 Guide, http://www.2002designguide.com/

AASHTO (1995) "Standard Specifications for Transportation Materials and Methods of Sampling and Testing", American Association of State Highway and Transportation Officials, Washington, D.C.

Abdullah, W.S., Obaidat, M.T., Abu-Sa'da, N.M. (1998) "Influence of Aggregate Type and Gradation on Voids of Asphalt Concrete Pavements", *Journal of Materials in Civil Engineering*, Vol. 10 No. 2, pp. 76-85

Akili, W. (1993) "Effect of Moisture on Laboratory-Prepared Asphalt Mixtures", *Journal of Testing and Evaluation*, Vol. 21 No. 1, pp.73-83

Ali, H.A., Tayabji, S.D. (1998) "Evaluation of Mechanistic-Empirical Performance Prediction Models for Flexible Pavements", *Transportation Research Record*, No. 1629, pp. 169-180

Allen, D.H., Haisler, W.E. (1985) *Introduction to Aerospace Structural Analysis*, John Wiley & Sons, Inc.

Anderson, R.M., Bahia, H.U. (1997) "Evaluation and Selection of Aggregate Gradations for Asphalt Mixtures Using Superpave", *Transportation Research Record*, No. 1583, pp. 91-97

Anderson, R.M., Bukowski, J.R., Turner, P.A. (1999) "Using Superpave Performance Tests To Evaluate Asphalt Mixtures", *Transportation Research Record*, No. 1681, pp. 106-112

Anthony, A.M., Berthelot, C.F. (2004) "Effect of Manufactured Fines on Physical and Mechanical Properties of Saskatchewan Dense Graded Hot Mix Asphalt Pavement Mixes", *Canadian Technical Asphalt Association Proceedings, 49th Annual Conference*, Vol. XLIX, pp. 381-396

Aschenbrener, T., MacKean, C. (1994) "Factors that Affect the Voids in the Mineral Aggregate of Hot-Mix Asphalt", *Transportation Research Record*, No. 1469, pp. 1-8

ASTM (1996) "Annual Book of ASTM Standards", American Society for Testing and Materials, West Conshohocken, PA

Baladi, G.Y. (1989) "Fatigue Life and Permanent Deformation Characteristics of Asphalt Concrete Mixes", *Transportation Research Record*, No. 1227, pp. 75-87

Baladi, G.Y., Thomas, A. (1994) "Mechanistic Evaluation of AASHTO Flexible Pavement Design Equations", *Transportation Research Record*, No. 1449, pp. 72-78

Barksdale, R.D. (1977) "Performance of Asphalt Concrete Pavements", *Transportation Engineering Journal*, Vol. 101, pp. 55-74

Berthelot, C.F., Crockford, B., White, S., Sparks, G. (1997) "Mechanistic Quality Control/Quality Assurance Evaluation of Saskatchewan Specific Pavement Studies-9A Asphalt Mixes", *Canadian Technical Asphalt Association Proceedings, 42th Annual Conference*, Vol. XLII, pp. 201-227

Berthelot, C.F., Crockford, B., Lytton R. (1999) "Comparison of Alternative Test Methods for Predicting Asphalt Concrete Rut Performance", *Canadian Technical Asphalt Association Proceedings, 44th Annual Conference*, Vol. XLVL, pp. 405-434

Berthelot, C.F. (1999) "Mechanistic Modelling of Saskatchewan SPS-9A Asphalt Concrete Pavements", Ph.D. Dissertation, Texas A&M University, Department of Civil Engineering

Berthelot, C.F. (2003) *CE 311 Continuum Mechanics Class Notes*

Berthelot, C.F., Widger, A., Gehlen T. (2004) "Mechanistic Investigation of Granular Base and Subbase Materials: A Saskatchewan Case Study"

Beshara, M. (2000) "Initial Rutting Assessment on CS 1-20 and CS 1-16"

Bischoff, D., Schmiedlin, R., Rettner, D., Watson, D., Jared, D. (1998) "Pounding the Pavement", *Civil Engineering (New York)*, Vol. 68 No. 11, pp.59-61

Blight, G.E., (1974) "Permanent Deformation in Asphaltic Materials", *Transportation Engineering Journal*, Vol. 100, pp. 263-276

Bouchard, G.P. (1992) "Effects of Aggregate Absorption and Crush Percentage on Bituminous Concrete", *ASTM Special Technical Publication*, No. 1147, pp. 35-44

Brown, S.F. (1976) "Laboratory Testing for Use in the Prediction of Rutting in Asphalt Pavements", *Transportation Research Record*, No. 616, pp. 22-27

Brown, E.R., Foo, K.Y. (1991) "Evaluation of Variability in Resilient Modulus Test Results (ASTM D4123)", *Journal of Testing and Evaluation*, Vol. 19 No. 1, pp. 1-13

Brown, E.R., Kandhal, P.S., Zhang, J. (2001) "Performance Testing for Hot Mix Asphalt", *NCAT Report No. 2001-05A*

Buchanan, M.S., E.R. Brown (2001) "Effect of Superpave Gyratory Compactor Type on Compacted Hot-Mix Asphalt Density", *Transportation Research Record*, No. 1761, pp. 50-60

Butcher, M. (1998) "Determining Gyratory Compaction Characteristics Using Servopac Gyratory Compactor", *Transportation Research Record*, No. 1630, pp. 89-97

Buttlar, W.G., Roque, R. (1994) "Development and Evaluation of the Strategic Highway Research Program Measurement and Analysis System for Indirect Tensile Testing at Low Temperatures", *Transportation Research Record*, No. 1454, pp. 163-171

Button, J.W, Perdomo, D., Lytton, R.L. (1990), "Influence of Aggregate on Rutting in Asphalt Concrete Pavements", *Transportation Research Record*, No. 1259, pp. 141-152

Button, J.W., Little, D.N., Jagadam, V., Pendleton, O.J. (1994) "Correlation of Selected Laboratory Compaction Methods with Field Compaction", *Transportation Research Record*, No. 1454, pp. 193-201

Carlberg, M. (2003) "The Effect of Coarse Aggregate Angularity on Rutting Performance of Saskatchewan Asphalt Concrete Mixes." M.Sc. Thesis, University of Saskatchewan, Department of Civil Engineering.

Carpenter, S.H., Vavrik, W.R. (2001) "Repeated Triaxial Testing During Mix Design for Performance Characterization", *Transportation Research Record*, No. 1767, pp. 76-84

Chehab, G.R., O'Quinn, E., Kim, Y.R. (2000) "Specimen Geometry Study for Direct Tension Test Based on Mechanical Tests and Air Void Variation in Asphalt Concrete Specimens Compacted by Superpave Gyratory Compactor", *Transportation Research Record*, No. 1723, pp. 125-132

Chen, W.-F. (1994) "Studies in Applied Mechanics 37B, Constitutive Equations for Engineering Materials Vol. 2: Plasticity and Modelling"

Christensen, D.W. Jr., Bonaquist, R.F., Handojo, T. (2002) "Field Shear Test Device for Quality Control Testing of Asphalt Concrete", *Asphalt Paving Technology: Association of Asphalt Paving Technologists-Proceedings of the Technical Sessions*, Vol. 71, pp. 386-416

Chua, K.M., Tenison, J. (2003) "Explaining the Hveem Stabilometer Test: Relating R-Value, S-Value, and the Elastic Modulus", *Journal of Testing and Evaluation*, Vol. 31 No. 4, pp.269-276

Consedine, R. L. (1998) "Superpave Comes to Canada", *Aggregates and Roadbuilding Magazine*, http://rocktoroad.com/superpave.html

Consuegra, A., Little, D.N., Von Quintus, H., Burati, J. (1989) "Comparative Evaluation of Laboratory Compaction Devices Based on Their Ability to Produce Mixtures with Engineering Properties Similar to Those Produced in the Field", *Transportation Research Record*, No. 1228, pp. 81-87

Corté, J.-F., Goux,M.-T. (1996) "Design of Pavment Structures: The French Technical Guide", *Transportation Research Record*, No. 1539, pp. 116-124

COS (2000) *"City of Saskatoon Standard Construction Specifications and Drawings: Roadways, Water and Sewer"*

Cragg, R., Pell, P.S. (1971) "Dynamic Stiffness of Bituminous Road Materials", *Asphalt Paving Technology: Association of Asphalt Paving Technologists-Proceedings of the Technical Sessions*, 1971, pp. 126-147

Crockford, W.W., Berthelot, C.F., Tritt, B., Sinadinos, C. (2002) "Triaxial Frequency Sweep Test" *Asphalt Paving Technology: Association of Asphalt Paving Technologists-Proceedings of the Technical Sessions*, pp. 712-724

Croney, D. (1977) "The Design and Performance of Road Pavements", *Department of the Environment, Department of Transport, Transport and Road Research Laboratory*

D'Angelo, J.A., Paugh, C., Harman, T.P., Bukowski, J. (1996) "Comparison of the Superpave Gyratory Compactor to the Marshall for Field Quality Control", *Asphalt Paving Technology: Association of Asphalt Paving Technologists-Proceedings of the Technical Sessions*, Vol. 64, pp 611-628

D'Angelo, J., Harman, T.P., Paugh, C.W. (2001) "Evaluation of Volumetric Properties and Gyratory Compaction Slope for the Quality Control of Hot Mix Asphalt Production", *Asphalt Paving Technology: Association of Asphalt Paving Technologists-Proceedings of the Technical Sessions*, Vol. 70, pp. 729-761

Davies, T. (2004) *Personal e-mail Correspondence*

Davis, R.L. (1994) "Engineering Properties of Asphalt Mixtures and Their Relationship to Performance"

Dietrich, L., Lekszycki, T., Turski, K. (1998) "Problems of Identification of Mechanical Characteristics of Viscoelastic Composites", *Acta Mechanica*, Vol. 126, No. 1-4, pp. 153-167

DHT (2003) "4102 – Specifications for Asphalt Concrete"

Epps, J.A., Monismith, C.L. (1971) "Fatigue of Asphalt Concrete Mixtures EM DASH Summary of Existing Information", *ASTM Special Technical Publication*, No. 508, pp. 19-45

Epps, A. (2000) "Design and Analysis System for Thermal Cracking in Asphalt Concrete", *Journal of Transportation Engineering ASCE*, Vol. 126 No. 4, pp. 300-307

Foster, C.R. (1993) "Densification of Asphalt Pavements by Traffic", *Airport Pavement Innovations Theory to Practice*, pp. 164-180

Gibson, N.H., Schwartz, C.W., Schapery, R.A., Witczak, M.W. (2003) "Viscoelastic, Viscoplastic, and Damage Modelling of Asphalt Concrete in Unconfined Compression", *Transportation Research Record*, No. 1860, pp. 3-15

Haas, R., Karan, M.A. (1993) "Canadian Pavement Management Systems", *Pacific Rim Trans Tech Conference*, pp. 75-81

Hadley, W.O., Hudson, W.R., Kennedy, T.W. (1970) "Correlation of Indirect Tensile Results with Stability and Cohesiometer Values for Asphalt-Treated Materials", *Association of Asphalt Paving Technologists-Proceedings of the Technical Sessions,* pp. 745-765

Hand, A., Stiady, J.L., White, T.D., Nourelding, A.S., Galal, K. (2001) " Gradation Effects on Hot-Mix Asphalt Performance", *Transportation Research Record*, No. 1767, pp. 152-157

Hanson, D.I., Mallick, R.B., Brown, E.R. (1994) "Five-Year Evaluation of HMA Properties at the AAMAS Test Projects", *Transportation Research Record*, No. 1454, pp. 143-143

Harichandran, R.S., Buch, N., Baladi, G.Y. (2001) "Flexible Pavement Design in Michigan, Transition from Empirical to Mechanistic Methods", *Transportation Research Record*, No. 1778, pp. 100-106

Harman, T., Bukowski, J.R., Moutier, F., Huber, G., McGennis R. (1999) "The History and Future Challenges of Gyratory Compaction", *Transportation Research Record* No. 1789, pp. 200-207

Harvey, J.T., Tsai, B.-W. (1996) "Effects of Asphalt Content and Air Void Content on Mix Fatigue and Stiffness", *Transportation Research Record*, No. 1543, pp. 38-45

Highway Research Board (1955) "Special Report 22, The WASHTO Road Test, Part 2: Test Data Analyses and Findings"

Highway Research Board (1961) "AASHO Road Test: Report", *National Research Council*

Hopman, P.C. (1994) "Review of Modelling the Mechanical Parameters of Asphalt Material", *Proceedings-Conference of the Australian Road Research Board*, Vol. 17, pp. 317-331

Huang, S.-C., Branthaver, J.F., Robertson, R.E., Kim, S.-S. (1998) "Effect of Film Thickness on the Rheological Properties of Asphalts in Contact with the Aggregate Surface", *Transportation Research Record*, No. 1638, pp. 31-39

Huang, Y.H. (1993) *Pavement Analysis and Design*, Prentice Hall, Englewood Cliffs N.J.

Huber, G.A. (1989) "Deformation? We've Already got the Solution", *Asphalt*, Vol. 3 No. 2, pp. 9-10, 13

Huber, G.A (1996) "Development of the Superpave Gyratory Compactor", *The Superpave Asphalt Reseach Program*
www.utexas.edu/research/Superpave/articles/gyr_hist.html

Huhtala, M., Alkio, R., Pihljamaki, J., Pienmaki, M., Halonan, P. (1990) "Behaviour of Bituminous Materials Under Moving Wheel Loads", ", *Asphalt Paving Technology: Association of Asphalt Paving Technologists-Proceedings of the Technical Sessions*, Vol. 59, pp. 422-442

Hveem, F.N. (1983) "Highway Recollections of F.N. Hveem", *Caltrans Committee on Preservation of Historical Heritage, California Department of Transportation*, Sacramento CA

Jeng, Y.-S., Liaw, C.-J., Liu, P. (1993) "Analysis of Crack Resistance of Asphalt Concrete Overlays: A Fracture Mechanics Approach", *Transportation Research Record*, No. 1388, pp.160-166

Kandhal, P.S. (1994) "Field and Laboratory Investigation of Stripping in Asphalt Pavements: State of the Art Report", *Transportation Research Record*, No. 1454, pp.36-47

Kandhal, P.S., Chakraborty, S. (1996) "Effect of Asphalt Film Thickness on Short- and Long-Term Aging of Asphalt Paving Mixtures", *Transportation Research Record*, No. 1535, pp. 83-90

Kandhal, P.S., Mallick, R.B. (2001) "Effect of Mix Gradation on Rutting Potential of Dense-Graded Asphalt Mixtures", *Transportation Research Record*, No. 1767, pp. 146-151

Kandhal, P.S., Dunning, M., Vavrick, W., Hugo, F., Weishahn, L., Hobson, K., Nady, R., Cooley, L.A. Jr. (2002) "Investigation of the Restricted Zone in the Superpave Aggregate Gradation Specification", *Asphalt Paving Technology: Association of Asphalt Paving Technologists-Proceedings of the Technical Sessions*, Vol. 71, pp. 479-534

Kennedy, T.W. (1977) "Pavement Design Characteristics of In-Service Asphalt Mixtures", *Transportation Research Record*, No. 659, pp. 24-32

Kim, Y.R., Kim, N., Khosla, N.P. (1992) "Effects of Aggregate Type and Gradation on Fatigue and Permanent Deformation of Asphalt Concrete", *ASTM Special Technical Publication*, No. 1147, pp. 310-328

Kim, Y.R., Shah, K.A., Khosla, N.P. (1992) "Influence of Test Parameters in SHRP P07 Procedure on Resilient Moduli of Asphalt Concrete Field Cores", *Annual Meeting of the Transportation Research Board*

Kim, Y.R., Lee, Y.-C. (1995) "Interrelationships Among Stiffness of Asphalt-Aggregate Mixtures", *Asphalt Paving Technology: Association of Asphalt Paving Technologists-Proceedings of the Technical Sessions*, Vol. 64, pp. 575-610

Kim, Y.R., Lee, Y.-C., Kim, H.J. (1995) "Correspondence Principle for Characterization of Asphalt Concrete", *Journal of Materials in Civil Engineering*, Vol. 7 No. 1, pp. 59-68

Kim, H., Haas, C.T., Rauch, A.F., Browne, C. (2002) "Wavelet-Based Three-Dimensional Descriptors of Aggregate Particles, *Transportation Research Record*, No. 1787, pp. 109-116

Kreide, M., Budija, M., Carswell, J. (2003) "The 'Original' Stone Mastic Asphalt: The German Experience", *Proceedings-Conference of the Australian Road Research Board*, Vol. 21, pp. 731-747

Leahy, R., Hicks, R.G., Monismith, C.L., Finn, F.N. (1996) "Framework for Performance-Based Approach to Mix Design and Analysis", *Asphalt Paving Technology: Association of Asphalt Paving Technologists-Proceedings of the Technical Sessions*, Vo. 64, pp. 431-473

Leahy, R., Hicks, R.G., Monismith, C.L. (1996) "Asphalt Update", *ASCE*, pp. 58-61

Lee, H.J., Kim, Y.R., Lee, S.W. (2003) "Prediction of Asphalt Mix Fatigue Life with Viscoelastic Material Properties", *Transportation Research Record*, No. 1832, pp. 139-147

Linden, R.N., Mahoney, J.P., Jackson, N.C. (1989) "Effect of Compaction on Asphalt Concrete Performance", *Transportation Research Record*, No. 1217, pp. 20-28

Majidzadeh, K., Khedr, S., El-Mojarrush M. (1979) "Evaluation of Permanent Deformation in Asphalt Concrete Pavements", *Transportation Research Record*, No. 715, pp. 21-31

Mallick, R.B. (1999) "Use of Superpave Gyratory Compactor to Characterize Hot-Mix Asphalt", *Transportation Research Record*, No. 1681, pp. 87-96

Malvern, L.E. (1969) *Introduction to the Mechanics of a Continuous Medium*, Prentice Hall, Inc.

Mamlouk, M.S., Yuan, Y.M., Tseng, N.T., Lee, G.C. (1983) "Analysis of Nonlinear Behavior of Asphalt Concrete During Marshall Test", *Journal of Testing & Evaluation*, Vol. 11 No. 5, pp. 327-332

Mamlouk, M.S., Sarofim, R.T. (1988) "Modulus of Asphalt Mixtures-An Unresolved Dilemma", *Transportation Research Record*, No. 1171, pp. 193-198

Matheson, M.J., Simmons, J.V. (1990) "Modified Mechanistic Design Accounting for Permanent Deformation of Flexible Pavement Layers", *Proceedings-Conference of the Australian Road Research Board*, pp. 347-363

Maupin, G.W. Jr. (1995) "Determination of Compaction Effort to Duplicate Pavement Voids for Corps of Engineers Gyratory Testing Machine", *Transportation Research Record*, No. 1492, pp. 13-17

McCann, M., Sebaaly, P.E. (2003) "Evaluation of Moisture Sensitivity and Performance of Lim in Hot-Mix Asphalt: Resilient Modulus, Tensile Strength, and Simple Shear Tests", *Transportation Research Record*, No. 1832, pp. 9-16

Mogawer, W.S., Stuart, K.D. (1994) "Evaluation of Stone Matrix Asphalt versus Dense-Graded Mixtures", *Transportation Research Record*, No. 1454, pp. 58-65

Mohamed, E.H.H. (1993) "Debonding Location in Asphalt Concrete Associated with Moisture Damage", *Journal of Materials in Civil Engineering*, Vol. 5 No. 4, pp. 497-509

Monismith, C.L., Epps, J.A. (1969) "Influence of Mixture Variables on the Flexural Properties of Asphalt Concrete", *Asphalt Paving Technology: Association of Asphalt Paving Technologists-Proceedings of the Technical Sessions*, Vol. 38, pp. 423-464

Monismith, C.L., Finn, F.N. (1977) "Flexible Pavement Design: State-of-the-Art—1975", *Transportation Engineering Journal*, Vol. 103 No. 1, pp. 1-53

Monismith, C.L. (1992) "Analytically Based Asphalt Pavement Design and Rehabilitation: Theory to Practice 1962-1992", *Transportation Research Record*, No. 1354, pp. 5-26

Oliver, J.W.H., Jameson, G.W., Sharp, K.G., Vertessy, N.J., Johnson-Clarke, J.R., Alderson, A.J. (1997) "Evaluation of Rut-Resistant Properties of Asphalt Mixes Under Field and Laboratory Conditions", *Transportation Research Record*, No. 1590, pp. 53-61

Papagiannakis, A.T., Abbas, A., Masad, E. (2002), "Micromechanical Analysis of Viscoelastic Properties of Asphalt Concretes", *Transportation Research Record*, No. 1789, pp. 113-120

Park, S.-W., Lytton, R.L. (2004) "Effect of Stress-Dependent Modulus and Poisson's Ratio on Structural Responses in Thin Asphalt Pavements", *Journal of Transportation Engineering*, Vol. 130 No. 3, pp. 387-394

Parker, F., Brown, E.R. (1992) "Effects of Aggregate Properties on Flexible Pavement Rutting in Alabama", *ASTM Special Technical Publication*, No. 1147, pp. 68-89

Partl, M.N., Vinton, T.S., Hicks, R.G. (1994) "Mechanical Properties of Stone Mastic Asphalt", *Proceedings of the Materials Engineering Conference*, No. 804, pp. 849-858

Partl, M.N., Vinton, T.S., Hicks, R.G., Younger, K. (1996) "Performance-Related Testing of Stone Mastic Asphalt", *Asphalt Paving Technology: Association of Asphalt Paving Technologists-Proceedings of the Technical Sessions*, Vol. 64, pp. 96-129

Patrick, J.E., Bailey, R. (2003) "Use of Pavement Deterioration Models in Pavement Design", *Proceedings–Conference of the Australian Road Research Board*, Vol. 21, pp. 1581-1595

Pellinen, T.K., Witczak, M.W. (2002) "Use of Stiffness of Hot-Mix Asphalt as a Simple Performance Test", *Transportation Research Record*, No. 1789, pp. 80-90

Rao, C., Tutumluer, E. (2000) "Determination of Volume of Aggregates: New Image Analysis Approach", *Transportation Research Record*, No. 1721, pp. 73-80

Rao, C., Tutumluer, E., Kim, I.T. (2002) "Quantification of Coarse Aggregate Angularity Based on Image Analysis", *Transportation Research Record*, No. 1787, pp. 117-124

Roberts, F.L., Kandhal, P.S., Brown, E.R., Lee, D., Kennedy, T.W. (1996) *Hot Mix Asphalt Materials, Mixture Design and Construction 2nd Edition, NAPA Education Foundation*

Romero, P., Anderson, R.M. (2001) "Variability of Asphalt Mixture Tests Using Superpave Shear Tester Repeated Shear at Constant Height Test", *Transportation Research Record*, No. 1767, pp. 95-101

Roque, R., Ruth, B.E. (1990) "Mechanisms and Modelling of Surface Cracking in Asphalt Pavements", *Asphalt Paving Technology: Association of Asphalt Paving Technologists-Proceedings of the Technical Sessions*, Vol. 59, pp. 396-421

Rowe, G.M., Brown, S.F., Sharrock, M.J., Bouldin, M.G. (1995) "Viscoelastic Analysis of Hot Mix Asphalt Pavement Structures", *Transportation Research Record*, No. 1482, pp. 44-51

Ruth, B.E. (ed.) (1985) "Evaluation and Prevention of Water Damage to Asphalt Pavement Materials", *ASTM Special Technical Publication*, 154 p.

Saadeh, S., Masad, E., Stuart, K., Abbas, A., Papagainnakis, T., Al-Khateeb, G. (2003) "Comparative Analysis of Axial and Shear Viscoplastic Properties of Asphalt Mixes", *Asphalt Paving Technology: Association of Asphalt Paving Technologists-Proceedings of the Technical Sessions*, Vol. 72, pp. 122-153

Sebaaly, P.E., Ridolfi, D., Gangavaram, R.S., Epps, J.A. (1997) "Selecting Most Desirable Hot-Mix Asphalt Mixtures", *Transportation Research Record*, No. 1590, pp. 99-107

Sebaaly, P.E., Lake, A., Epps, J. (2002) "Evaluation of Low-Temperature Properties of HMA Mixtures", *Journal of Transportation Engineering*, Vol. 128 No. 6, pp. 578-586

Shen, W., Kirkner, D.J. (2001) "Thermal Cracking of Viscoelastic Asphalt-Concrete Pavement", *Journal of Engineering Mechanics*, Vol. 127 No. 7, pp. 700-709

Shenoy, A., Romero, P. (2002) "Standardized Procedure for Anlysis of Dynamic Modulus $|E^*|$ Data to Predict Asphalt Pavement Distresses", *Transportation Research Record*, No. 1789, pp. 173-182

Shook, J.F. (1984) "Structural Analysis of Asphalt Pavements Using Computers", *Transportation Forum – Transportation Association of Canada*, Vol. 1 No. 2, pp. 5-13
Sontowski, P. (1995) "How to Prevent Asphalt Pavement Raveling", *Better Roads*, Vol. 65 No. 3, pp.23-24

Sousa, J., Monismith, C.L. (1988) "Dynamic Properties of Asphalt Concrete", *Journal of Testing and Evaluation*, Vol. 16 No. 4, pp. 350-363

Sousa, J., Solaimanian, M. (1994) "Abridged Procedure to Determine Permanent Deformation of Asphalt Concrete Pavements", *Transportation Research Record*, No. 1448, pp. 25-33

SHRP-A-357 (1993) "Development and Validation of Performance Prediction Models and Specifications for Asphalt Binders and Paving Mixes"

SHRP (1994) "Superior Performing Asphalt Pavements (Superpave): The Product of the SHRP Asphalt Research Program", *National Academy of Sciences*

SHRP-A-408 (1994) "Level One Mix Design: Materials Selection, Compaction, and Conditioning"

SHRP-A-415 (1994) "Permanent Deformation Response of Asphalt Aggregate Mixes"

"Superpave Mix Design" (1996) *Asphalt Institute Superpave Series No. 2 (SP-2)*

Tayebali, A.A., Deacon, J.A., Monismith, C.L. (1995) "Comparison of Axial and Diametral Resilient Stiffness of Asphalt-Aggregate Mixes", *Transportation Research Record*, No. 1492, pp. 135-143

Terrel, R.L. (1971) "Fatigue Behaviour: Field Observations and Analytical Predictions", *ASTM Special Technical Publication*, No. 508, pp. 117-143

Theyse, H.L., De Beer, M., Rust, F.C. (1996) "Overview of South African Mechanistic Pavement Design Method", *Transportation Research Record*, No. 1539, pp. 6-17

U.S. Army Corps of Engineers, War Department, Mississippi River Commission (1944) "A Stability Method and Apparatus for the Design and Control of Asphalt Paving

Mixtures in the Field", *Interim Report No. 1, U.S. Waterways Experiment Station, Vicksburg, MS*

Uzan, J. (1996) "Asphalt Concrete Characterization for Pavement Performance Prediction", *Asphalt Paving Technology: Association of Asphalt Paving Technologists-Proceedings of the Technical Sessions*, Vol. 65, pp. 573-606

van de Loo, P.J. (1976) "Practical Approach to the Prediction of Rutting in Asphalt Pavements: The Shell Method", *Transportation Research Record*, No. 616, pp. 15-21

Wallace, H.A., Martin, J.R. (1967) *Asphalt Pavement Engineering*

Wang, J.-N., Yang, C.-K., Luo, T.-Y. (2001) "Mechanistic Analysis of Asphalt Pavements, Using Superpave Shear Tester and Hamburg Wheel-Tracking Device", *Transportation Research Record*, No. 1767, pp. 102-110

Watson, D.E., Moore, K.A., Williams, K., Cooley, L.A. Jr. (2003) "Refinement of New-Generation Open-Graded Friction Course Mix Design", *Transportation Research Record*, No. 1832, pp. 78-85

Webster's Third New International Dictionary, Merriam-Webster Incorporated (1993)

Weissman, S.L., Harvey, J., Sackman, J.L., Long, F. (1999) "Selection of Laboratory Test Specimen Dimension for Permanent Deformation of Asphalt Concrete Pavements", *Transportation Research Record*, No. 1681, pp. 113-120

West Virginia Department of Transportation Division of Highways Design Directive DD–644 (2003) "Hot Mix Asphalt"

Whitmoyer, S.L., Kim, Y.R. (1994) "Determining Asphalt Concrete Properties via the Impact Resonant Method", *Journal of Testing and Evaluation*, Vol. 22 No. 2, pp.139-148

Witczak, M.W., Pellinen, T.K., El-Basyouny, M.M. (2002) "Pursuit of the Simple Performance Test for Asphalt Concrete Fracture/Cracking", *Asphalt Paving Technology: Association of Asphalt Paving Technologists-Proceedings of the Technical Sessions*, Vol. 71, pp. 767-778

Zafir, Z., Siddharthan, R., Sebaaly, P.E. (1994) "Dynamic Pavement-Strain Histories from Moving Traffic Load", *Journal of Transportation Engineering*, Vol. 120 No. 5, pp. 821-842

APPENDIX A: GYRATORY ESTIMATED BULK SPECIFIC GRAVITY PROFILES

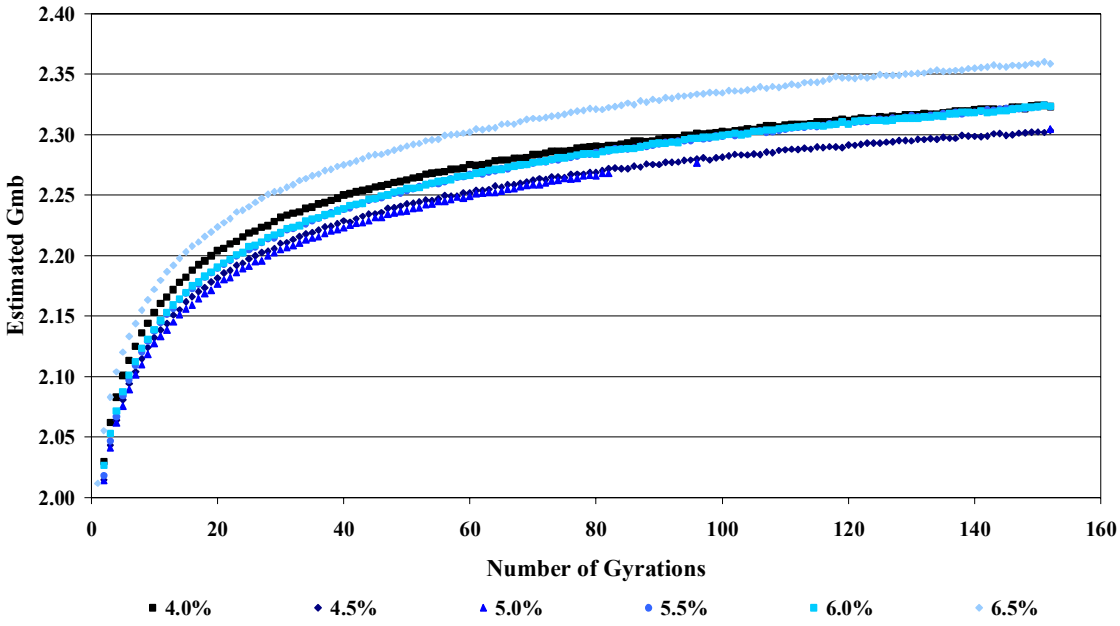

Figure A. 1 Fine Blend Gradation Gyratory Estimated Bulk Specific Gravity

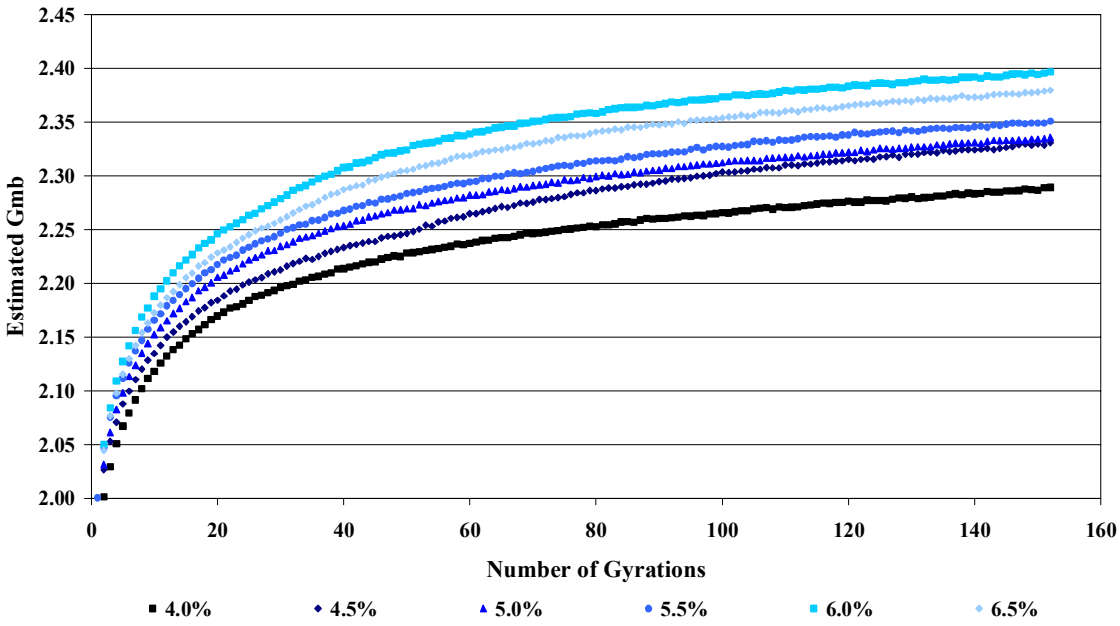

Figure A. 2 Middle Blend Gradation Gyratory Estimated Bulk Specific Gravity

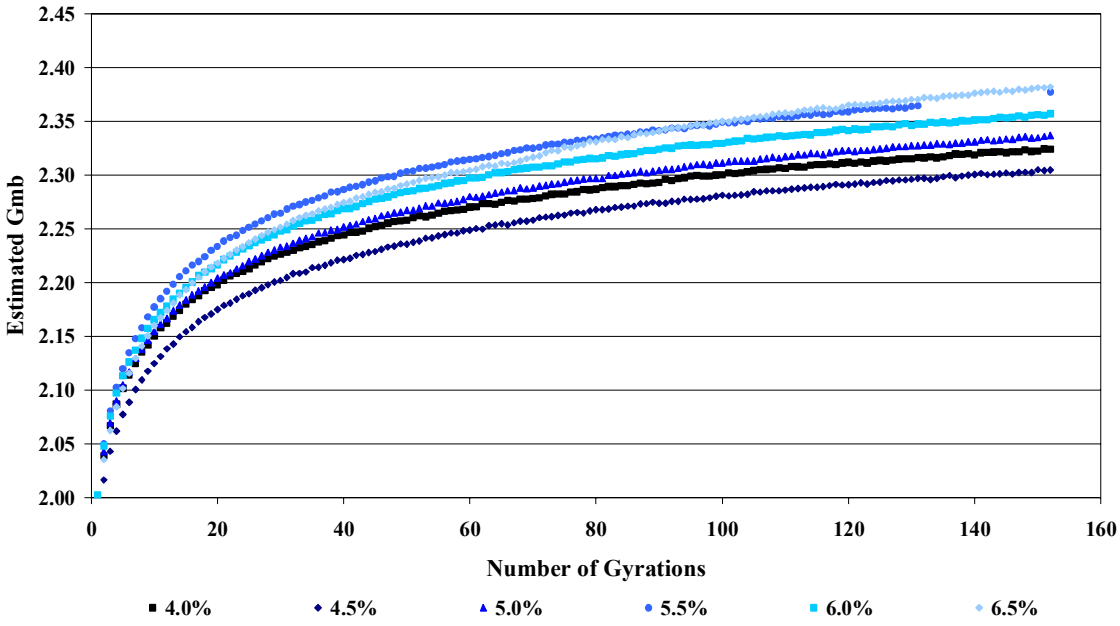

Figure A. 3 Coarse Blend Gradation Gyratory Estimated Bulk Specific Gravity

APPENDIX B: GYRATORY VOIDS IN TOTAL MIX PROFILES

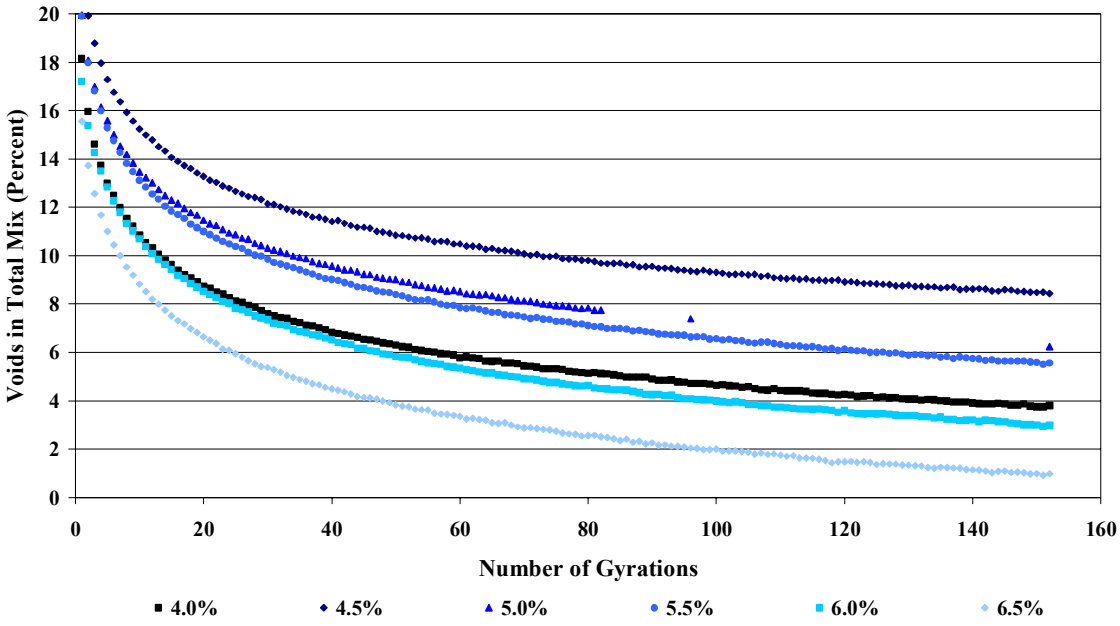

Figure B. 1 Fine Blend Gradation Gyratory Voids in Total Mix

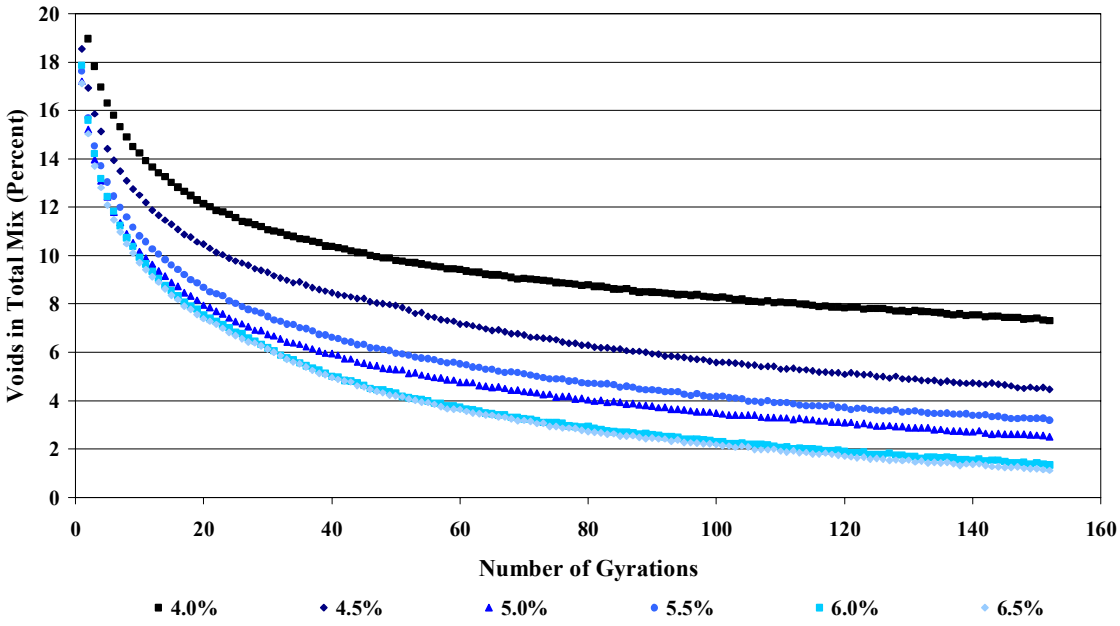

Figure B. 2 Middle Blend Gradation Gyratory Voids in Total Mix

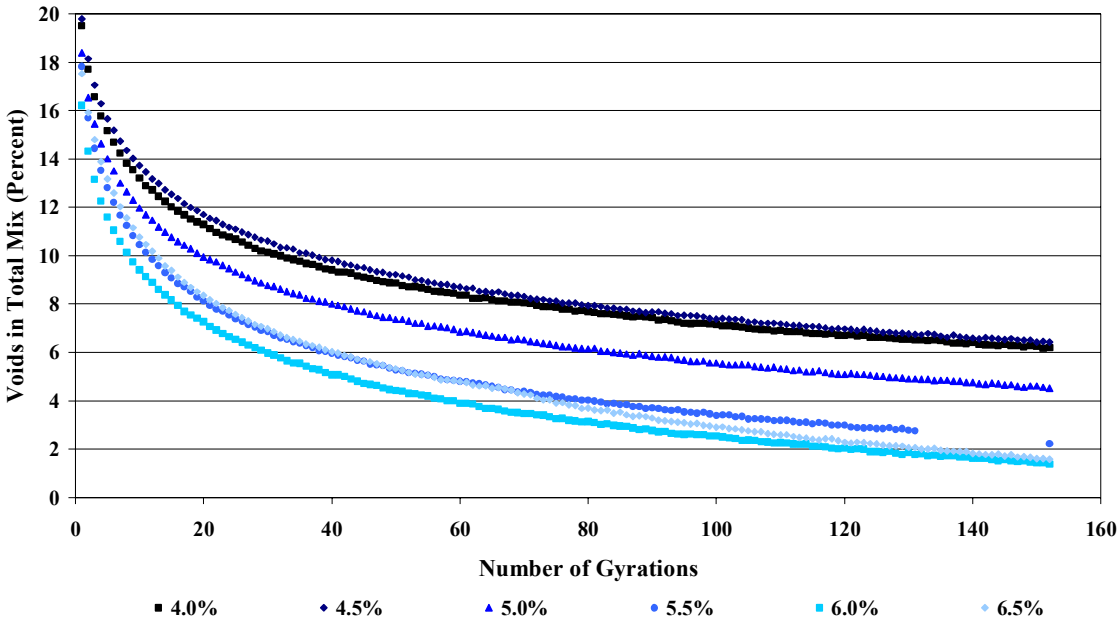

Figure B. 3 Coarse Blend Gradation Gyratory Voids in Total Mix

APPENDIX C: MATERIAL PROPERTY TREND LINE COEFFICIENTS

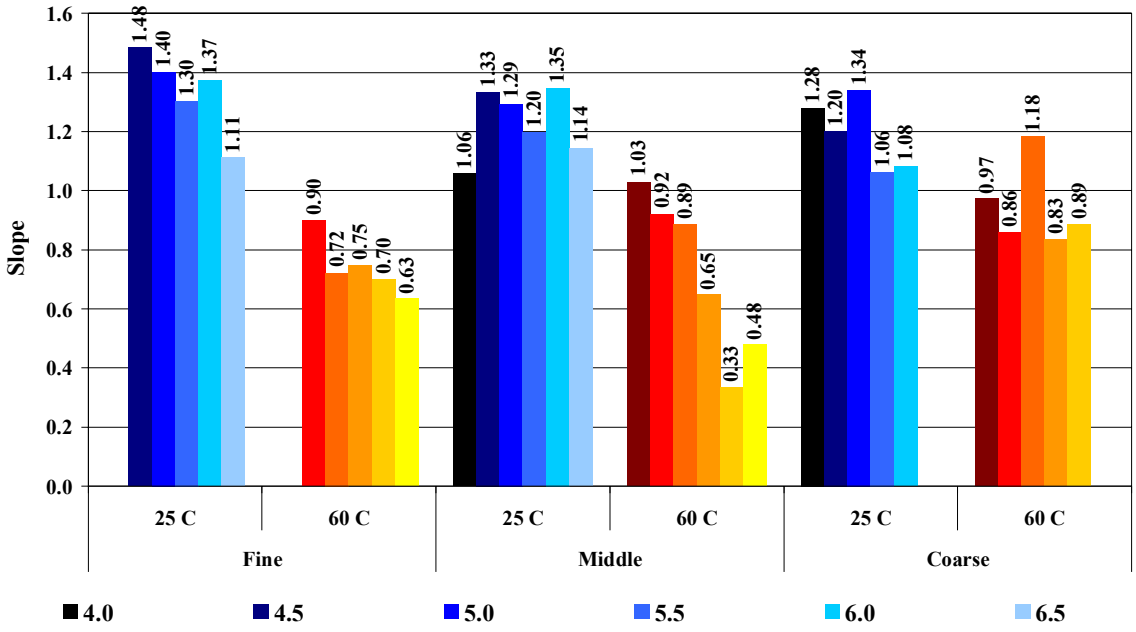

Figure C. 1 Dynamic Modulus Plotted versus Frequency Linear Trend Lines Slopes

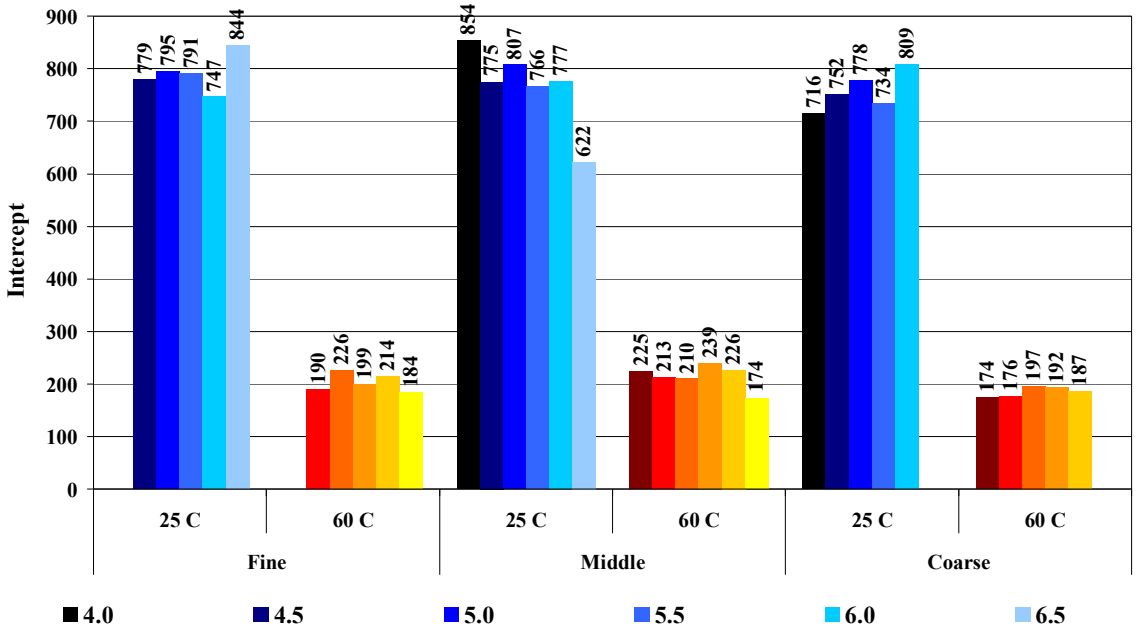

Figure C. 2 Dynamic Modulus Plotted versus Frequency Linear Trend Lines Intercepts

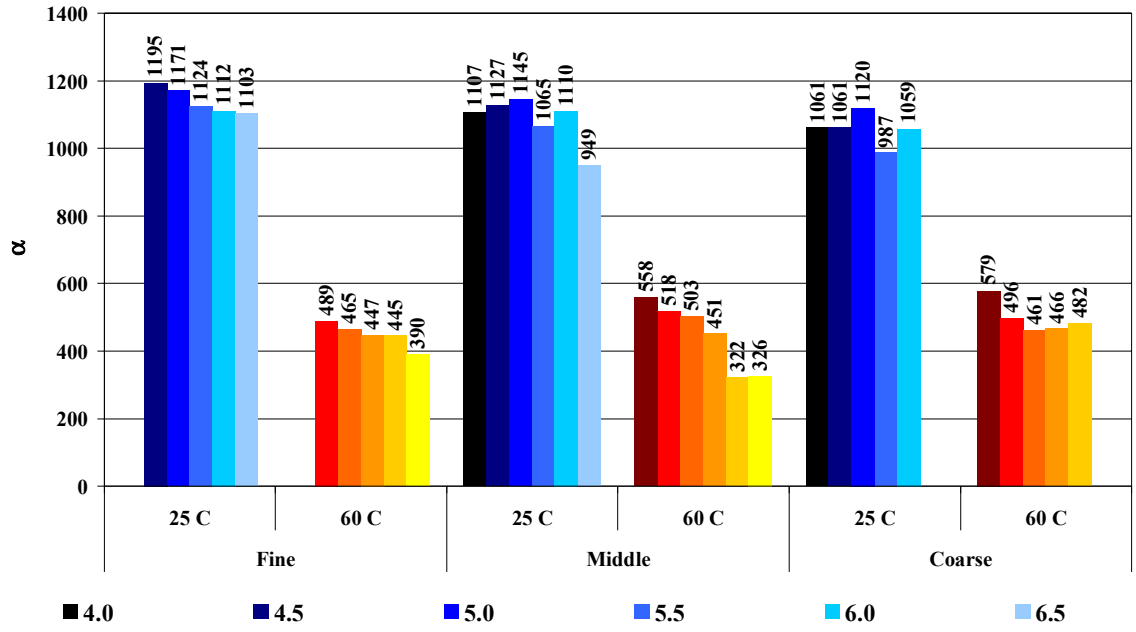

Figure C. 3 Dynamic Modulus Plotted versus Deviatoric Stress State Power Law Trend Lines α

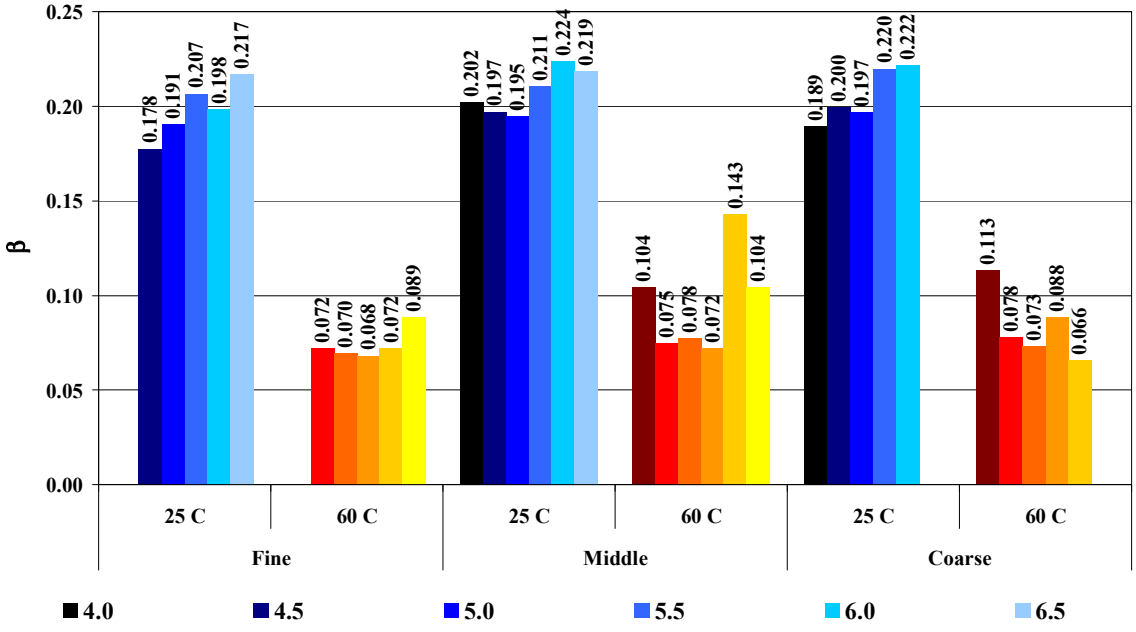

Figure C. 4 Dynamic Modulus Plotted versus Deviatoric Stress State Power Law Trend Lines β

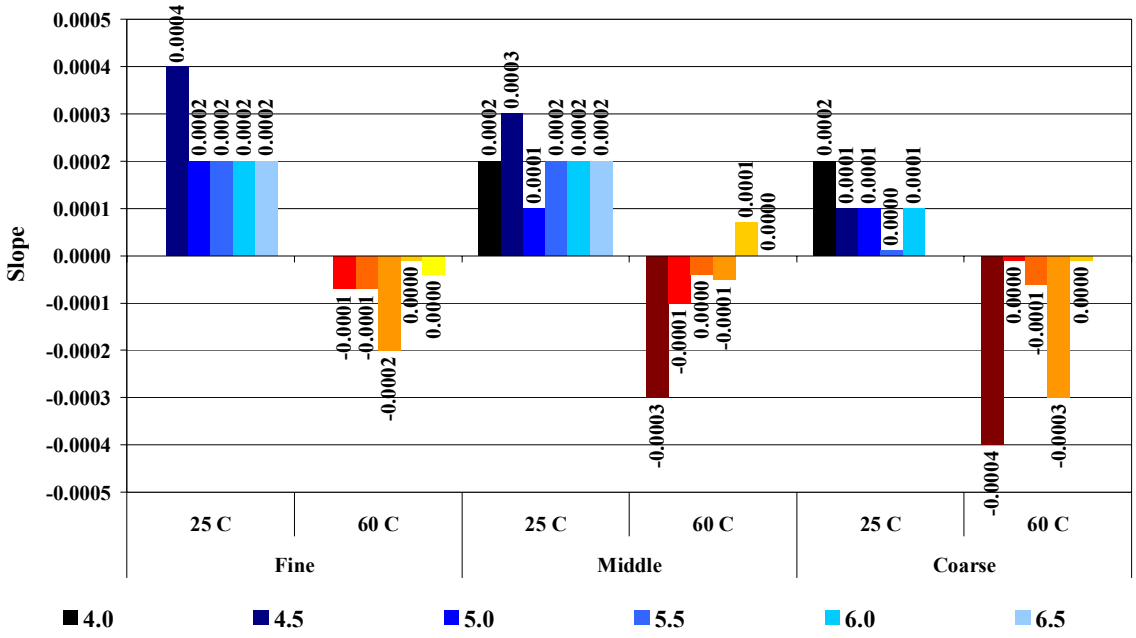

Figure C. 5 Poisson's Ratio Plotted versus Frequency Linear Trend Lines Slopes

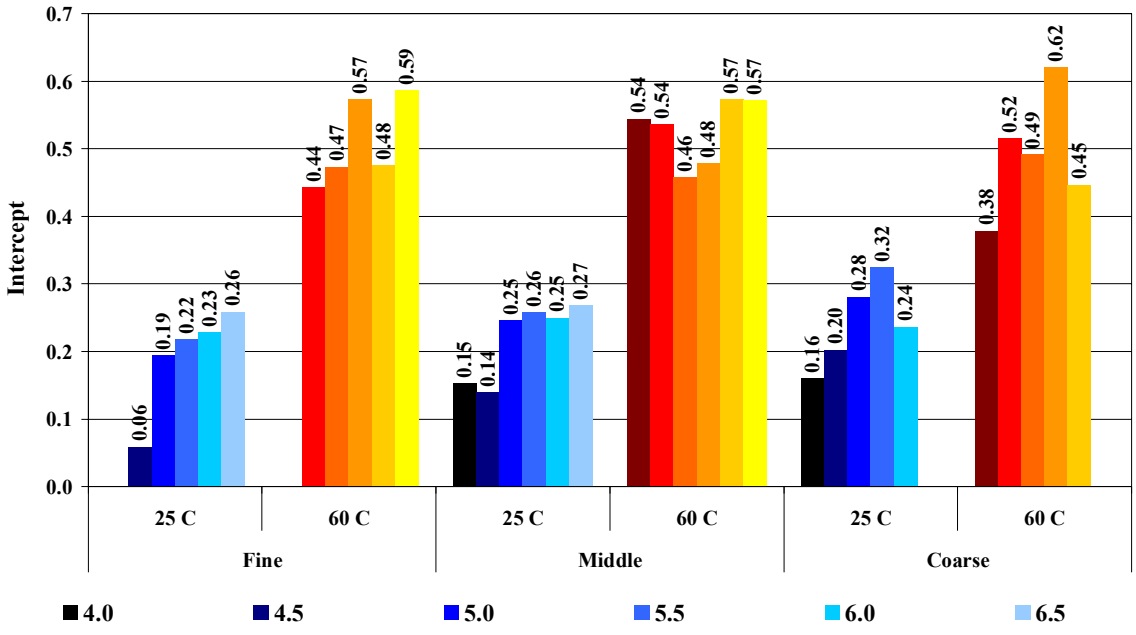

Figure C. 6 Poisson's Ratio Plotted versus Frequency Linear Trend Lines Intercepts

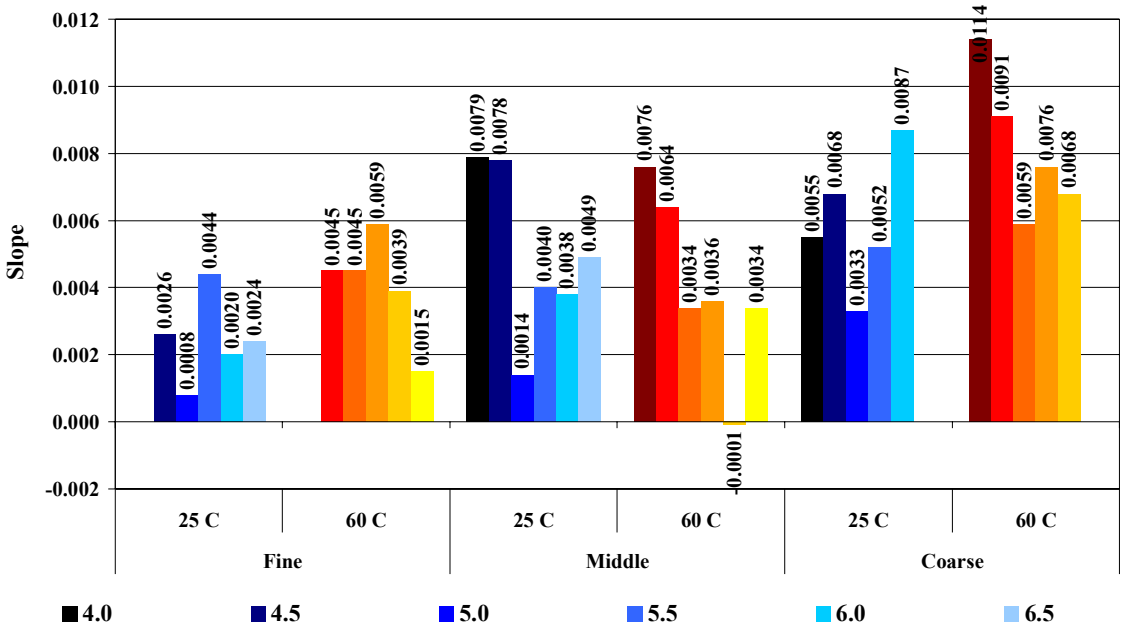

Figure C. 7 Poisson's Ratio Plotted versus Deviatoric Stress State Linear Trend Lines Slopes

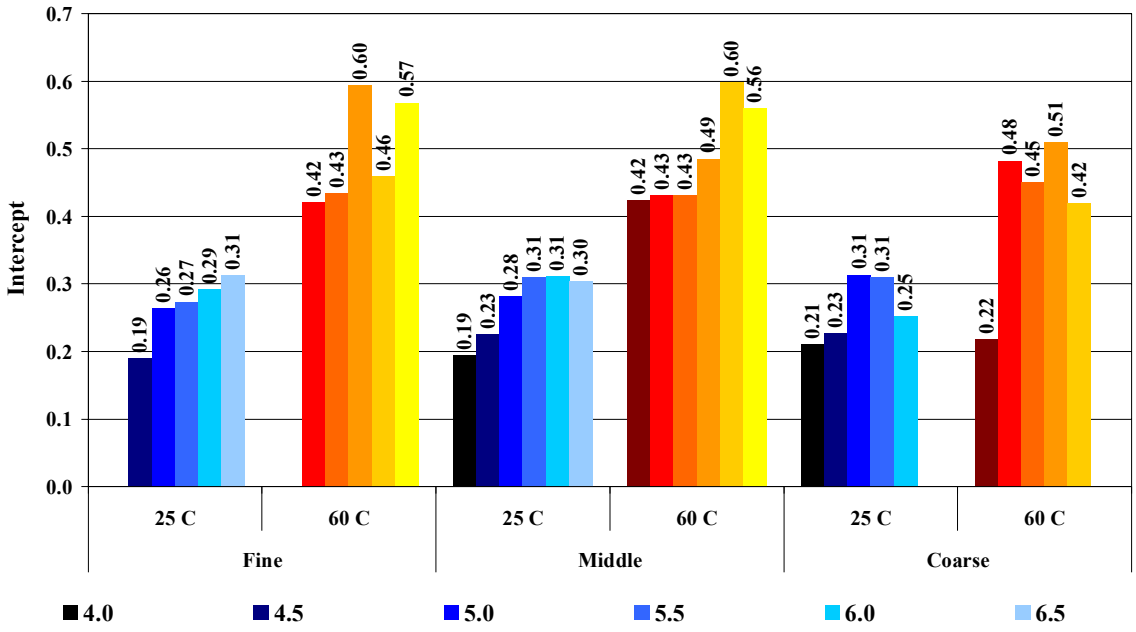

Figure C. 8 Poisson's Ratio Plotted versus Deviatoric Stress State Linear Trend Lines Intercepts

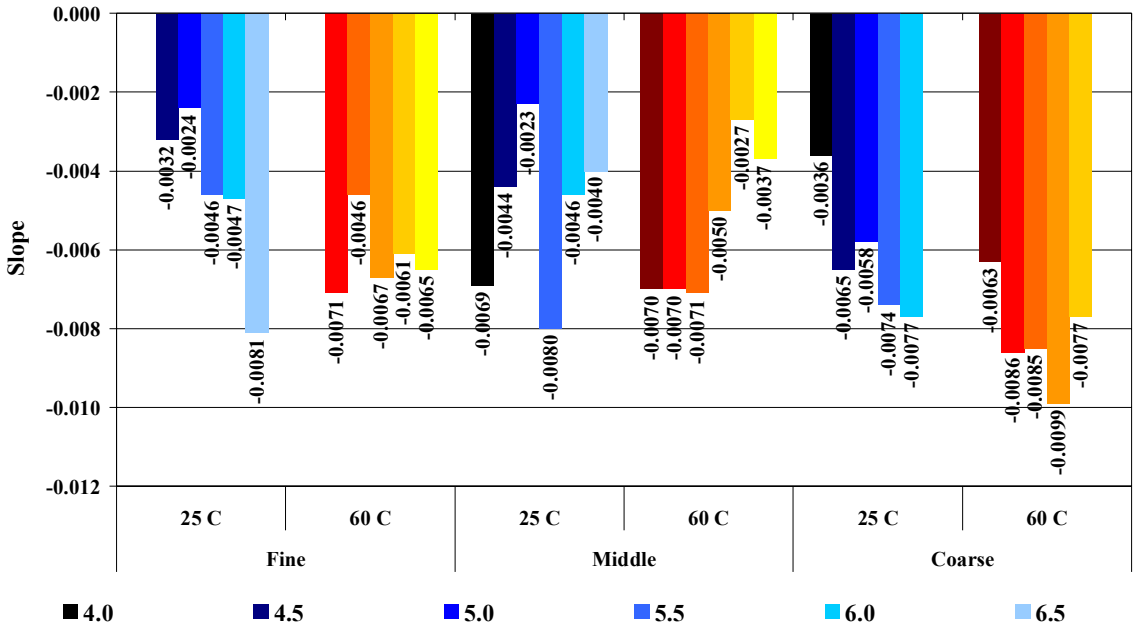

Figure C. 9 Phase Angle Plotted versus Frequency Linear Trend Lines Slopes

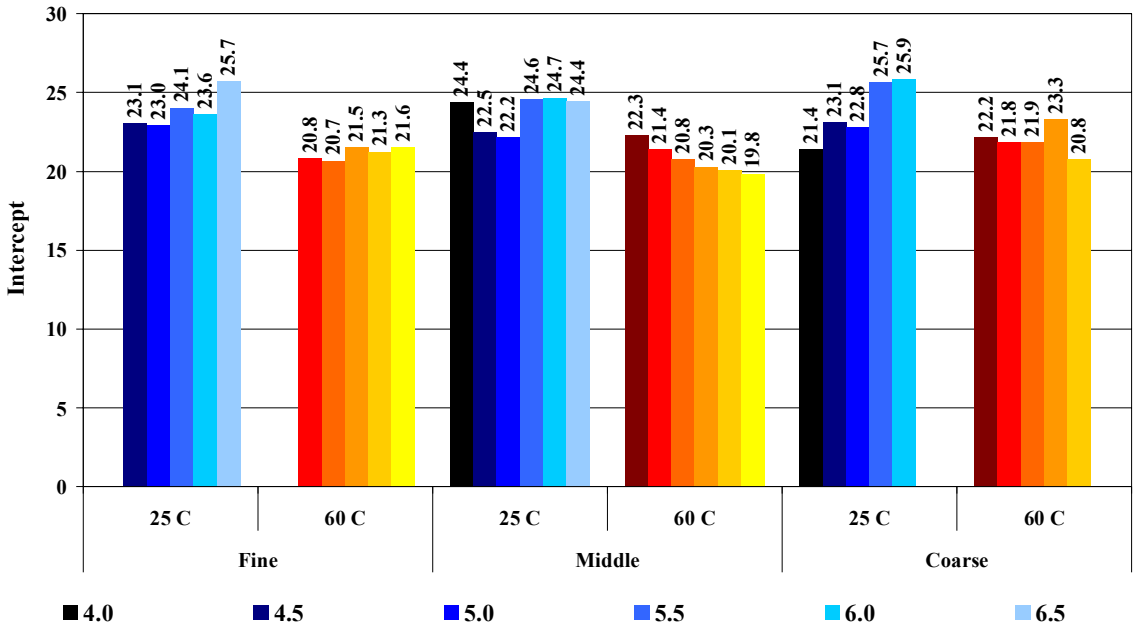

Figure C. 10 Phase Angle Plotted versus Frequency Linear Trend Lines Intercepts

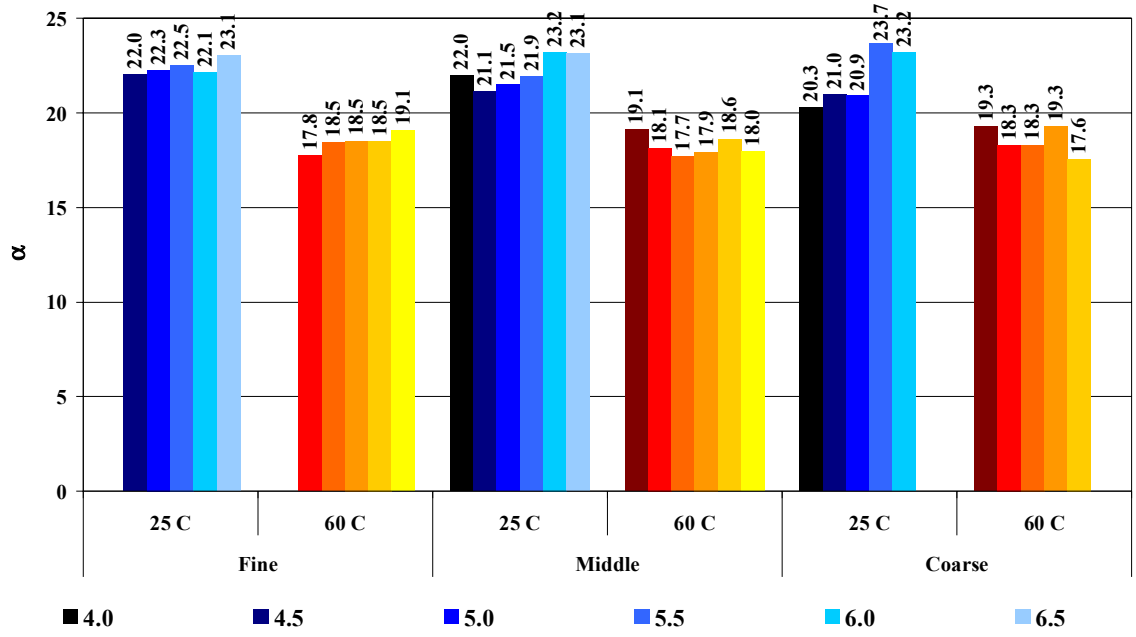

Figure C. 11 Phase Angle Plotted versus Deviatoric Stress State Power Law Trend Lines α

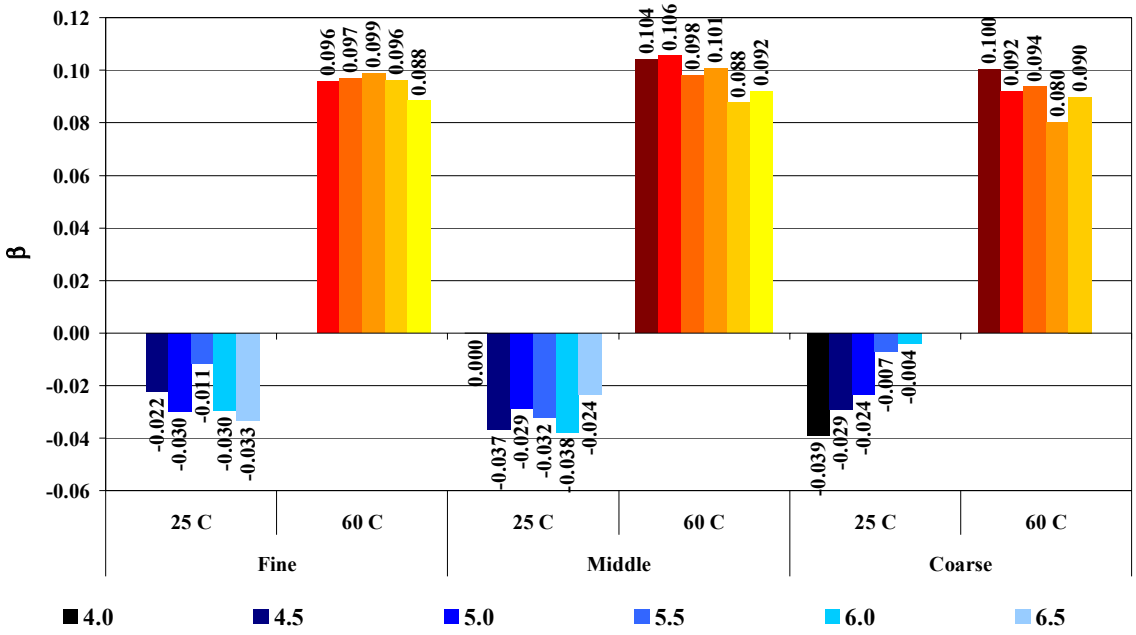

Figure C. 12 Phase Angle Plotted versus Deviatoric Stress State Power Law Trend Lines β

APPENDIX D: DYNAMIC MODULUS

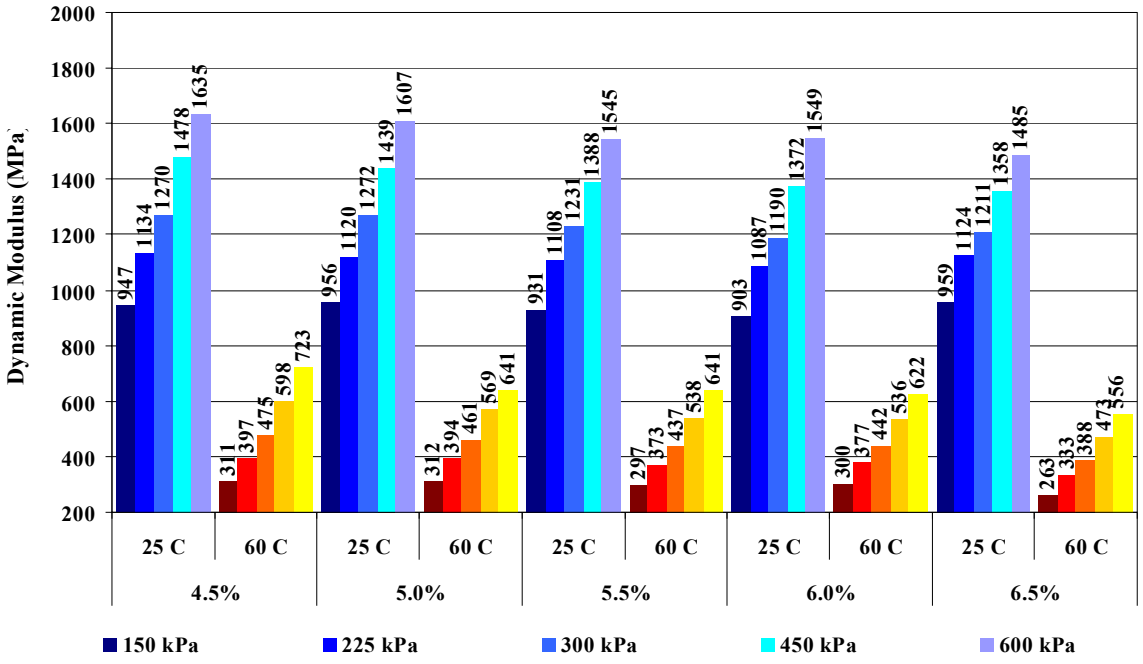

Figure D. 1 Fine Blend Dynamic Modulus by Deviatoric Stress State and Temperature Plotted versus Frequency

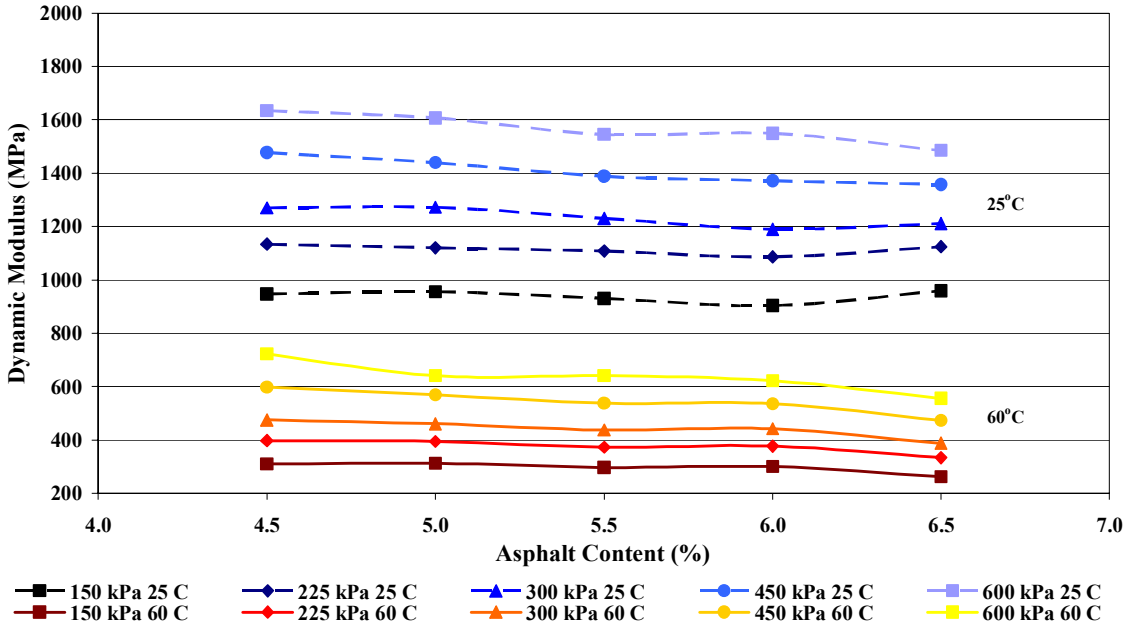

Figure D. 2 Fine Blend Dynamic Modulus by Deviatoric Stress State versus Asphalt Content and Temperature Plotted versus Frequency

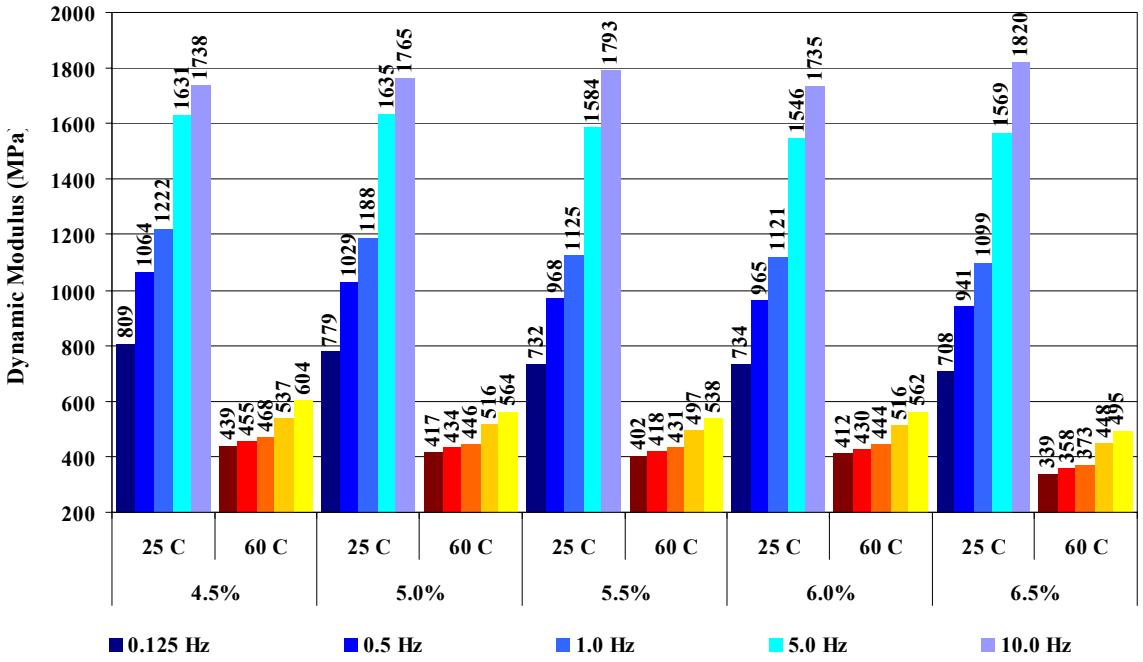

Figure D. 3 Fine Blend Dynamic Modulus by Frequency and Temperature Plotted versus Deviatoric Stress State

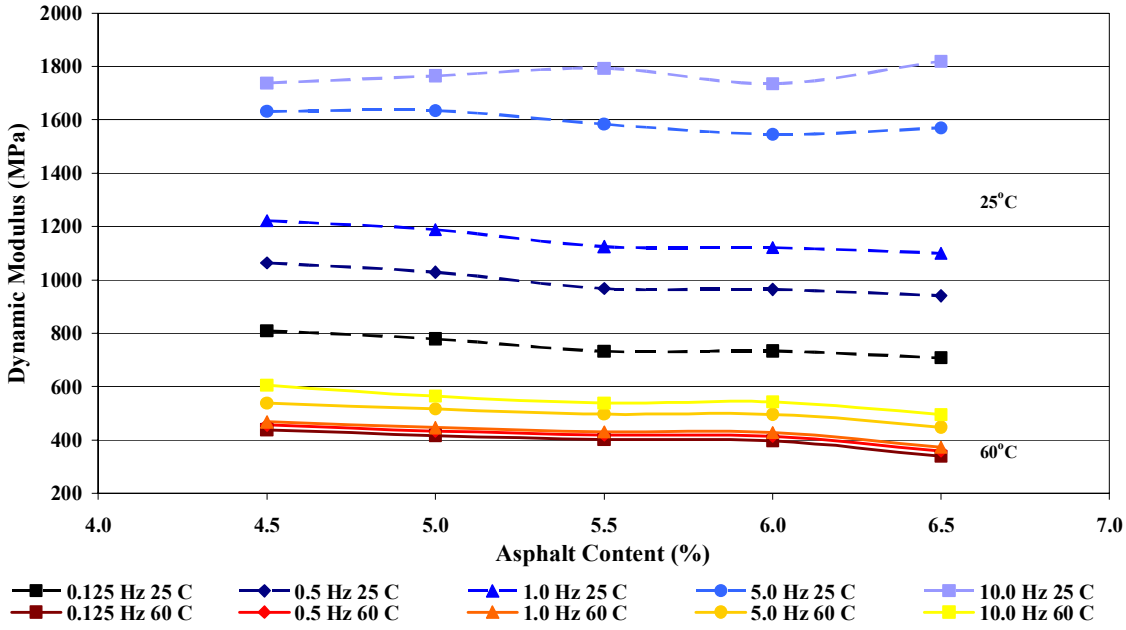

Figure D. 4 Fine Blend Dynamic Modulus versus Asphalt Content by Frequency and Temperature Plotted versus Deviatoric Stress State

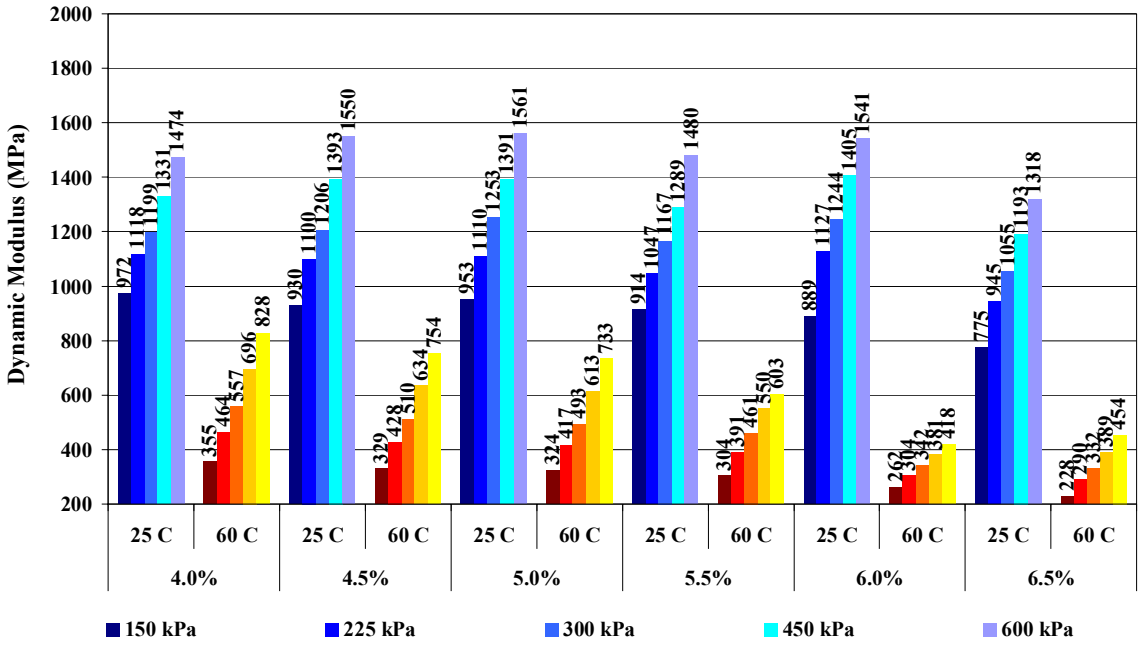

Figure D. 5 Middle Blend Dynamic Modulus by Deviatoric Stress State and Temperature Plotted versus Frequency

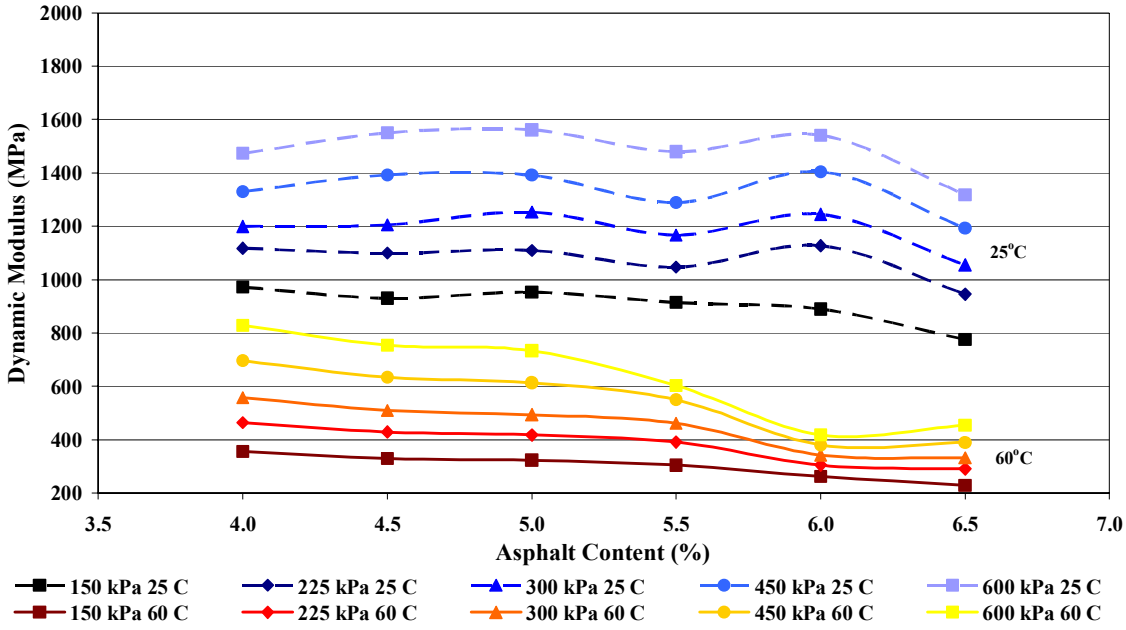

Figure D. 6 Middle Blend Dynamic Modulus versus Asphalt Content by Deviatoric Stress State and Temperature Plotted versus Frequency

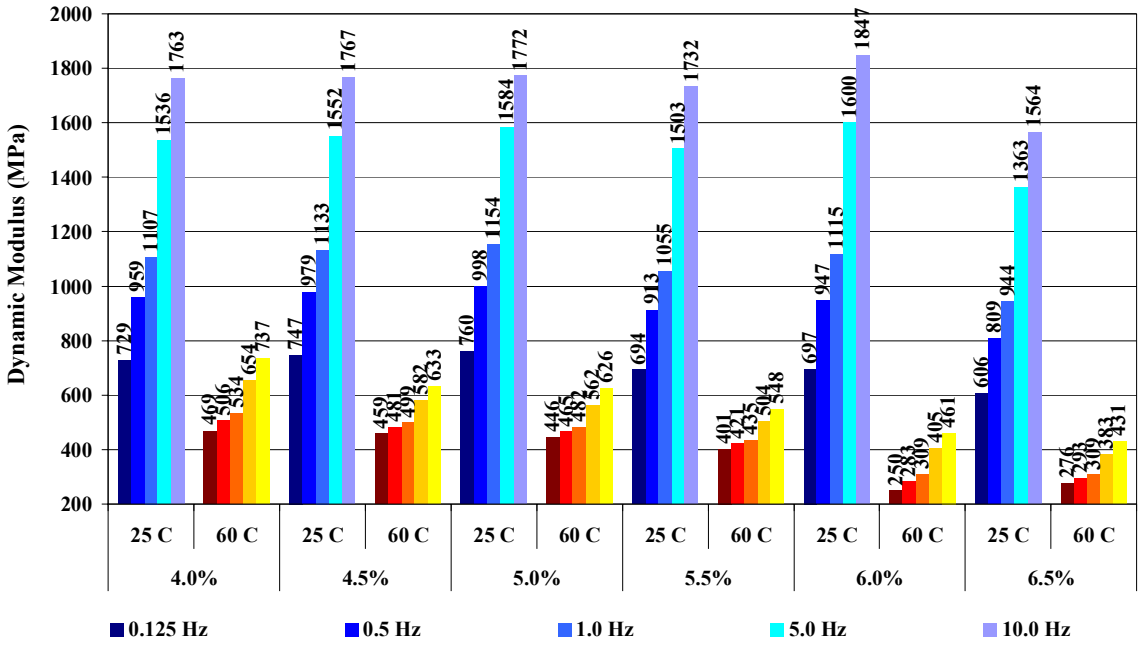

Figure D. 7 Middle Blend Dynamic Modulus by Frequency and Temperature Plotted versus Deviatoric Stress State

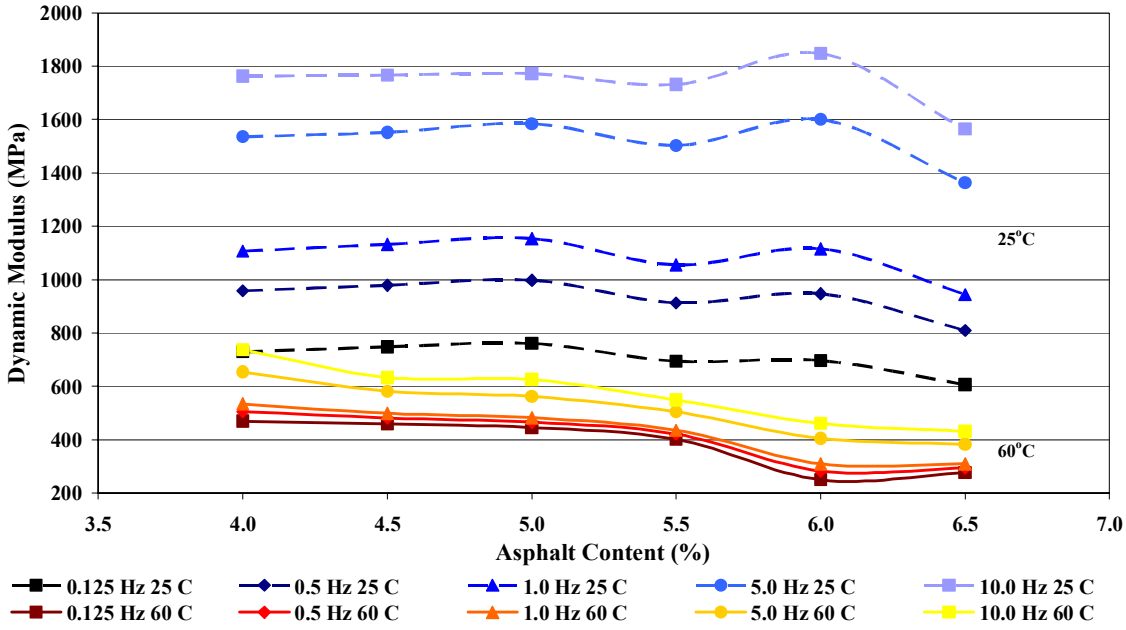

Figure D. 8 Middle Blend Dynamic Modulus versus Asphalt Content by Frequency and Temperature Plotted versus Deviatoric Stress State

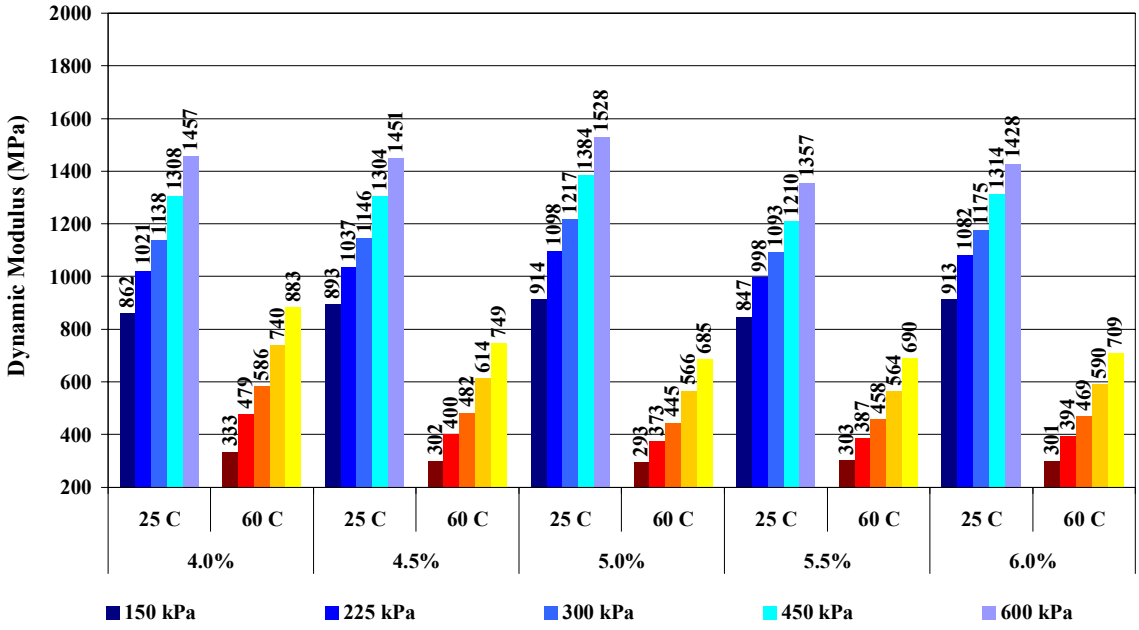

Figure D. 9 Coarse Blend Dynamic Modulus by Deviatoric Stress State and Temperature Plotted versus Frequency

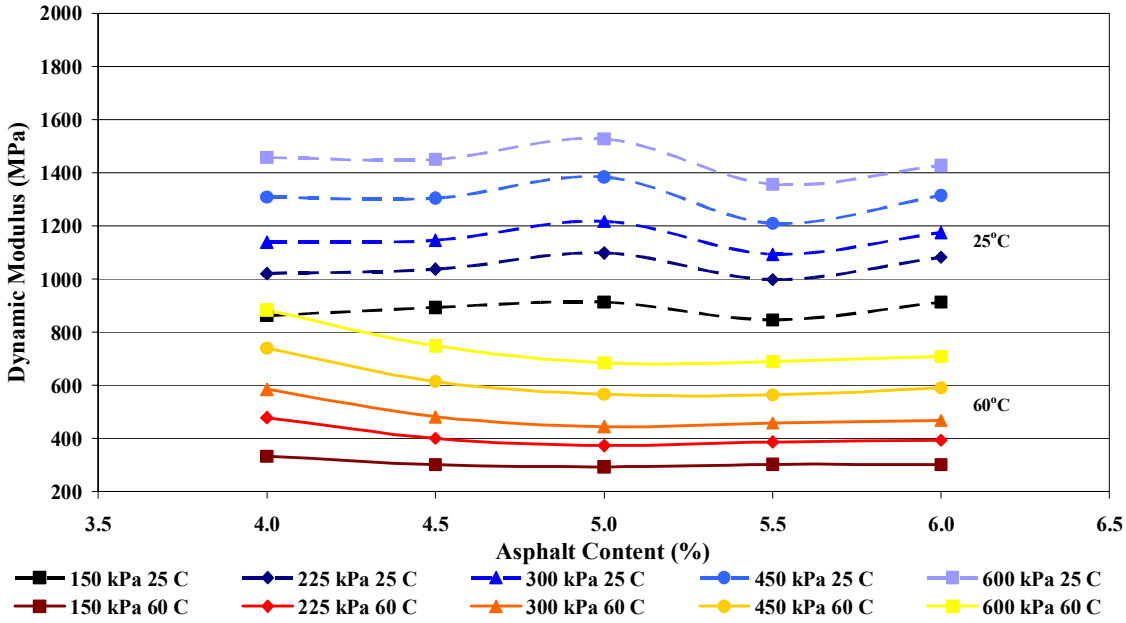

Figure D. 10 Coarse Blend Dynamic Modulus versus Asphalt Content by Deviatoric Stress State and Temperature Plotted versus Frequency

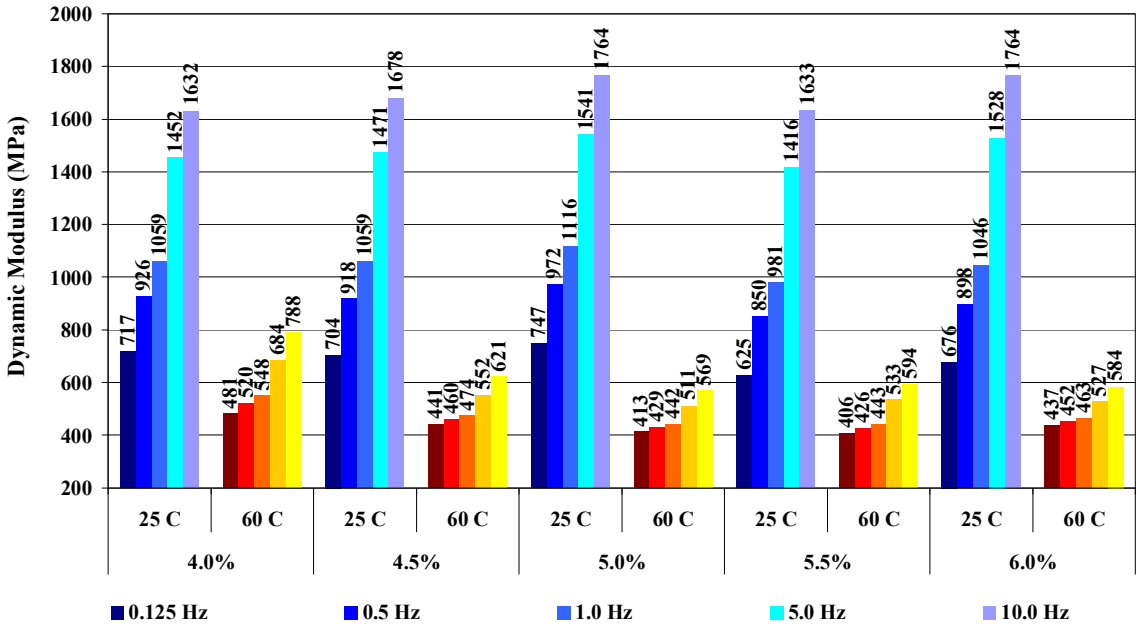

Figure D. 11 Coarse Blend Dynamic Modulus by Frequency and Temperature Plotted versus Deviatoric Stress State

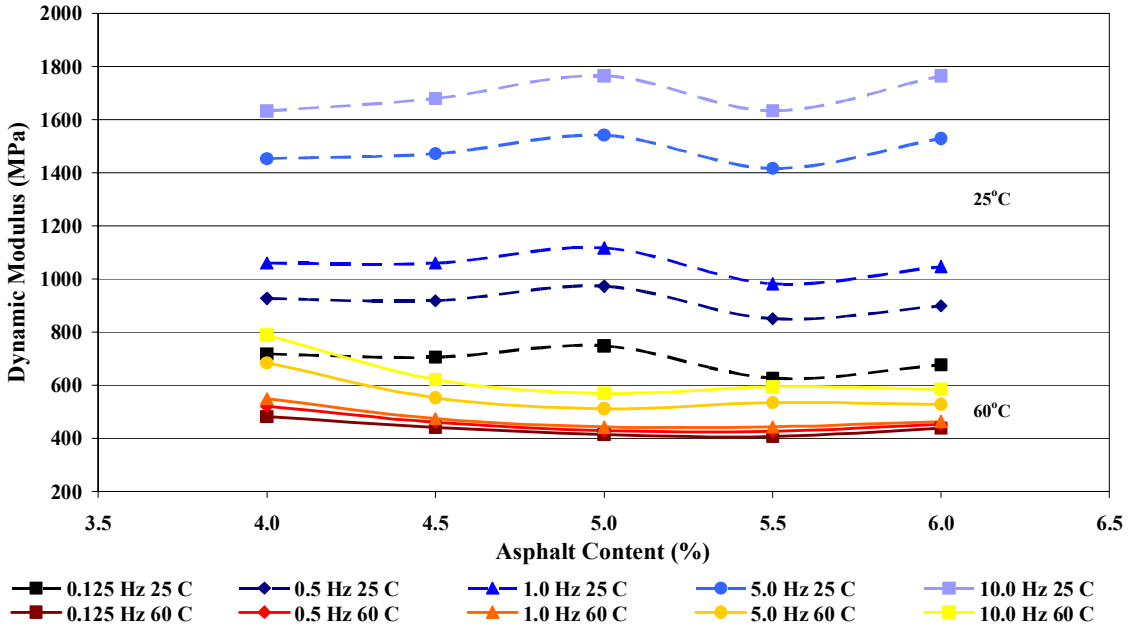

Figure D. 12 Coarse Blend Dynamic Modulus versus Asphalt Content by Frequency and Temperature Plotted versus Deviatoric Stress State

APPENDIX E: POISSON'S RATIO

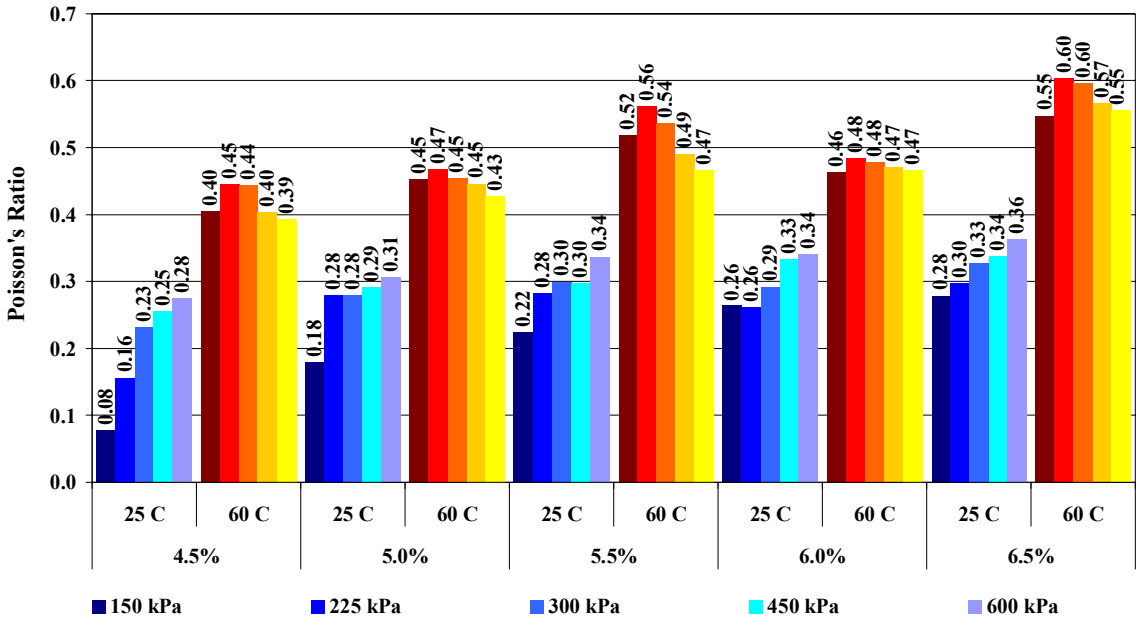

Figure E. 1 Fine Blend Poisson's Ratio by Deviatoric Stress State and Temperature Plotted versus Frequency

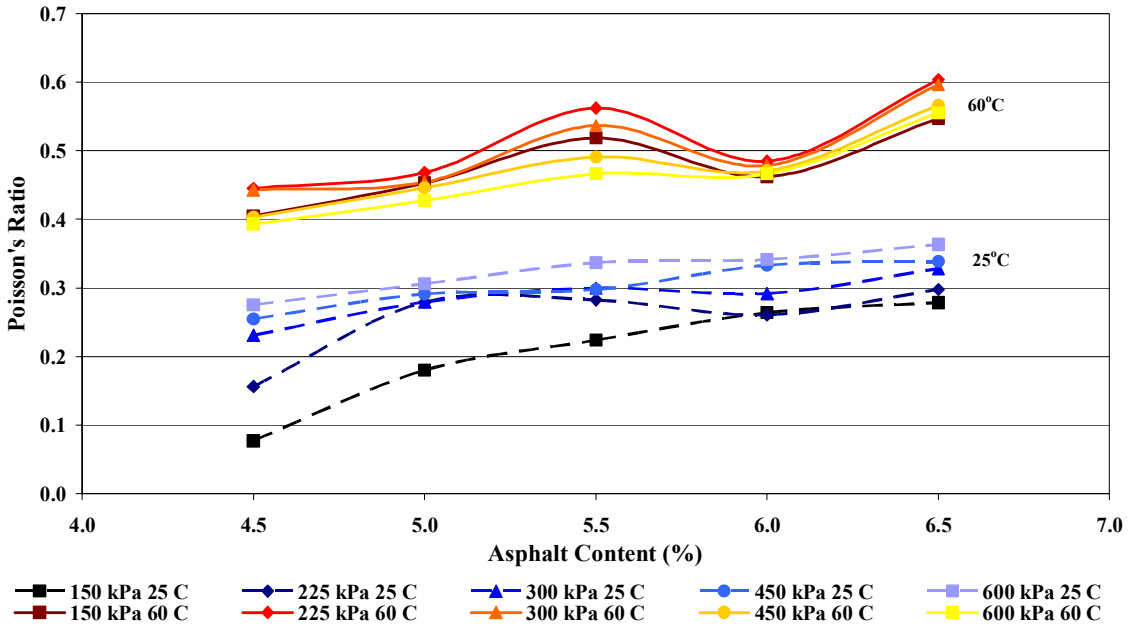

Figure E. 2 Fine Blend Gradation Poisson's Ratio versus Asphalt Content by Deviatoric Stress State and Temperature Plotted versus Frequency

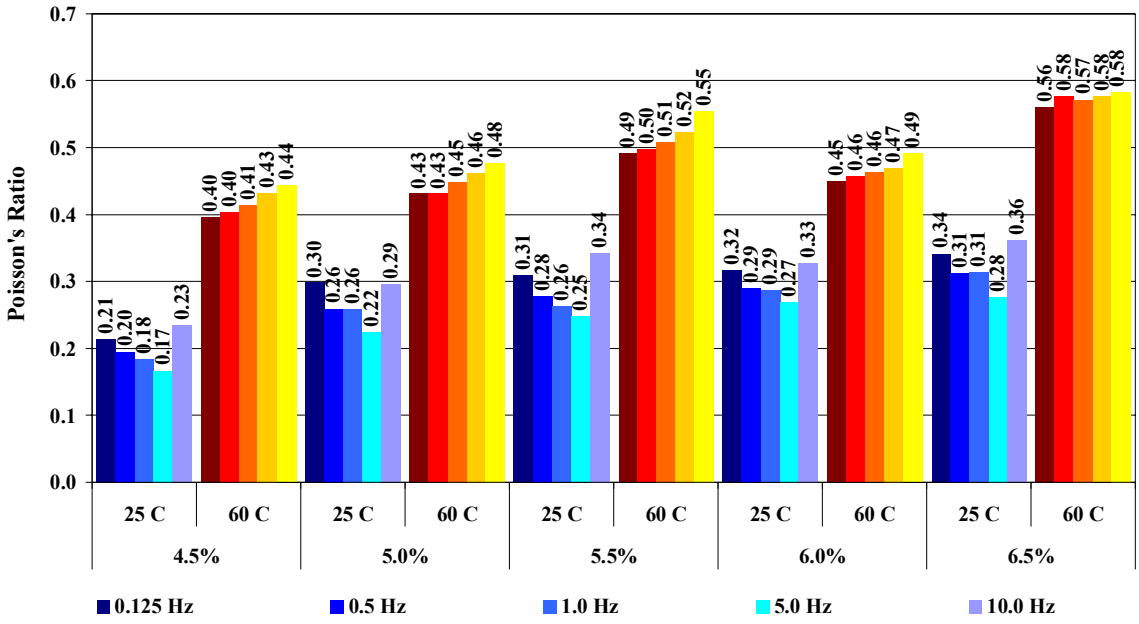

Figure E. 3 Fine Blend Poisson's Ratio by Frequency and Temperature Plotted versus Deviatoric Stress State

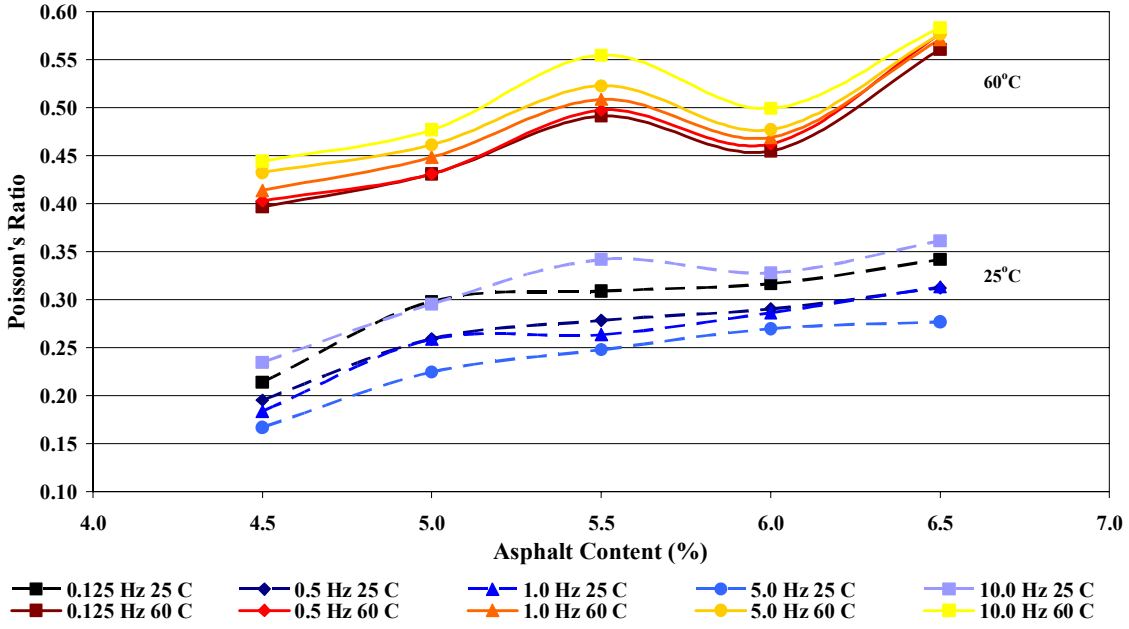

Figure E. 4 Fine Blend Poisson's Ratio versus Asphalt Content by Frequency and Temperature Plotted versus Deviatoric Stress State

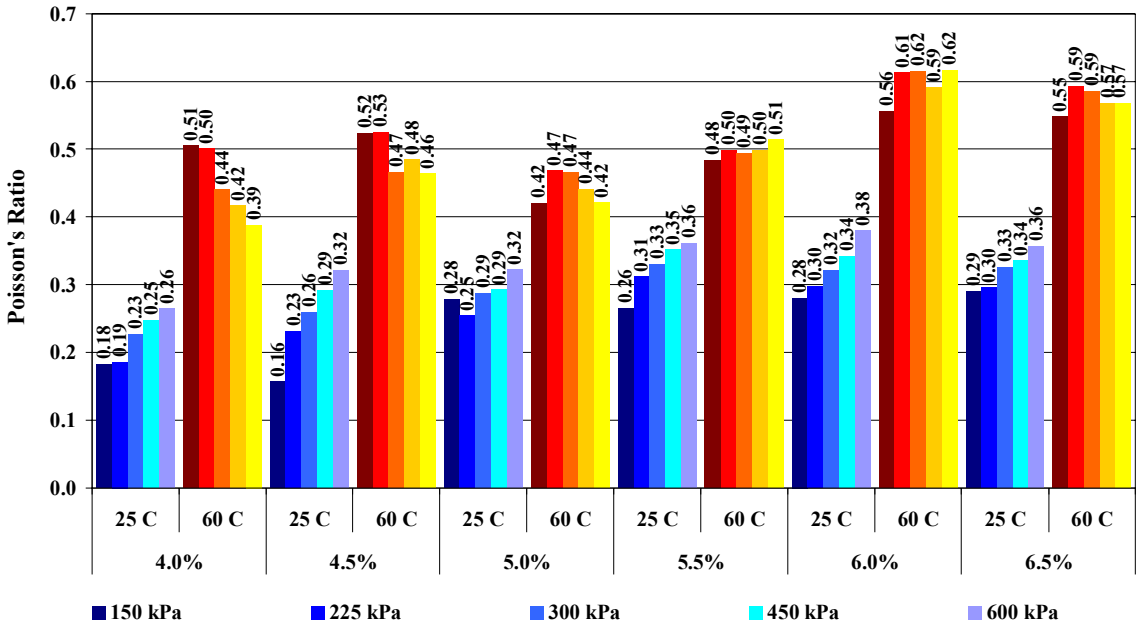

Figure E. 5 Middle Blend Poisson's Ratio by Deviatoric Stress State and Temperature Plotted versus Frequency

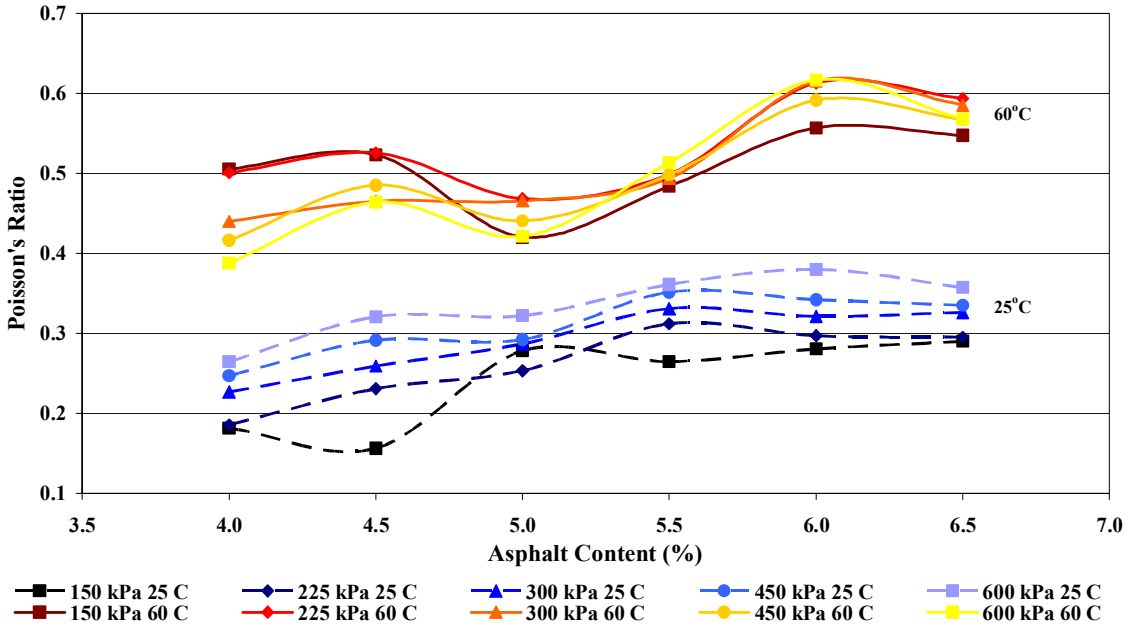

Figure E. 6 Middle Blend Poisson's Ratio versus Asphalt Content by Deviatoric Stress State and Temperature Plotted versus Frequency

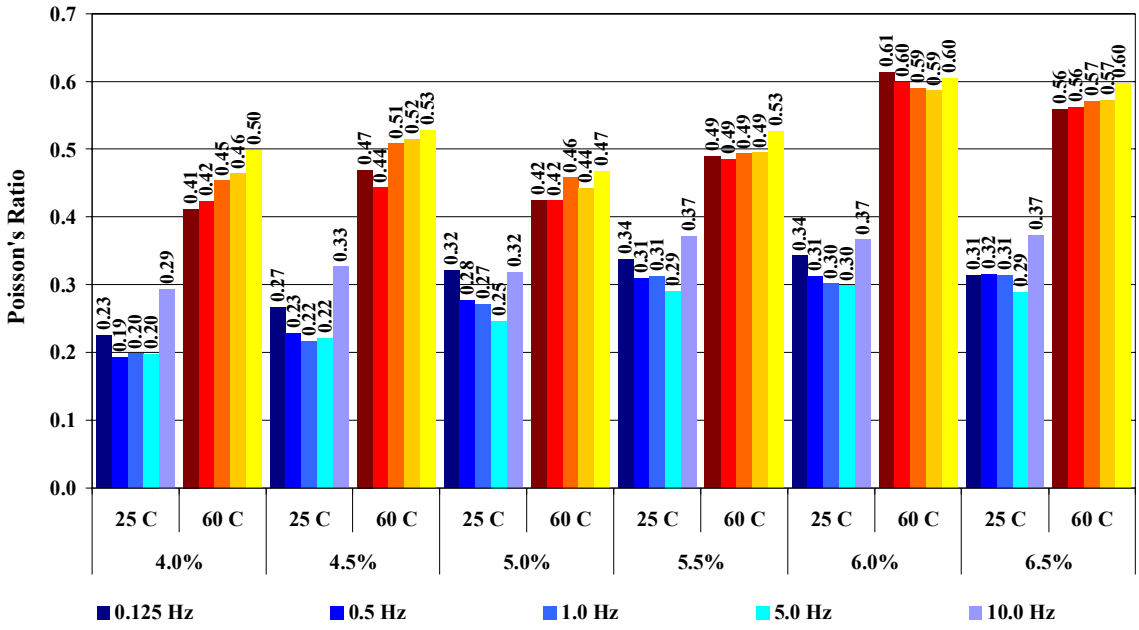

Figure E. 7 Middle Blend Poisson's Ratio by Frequency and Temperature Plotted versus Deviatoric Stress State

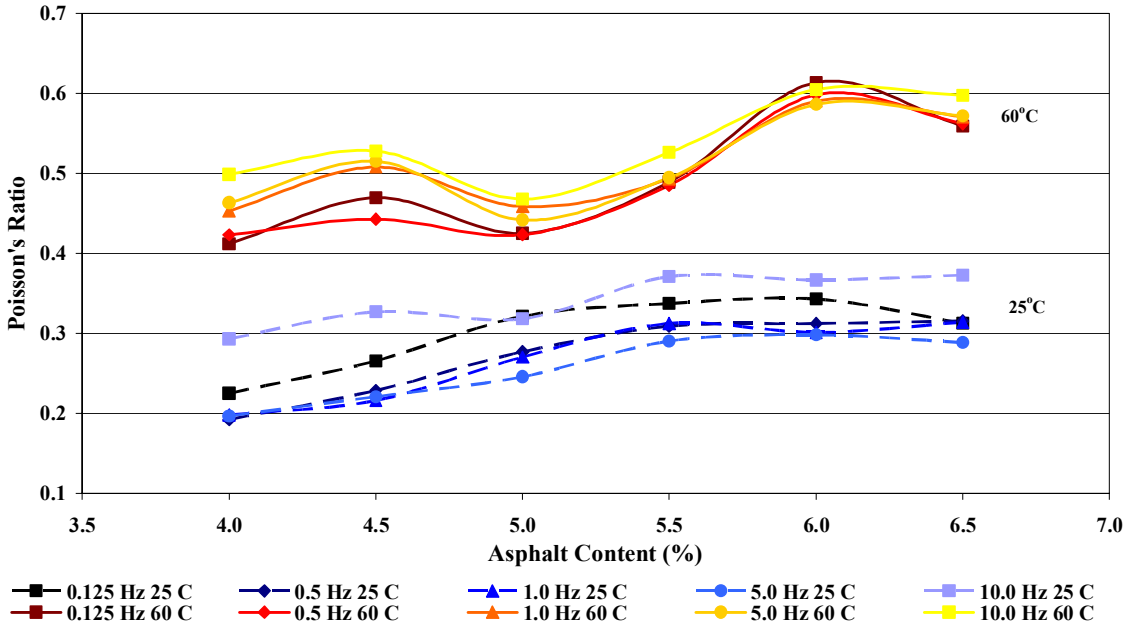

Figure E. 8 Middle Blend Poisson's Ratio versus Asphalt Content by Frequency and Temperature Plotted versus Deviatoric Stress State

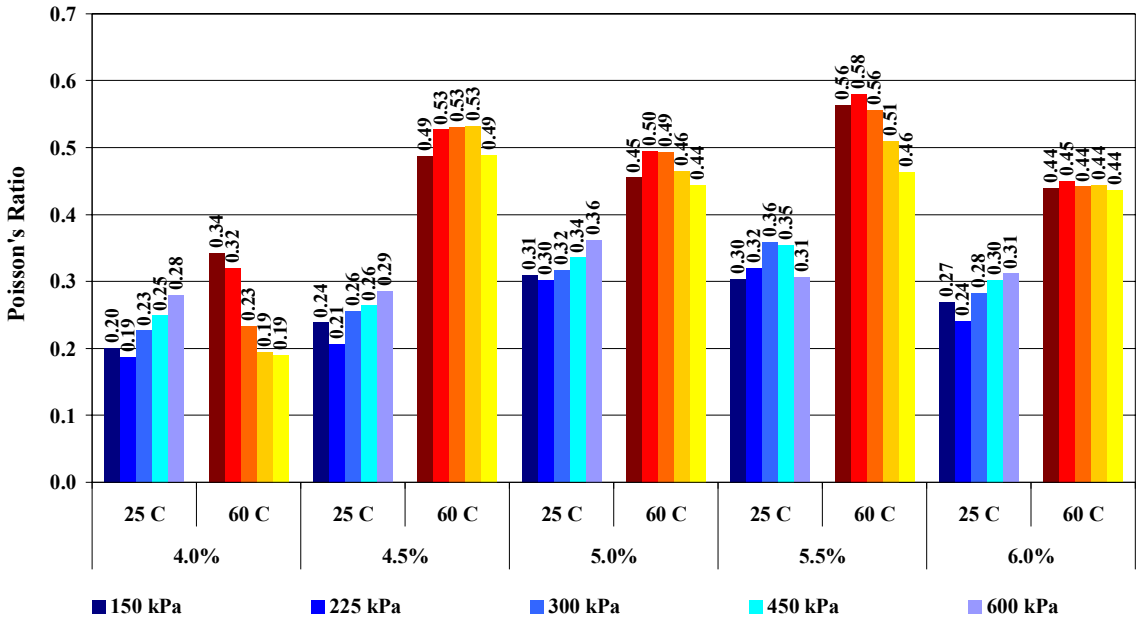

Figure E. 9 Coarse Blend Poisson's Ratio by Deviatoric Stress State and Temperature Plotted versus Frequency

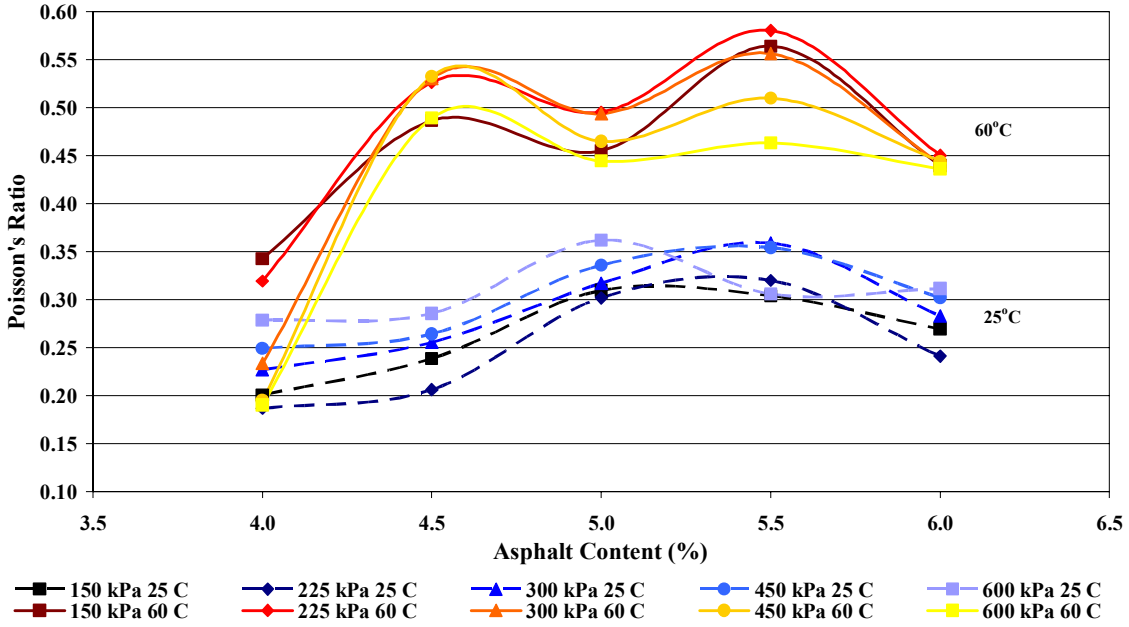

Figure E. 10 Coarse Blend Poisson's Ratio versus Asphalt Content by Deviatoric Stress State and Temperature Plotted versus Frequency

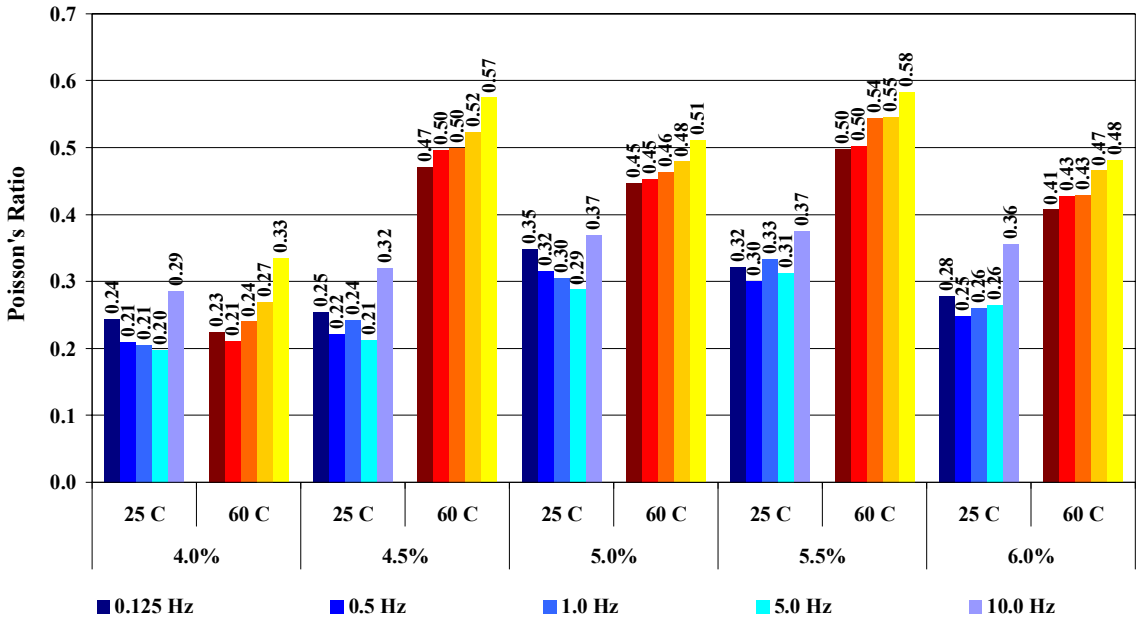

Figure E. 11 Coarse Blend Poisson's Ratio by Frequency and Temperature Plotted versus Deviatoric Stress State

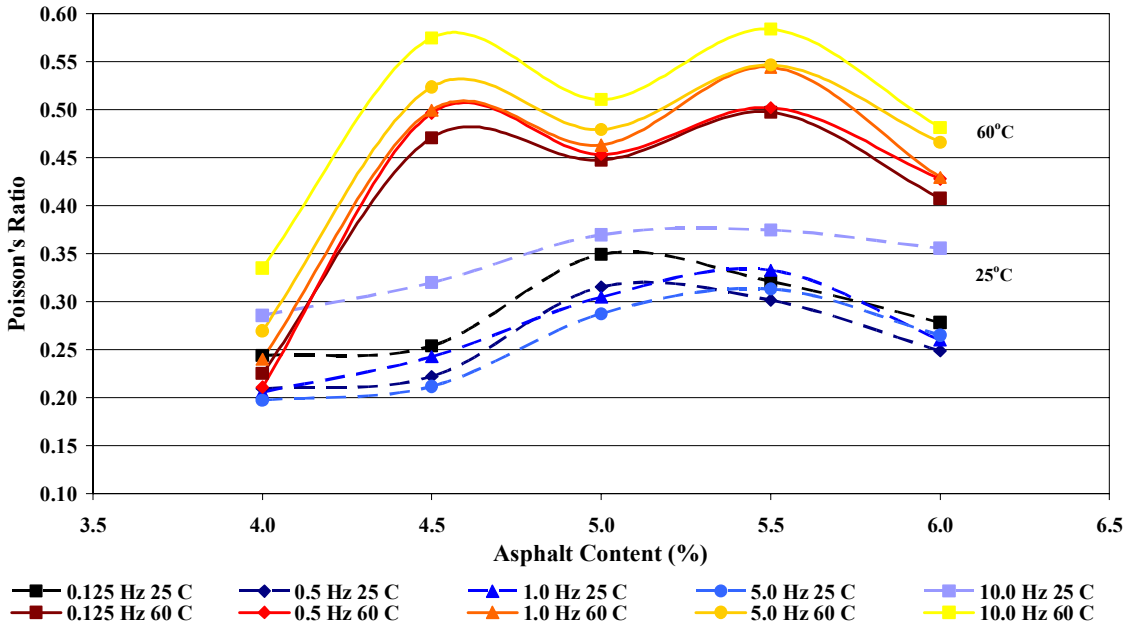

Figure E. 12 Coarse Blend Poisson's Ratio versus Asphalt Content by Frequency and Temperature Plotted versus Deviatoric Stress State

APPENDIX F: PHASE ANGLE

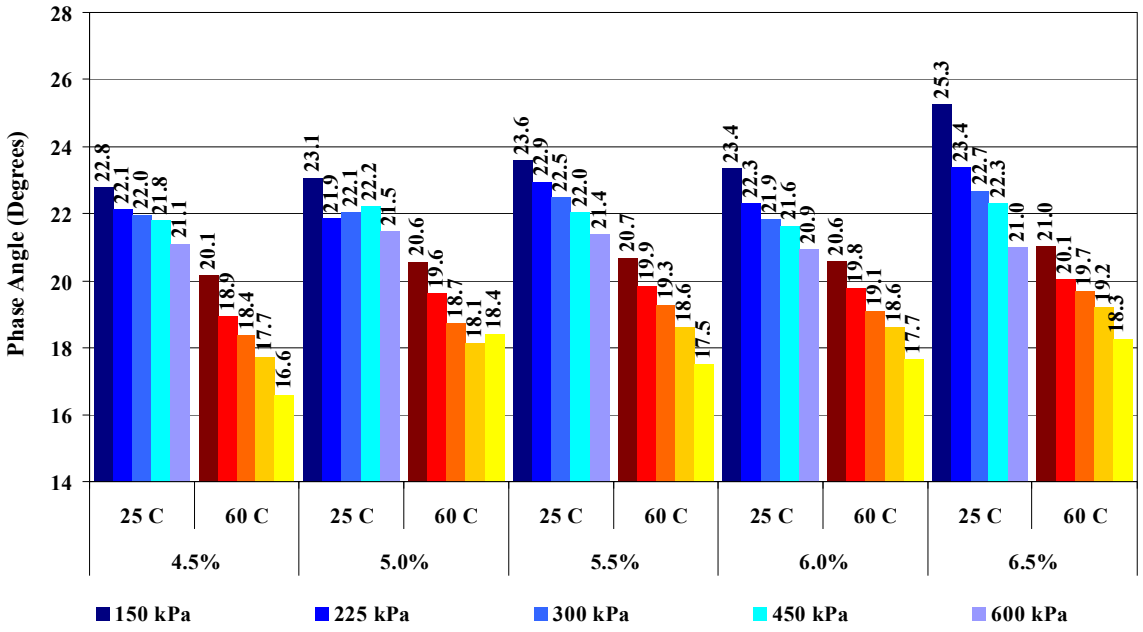

Figure F. 1 Fine Blend Phase Angle by Deviatoric Stress State and Temperature Plotted versus Frequency

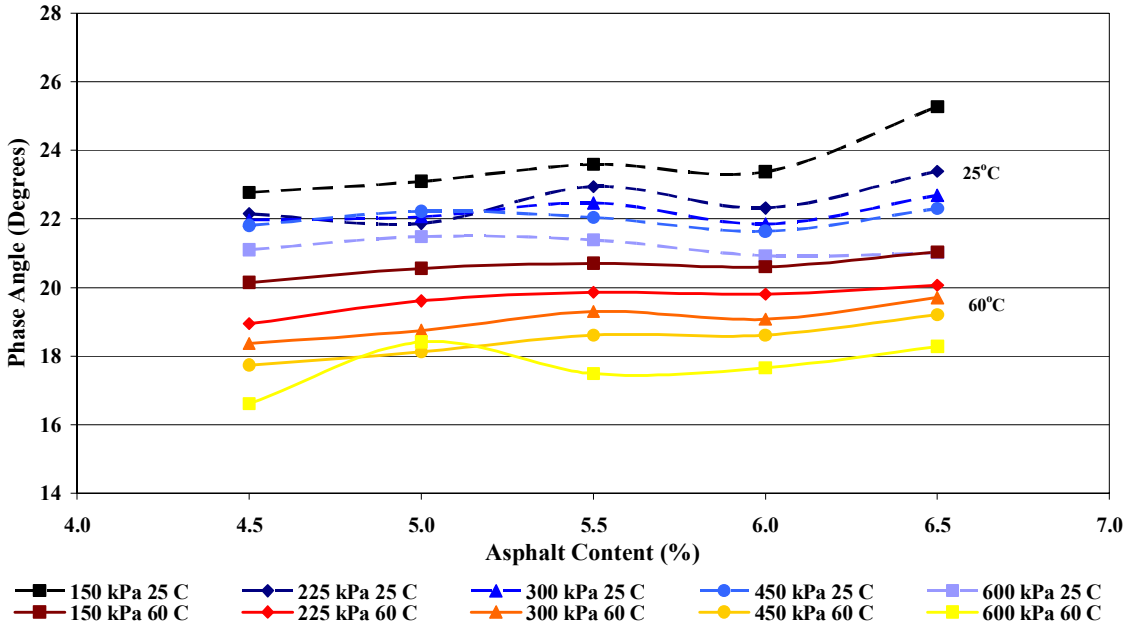

Figure F. 2 Fine Blend Gradation Phase Angle versus Asphalt Content by Deviatoric Stress State and Temperature Plotted versus Frequency

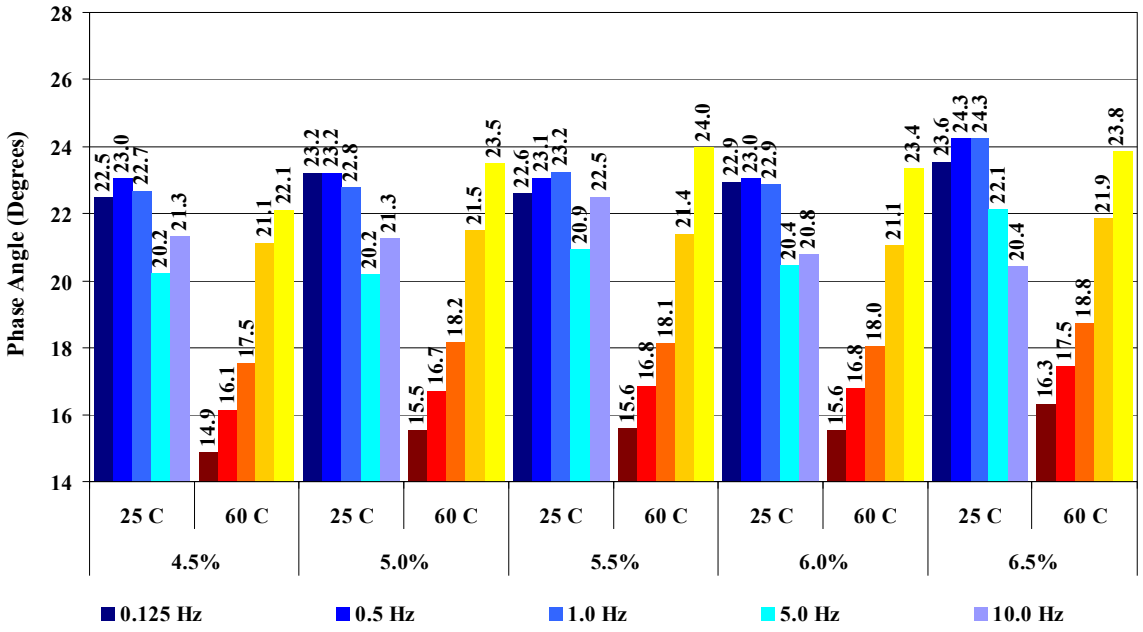

Figure F. 3 Fine Blend Phase Angle by Frequency and Temperature Plotted versus Deviatoric Stress State

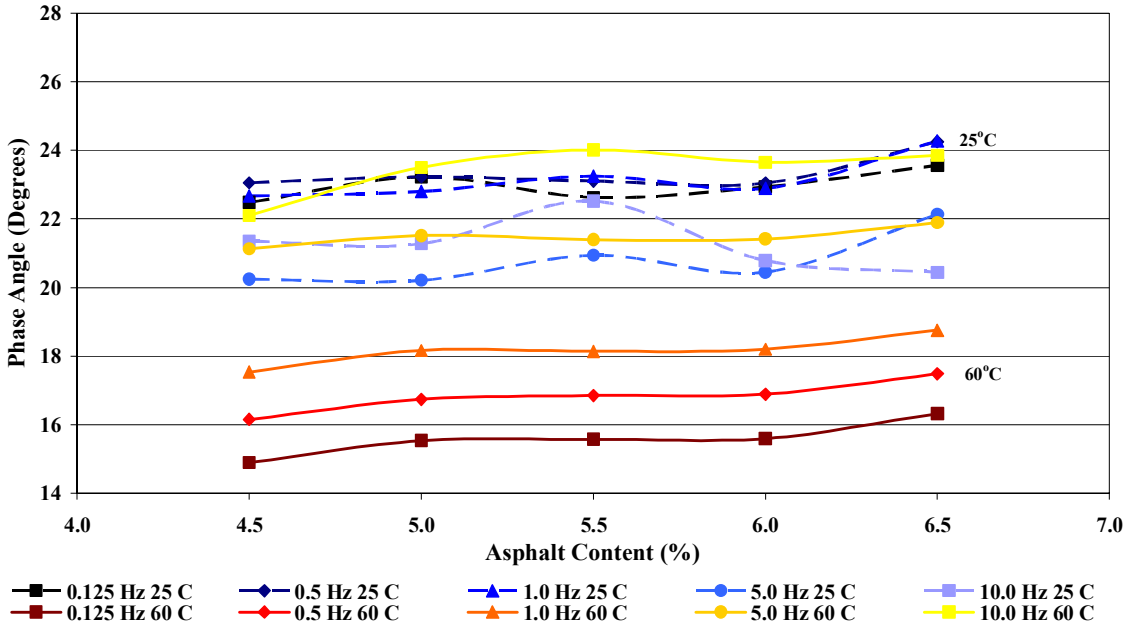

Figure F. 4 Fine Blend Gradation Phase Angle versus Asphalt Content by Frequency and Temperature Plotted versus Deviatoric Stress State

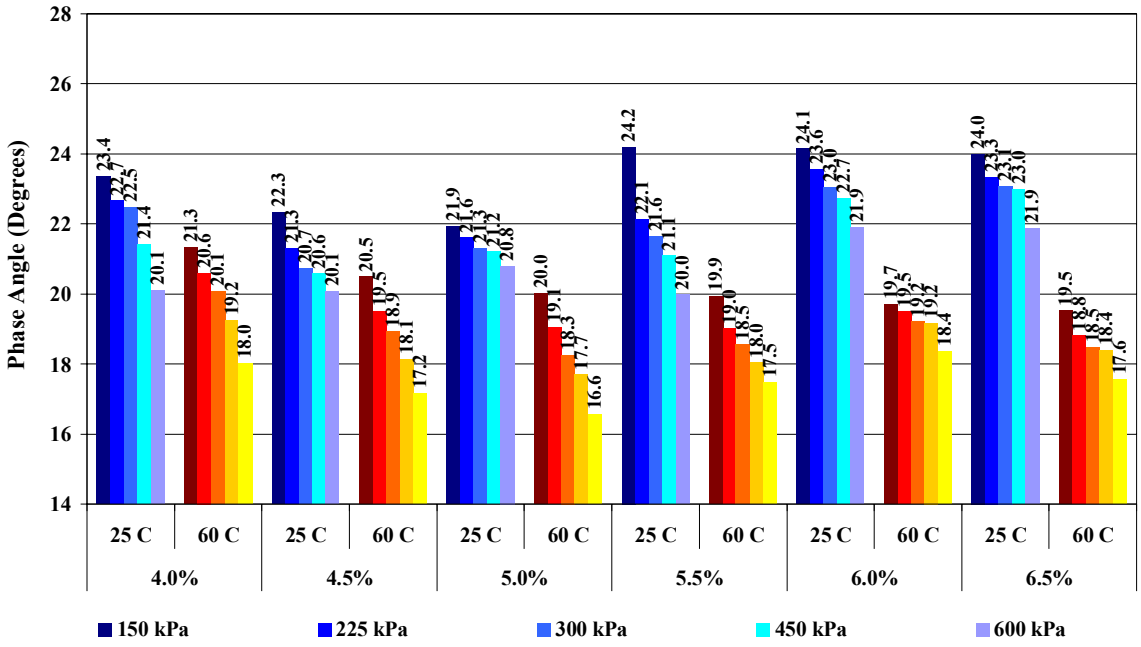

Figure F. 5 Middle Blend Phase Angle by Deviatoric Stress State and Temperature Plotted versus Frequency

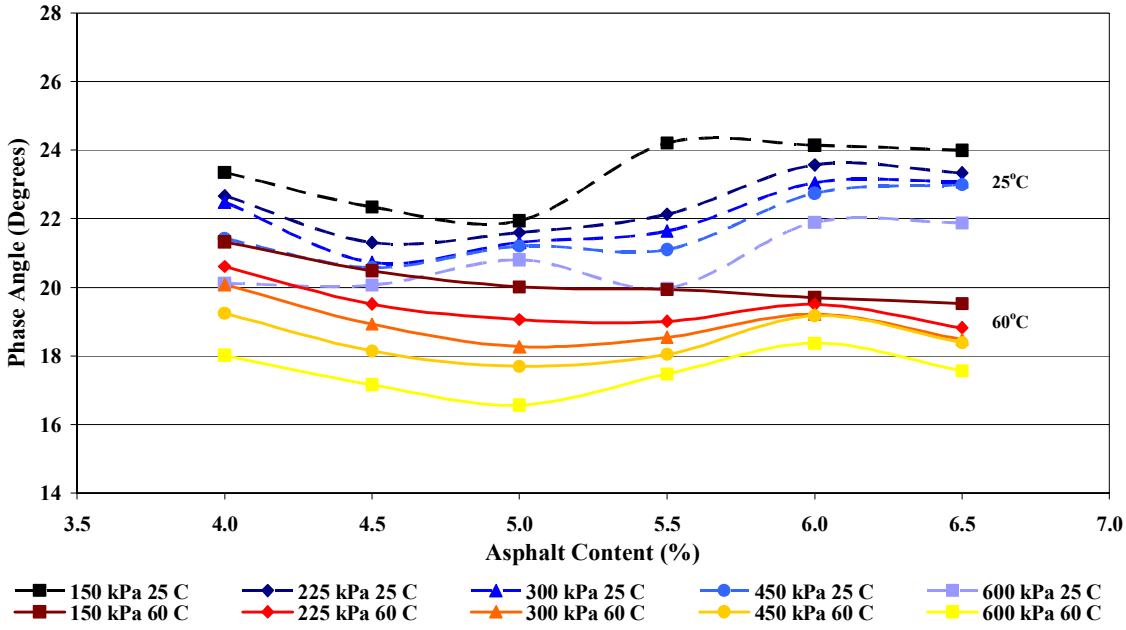

Figure F. 6 Middle Blend Phase Angle versus Asphalt Content by Deviatoric Stress State and Temperature Plotted versus Frequency

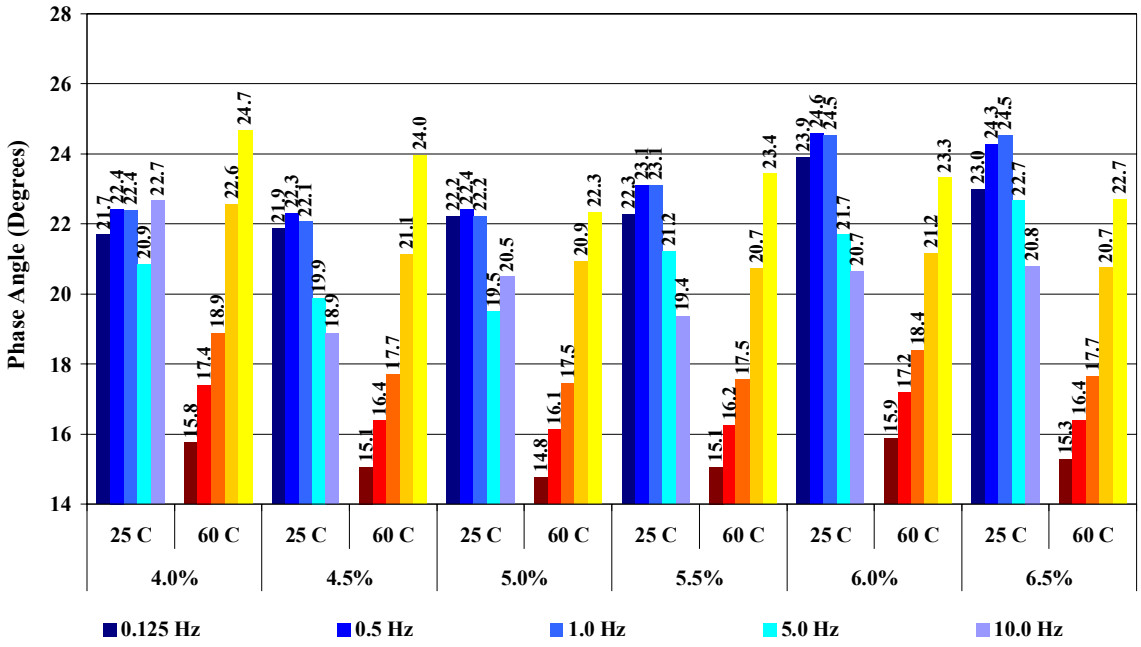

Figure F. 7 Middle Blend Phase Angle by Frequency and Temperature Plotted versus Deviatoric Stress State

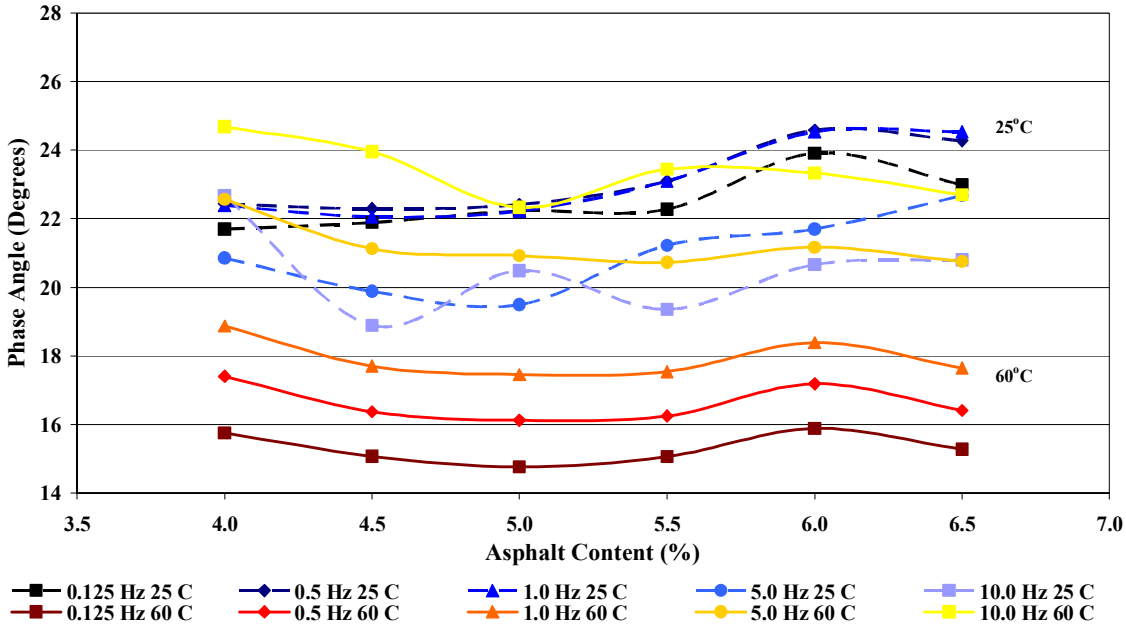

Figure F. 8 Middle Blend Phase Angle versus Asphalt Content by Frequency and Temperature Plotted versus Deviatoric Stress State

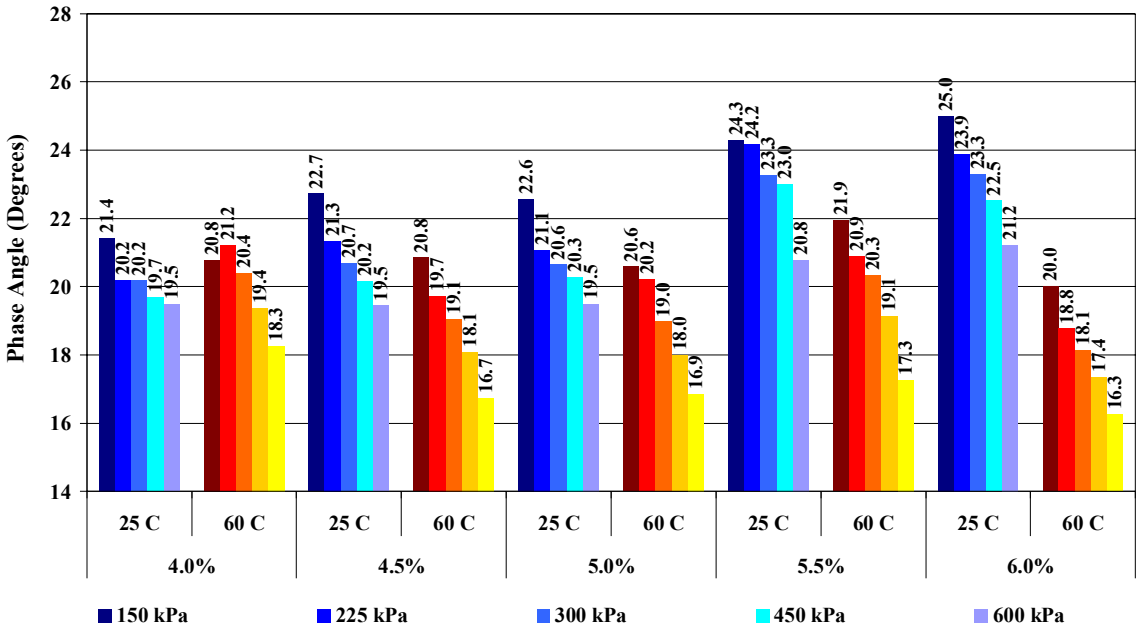

Figure F. 9 Coarse Blend Phase Angle by Deviatoric Stress State and Temperature Plotted versus Frequency

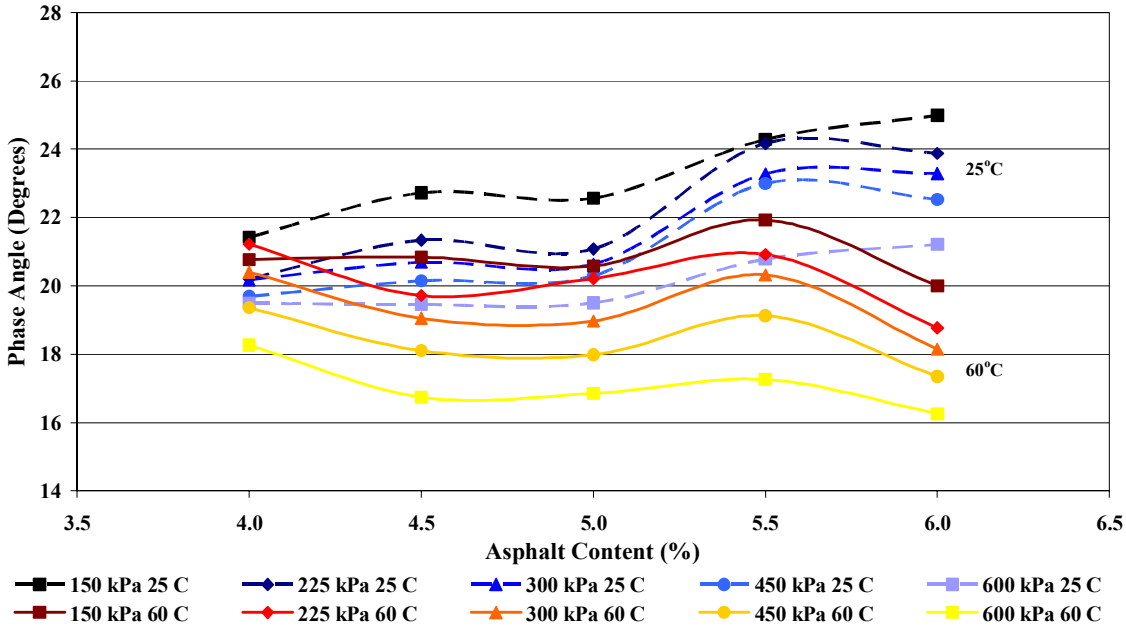

Figure F. 10 Coarse Blend Phase Angle by Deviatoric Stress State versus Asphalt Content and Temperature Plotted versus Frequency

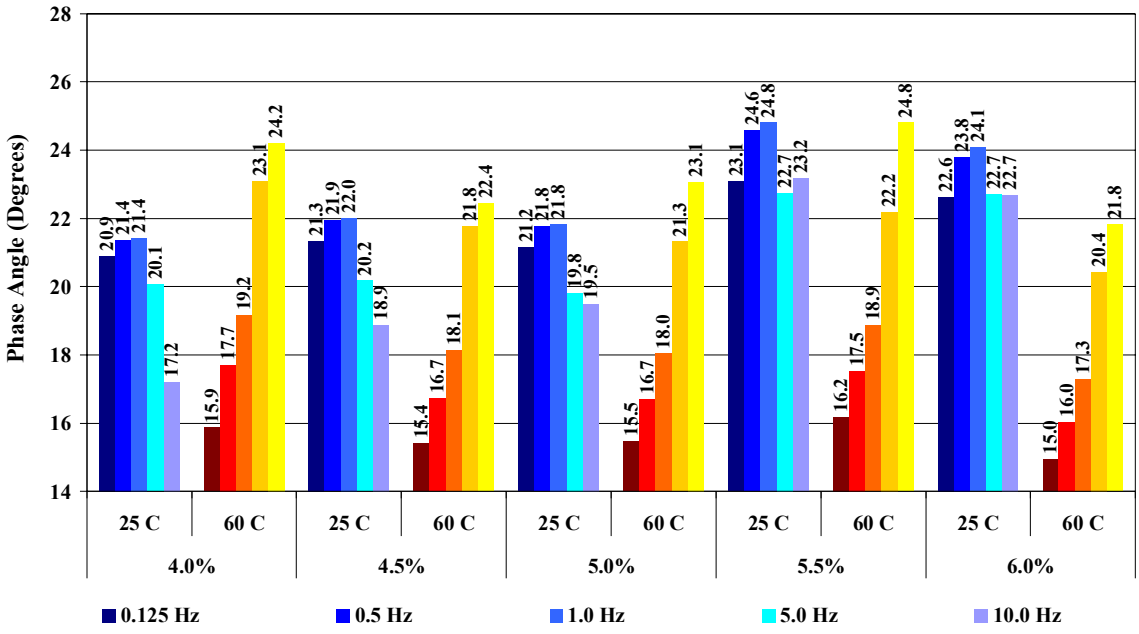

Figure F. 11 Coarse Blend Phase Angle by Frequency and Temperature Plotted versus Deviatoric Stress STate

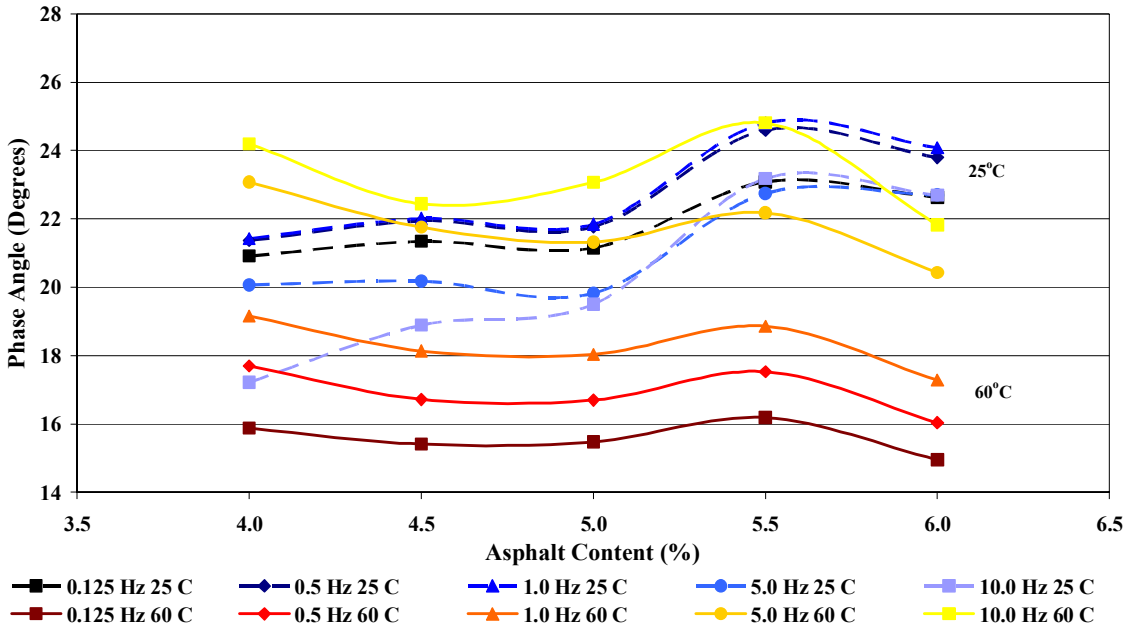

Figure F. 12 Coarse Blend Phase Angle versus Asphalt Content by Frequency and Temperature Plotted versus Deviatoric Stress State

APPENDIX G: DYNAMIC MODULUS RANGE FOR ACCEPTABLE VTM SPECIFICATIONS

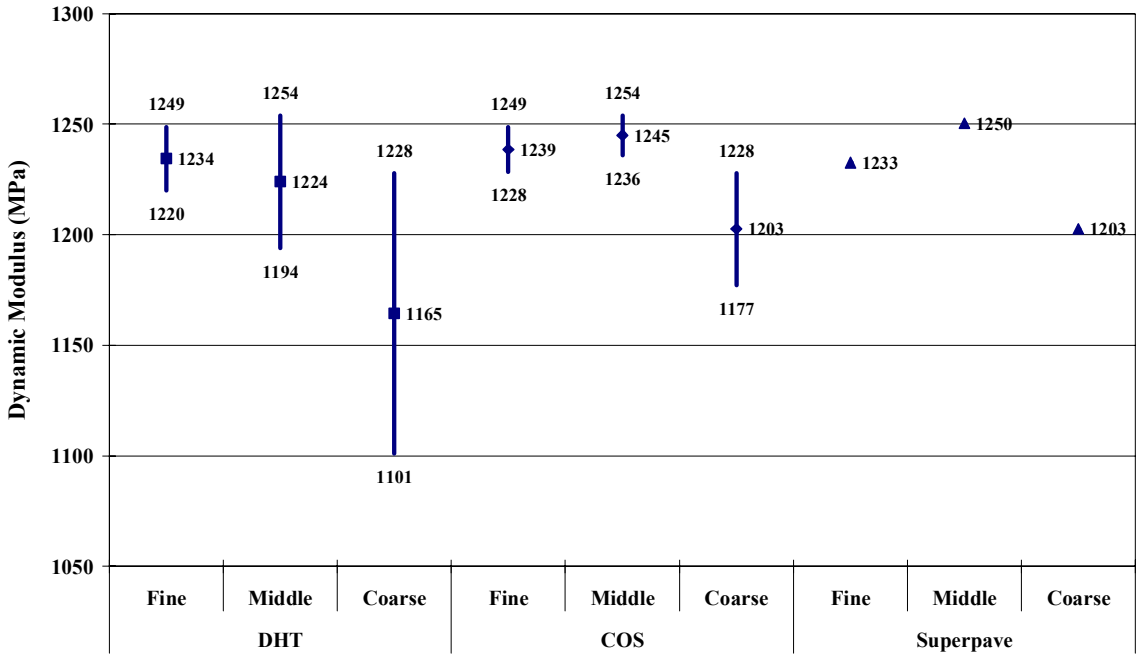

Figure G. 1 Dynamic Modulus Range Plotted versus Frequency and Deviatoric Stress State at 25°C for Ranges of Acceptable VTM Specifications

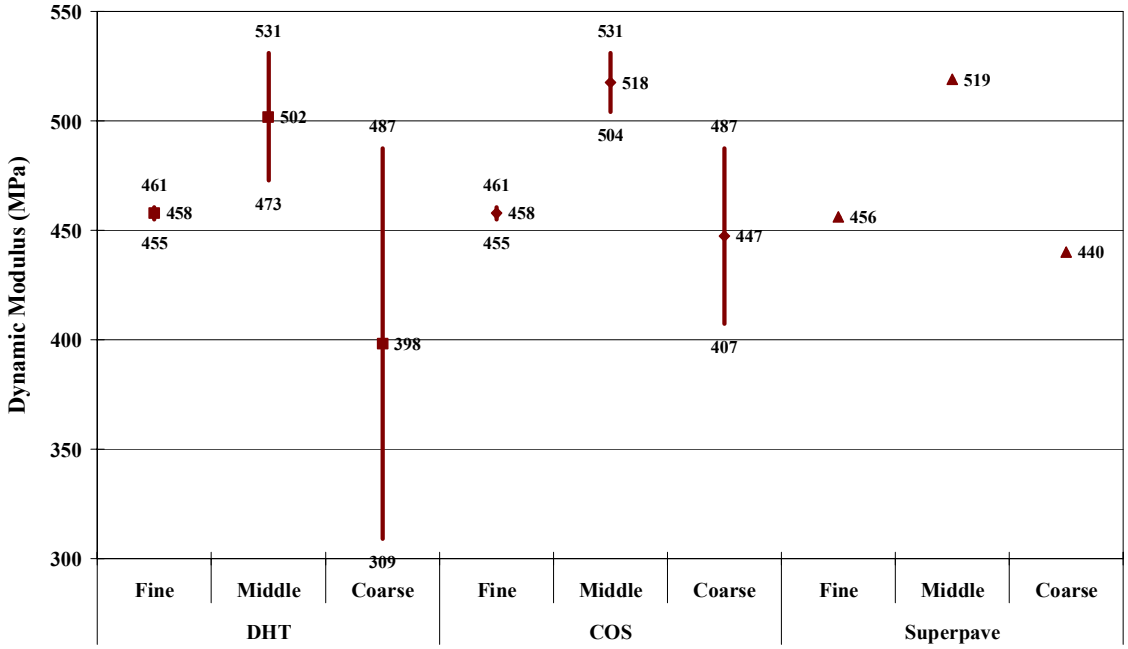

Figure G. 2 Dynamic Modulus Range Plotted versus Frequency and Deviatoric Stress State at 60°C for Ranges of Acceptable VTM Specifications

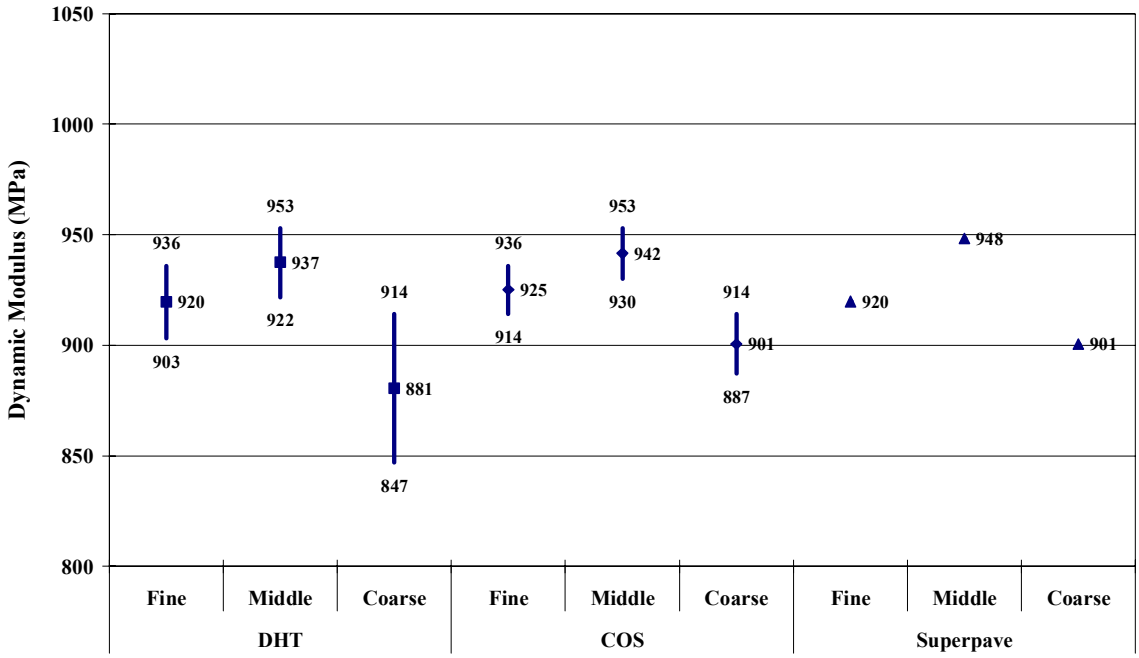

Figure G. 3 Dynamic Modulus Range Plotted versus Frequency at 25°C for Range of VTM Specifications Met – 150 kPa

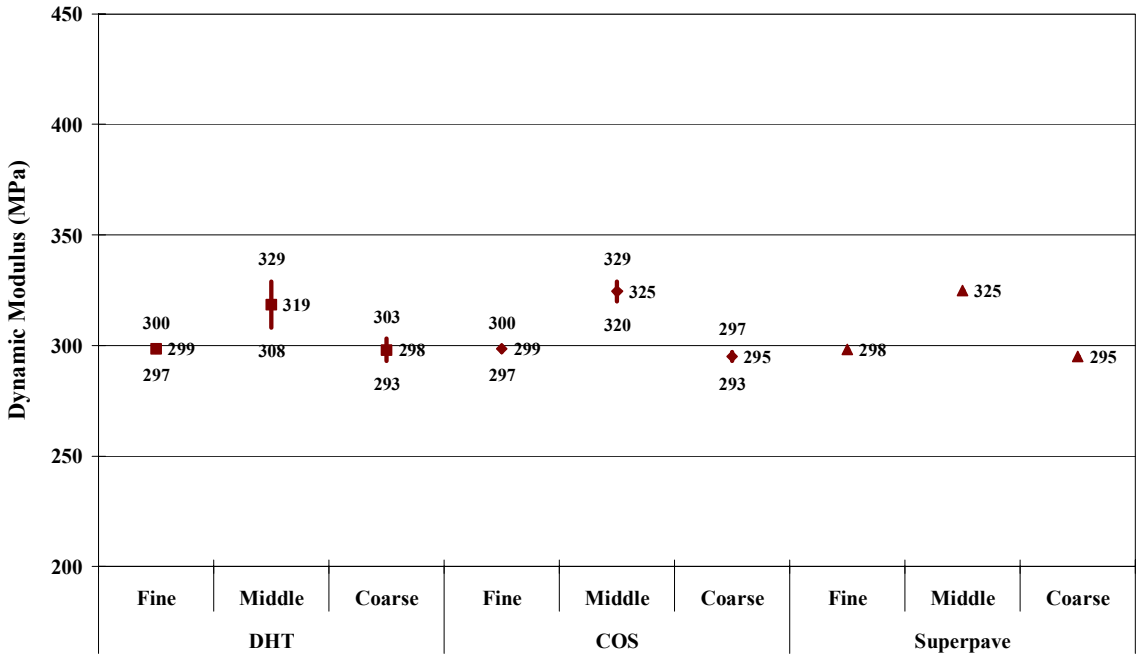

Figure G. 4 Dynamic Modulus Range Plotted versus Frequency at 60°C for Range of VTM Specifications Met – 150 kPa

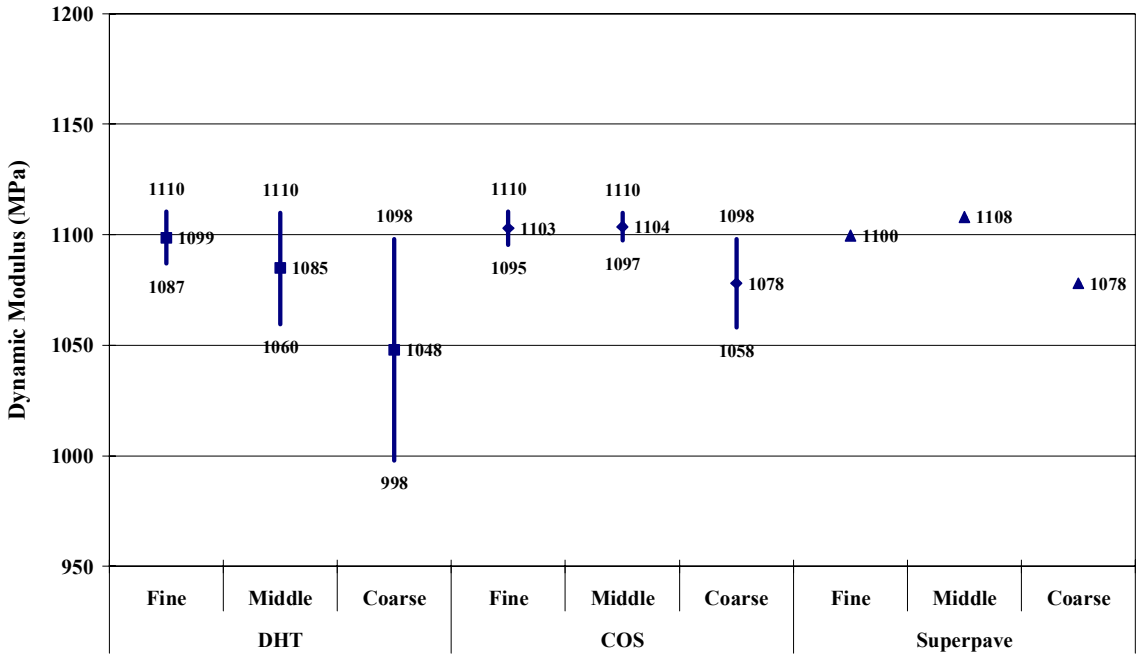

Figure G. 5 Dynamic Modulus Range Plotted versus Frequency at 25°C for Range of VTM Specifications Met – 225 kPa

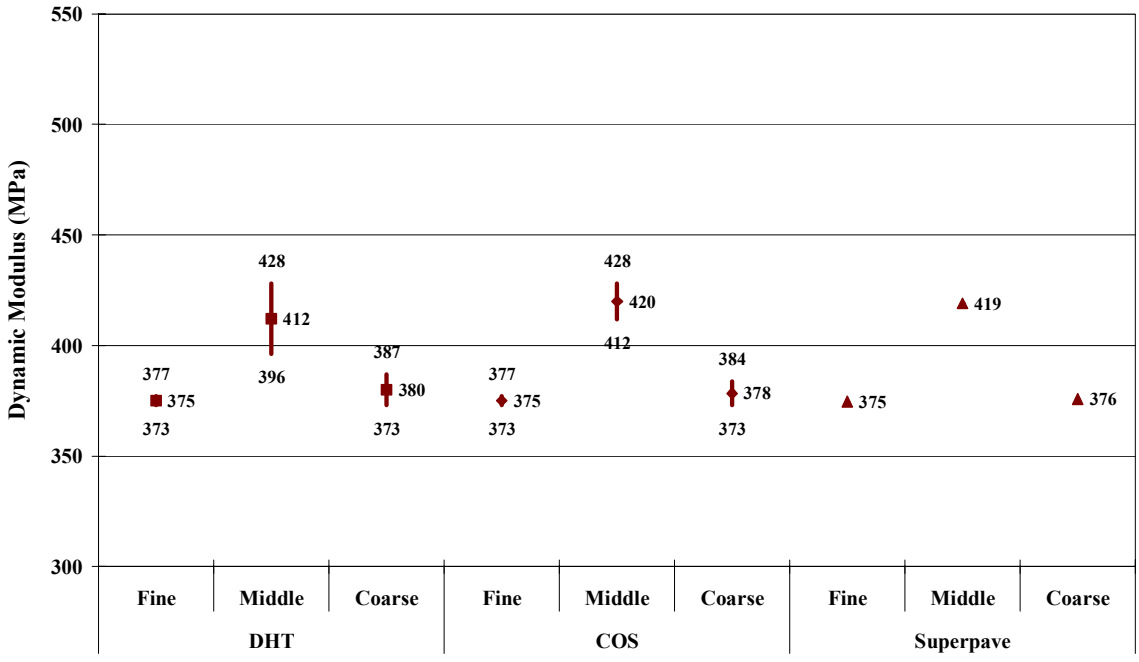

Figure G. 6 Dynamic Modulus Range Plotted versus Frequency at 60°C for Range of VTM Specifications Met – 225 kPa

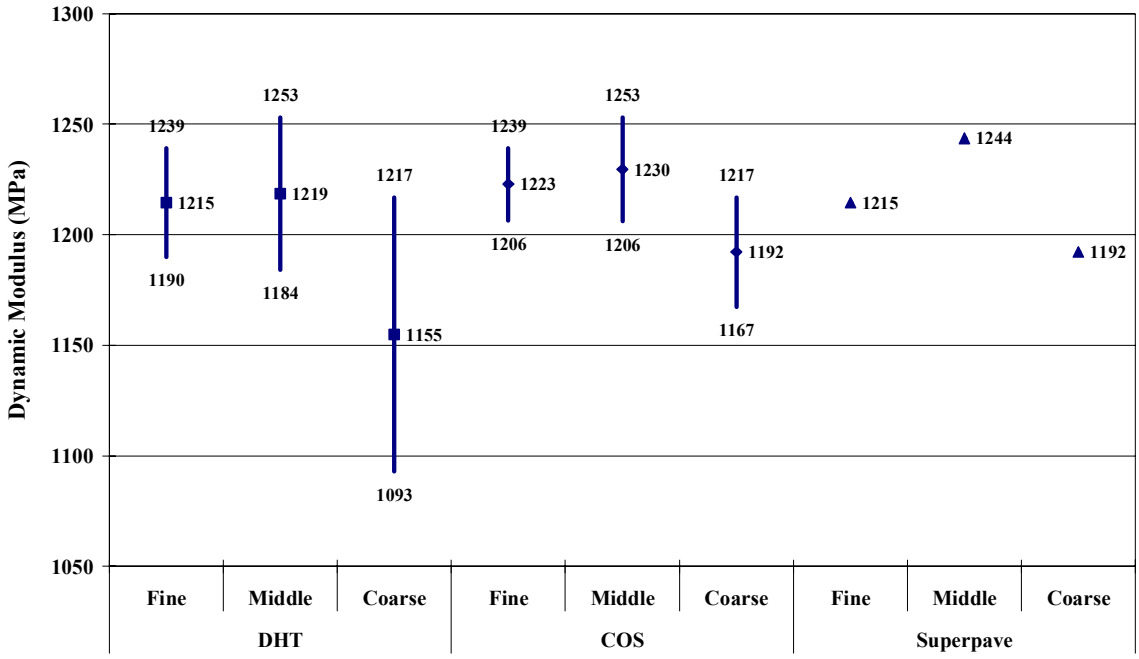

Figure G. 7 Dynamic Modulus Range Plotted versus Frequency at 25°C for Range of VTM Specifications Met – 300 kPa

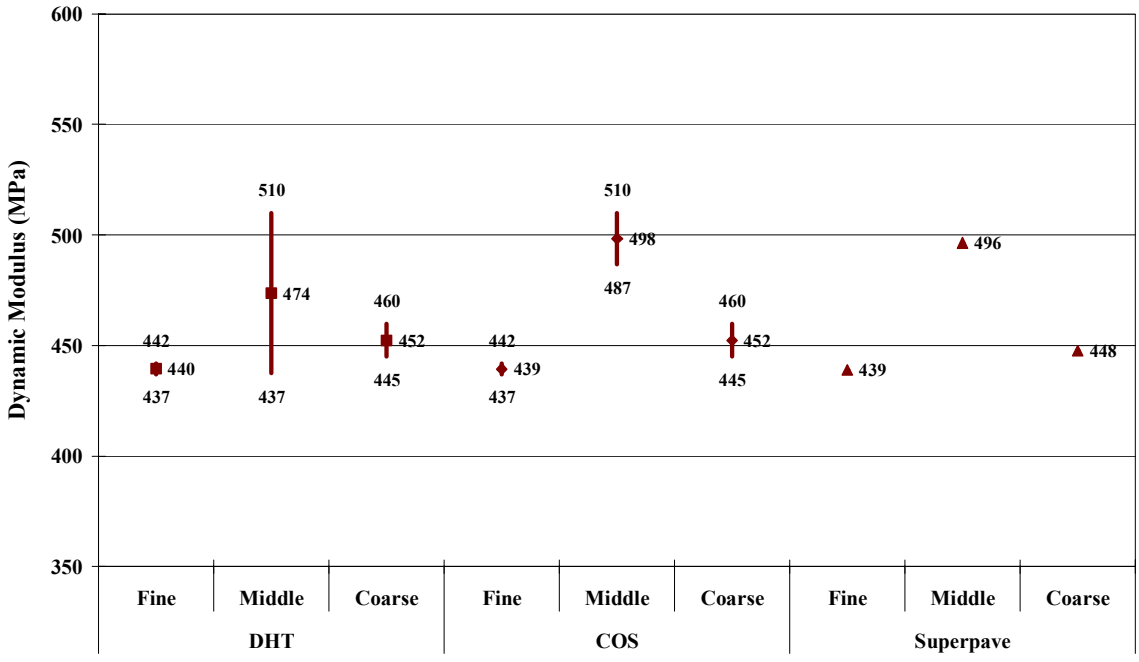

Figure G. 8 Dynamic Modulus Range Plotted versus Frequency at 60°C for Range of VTM Specifications Met – 300 kPa

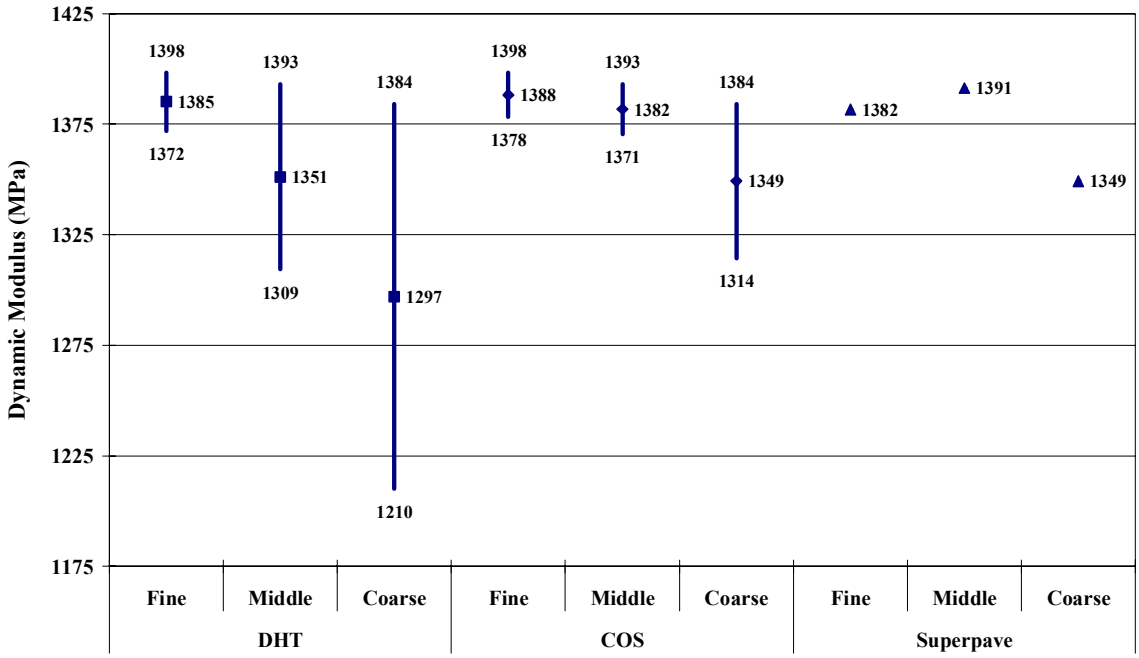

Figure G. 9 Dynamic Modulus Range Plotted versus Frequency at 25°C for Range of VTM Specifications Met – 450 kPa

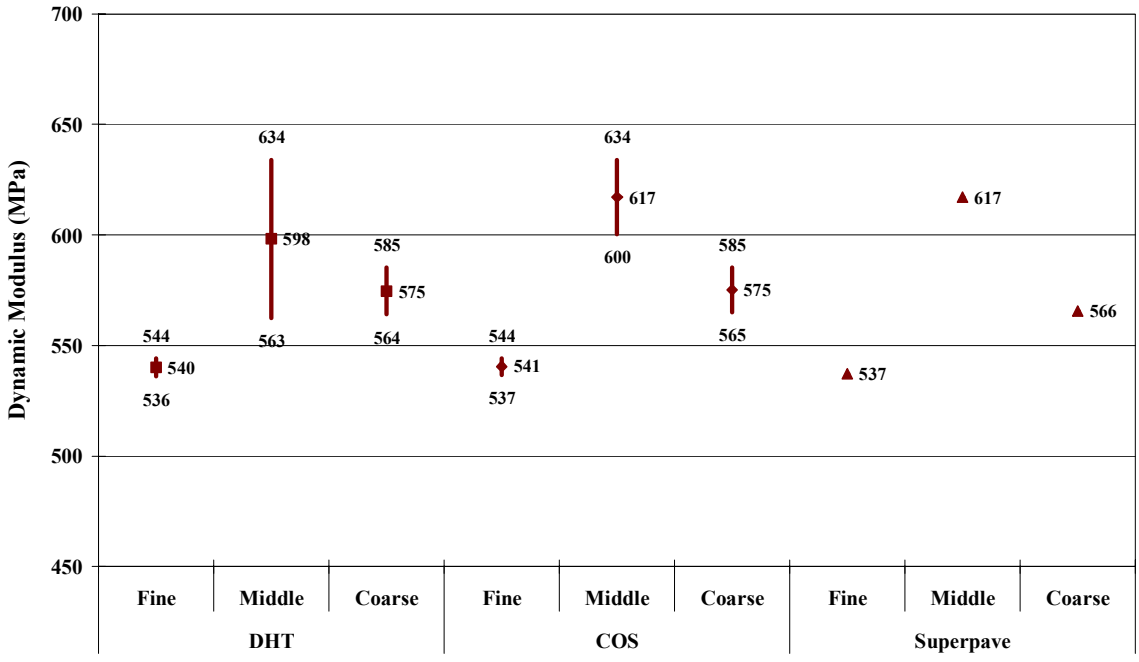

Figure G. 10 Dynamic Modulus Range Plotted versus Frequency at 60°C for Range of VTM Specifications Met – 450 kPa

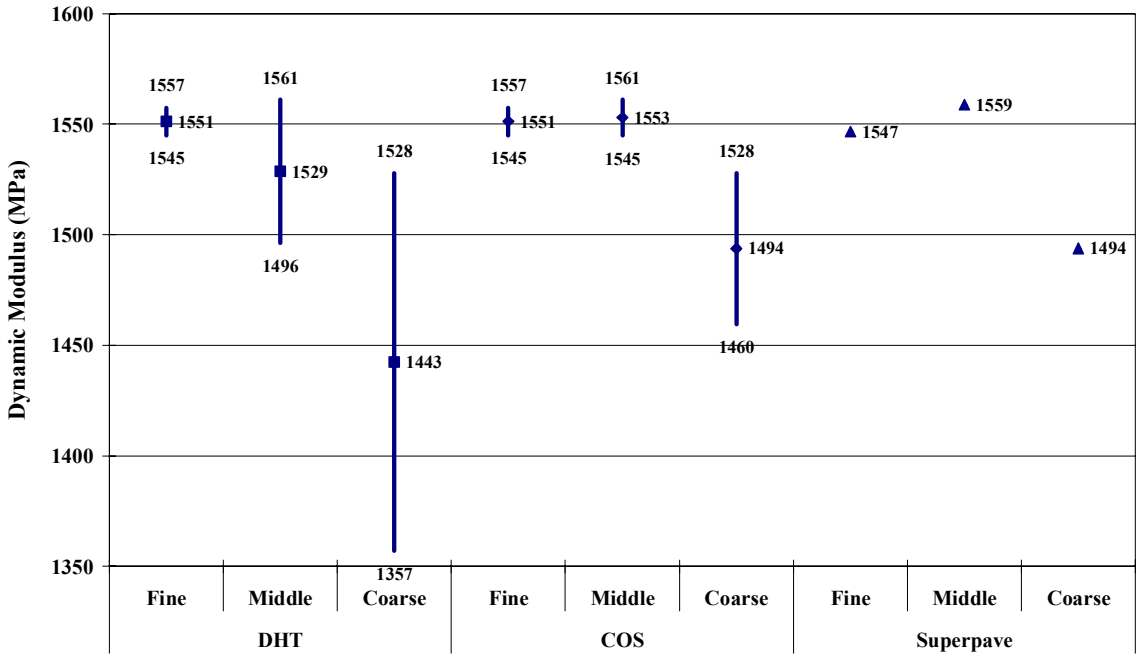

Figure G. 11 Dynamic Modulus Range Plotted versus Frequency at 25°C for Range of VTM Specifications Met – 600 kPa

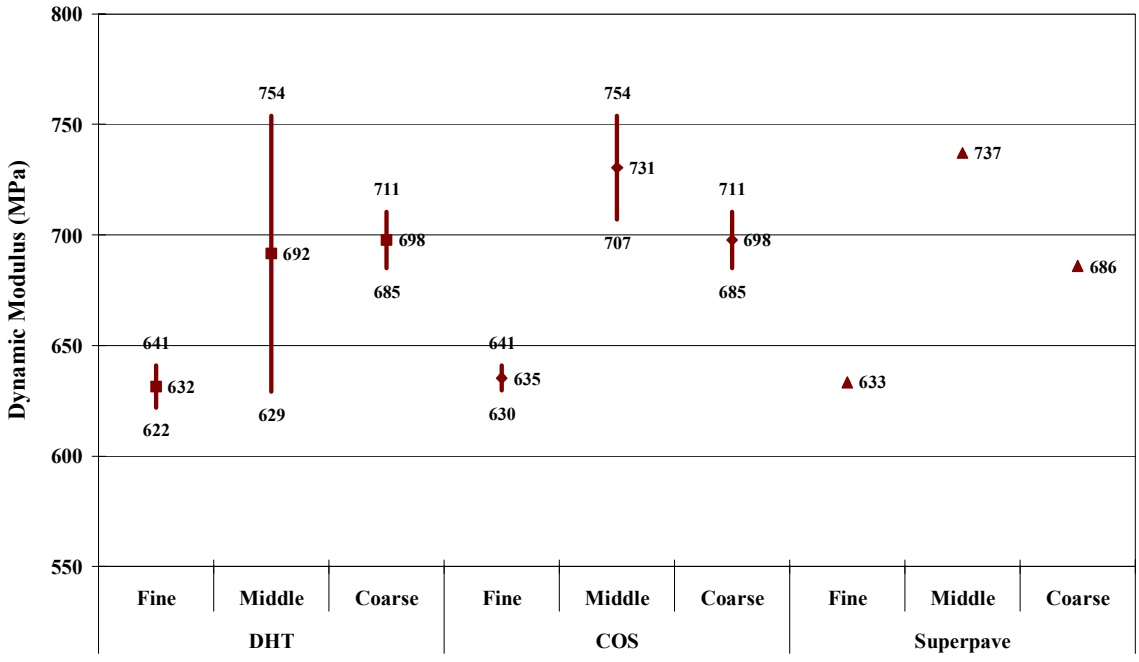

Figure G. 12 Dynamic Modulus Range Plotted versus Frequency at 60°C for Range of VTM Specifications Met – 600 kPa

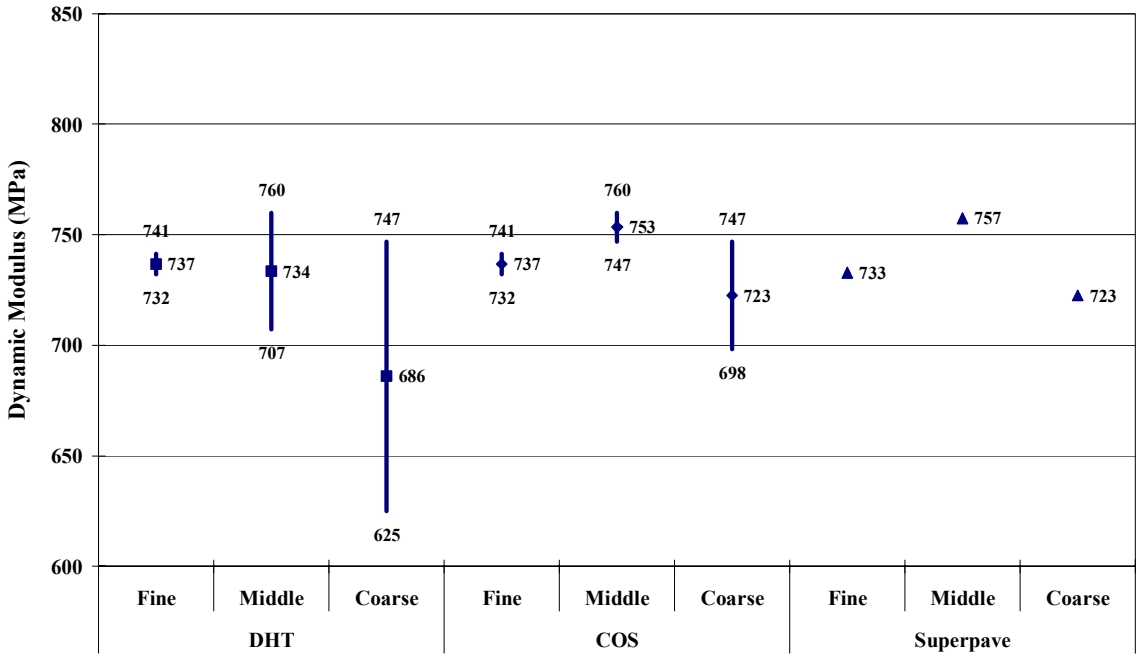

Figure G. 13 Dynamic Modulus Range Plotted versus Deviatoric Stress State at 25°C for Range of VTM Specifications Met at 0.125 Hz

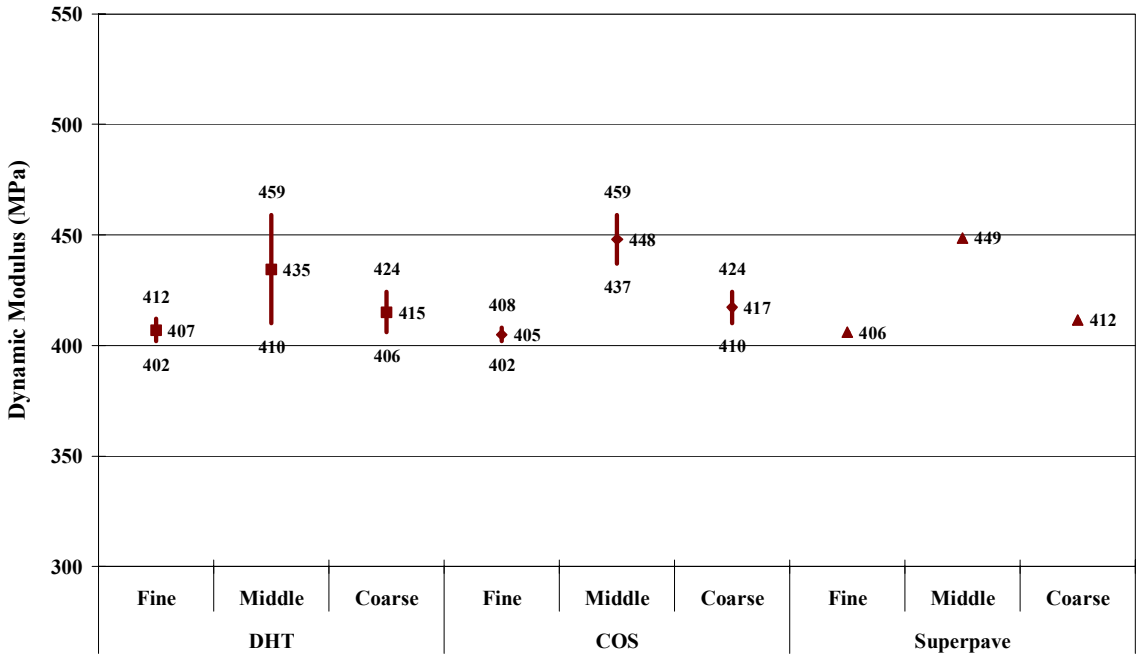

Figure G. 14 Dynamic Modulus Range Plotted versus Deviatoric Stress State at 60°C for Range of VTM Specifications Met at 0.125 Hz

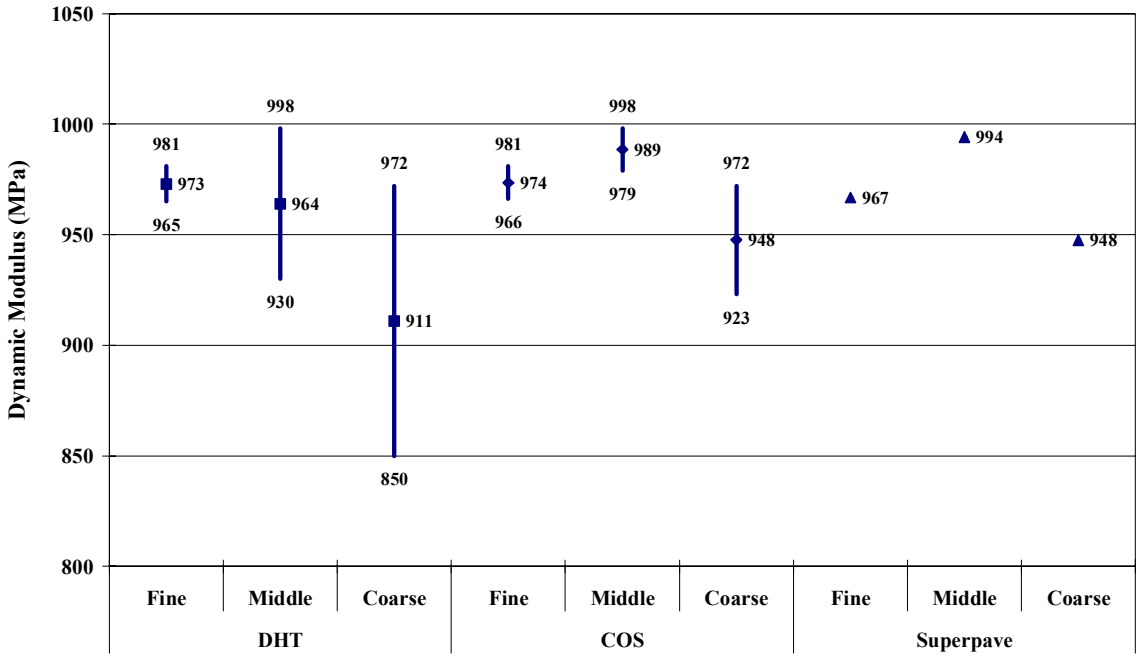

Figure G. 15 Dynamic Modulus Range Plotted versus Deviatoric Stress State at 25°C for Range of VTM Specifications Met at 0.5 Hz

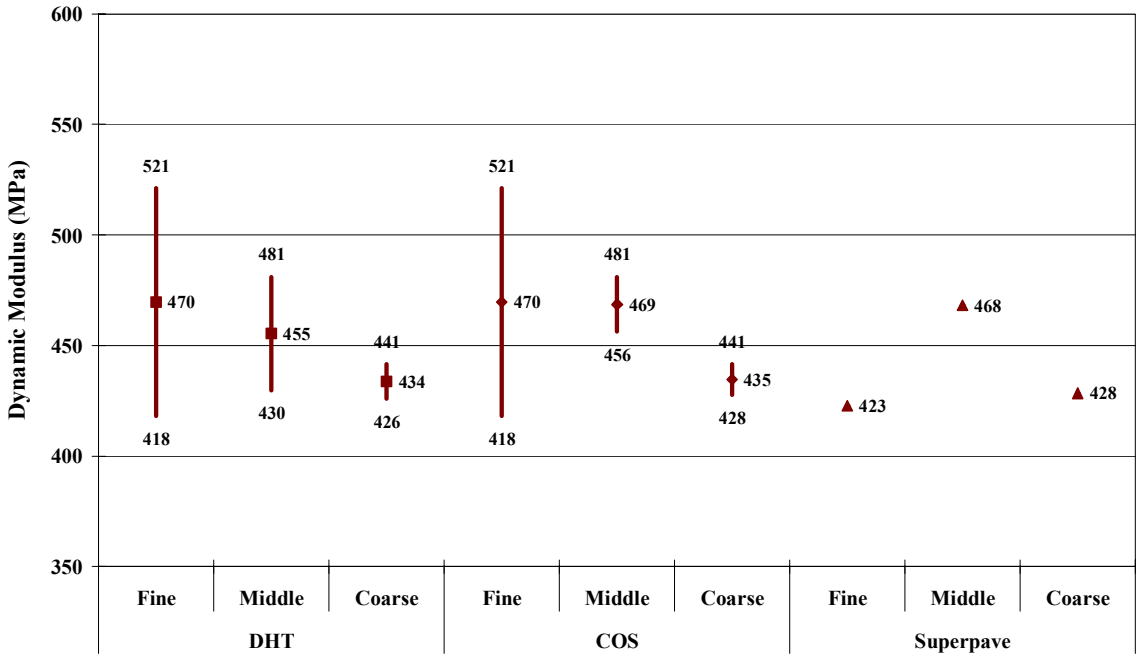

Figure G. 16 Dynamic Modulus Range Plotted versus Deviatoric Stress State at 60°C for Range of VTM Specifications Met at 0.5 Hz

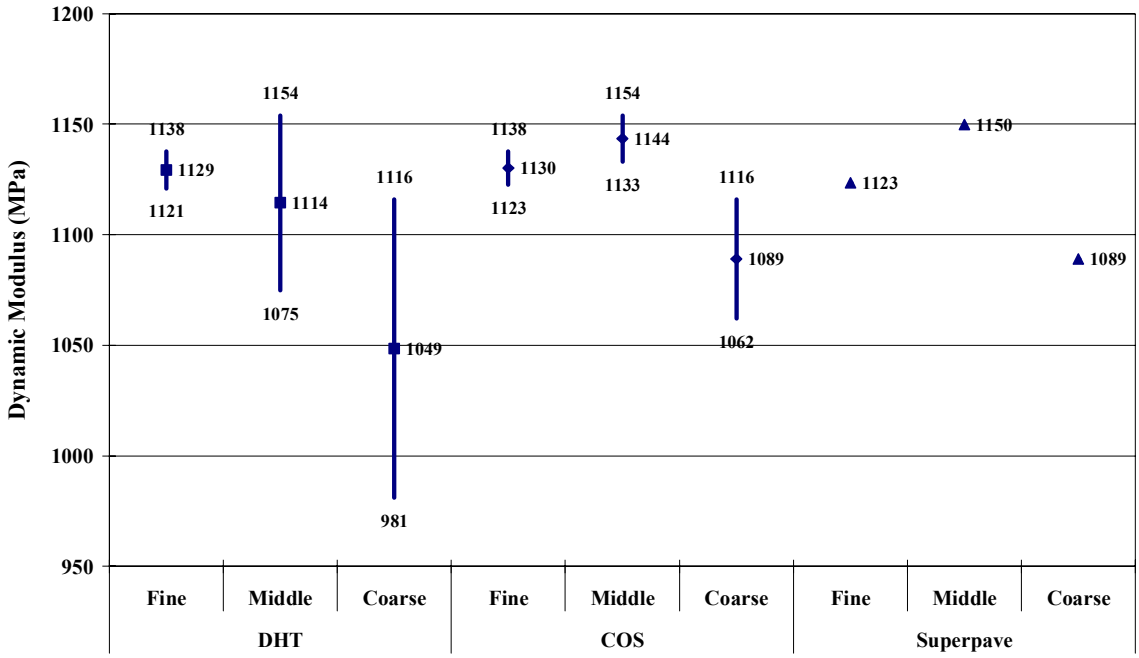

Figure G. 17 Dynamic Modulus Range Plotted versus Deviatoric Stress State at 25°C for Range of VTM Specifications Met at 1.0 Hz

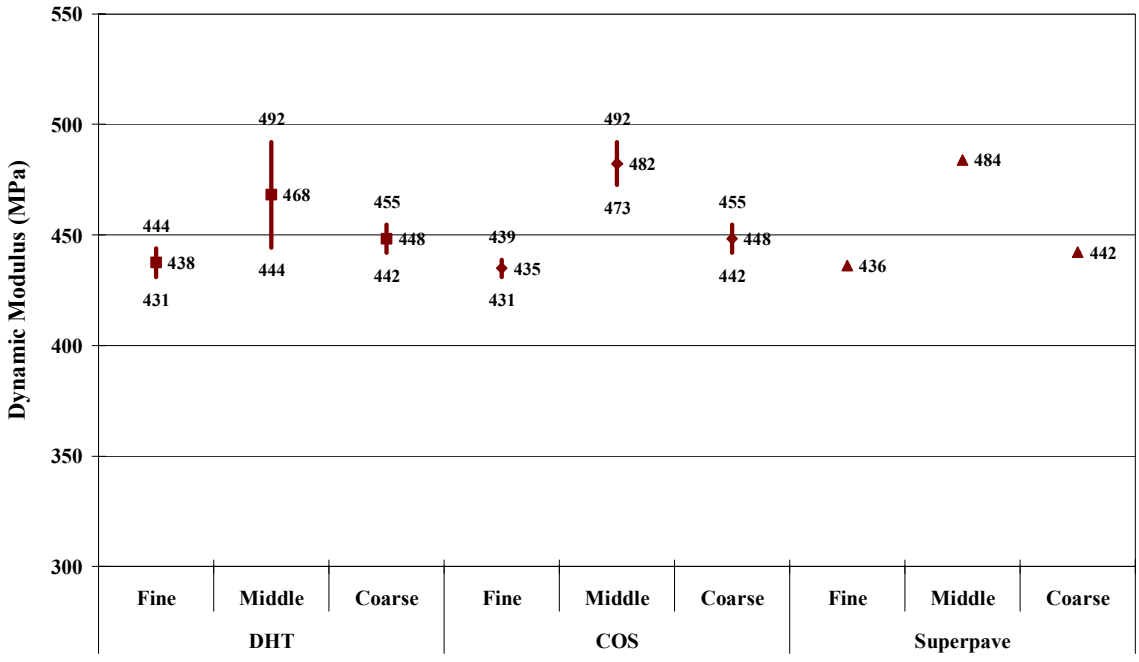

Figure G. 18 Dynamic Modulus Range Plotted versus Deviatoric Stress State at 60°C for Range of VTM Specifications Met at 1.0 Hz

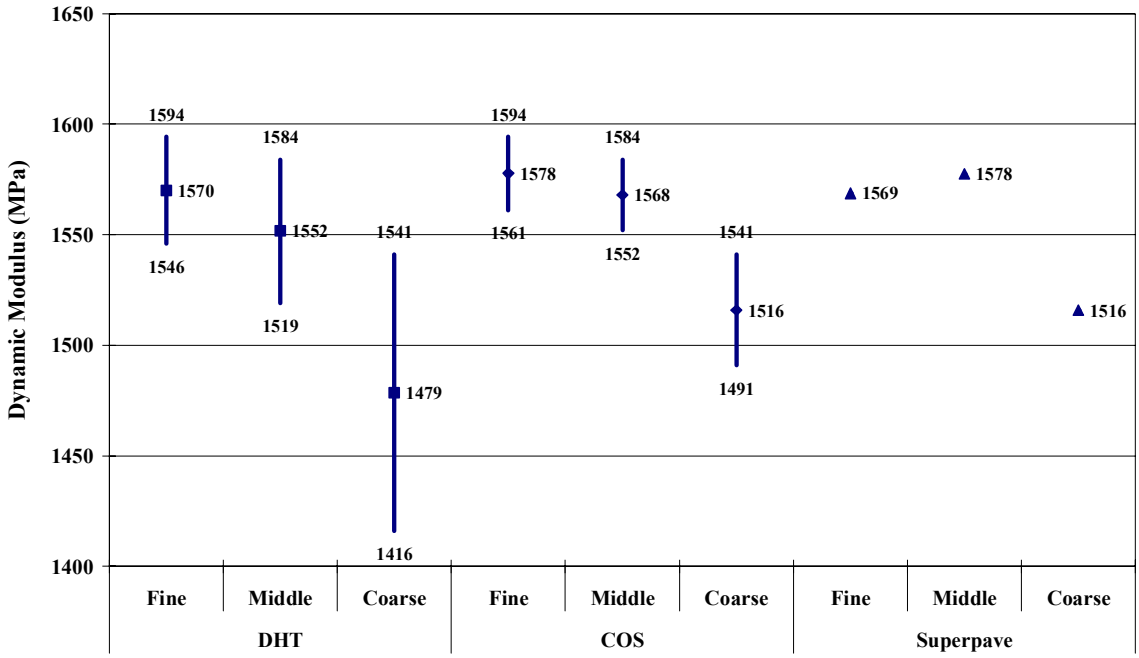

Figure G. 19 Dynamic Modulus Range Plotted versus Deviatoric Stress State at 25°C for Range of VTM Specifications Met at 5.0 Hz

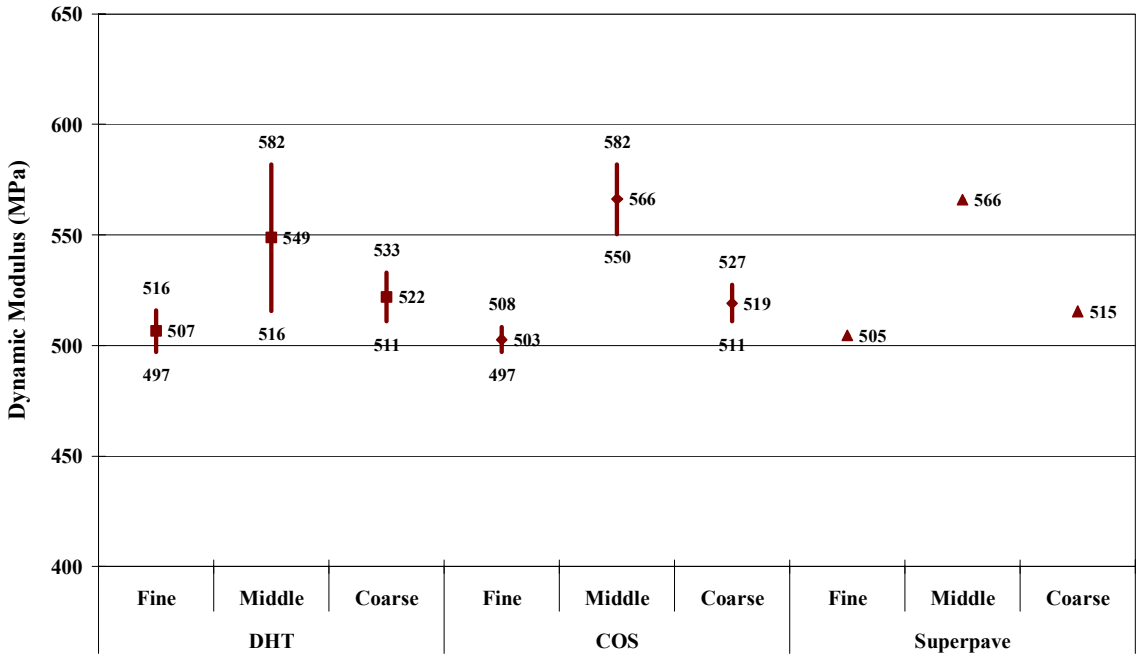

Figure G. 20 Dynamic Modulus Range Plotted versus Deviatoric Stress State at 60°C for Range of VTM Specifications Met at 5.0 Hz

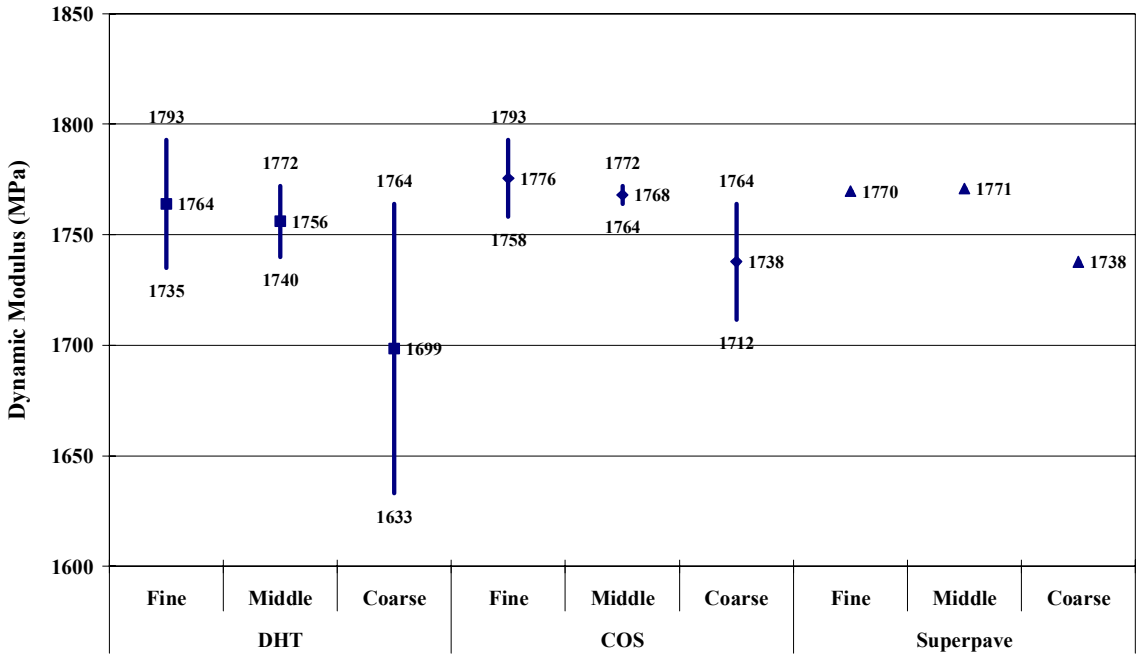

Figure G. 21 Dynamic Modulus Range Plotted versus Deviatoric Stress State at 25°C for Range of VTM Specifications Met at 10.0 Hz

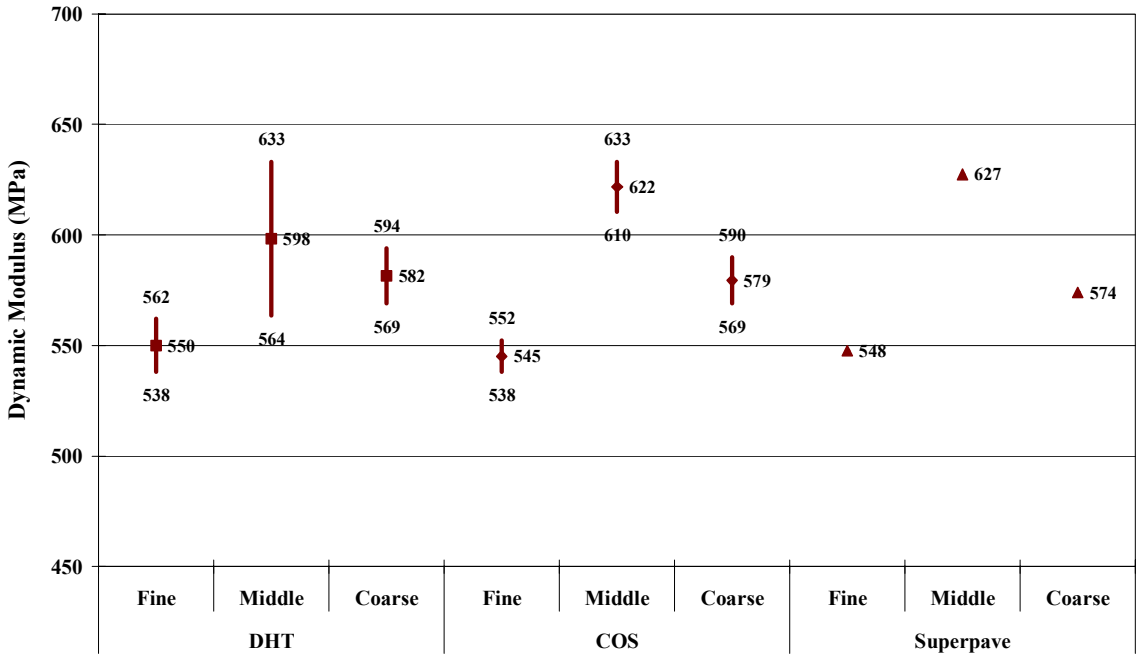

Figure G. 22 Dynamic Modulus Range Plotted versus Deviatoric Stress State at 60°C for Range of VTM Specifications Met at 10.0 Hz

APPENDIX H: POISSONS' RATIO RANGE FOR ACCEPTABLE VTM SPECIFICATIONS

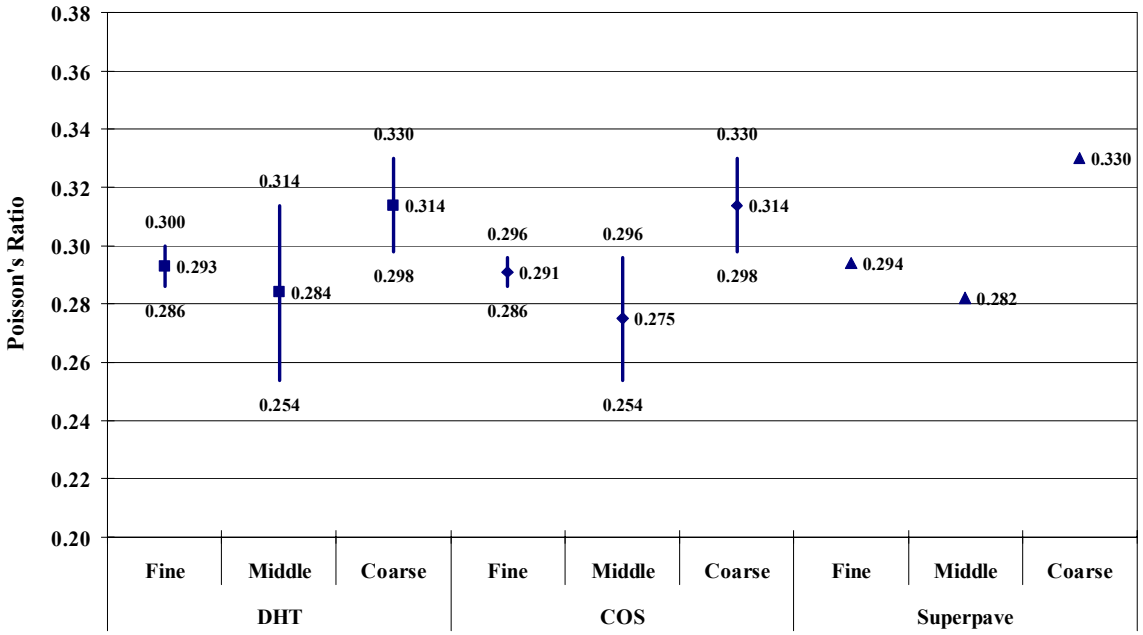

Figure H. 1 Poisson's Ratio Range Plotted versus Deviatoric Stress State and Frequency at 25°C for Ranges of Acceptable VTM Specifications

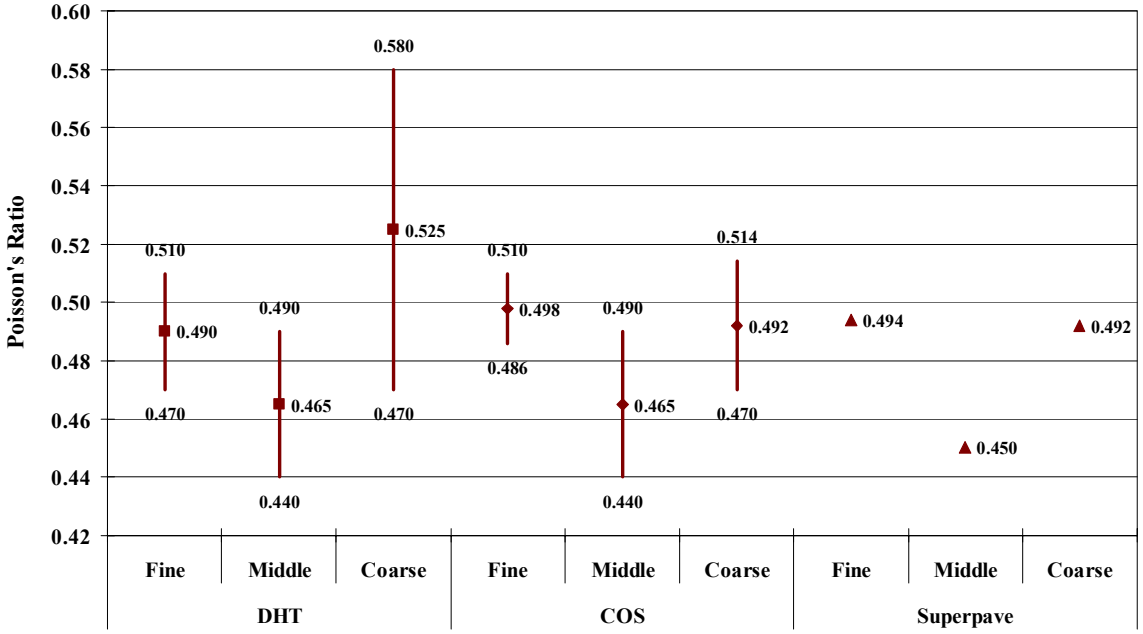

Figure H. 2 Poisson's Ratio Range Plotted versus Deviatoric Stress State and Frequency at 60°C for Ranges of Acceptable VTM Specifications

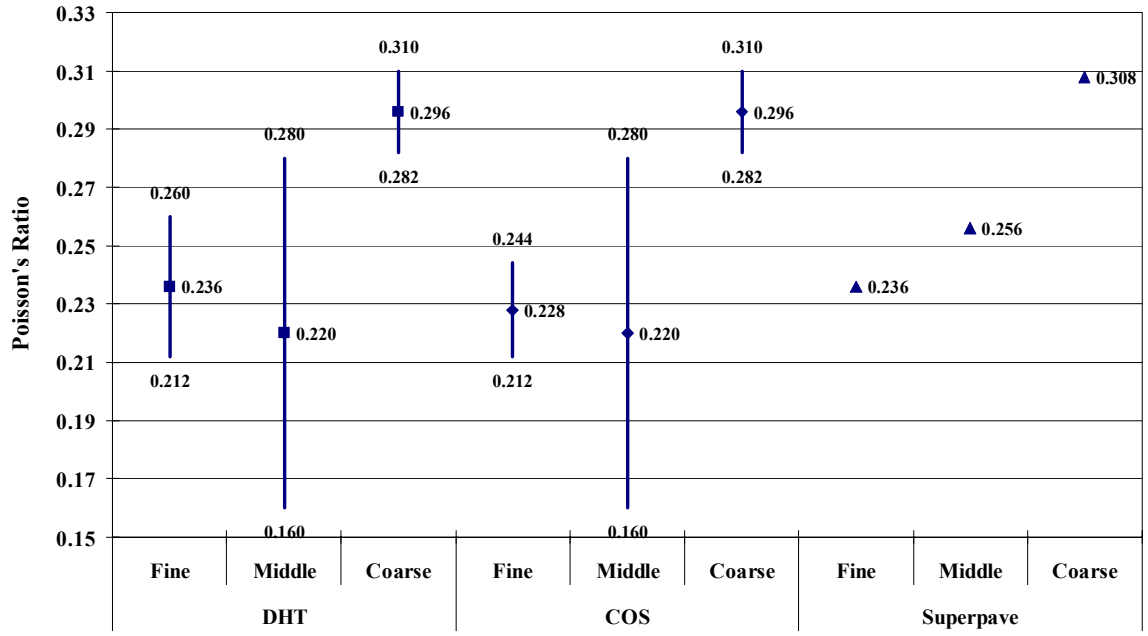

Figure H. 3 Poisson's Ratio Range Plotted versus Frequency at 25°C for Range of VTM Specifications Met at 150 kPa

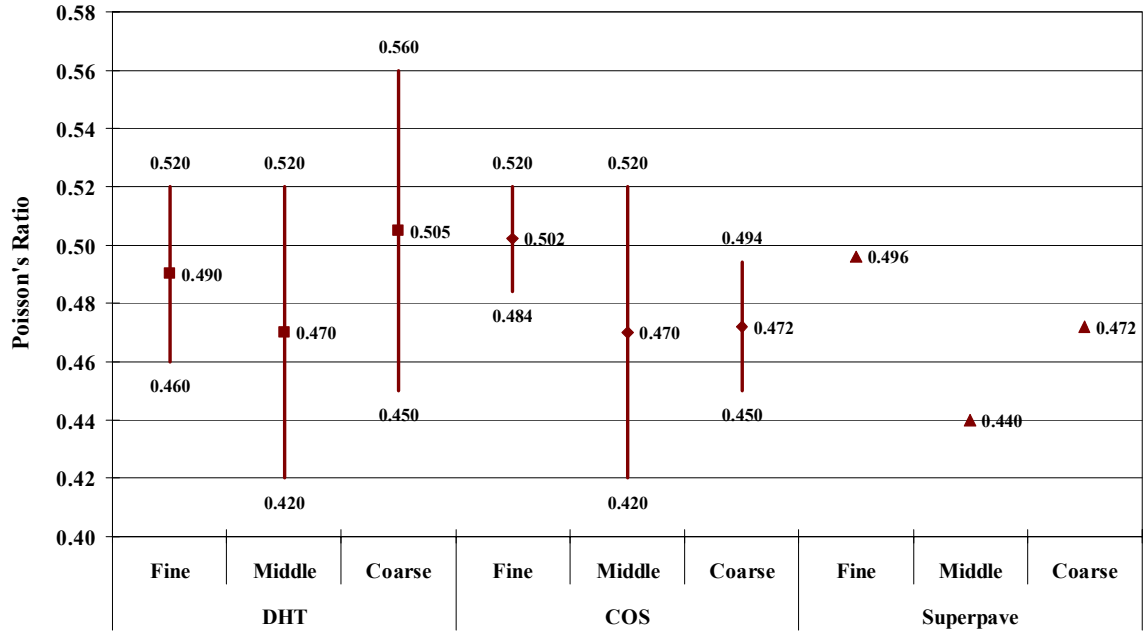

Figure H. 4 Poisson's Ratio Range Plotted versus Frequency at 60°C for Range of VTM Specifications Met at 150 kPa

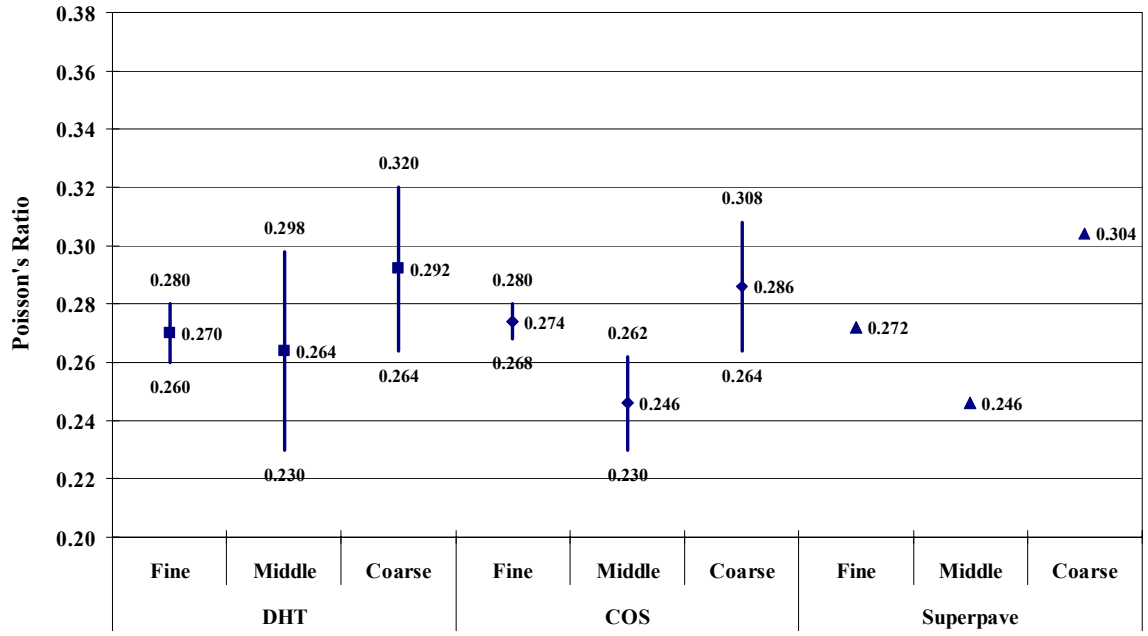

Figure H. 5 Poisson's Ratio Range Plotted versus Frequency at 25°C for Range of VTM Specifications Met at 225 kPa

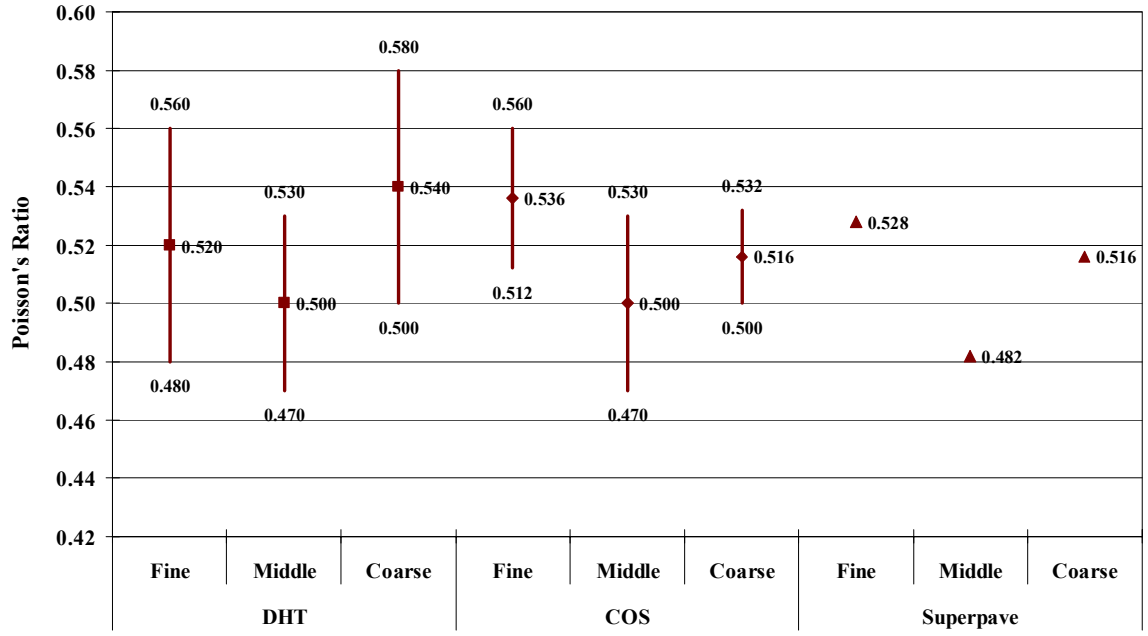

Figure H. 6 Poisson's Ratio Range Plotted versus Frequency at 60°C for Range of VTM Specifications Met at 225 kPa

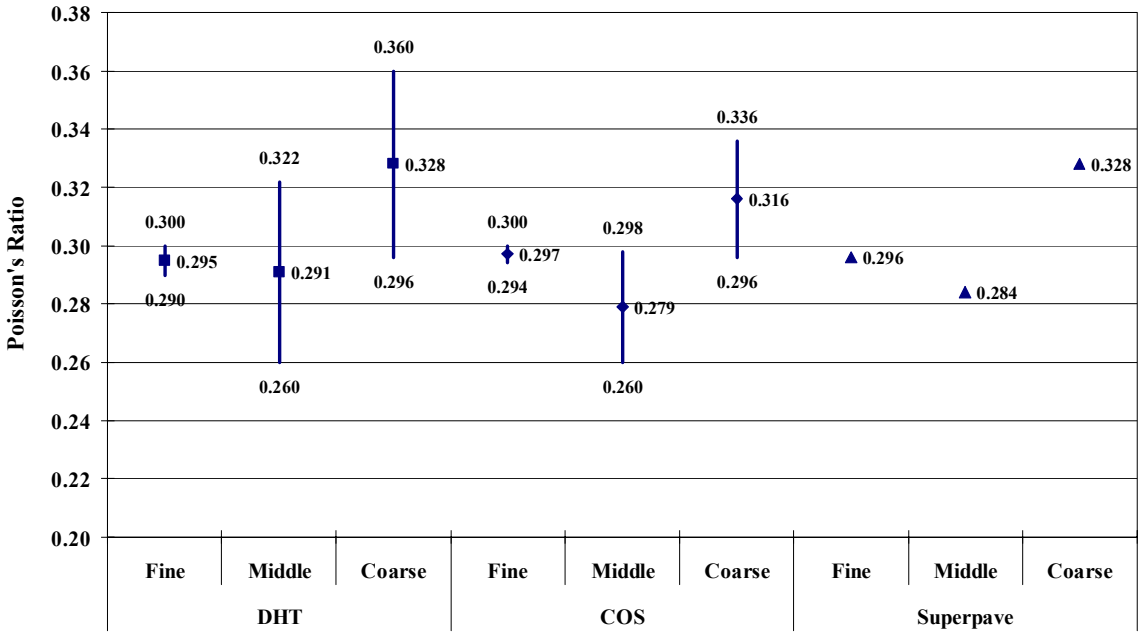

Figure H. 7 Poisson's Ratio Range Plotted versus Frequency at 25°C for Range of VTM Specifications Met at 300 kPa

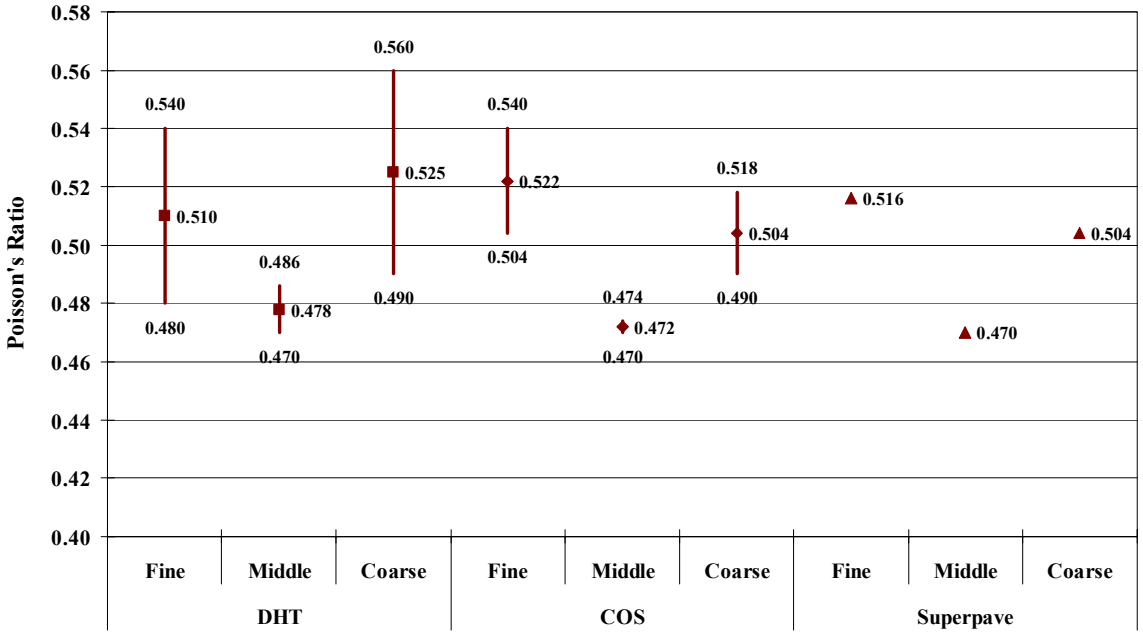

Figure H. 8 Poisson's Ratio Range Plotted versus Frequency at 60°C for Range of VTM Specifications Met at 300 kPa

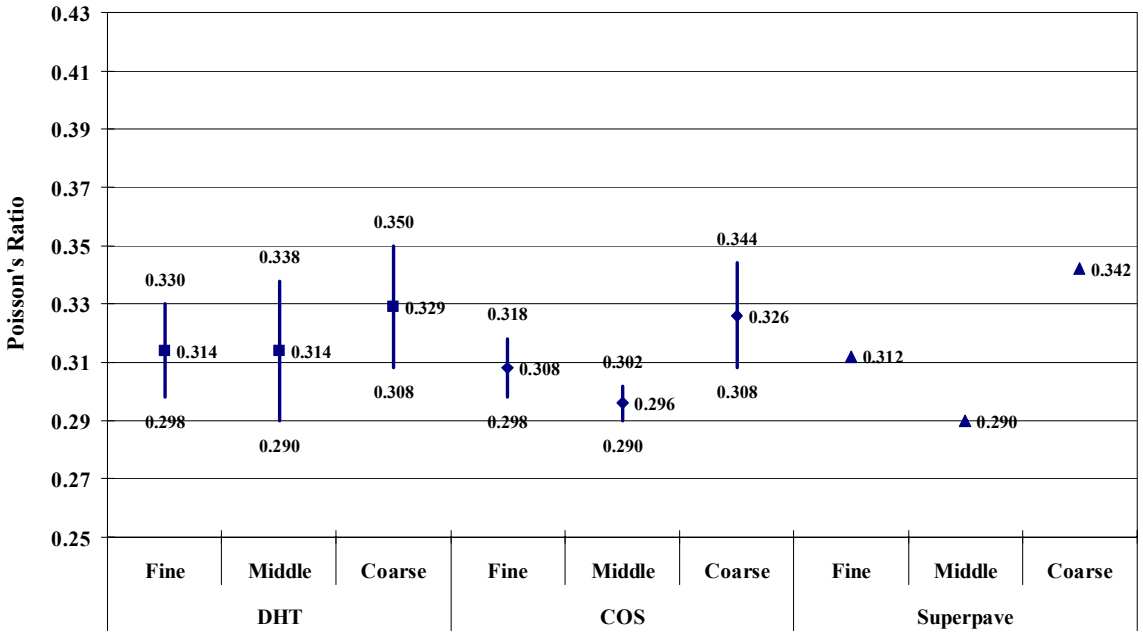

Figure H. 9 Poisson's Ratio Range Plotted versus Frequency at 25°C for Range of VTM Specifications Met at 450 kPa

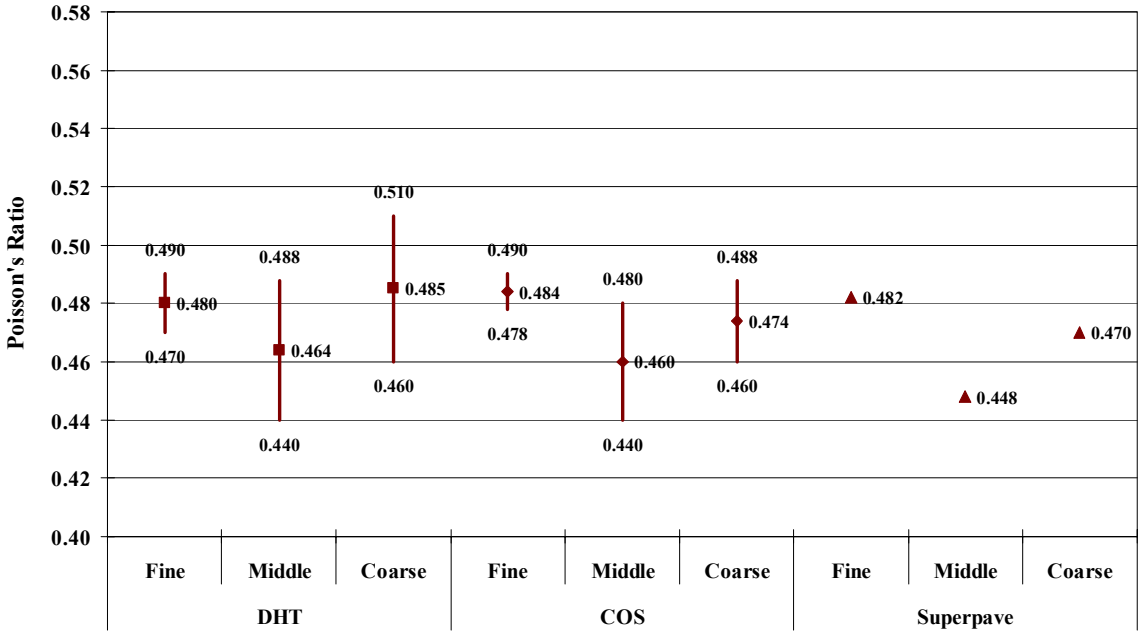

Figure H. 10 Poisson's Ratio Range Plotted versus Frequency at 60°C for Range of VTM Specifications Met at 450 kPa

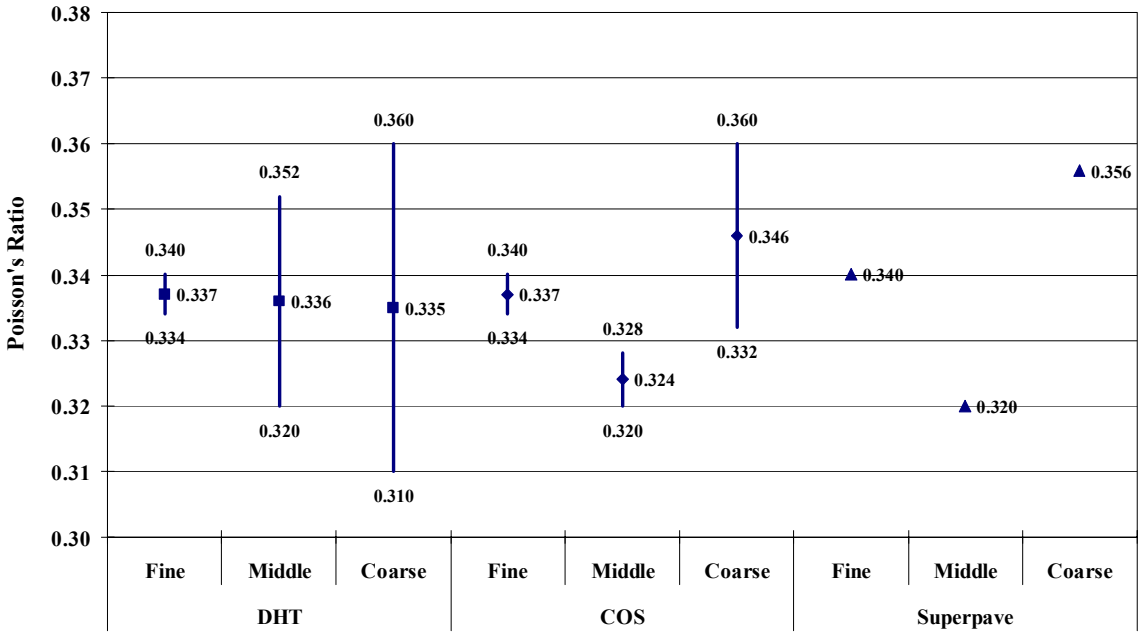

Figure H. 11 Poisson's Ratio Range Plotted versus Frequency at 25°C for Range of VTM Specifications Met at 600 kPa

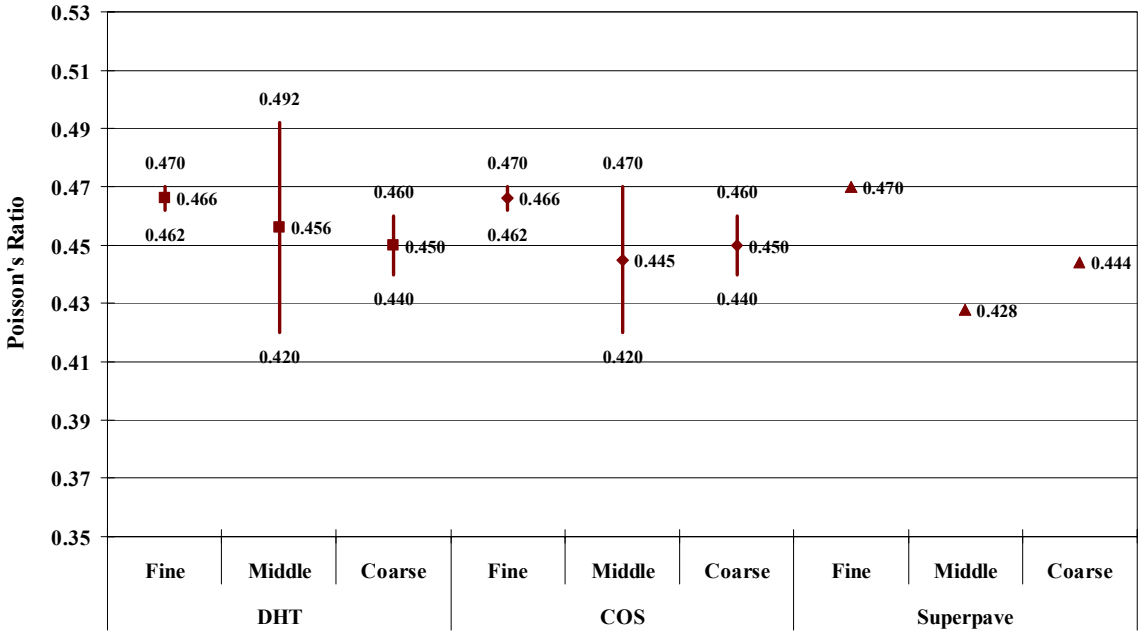

Figure H. 12 Poisson's Ratio Range Plotted versus Frequency at 60°C for Range of VTM Specifications Met at 600 kPa

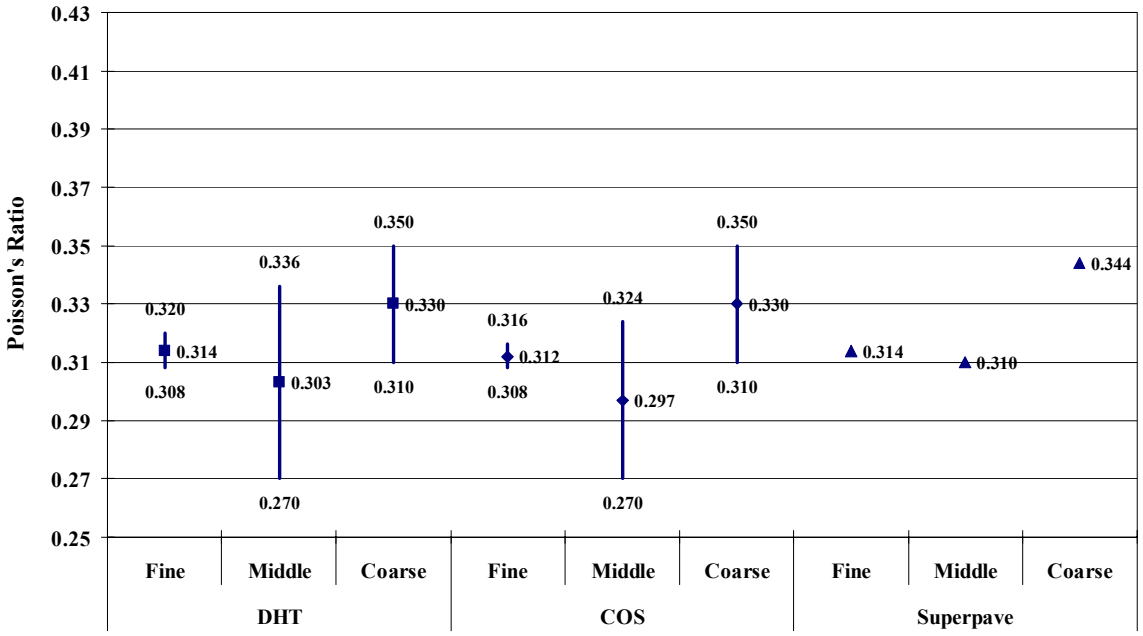

Figure H. 13 Poisson's Ratio Range Plotted versus Deviatoric Stress State at 25°C for Range of VTM Specifications Met at 0.125 Hz

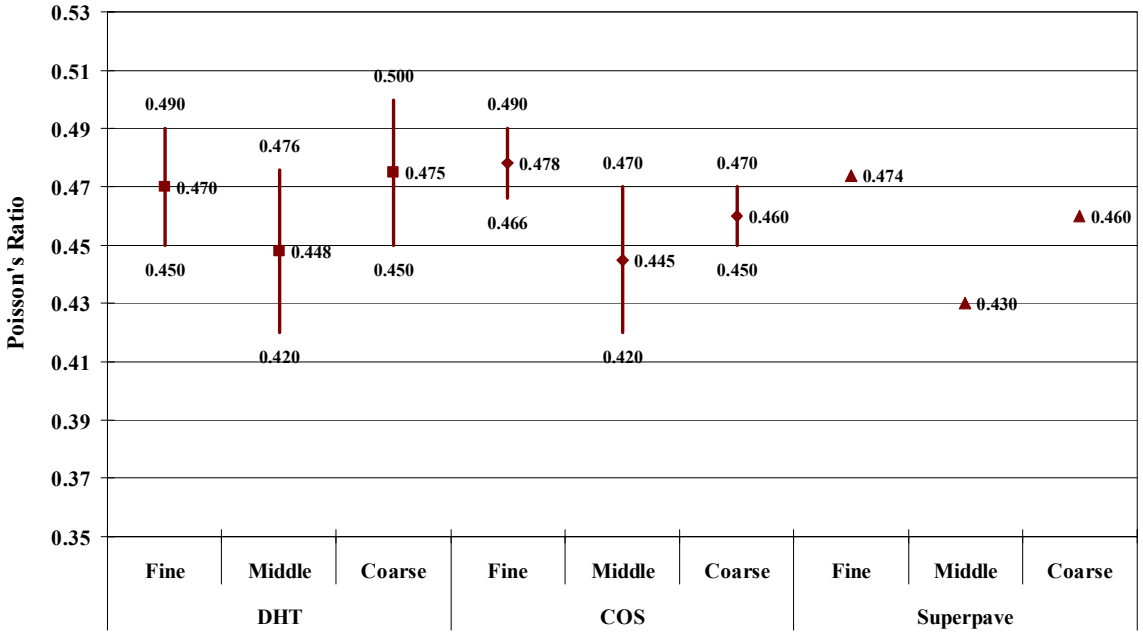

Figure H. 14 Poisson's Ratio Range Plotted versus Deviatoric Stress State at 60°C for Range of VTM Specifications Met at 0.125 Hz

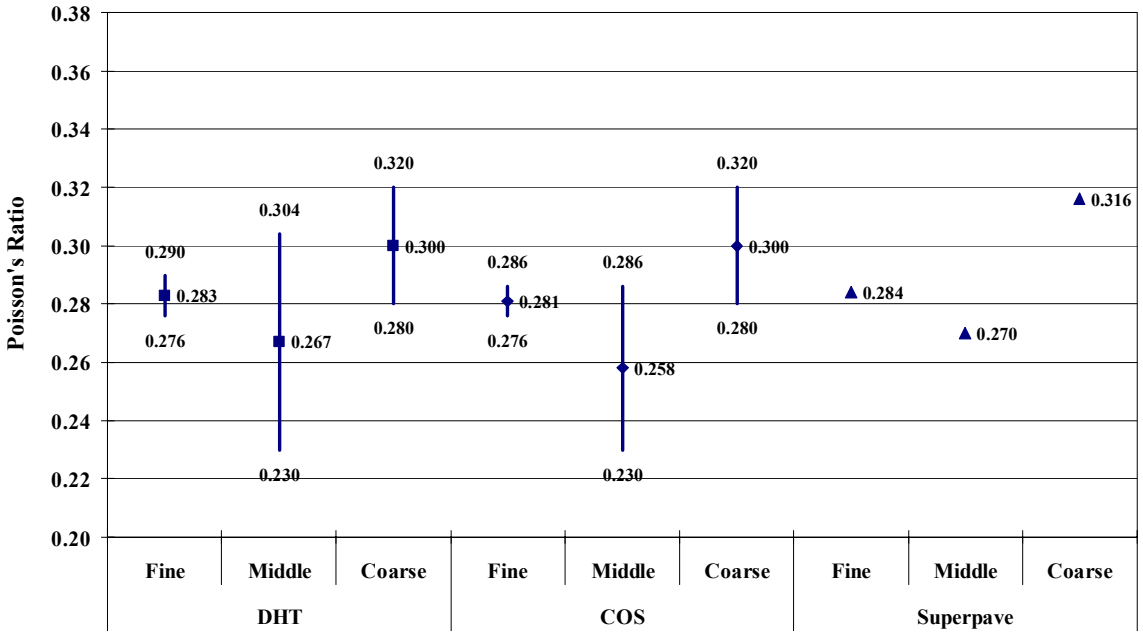

Figure H. 15 Poisson's Ratio Range Plotted versus Deviatoric Stress State at 25°C for Range of VTM Specifications Met at 0.5 Hz

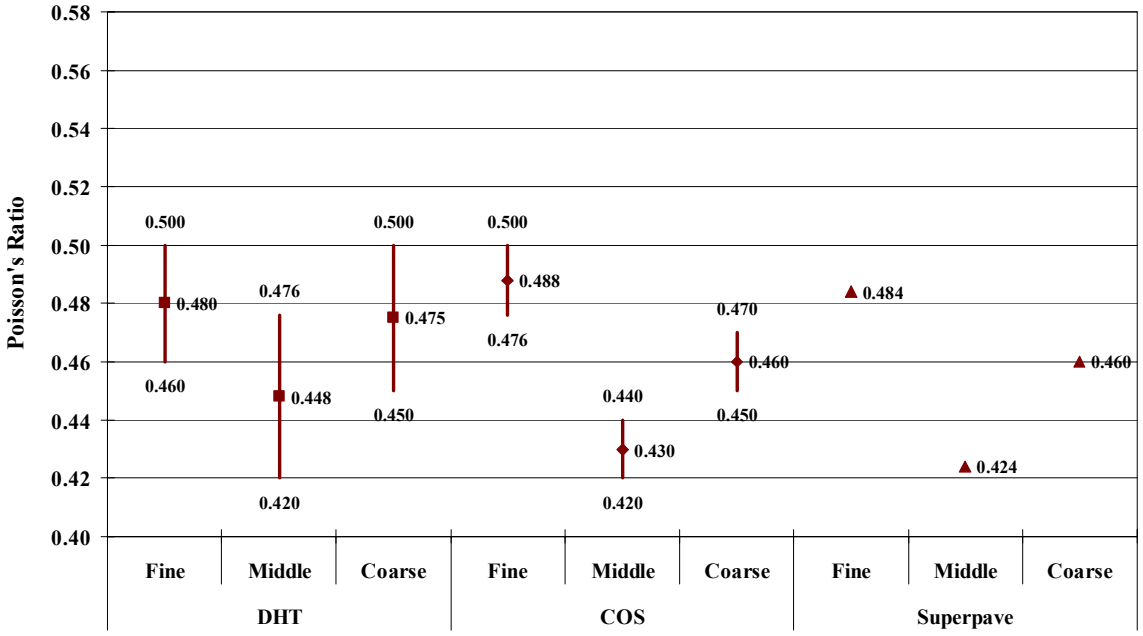

Figure H. 16 Poisson's Ratio Range Plotted versus Deviatoric Stress State at 60°C for Range of VTM Specifications Met at 0.5 Hz

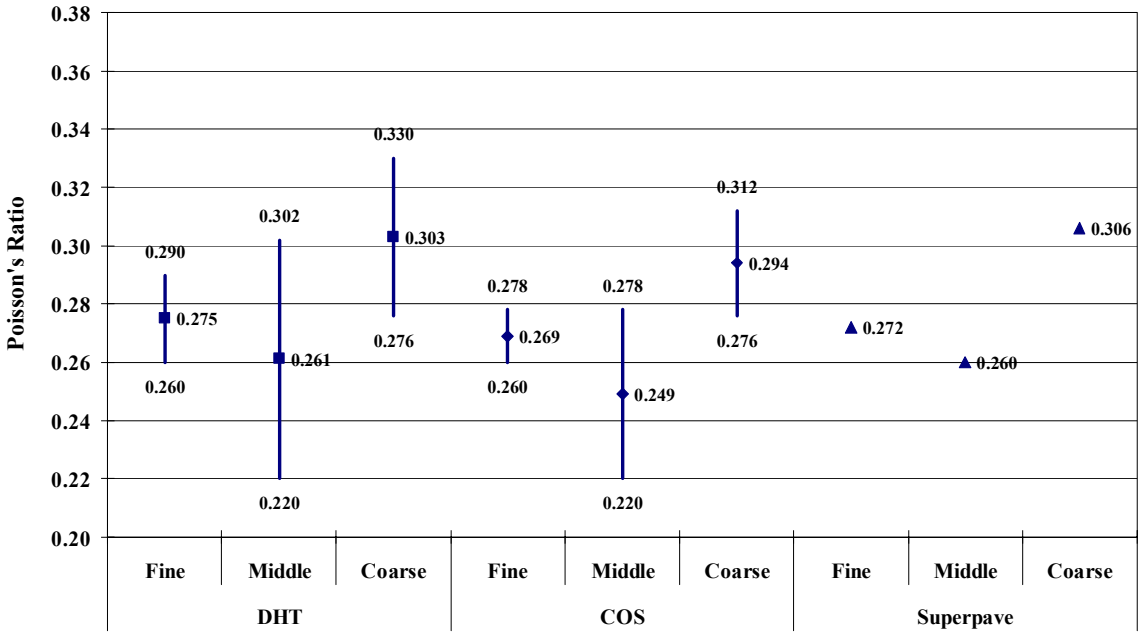

Figure H. 17 Poisson's Ratio Range Plotted versus Deviatoric Stress State at 25°C for Range of VTM Specifications Met at 1.0 Hz

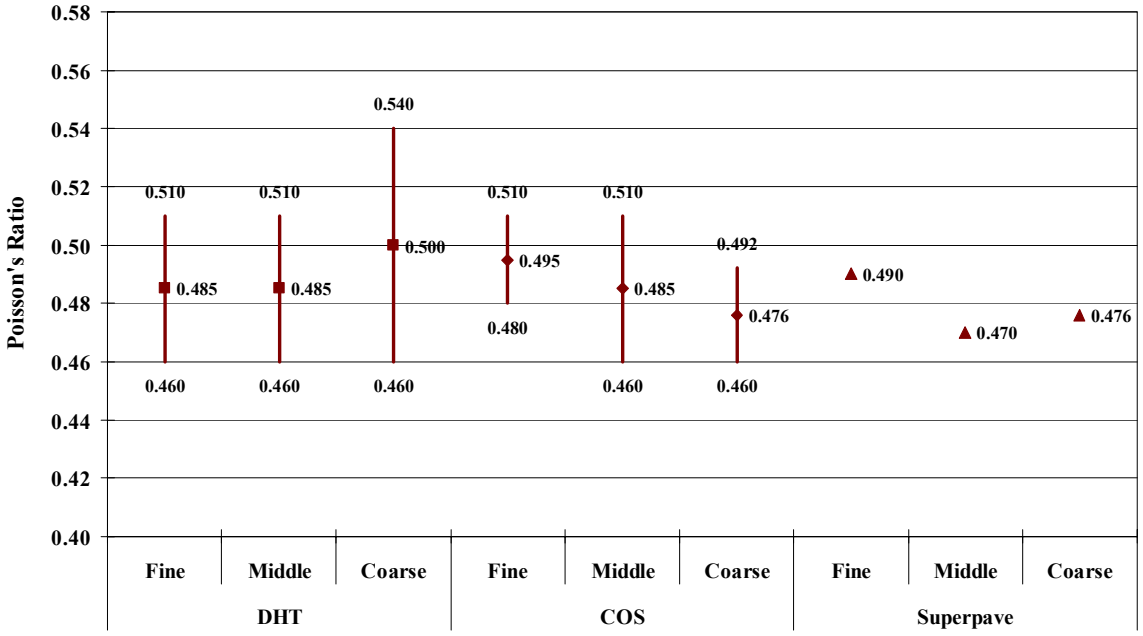

Figure H. 18 Poisson's Ratio Range Plotted versus Deviatoric Stress State at 60°C for Range of VTM Specifications Met at 1.0 Hz

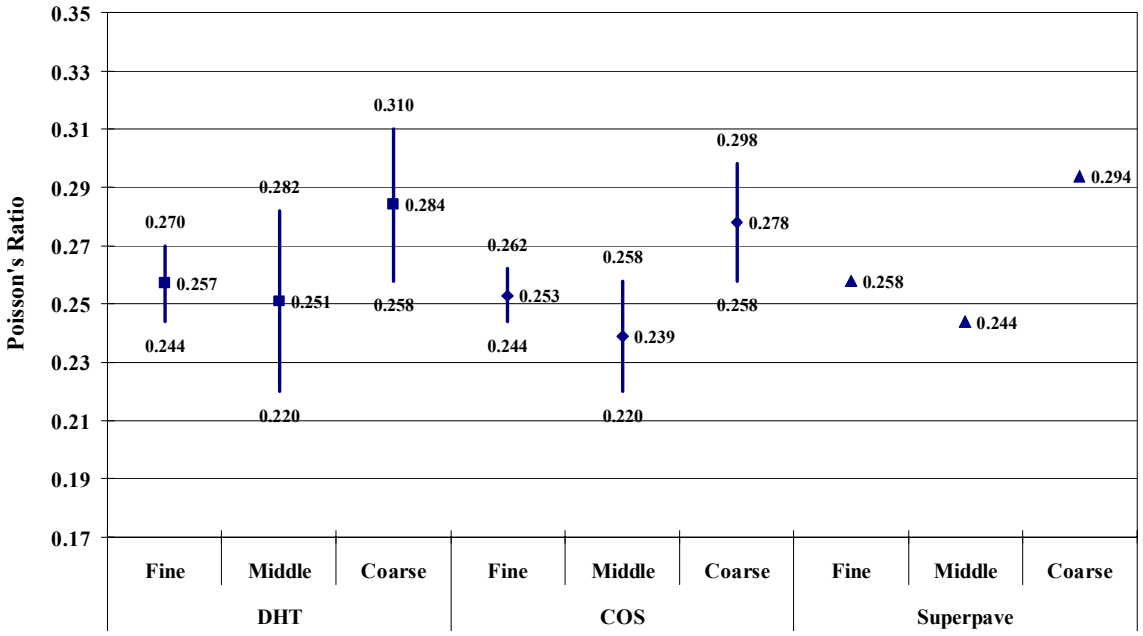

Figure H. 19 Poisson's Ratio Range Plotted versus Deviatoric Stress State at 25°C for Range of VTM Specifications Met at 5.0 Hz

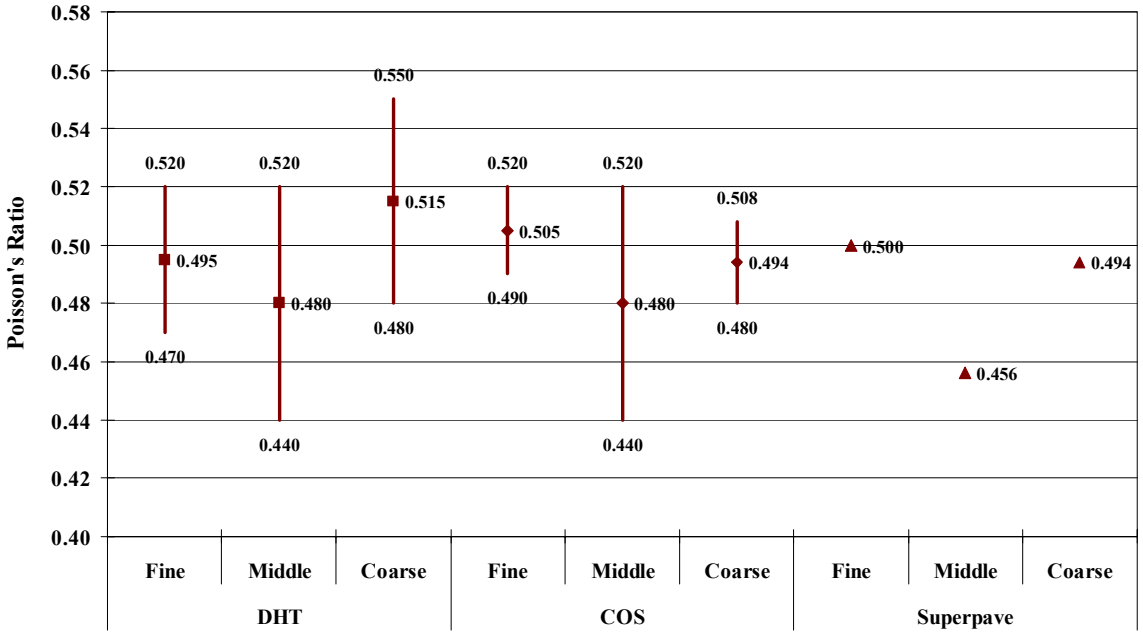

Figure H. 20 Poisson's Ratio Range Plotted versus Deviatoric Stress State at 60°C for Range of VTM Specifications Met at 5.0 Hz

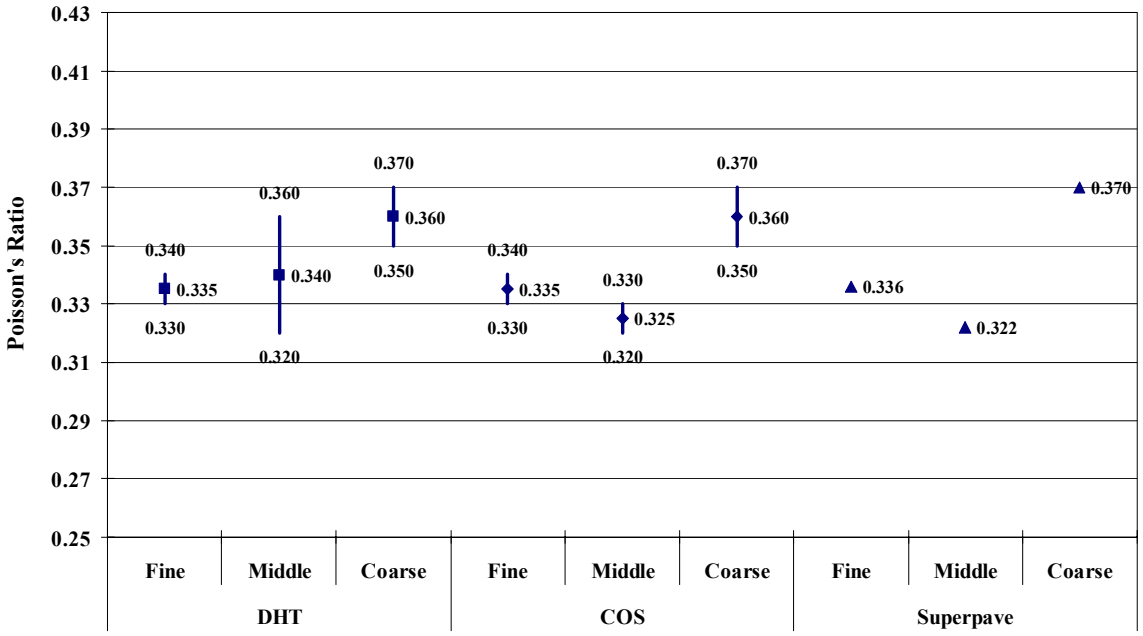

Figure H. 21 Poisson's Ratio Range Plotted versus Deviatoric Stress State at 25°C for Range of VTM Specifications Met at 10.0 Hz

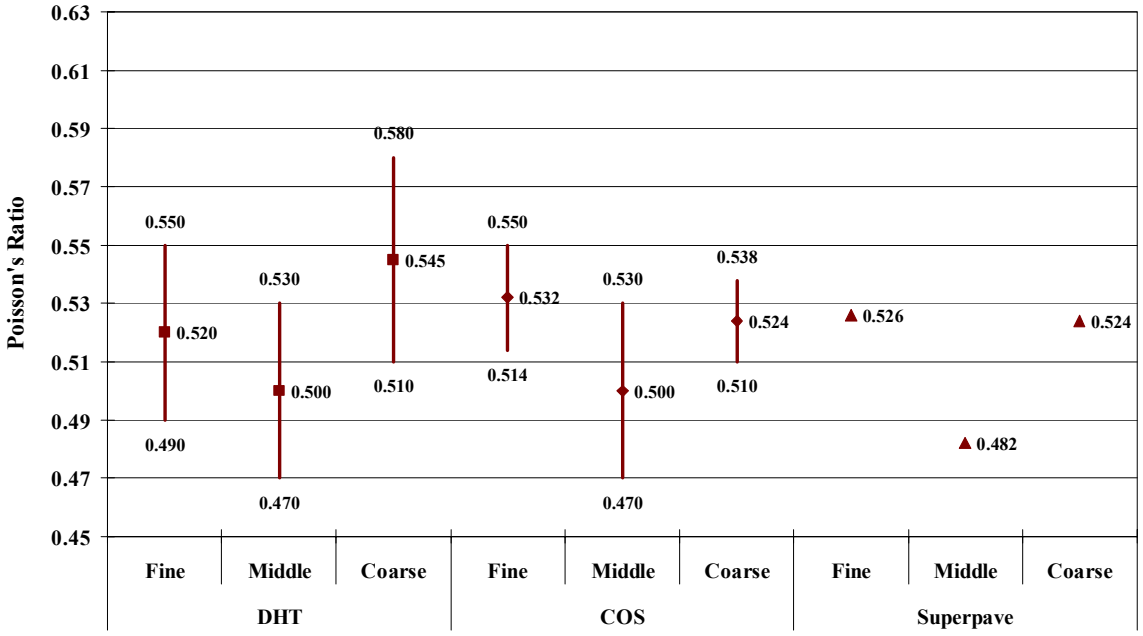

Figure H. 22 Poisson's Ratio Range Plotted versus Deviatoric Stress State at 60°C for Range of VTM Specifications Met at 10.0 Hz

APPENDIX I: PHASE ANGLE RANGE FOR ACCEPTABLE VTM SPECIFICATIONS

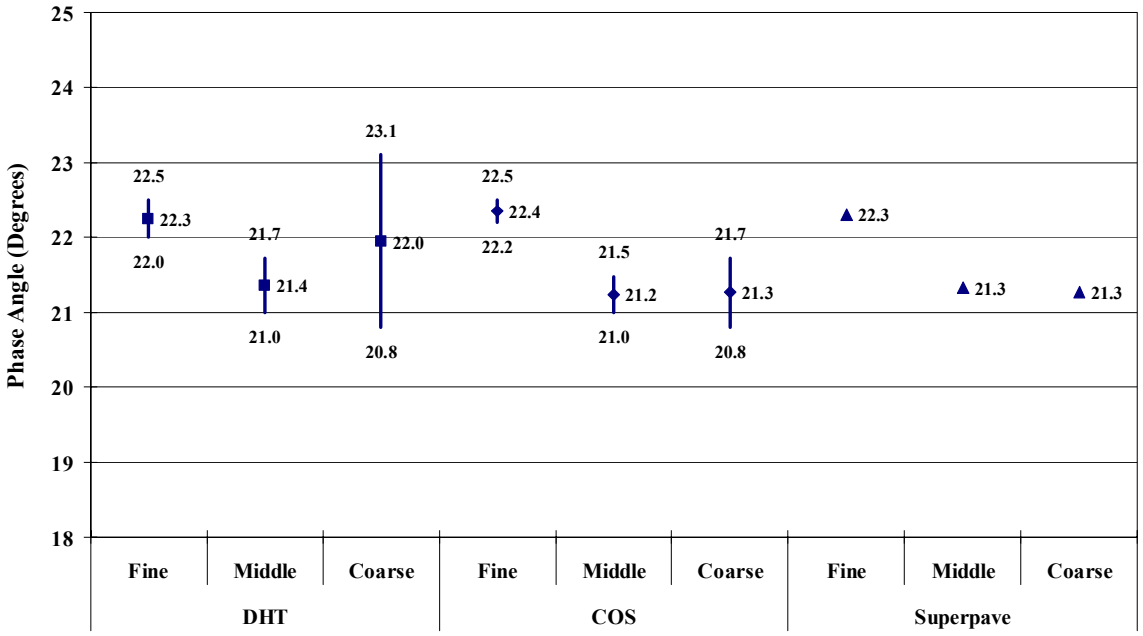

Figure I. 1 Phase Angle Range Plotted versus Deviatoric Stress State and Frequency at 25°C for Ranges of Acceptable VTM Specifications

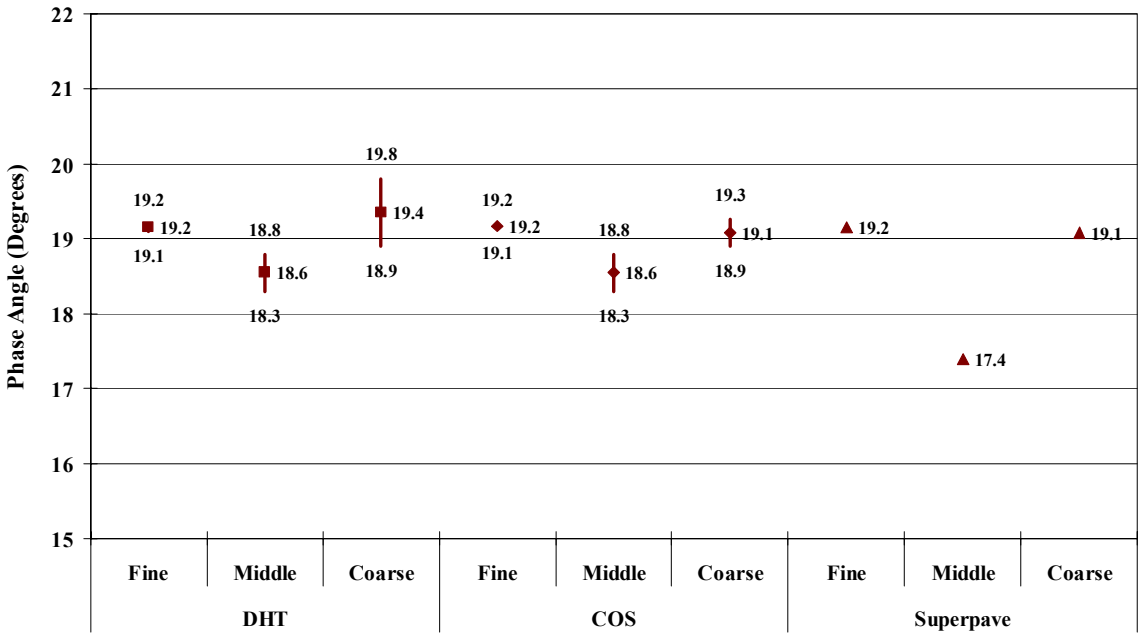

Figure I. 2 Phase Angle Range Plotted versus Deviatoric Stress State and Frequency at 60°C for Ranges of Acceptable VTM Specifications

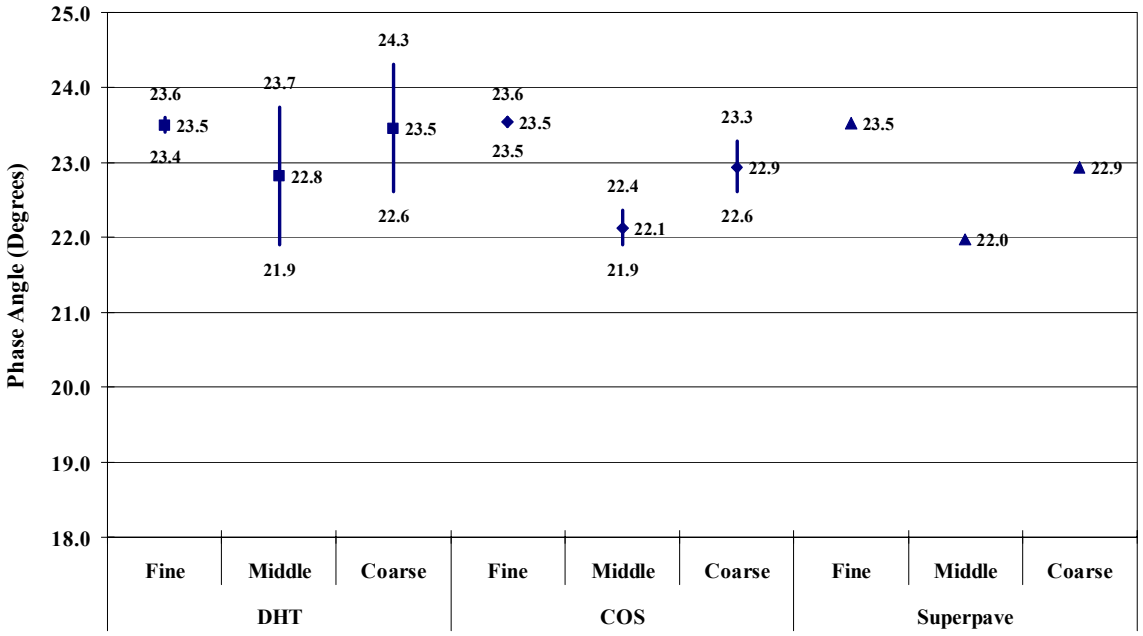

Figure I. 3 Phase Angle Range Plotted versus Frequency at 25°C for Range of VTM Specifications Met at 150 kPa

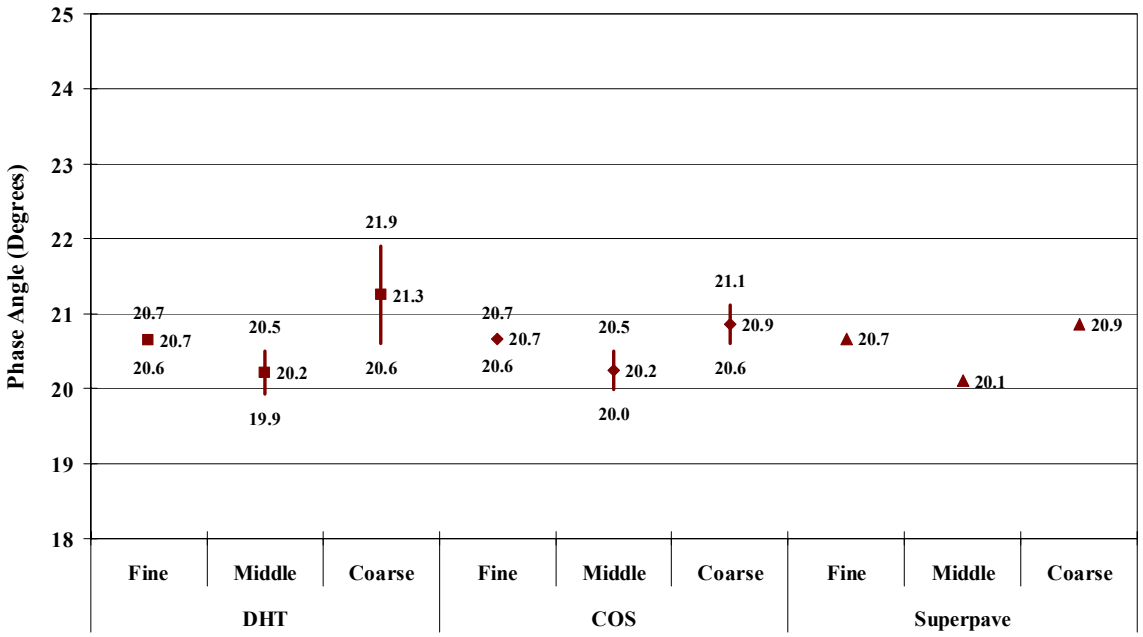

Figure I. 4 Phase Angle Range Plotted versus Frequency at 60°C for Range of VTM Specifications Met at 150 kPa

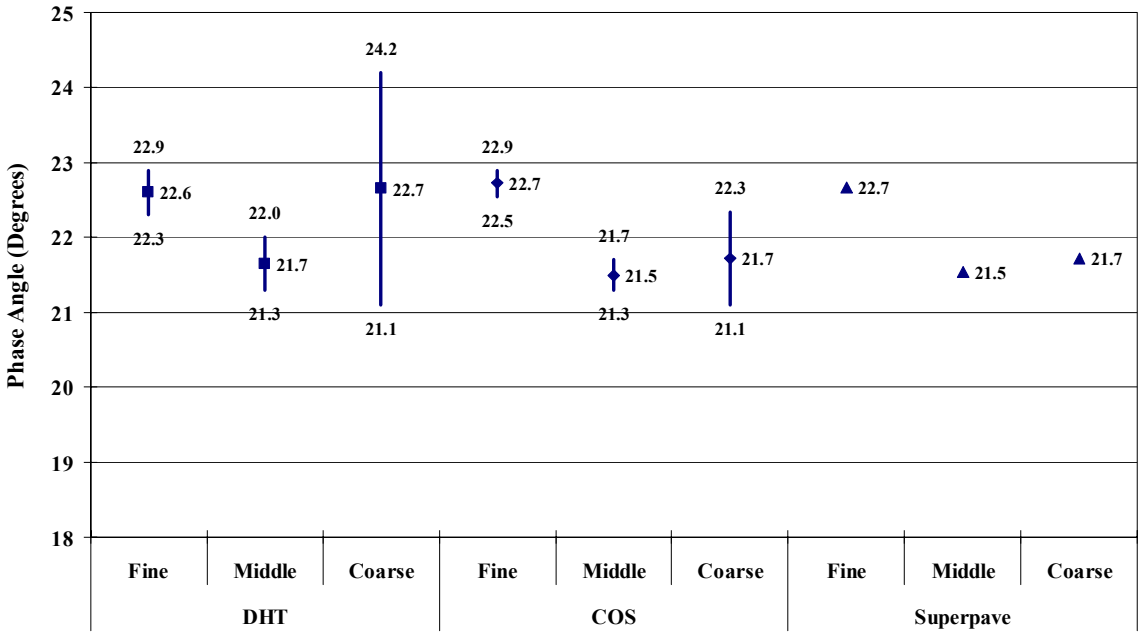

Figure I. 5 Phase Angle Range Plotted versus Frequency at 25°C for Range of VTM Specifications Met at 225 kPa

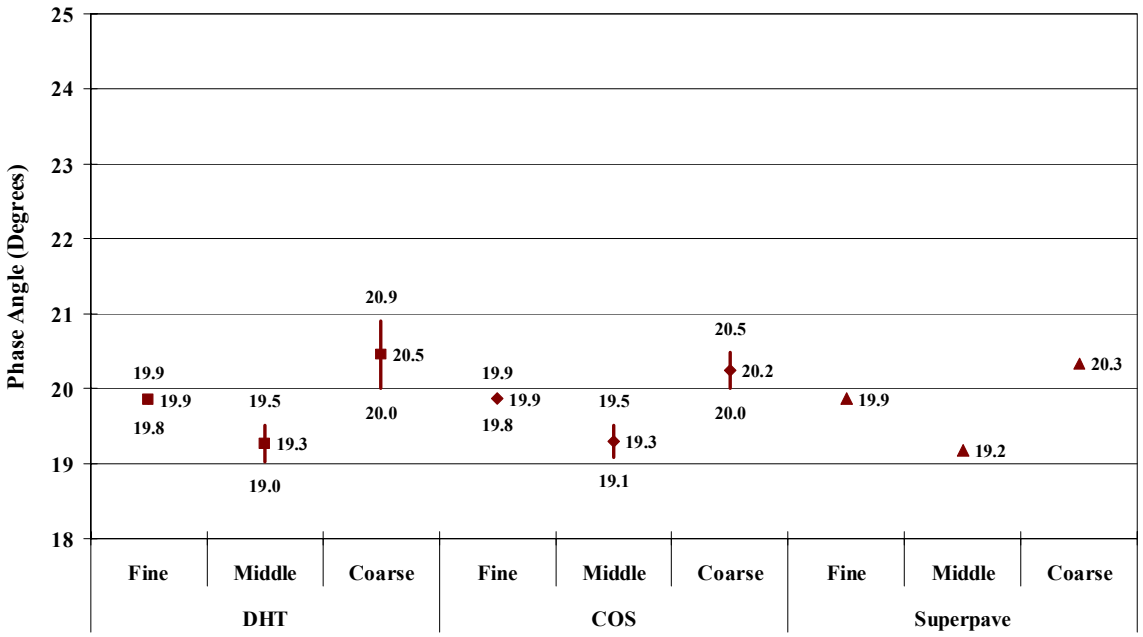

Figure I. 6 Phase Angle Range Plotted versus Frequency at 60°C for Range of VTM Specifications Met at 225 kPa

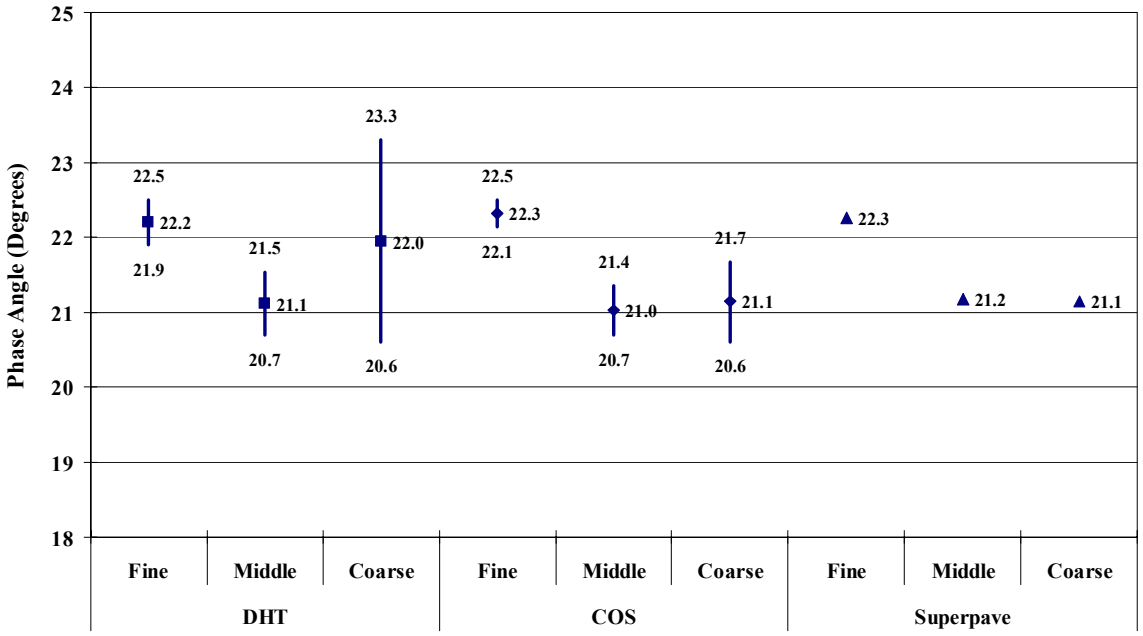

Figure I. 7 Phase Angle Range Plotted versus Frequency at 25°C for Range of VTM Specifications Met at 300 kPa

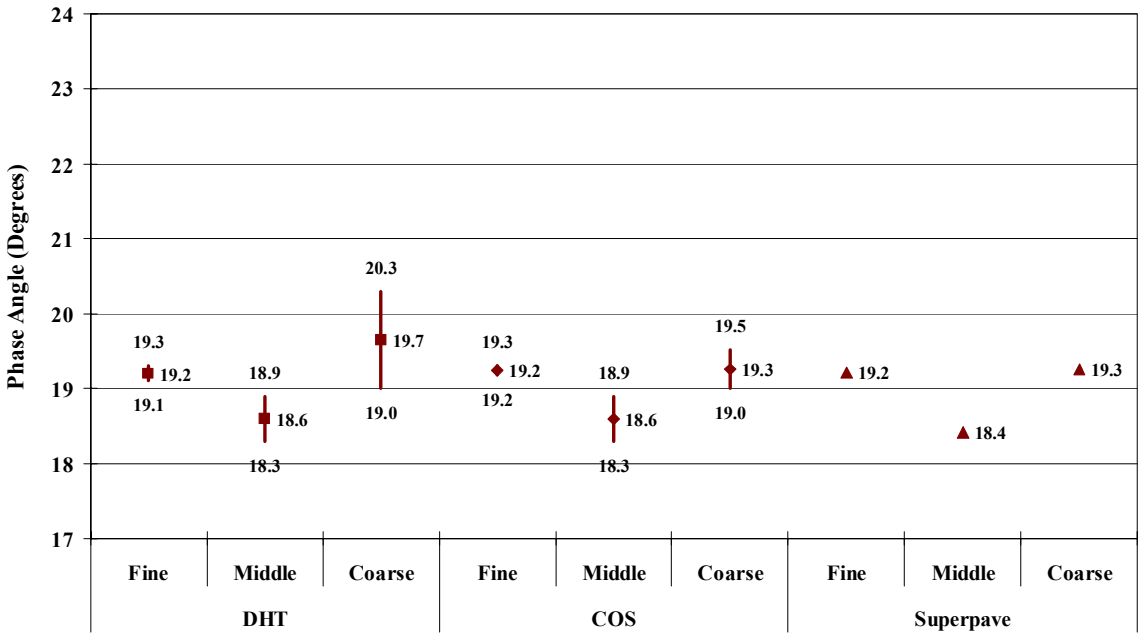

Figure I. 8 Phase Angle Range Plotted versus Frequency at 60°C for Range of VTM Specifications Met at 300 kPa

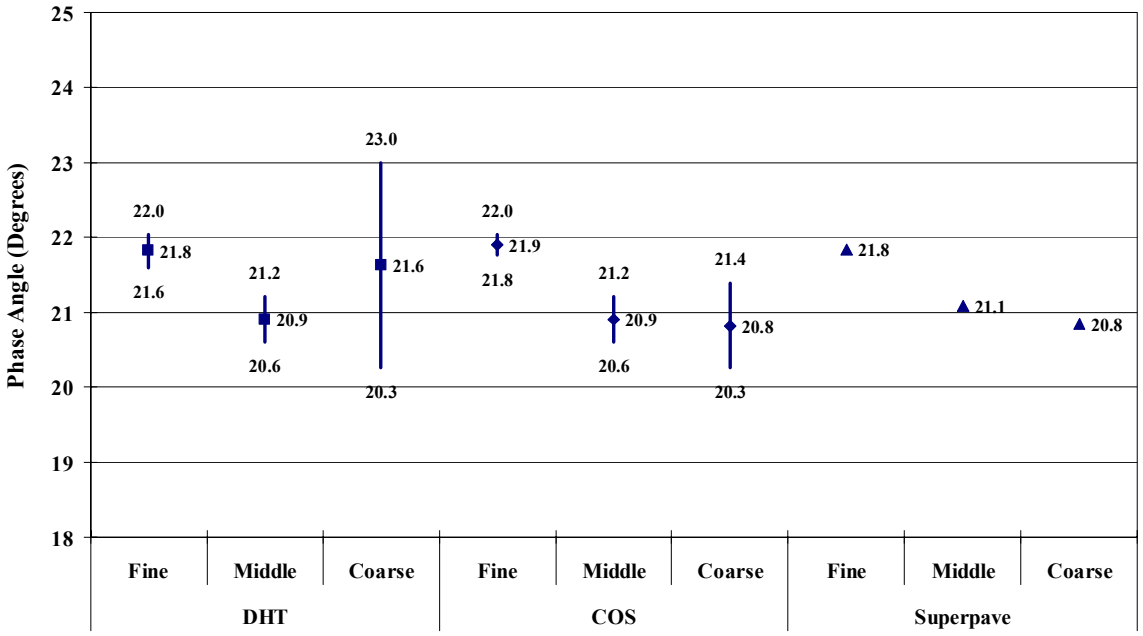

Figure I. 9 Phase Angle Range Plotted versus Frequency at 25°C for Range of VTM Specifications Met at 450 kPa

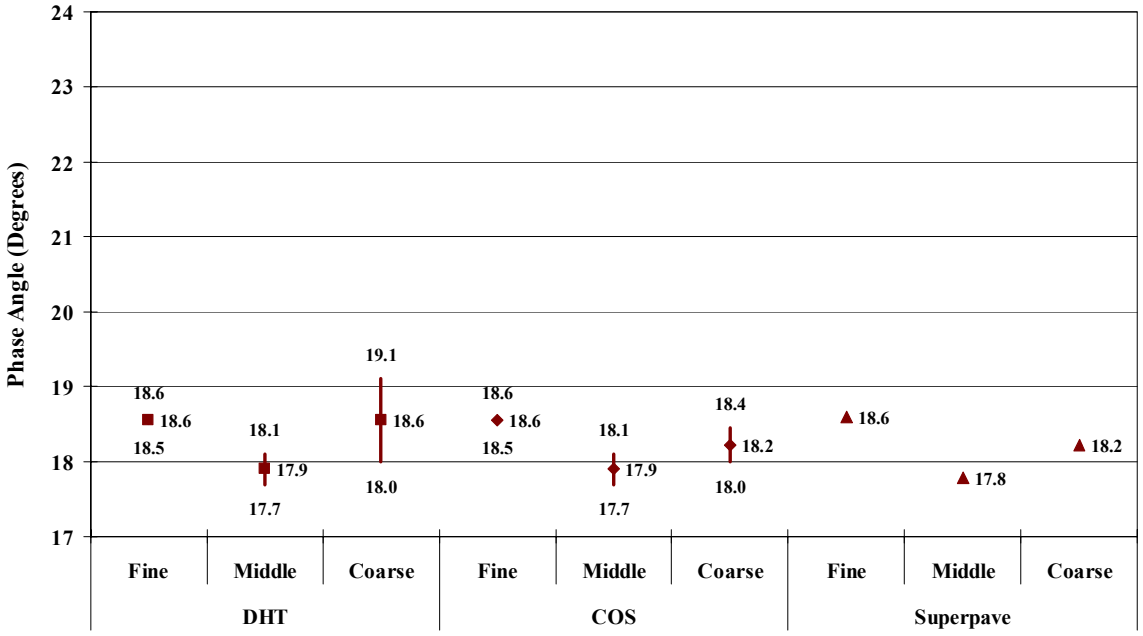

Figure I. 10 Phase Angle Range Plotted versus Frequency at 60°C for Range of VTM Specifications Met at 450 kPa

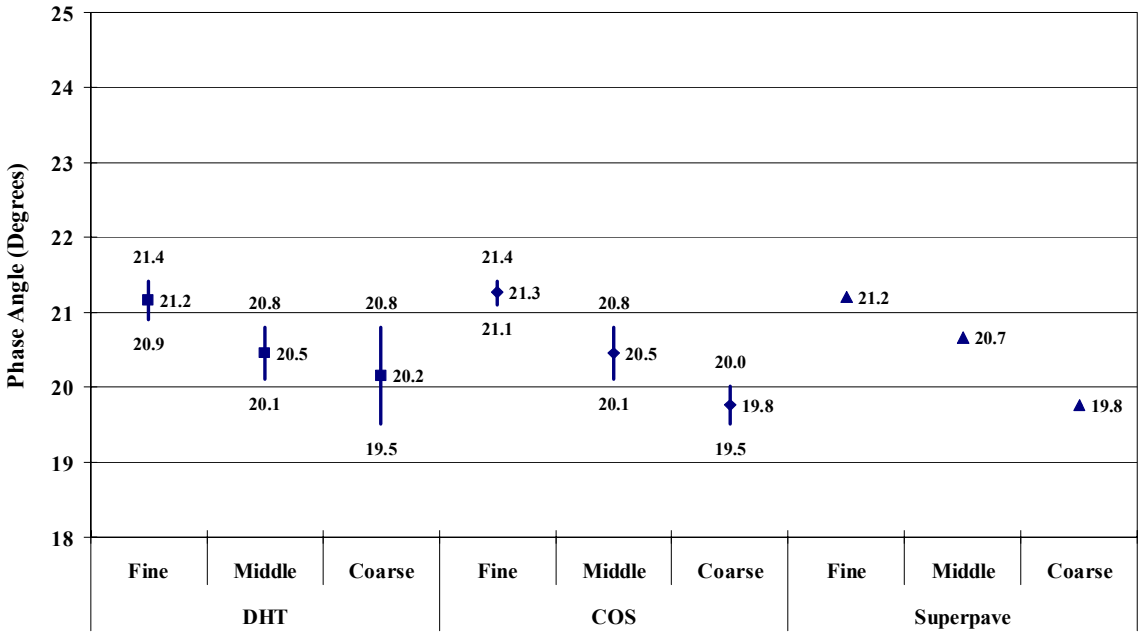

Figure I. 11 Phase Angle Range Plotted versus Frequency at 25°C for Range of VTM Specifications Met at 600 kPa

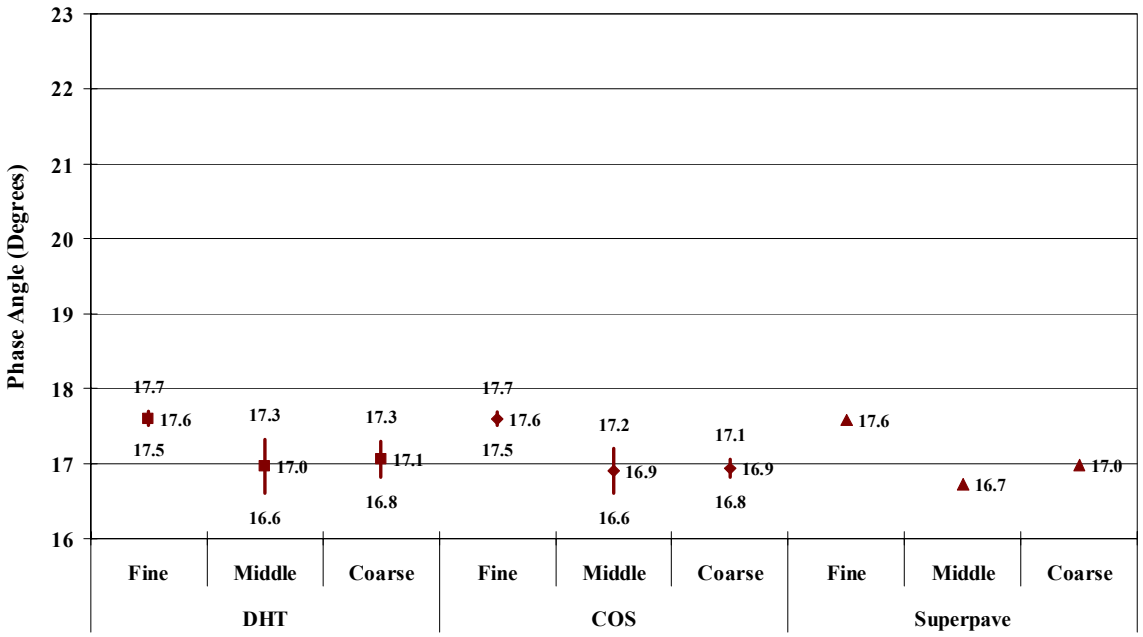

Figure I. 12 Phase Angle Range Plotted versus Frequency at 60°C for Range of VTM Specifications Met at 600 kPa

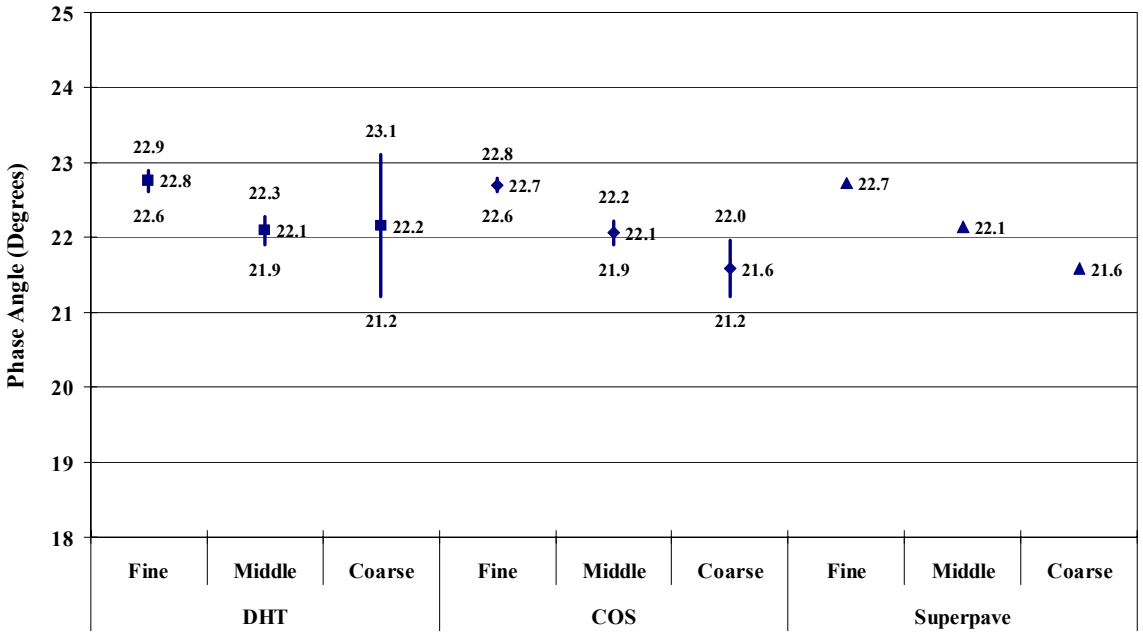

Figure I. 13 Phase Angle Range Plotted versus Deviatoric Stress State at 25°C for Range of VTM Specifications Met at 0.125 Hz

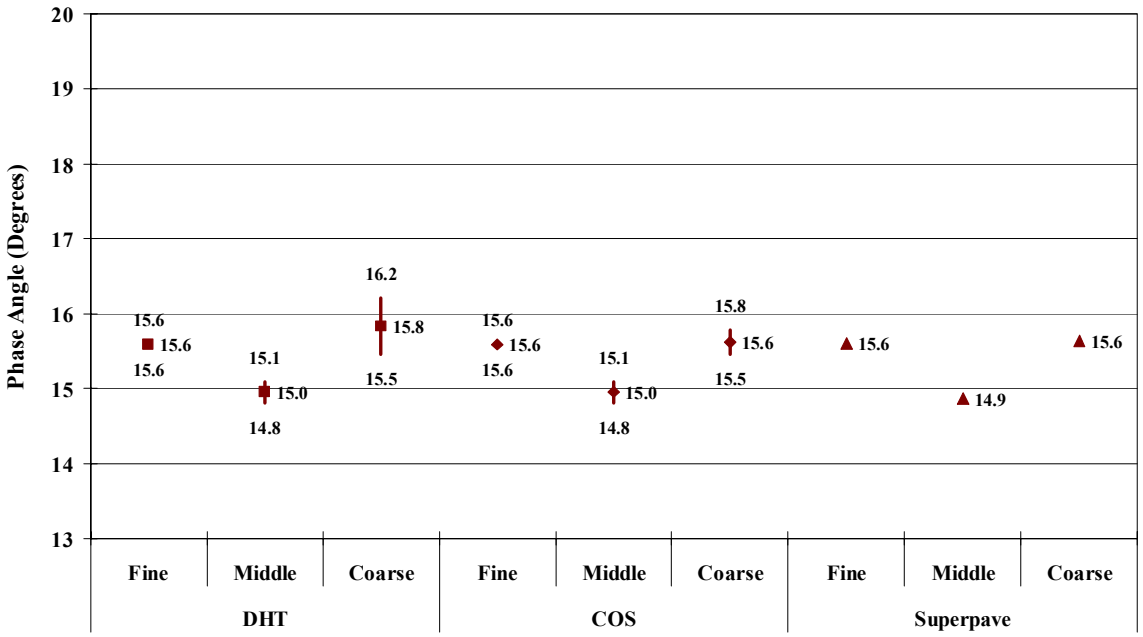

Figure I. 14 Phase Angle Range Plotted versus Deviatoric Stress State at 60°C for Range of VTM Specifications Met at 0.125 Hz

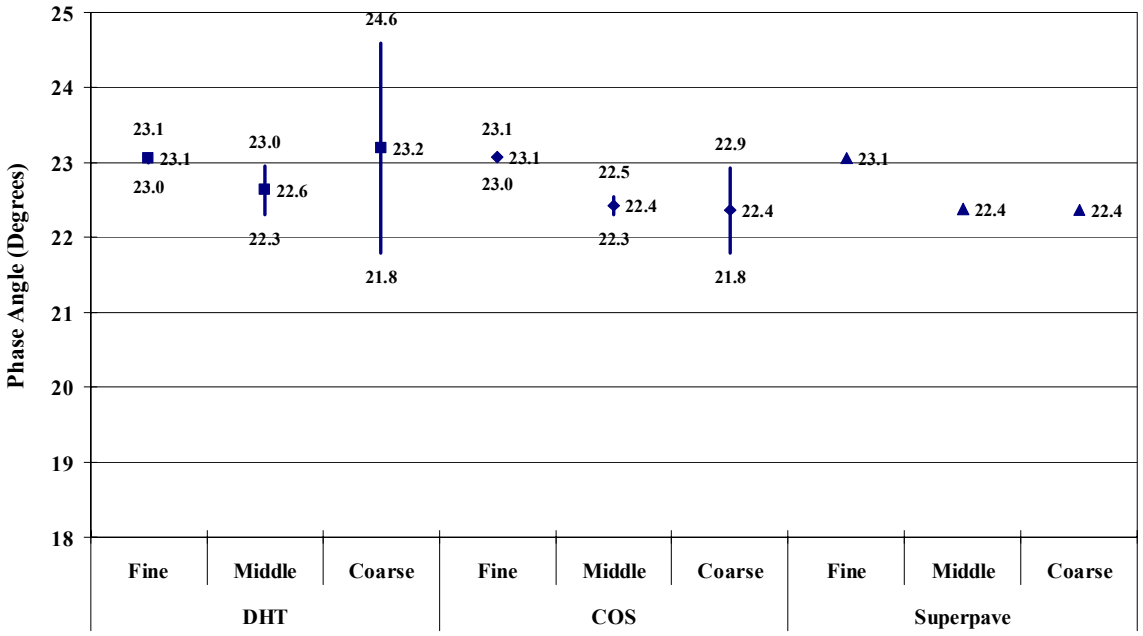

Figure I. 15 Phase Angle Range Plotted versus Deviatoric Stress State at 25°C for Range of VTM Specifications Met at 0.5 Hz

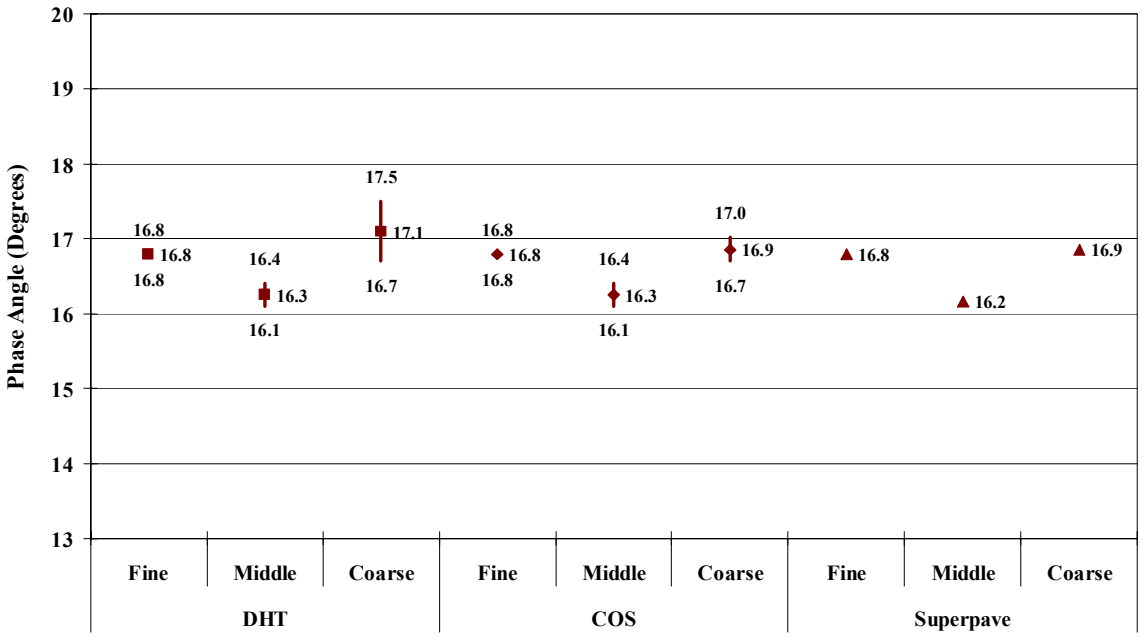

Figure I. 16 Phase Angle Range Plotted versus Deviatoric Stress State at 60°C for Range of VTM Specifications Met at 0.5 Hz

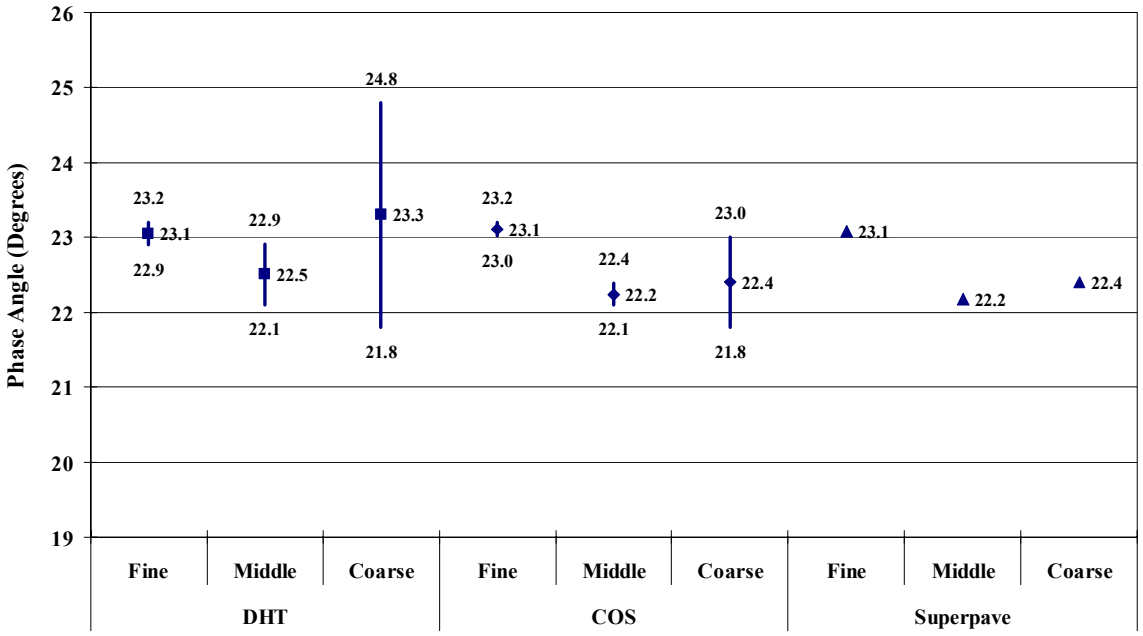

Figure I. 17 Phase Angle Range Plotted versus Deviatoric Stress State at 25°C for Range of VTM Specifications Met at 1.0 Hz

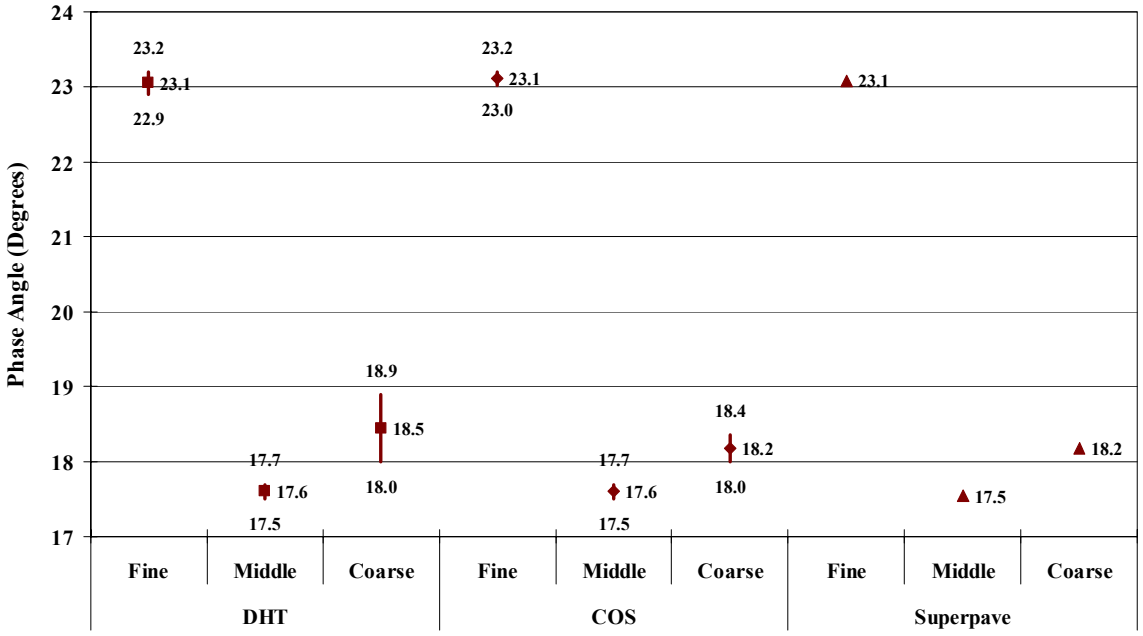

Figure I. 18 Phase Angle Range Plotted versus Deviatoric Stress State at 60°C for Range of VTM Specifications Met at 1.0 Hz

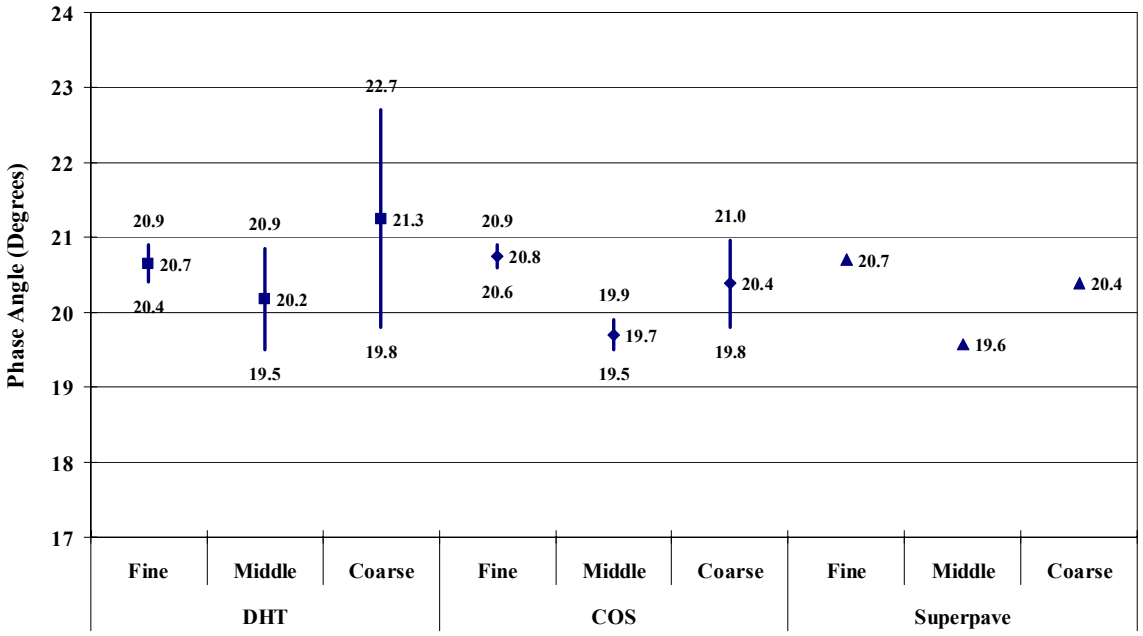

Figure I. 19 Phase Angle Range Plotted versus Deviatoric Stress State at 25°C for Range of VTM Specifications Met at 5.0 Hz

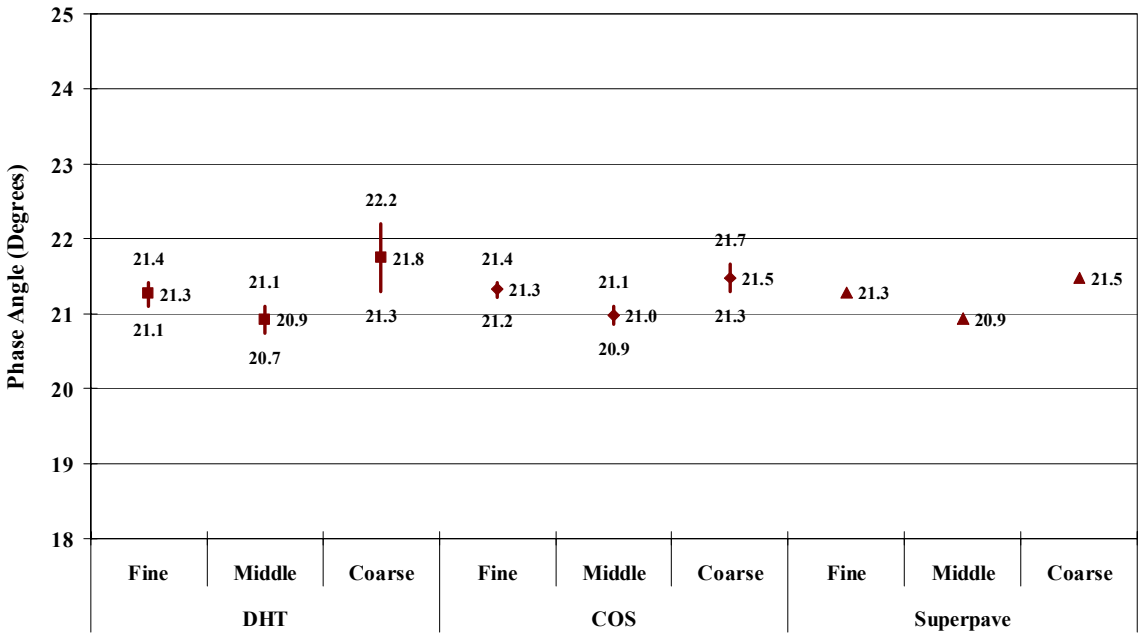

Figure I. 20 Phase Angle Range Plotted versus Deviatoric Stress State at 60°C for Range of VTM Specifications Met at 5.0 Hz

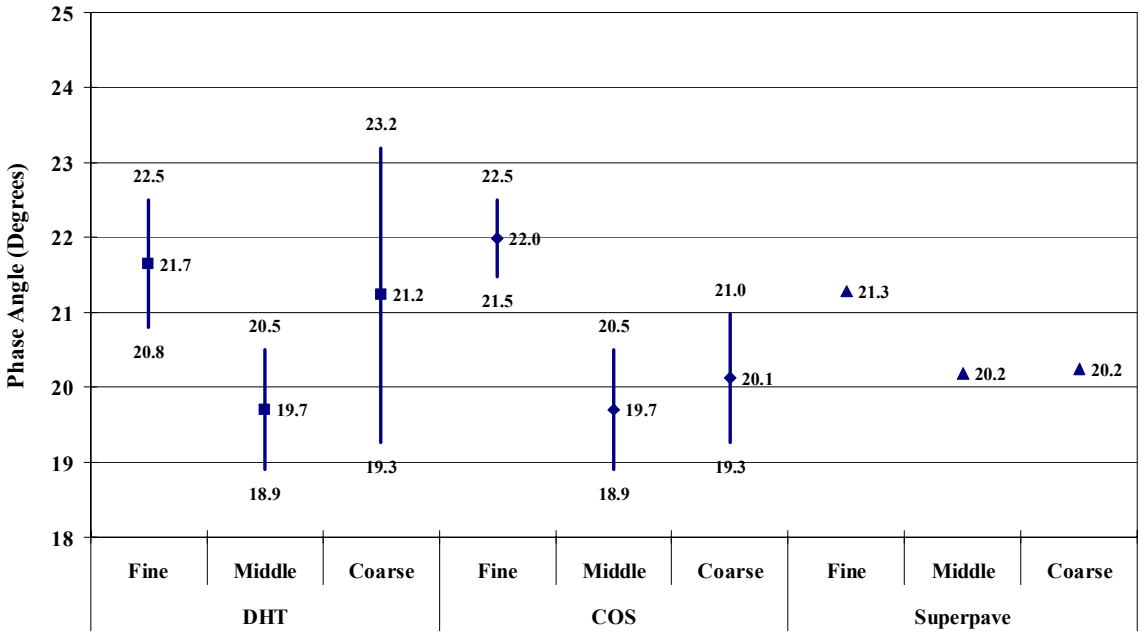

Figure I. 21 Phase Angle Range Plotted versus Deviatoric Stress State at 25°C for Range of VTM Specifications Met at 10.0 Hz

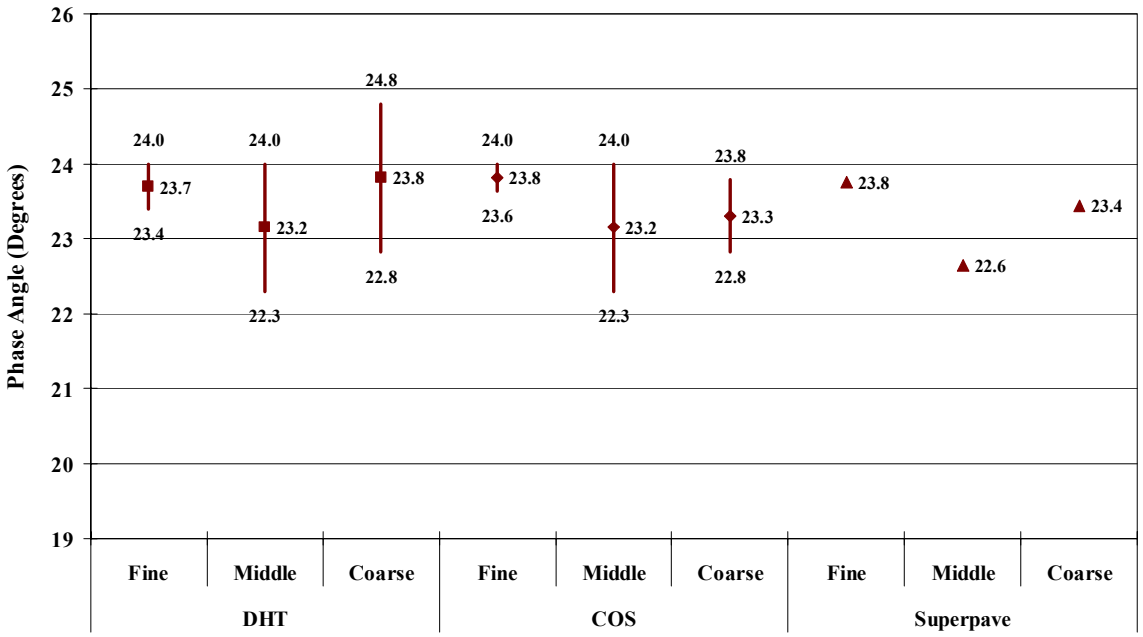

Figure I. 22 Phase Angle Range Plotted versus Deviatoric Stress State at 60°C for Range of VTM Specifications Met at 10.0 Hz